

CALIFORNIA INSTITUTE OF TECHNOLOGY

EARTHQUAKE ENGINEERING RESEARCH LABORATORY

THE RESPONSE OF NONLINEAR
MULTI-STORY STRUCTURES SUBJECTED
TO EARTHQUAKE EXCITATION

by

Melbourne F. Giberson

A report on research conducted under a
grant from the National Science Foundation

Pasadena, California

1967

THE RESPONSE OF NONLINEAR
MULTI-STORY STRUCTURES SUBJECTED
TO EARTHQUAKE EXCITATION

Thesis by
Melbourne Fernald Giberson

In Partial Fulfillment of the Requirements
For the Degree of
Doctor of Philosophy

California Institute of Technology
Pasadena, California

1967

(Submitted May 15, 1967)

ACKNOWLEDGMENTS

The author wishes to express his sincere appreciation to his advisor, Professor D. E. Hudson, for his valuable assistance and guidance throughout this investigation. The author is also grateful to Professors W. D. Iwan and P. C. Jennings for their helpful advice and the interest they took in this project.

The author appreciates the additional detailed information provided by R. W. Clough, Professor of Civil Engineering at the University of California at Berkeley, K. Lee Benuska and Ian Stubbs of T. Y. Lin & Associates which helped in interpreting the FHA Study⁽¹⁾ and their report to the Office of Civil Defense⁽²⁾. The personnel of the Caltech Computer Center are to be thanked for their programming advice and their cooperation when the extensive plotting was performed. Helpful suggestions concerning the manuscript provided by fellow graduate students are also very much appreciated.

The author further wishes to express his deep gratitude to his wife, Susan, for her patience, understanding and aid throughout his years of graduate study.

The financial support received from the California Institute of Technology and the National Science Foundation is gratefully acknowledged. Additional funds for the computation time provided by the Engineering Division of the National Science Foundation are also gratefully acknowledged.

ABSTRACT

The dynamic responses of a 20-story nonlinear structural frame representative of a modern high rise building are analyzed with the aid of a digital computer. Related analytical studies of continuous systems are carried out. Quantitative information is provided on the importance of a wide range of modes to the various responses of a multi-story structure during an earthquake. The effect of yielding on the response is observed. The magnitude of the structural responses are compared with common measurements of earthquake strength.

At the ends of each girder and column of the structural frame are yield hinges which have bilinear bending moment-rotation hysteretic characteristics. Two beam models having such characteristics are studied; one of these models can treat curvilinear hysteretic behavior. Three definitions of ductility factor are discussed, one of which is applicable to both bilinear and curvilinear hysteresis loops. In the computer program, the frame is subjected to the time history of an earthquake accelerogram, the equations of motion are step-wise integrated, and the various structural responses - displacement, bending moments, incurred yielding, etc. - are determined.

The agreement between the response parameters resulting from excitation by seven different earthquake ground motions indicates that these response characteristics are determined more by the properties of the structure than by the earthquake. These results throw some light on extreme value statistics of the response of yielding structures subjected to earthquakes. The characteristic patterns observed in the computed responses of the nonlinear structure can be related to analytical studies of linear elastic, shear-type, uniform and tapered continuous cantilever beams.

iv
TABLE OF CONTENTS

| <u>PART</u> | | <u>PAGE</u> |
|-------------|--|-------------|
| I | INTRODUCTION | 1 |
| II | MODELS OF BEAMS WITH NONLINEAR CHARACTERISTICS AND ASSOCIATED DEFINITIONS OF DUCTILITY FACTOR | 6 |
| | 2.1 Introduction | 6 |
| | 2.2 Nomenclature Pertaining to Hysteresis Loops | 8 |
| | 2.3 Three Definitions of "Ductility Factor" for Simple Yielding Systems | 9 |
| | 2.4 Two Systems for Modeling a Simple Yielding System with Bilinear Hysteretic Characteristics | 16 |
| | 2.5 Two Models of Nonlinear Beams | 22 |
| | 2.6 Simple Yielding Systems for Nonlinear Beams | 39 |
| | 2.7 Ductility Factors for Nonlinear Beams | 44 |
| III | EQUATIONS OF MOTION FOR NONLINEAR TALL STRUCTURES | 49 |
| | 3.1 Introduction | 49 |
| | 3.2 A Class of Nonlinear Tall Structures | 49 |
| | 3.3 Damping | 58 |
| | 3.4 Equations of Motion | 62 |
| | 3.5 Solution of the Equations of Motion | 74 |
| IV | VERIFICATION OF THE COMPUTER PROGRAM | 83 |
| | 4.1 Introduction | 83 |
| | 4.2 Error Checks in the Program | 83 |
| | 4.3 The Wilson-Clough Integration Technique | 85 |
| | 4.4 Excitation of the Linear A/20/2.2/2/6 Frame Near Its Third Natural Frequency | 87 |
| | 4.5 A Comparison With Results of the FHA Study | 91 |

| <u>PART</u> | | <u>PAGE</u> |
|-------------------|--|-------------|
| V | MODAL ANALYSIS OF CONTINUOUS CANTILEVER BEAMS AND OF TALL STRUCTURES | 93 |
| | 5.1 Introduction | 93 |
| | 5.2 Modal Analysis of Continuous Cantilever Beams | 95 |
| | 5.3 Modal Analysis of Discretized Models of Tall Structures | 115 |
| VI | RESPONSE RESULTS | 124 |
| | 6.1 Introduction | 124 |
| | 6.2 Comparison of the Linear and Nonlinear Responses of a Structural Frame | 127 |
| | 6.3 Response of the Nonlinear A/20/2.2/2/6 Frame Subjected to Earthquake Excitation | 138 |
| | 6.4 Relationships Between Structural Responses and the Strength of an Earthquake | 157 |
| VII | CONCLUSIONS | 161 |
| <u>APPENDICES</u> | | |
| A | RESPONSE PLOTS FOR A NONLINEAR MULTI-STORY STRUCTURE SUBJECTED TO SEVERAL EARTHQUAKE EXCITATIONS | 165 |
| B | DISCUSSION OF THE YIELD CRITERIA USED IN THE FHA STUDY | 194 |
| C | DISCUSSION OF THE TREATMENT OF SYMMETRY FOR THE TWO-COMPONENT BEAM MODEL | 202 |
| D | FUTURE STUDIES | 208 |
| E | LISTING OF THE COMPUTER PROGRAM | 210 |
| | REFERENCES | 228 |

CHAPTER I

INTRODUCTION

Until recently, comparatively little has been known about the response of multi-story structures subjected to earthquakes. Consequently, in regions where earthquakes have occurred relatively frequently, building codes imposed stringent height limits on structures. In the past few years, however, there has been a significant improvement in the understanding of how structures respond to earthquakes, and, as a result, in some cities height restrictions have been relaxed for structures which are designed on the basis of the dynamic forces, deformation, and yielding which would be induced by a strong earthquake.

A common type of high-rise building being constructed today (1967) uses glass and light-weight walls extensively, relying on large columns and girders for support. The investigation described in this report was undertaken in order to provide additional information on how this kind of multi-story structure responds to earthquake excitation.

The initial work on problems encountered in designing earthquake resistant multi-story structures was done during the 1920's and early 1930's by K. Muto⁽³⁾ and K. Suyehiro⁽⁴⁾ of Japan and M. A. Biot^(5,6) and J. R. Freeman⁽⁷⁾ in the United States. Although the equations of motion for earthquake excited multi-story structures were well known, the time history solutions of the responses of multi-story structures could not be obtained because neither analog

nor digital computers were available to make the extensive calculations necessary.

Through the years the one degree of freedom system has received extensive study by several investigators using analytical techniques and, as they become available, analog and digital computers. Among them are D. F. Hudson⁽⁸⁾, G. W. Housner⁽⁹⁾, T. K. Caughey⁽¹⁰⁾, G. V. Berg⁽¹¹⁾, S. S. Thomaides⁽¹¹⁾, J. Penzien⁽¹²⁾, W. D. Iwan⁽¹³⁾, Paul C. Jennings⁽¹⁴⁾, C. V. Chelapati⁽¹⁵⁾, and L. D. Lutes⁽¹⁶⁾. In addition to direct application to the one degree of freedom system, the results of their investigations also provide significant insight into the understanding of how multi-story structures respond to earthquake excitation.

One early study in multi-story structures appeared in 1938. In that study, L. S. Jacobsen and R. S. Ayre⁽¹⁷⁾ experimentally determined the dynamic shears for at least the first four modes of a sixteen story model of an office building using a decaying sinusoidal base excitation of finite duration. The results indicated that the higher modes are important for shear forces in the upper floors.

With the advent of analog and digital computers, the equations of motion of multi-story structures subjected to earthquake excitation could be solved. The earlier research work on multi-story structures using these tools was performed by T. P. Tung⁽¹⁸⁾, Richard L. Jennings^(19,20), N. M. Newmark^(18,20,23), R. W. Clough⁽²¹⁾, J. A. Blume^(22,23), J. E. Goldberg⁽²⁴⁾, J. L. Bogdanoff⁽²⁴⁾, Z. L. Moh⁽²⁴⁾, L. Corning⁽²³⁾, J. Penzien⁽²⁵⁾ and many others. More recent work of this nature has been carried out by J. I.

Bustamente⁽²⁶⁾, H. Umemura⁽²⁷⁾, Y. Osawa⁽²⁷⁾, A. Shibata⁽²⁷⁾, and G. V. Berg⁽²⁸⁾, to mention a few.

A number of researchers have visualized this problem as a wave propagation problem in a continuous cantilever beam. Among them are K. Muto^(3,29), H. Suyehiro⁽⁴⁾, H. M. Westergaard⁽³⁰⁾, L. S. Jacobsen⁽³¹⁾, K. Kanai⁽³²⁾, G. N. Bycroft^(33,34,35), M. J. Murphy⁽³⁵⁾ and L. W. Harrison⁽³⁵⁾.

During the five years preceding 1967 a large amount of research on multi-story structures using high capacity-high speed digital computers has been done by R. W. Clough^(36,37,38,39,1) and his co-workers E. L. Wilson^(37,38,39), I. P. King^(37,38), K. L. Benuska⁽³⁹⁾, and T. Y. Lin & Associates⁽²⁾.

Many of these authors have noted that several modes can be excited in a multi-story structure and that the "higher" modes must be considered in the interfloor shear force in the upper portion of the structure. In this report, quantitative information is provided on the importance of all modes including the "higher" ones to the various responses of a multi-story structure during an earthquake.

In Chapter II two different models of a nonlinear beam which can be used to represent each girder and column in a structural frame are presented and compared. One beam model can have different curvilinear or bilinear bending moment-rotation hysteresis loops located at the yield joints at each end of the beam. The other model is restricted to having bilinear hysteresis loops at the ends. Three definitions of ductility factor applicable to these beams are given and discussed.

The properties of the class of nonlinear multi-story structures considered in this report are listed in Chapter III. In addition, the damping mechanisms are described and the equations of motion for this system are derived. Using the Wilson-Clough integration technique⁽⁴⁰⁾, the equations of motion are put into a form suitable for solution by the 7090/7094 digital computer at the Computer Center of the California Institute of Technology.

As an overall check on the computer program for analyzing the response of nonlinear multi-story structures, several tests on it were carried out which are briefly described in Chapter IV. One of these was a comparison with results for a corresponding system presented in the FHA Study⁽¹⁾.

In Chapter V uniform and tapered, shear-type, linear elastic, continuous cantilever beams are analytically studied in order to determine the importance of "higher modes" to the responses, i.e., displacement, strain, shear force, and total acceleration, at various positions in an earthquake excited structure. "Whiplash" is discussed and a definition suggested. A method of determining "equivalent" modal participation factors for nonlinear structures is presented and examples of the "equivalent" modal contributions to displacements and interfloor displacements (strain) are given.

Chapter VI treats the response results for a nonlinear twenty story structure subjected to earthquake excitation. The effect of yielding is observed by comparing the responses for the nonlinear structure with those for the corresponding linear structure. Time history response plots, displacement envelopes, and ductility factors

for the nonlinear structure subjected to the entire duration of several earthquakes are presented and analyzed. The effects of various modes are observed by comparing time history response plots of the multi-story structure with those for one degree of freedom linear oscillators representing the individual modes. Three common measurements of the strength of an earthquake are given and are compared with the magnitudes of the corresponding structural responses for the earthquakes used.

CHAPTER II

MODELS OF BEAMS WITH NONLINEAR CHARACTERISTICS
AND ASSOCIATED DEFINITIONS OF DUCTILITY FACTOR2.1 Introduction

The primary purpose of this chapter is to describe and compare two different models of a nonlinear beam which can be used to represent each girder and column in a discretized model of a nonlinear tall structure. One beam model has identical bilinear bending moment-end rotation hysteresis loops at the yield joints located at each end of the beam. The other model is more versatile since it can have different curvilinear or bilinear bending moment-end rotation hysteresis loops at each end.

In order to develop concepts and terminology useful in discussing yielding beams, simple yielding systems are studied first. In this study the term "simple yielding system" always refers to a system with only one yield joint. A yield joint is similar to a Coulomb slider, but is more general since it can have a curvilinear force-deflection (or bending moment-rotation) relationship. In particular, certain nomenclature pertaining to hysteresis loops is presented, two different simple yielding systems are studied, and three definitions of ductility factor for these simple systems are given. Two independent models of beams with yield joints at each end are presented as extensions from the simple yielding systems. Three definitions of ductility factor which apply to yielding beams are also discussed.

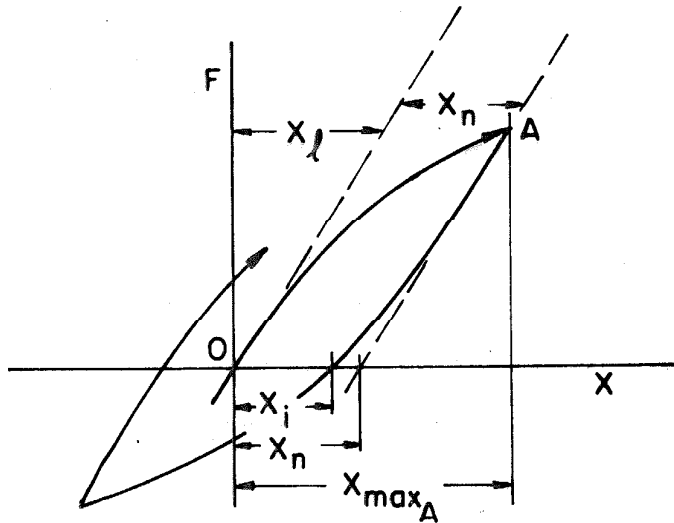


Fig. 2.1 Curvilinear
Hysteresis Loop

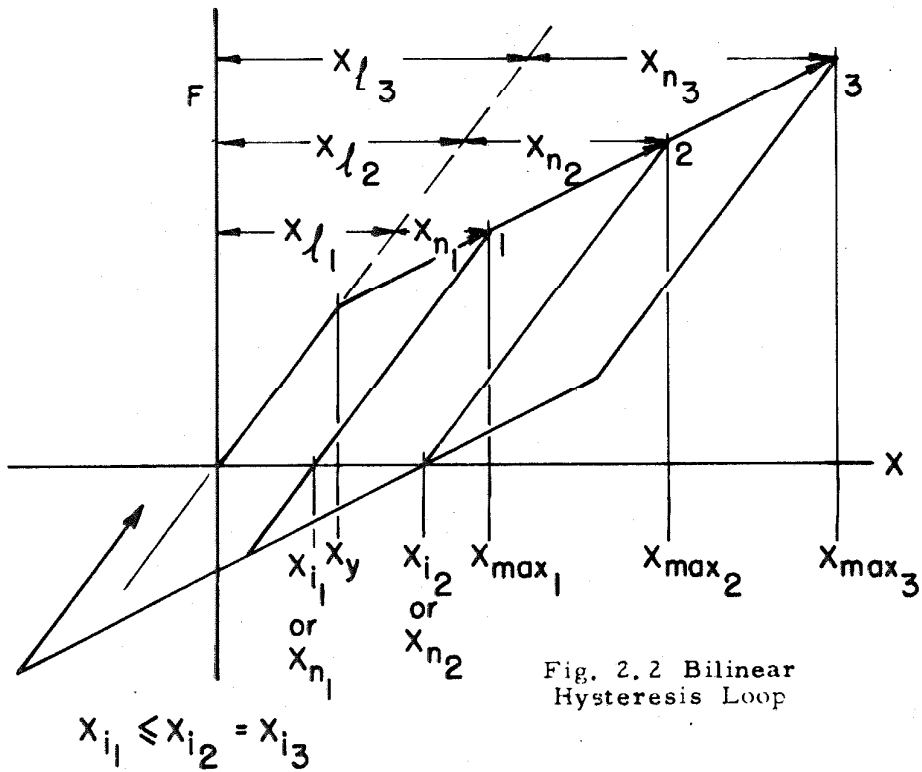


Fig. 2.2 Bilinear
Hysteresis Loop

2.2 Nomenclature Pertaining to Hysteresis Loops

The nomenclature pertaining to hysteresis loops as used in this report is defined in this section. A typical curvilinear hysteresis loop is shown in Fig. 2.1 and a typical bilinear hysteresis loop is depicted in Fig. 2.2. For both of these loops, the following nomenclature applies:

$$\begin{aligned}
 |x|_{\max} &= \text{maximum absolute displacement,} \\
 x_y &= \text{displacement at yield (yield level),} \\
 x_n &= \text{nonlinear displacement: departure from the initial tangent (absolute value),} \\
 x_l = |x|_{\max} - x_n &= \text{linear displacement: displacement along the initial tangent at the force level of } |x|_{\max} \text{ (absolute value),} \\
 x_i &= \text{irrecoverable displacement or permanent set (absolute value), and} \\
 x_r = |x|_{\max} - x_i &= \text{recoverable displacement (absolute value).}
 \end{aligned}$$

Hence,

$$x_l + x_n = x_r + x_i,$$

or

$$x_r = x_l + x_n - x_i. \quad (2.1)$$

From Fig. 2.1 and Fig. 2.2 it is seen that

$$x_i \leq x_n \quad \text{and} \quad x_l \leq x_r. \quad (2.2)$$

Note that for the bilinear hysteresis loop of Fig. 2.2 with

$$|x|_{\max} \leq x_{\max_2}, \quad (2.3)$$

the irrecoverable displacement is identical to the nonlinear displacement, and the linear displacement is identical to the recoverable displacement:

$$x_l = x_n \quad \text{and} \quad x_r = x_l \quad . \quad (2.4)$$

The bilinear hysteresis loop with the maximum displacement restricted by Eq. 2.3 is the one of primary interest in this report.

Looking at Fig. 2.1 and Fig. 2.2, it appears that in many instances the irrecoverable displacement can be much smaller than the corresponding nonlinear displacement. Furthermore, failure is probably more closely related to the nonlinear displacement than to the irrecoverable displacement. Consequently, one definition of ductility based on the nonlinear displacement rather than the irrecoverable displacement is given in the next section.

2.3 Three Definitions of "Ductility Factor" for Simple Yielding Systems

In this report, the term "ductility factor" is used as a measure of the amount of yielding incurred in a system. However, a "ductility factor" has no precise meaning until the method of measuring it has been defined. The purpose of this section is to make three definitions of the term "ductility factor" for the nonlinear spring of the simple yielding system of Fig. 2.3. All three definitions apply to the bilinear hysteresis loop shown in Fig. 2.4 and one of them also applies to the more general curvilinear hysteresis loop of Fig. 2.5.

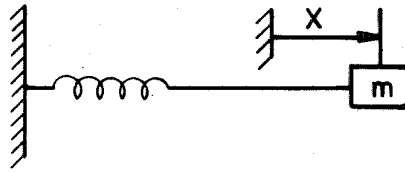


Fig. 2.3 Simple Yielding System With Nonlinear Spring

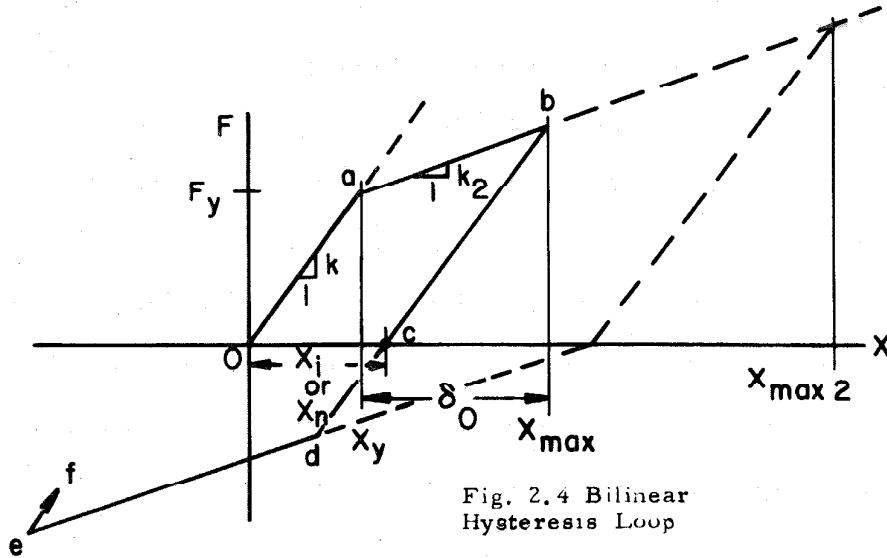


Fig. 2.4 Bilinear Hysteresis Loop

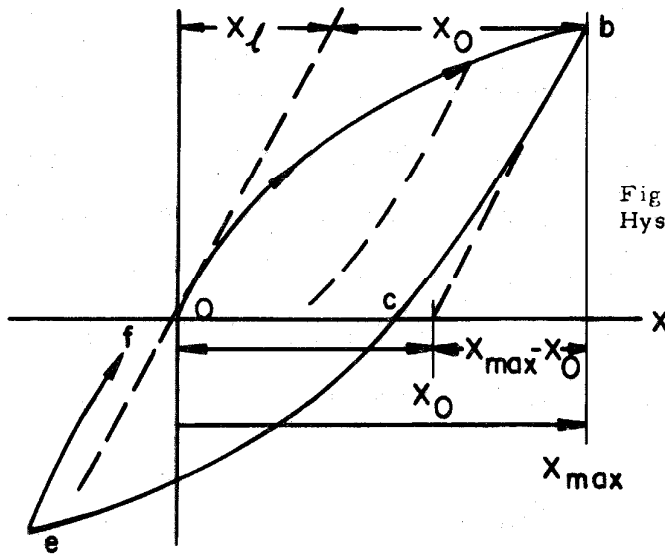


Fig 2.5 Curvilinear Hysteresis Loop

The next section, Section 2.4, treats two systems composed of linear springs and Coulomb sliders which can be used to model a simple yielding system with bilinear hysteretic characteristics. However, for the purposes of this section, it is only necessary to consider the simple yielding system of Figs. 2.3, 2.4, and 2.5.

For the nonlinear spring of the system of Fig. 2.3, one possible hysteresis loop is the path 0, a, b, c, d, e, f in Fig. 2.4. On this path only linear displacement is incurred until the displacement x exceeds x_y at point (a), whereupon it yields. At point (b) the displacement $|x|_{\max}$ is composed of the linear displacement, x_y , and additional displacement incurred during yielding, δ_o , where

$$\delta_o = |x|_{\max} - x_y .$$

Furthermore, using the terminology of Section 2.2, δ_o has both "linear" and "nonlinear" components. Now, if the spring is released so that the force becomes zero, the equilibrium displacement is the irrecoverable displacement x_i , at point (c). Note that for this example, $|x|_{\max}$ is less than x_{\max_2} ; consequently, the nonlinear displacement x_n and irrecoverable displacement x_i are equal:

$$x_n = x_i \quad (\text{if } |x|_{\max} \leq x_{\max_2}) . \quad (2.5)$$

From geometrical considerations, x_n is found from Fig. 2.4 to be

$$x_n = \left(1 - \frac{k_2}{k}\right) \cdot \delta_o . \quad (2.6)$$

Hence, the additional linear displacement incurred in going from point (a) to point (b) is

$$\delta_o - x_n = \left(\frac{k_2}{k}\right) \cdot \delta_o . \quad (2.7)$$

Therefore, the total linear displacement incurred in traversing from (0) to (a) to (b) is

$$x_l = x_y + \left(\frac{k_2}{k}\right) \cdot \delta_o . \quad (2.8)$$

The first definition of ductility factor, μ_1 , is simply a measure of the maximum absolute displacement at point (b), $|x|_{\max}$, (see Fig. 2.4) with respect to the yield displacement, x_y , without regard to the second slope, k_2 :

$$\mu_1 = \frac{|x|_{\max}}{x_y} \quad (2.9)$$

or

$$\mu_1 = 1 + \frac{\delta_o}{x_y} . \quad (2.10)$$

Although Eq. 2.10 can be used to measure the yielding for any bilinear hysteresis loop, its most appropriate application is to the ideally elasto-plastic hysteresis loop, i.e., a bilinear hysteresis loop with the second slope identically equal to zero, $k_2 \equiv 0$. In this

case, all of the displacement from the yield displacement at point (a) to point (b) is nonlinear:

$$x_n = \delta_o = |x|_{\max} - x_y, \quad (k_2 \equiv 0) \quad (2.11)$$

and the total linear displacement at point (b) is the yield displacement, x_y :

$$x_l = x_y \quad (k_2 \equiv 0) . \quad (2.12)$$

Furthermore, the total energy dissipated, E_D in a complete, symmetric hysteresis loop with $k_2 \equiv 0$ is proportional to $(\mu_1 - 1)$ and is given by

$$E_D = 4F_y \cdot \delta_o \quad (k_2 \equiv 0) \quad (2.13)$$

where

$$F_y = k \cdot x_y . \quad (2.14)$$

The amount of energy dissipated is of interest since, in some cases, dissipating energy by yielding can limit the amplitudes of the response.

Now, for systems with $k_2 \neq 0$, a second definition of ductility factor which measures the nonlinear displacement (instead of the maximum absolute displacement) at point (b) with respect to the yield displacement is

$$\mu_2 = 1 + \frac{x_n}{x_y} \quad (2.15)$$

which, by substituting Eq. 2.6 for x_n , becomes

$$\mu_2 = 1 + \left(1 - \frac{k_2}{k}\right) \frac{\delta_o}{x_y} . \quad (2.16)$$

In this case, the total energy dissipated in a complete symmetric hysteresis loop is proportional to $(\mu_2 - 1)$:

$$E_D = 4F_y \cdot \left(1 - \frac{k_2}{k}\right) \cdot \delta_o . \quad (2.17)$$

For the first two definitions of ductility factor, it is necessary to have a well-defined yield level. However, most curvilinear hysteresis loops do not have an inherently well-defined yield level. Nevertheless, for any hysteresis loop, except one with a vertical initial tangent, the nonlinear and linear displacements are well defined. For these loops a third definition of ductility factor relating the maximum absolute displacement, $|x|_{\max}$, at point (b) (see Fig. 2.4) to the linear displacement, x_ℓ , can be made:

$$\mu_3 = \frac{|x|_{\max}}{x_\ell}$$

or

$$\mu_3 = 1 + \frac{x_n}{x_\ell} . \quad (2.18)$$

However, the energy dissipated either in a curvilinear or in a bilinear hysteresis loop cannot be directly related to $(\mu_3 - 1)$ as was done above for $(\mu_2 - 1)$ in Eq. (2.17).

When used for the bilinear hysteresis loop of Fig. 2.4, the

third definition can be written in another form. For the maximum absolute displacement in this loop (at point (b)), x_l and x_n are given by Eq. 2.6 and Eq. 2.8, respectively. Substituting these into Eq. 2.18, μ_3 becomes

$$\mu_3 = 1 + \frac{\left(1 - \frac{k_2}{k}\right) \cdot \delta_o}{x_y + \left(\frac{k_2}{k} \cdot \delta_o\right)} \quad (2.19)$$

In order to show how these three definitions differ for bilinear hysteresis loops, the following numerical examples are considered:

Let $x_y = 1$ and $|x|_{\max} = 5$ for systems with $k_2/k = 0.05$ and $k_2/k = 0.95$. The various ductility factors are:

| Definition | $\frac{k_2}{k} = 0.05$ | $\frac{k_2}{k} = 0.95$ |
|--|------------------------|------------------------|
| $\mu_1 \equiv 1 + \frac{\delta_o}{x_y}$ | 5.0 | 5.0 |
| $\mu_2 \equiv 1 + \left(1 - \frac{k_2}{k}\right) \cdot \frac{\delta_o}{x_y}$ | 4.8 | 1.2 |
| $\mu_3 \equiv 1 + \frac{\left(1 - \frac{k_2}{k}\right) \cdot \delta_o}{x_y + \left(\frac{k_2}{k} \cdot \delta_o\right)}$ | 4.17 | 1.17 |

(Note that when $k_2/k = 0$, $\mu_1 = \mu_2 = \mu_3$.) From these examples, one can see that the choice of the definition of ductility factor can make a sizeable difference in the resulting numerical value.

If only bilinear hysteresis loops are of interest, the second definition, μ_2 , is a better indication of the amount of yielding

incurred as well as of the energy dissipated than the first, μ_1 . On the other hand, if one wishes to compare the ductility factors of curvilinear systems to those of bilinear systems, the third definition, μ_3 , is best.

2.4 Two Systems for Modeling a Simple Yielding System With Bilinear Hysteretic Characteristics

This section treats two systems composed of linear springs and Coulomb sliders (see Fig. 2.6 and Fig. 2.7) which are used to model the simple yielding system of Fig. 2.3 with the bilinear hysteresis loop of Fig. 2.4. The purpose of studying these systems is to form a base from which to extend to the more complex problem of nonlinear beams.

As seen in Figs. 2.6, 2.7, 2.8 and 2.9, the primary difference between these two simple yielding systems is the arrangement of the springs and Coulomb sliders. In one, the springs are in series, and in the other, the springs are in parallel. Consequently, the general equations relating forces to displacements as well as those relating the ductility factors to the displacement incurred during yielding have different functional dependencies for the two systems. Concerning the functional dependence of the ductility factor for the springs-in-series system of Fig. 2.6 and Fig. 2.8, the incurred yielding (the amount of slip in the Coulomb slider), δ' , is purely the nonlinear* displacement and the corresponding linear* displacement is

* See Section 2.2 for definitions of linear and nonlinear displacements.

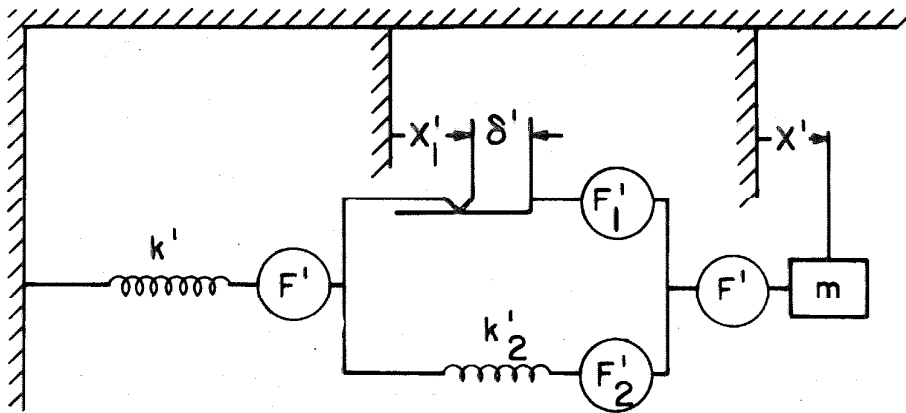


Fig. 2.6 Springs-in-Series

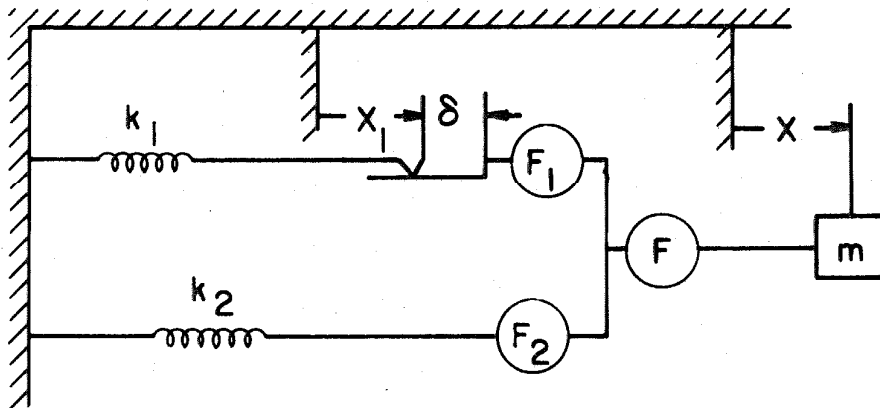


Fig. 2.7 Springs-in-Parallel

SPRINGS-IN-SERIES

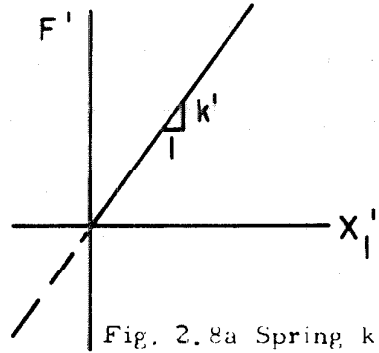
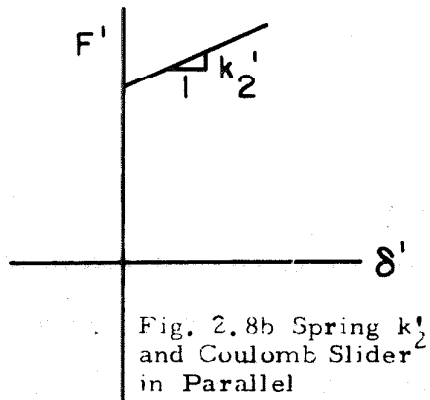
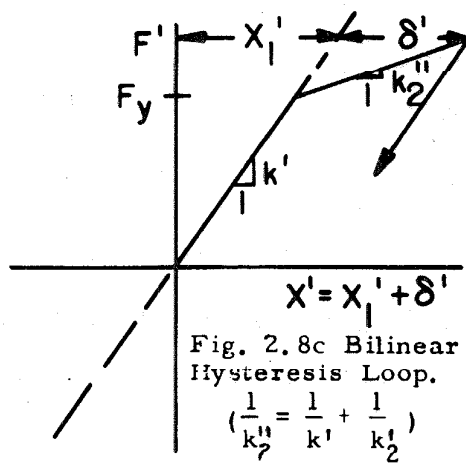
Fig. 2.8a Spring k' Fig. 2.8b Spring k'_2 and Coulomb Slider in Parallel

Fig. 2.8c Bilinear Hysteresis Loop.

$$\left(\frac{1}{k''_2} = \frac{1}{k'} + \frac{1}{k'_2}\right)$$

SPRINGS-IN-PARALLEL

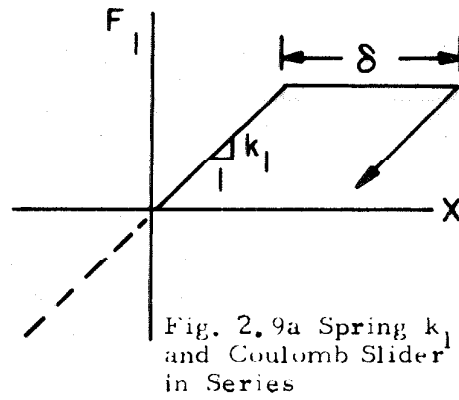
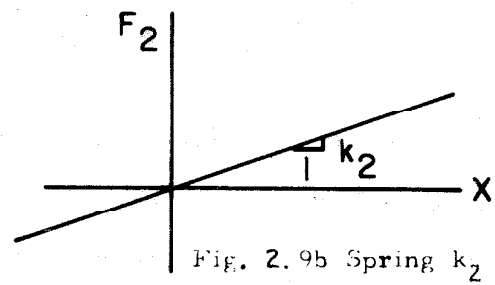
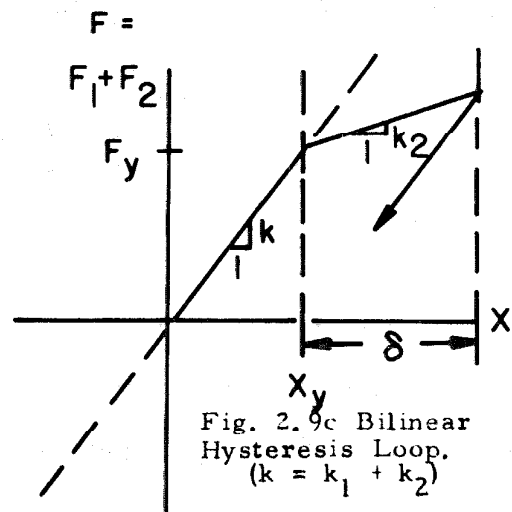
Fig. 2.9a Spring k_1 and Coulomb Slider in SeriesFig. 2.9b Spring k_2 

Fig. 2.9c Bilinear Hysteresis Loop.

$$(k = k_1 + k_2)$$

$$|x|_{\max} - \delta' .$$

Since δ' , as shown in Fig. 2.8c, corresponds to x_n of Fig. 2.4, the ductility factor for this system by the third definition, Eq. 2.19, is

$$\mu_{3 \text{ series}} = 1 + \frac{\delta'}{|x|_{\max} - \delta'}$$

or

$$\mu_{3 \text{ series}} = 1 + \frac{\delta'}{x'_1} . \quad (2.20)$$

In the springs-in-parallel system of Figs. 2.7 and 2.9, the displacement incurred during yielding, δ , is the sum of both the nonlinear and the linear displacements incurred by the entire system beyond the yield point. Since δ of Fig. 2.9c corresponds to δ_0 of Fig. 2.4, the ductility factor for this system, by the third definition, Eq. 2.19, is

$$\mu_{3 \text{ parallel}} = 1 + \frac{\left(1 - \frac{k_2}{k}\right) \delta}{x_y + \frac{k_2}{k} \delta} \quad (2.21)$$

where $k = k_1 + k_2$.

In the following vis-à-vis presentation, the different functional dependencies of the forces upon displacements in the two systems are studied.

Springs-in-Series
(Fig. 2.6 and Fig. 2.8)

General equations:

$$F' = F'_1 + F'_2;$$

$$x' = x'_1 + \delta';$$

in incremental form:

$$\Delta F' = \Delta F'_1 + \Delta F'_2; \quad (2.22.1)$$

$$\Delta x' = \Delta x'_1 + \Delta \delta'. \quad (2.23.1)$$

For small displacements:

$$F' = k'x'.$$

Spring k'_1 :

$$F'_1 = k'_1 x'_1;$$

$$\Delta F'_1 = k'_1 \Delta x'_1. \quad (2.24.1)$$

Spring k'_2 :

$$F'_2 = k'_2 \delta';$$

$$\Delta F'_2 = k'_2 \Delta \delta'. \quad (2.25.1)$$

Coulomb slider:

If F'_y is the yield limit for the force F' , then

$$F'_{1y} = F'_y$$

Springs-in-Parallel
(Fig. 2.7 and Fig. 2.9)

General equations:

$$F = F_1 + F_2;$$

$$x = x_1 + \delta;$$

in incremental form:

$$\Delta F = \Delta F_1 + \Delta F_2; \quad (2.22.2)$$

$$\Delta x = \Delta x_1 + \Delta \delta. \quad (2.23.2)$$

For small displacements:

$$F = kx$$

where

$$k = k_1 + k_2;$$

or

$$k_1 \equiv qk, \quad k_2 \equiv pk,$$

and

$$p + q = 1.$$

Spring k_1 :

$$F_1 = k_1 x_1;$$

$$\Delta F_1 = k_1 \Delta x_1. \quad (2.24.2)$$

Spring k_2 :

$$F_2 = k_2 \delta;$$

$$\Delta F_2 = k_2 \Delta \delta. \quad (2.25.2)$$

Coulomb slider:

If F_y is the yield limit for the force F , then

$$F_{1y} = q \cdot F_y$$

Springs-in-Series, cont.

is the yield limit for the Coulomb slider:

$$|F'_1| \leq F'_{1y}.$$

Yield Criteria:

When

$$|F'_1| < F'_{1y} \text{ (linear state),}$$

$$\Delta\delta' = 0.$$

Hence,

$$\Delta F' = k' \cdot \Delta x'. \quad (2.26.1)$$

When

$$|F'_1| = F'_{1y} \text{ (nonlinear state)}$$

$$\Delta F'_1 = 0.$$

Hence, from Eq. 2.22.1,

$$\Delta F' = \Delta F'_2$$

and with Eq. 2.25.1,

$$\Delta F' = k'_2 \cdot \Delta\delta'. \quad (2.27.1)$$

Also, in this state

$$\Delta F' = k''_2 \cdot \Delta x'$$

where k''_2 , as shown in

Fig. 2.8c, is given by

$$\frac{1}{k''_2} = \frac{1}{k'} + \frac{1}{k'_2}.$$

Springs-in-Parallel, cont.

is the yield level for the Coulomb slider:

$$|F_1| \leq F_{1y}.$$

Yield Criteria:

When

$$|F_1| < F_{1y} \text{ (linear state),}$$

$$\Delta\delta = 0.$$

Hence,

$$\Delta x_1 = \Delta x, \text{ and}$$

$$\Delta F = k \cdot \Delta x. \quad (2.26.2)$$

When

$$|F_1| = F_{1y} \text{ (nonlinear state)}$$

$$\Delta F_1 = 0.$$

Hence,

$$\Delta x_1 = 0$$

and

$$\Delta\delta = \Delta x.$$

From Eq. 2.22.2, with $\Delta F_1 = 0$,

$$\Delta F = \Delta F_2 \quad (2.27.2)$$

and

$$\Delta F = k_2 \Delta x,$$

i.e., any increase of the force above the yield level is done via spring k_2 only.

In order to make the bilinear spring systems appear the same to mass (m) in Fig. 2.6 and Fig. 2.7, let

$$x' = x \quad , \quad (\Delta x' = \Delta x) \quad ;$$

and

$$F' = F \quad ; \quad (\Delta F' = \Delta F) \quad .$$

Then, from Eq. 2.26.1 and Eq. 2.26.2 for the linear state, it is found that

$$k' = k$$

and, correspondingly, for the nonlinear state, it is found that

$$k_2'' = k_2 \quad .$$

Hence, by substitution, an equation for k_2' in terms of k and k_2 arises:

$$\frac{1}{k_2'} = \frac{1}{k_2} - \frac{1}{k} \quad .$$

This shows that it is possible to adjust the spring constants of these two simple yielding systems so that they appear the same from the outside in both states of yield. As will be seen in the next section, it is not possible to adjust the spring constants of the two models of nonlinear beams so that they appear the same in all states of yield.

2.5 Two Models of Nonlinear Beams

The two beam models presented in this section have nonlinear hysteretic bending moment-end rotation characteristics; consequently, they are more complicated than the simple yielding systems of the previous sections. It should be noted that the "one-component" beam model, Fig. 2.10, is an extension of the springs-in-series system,

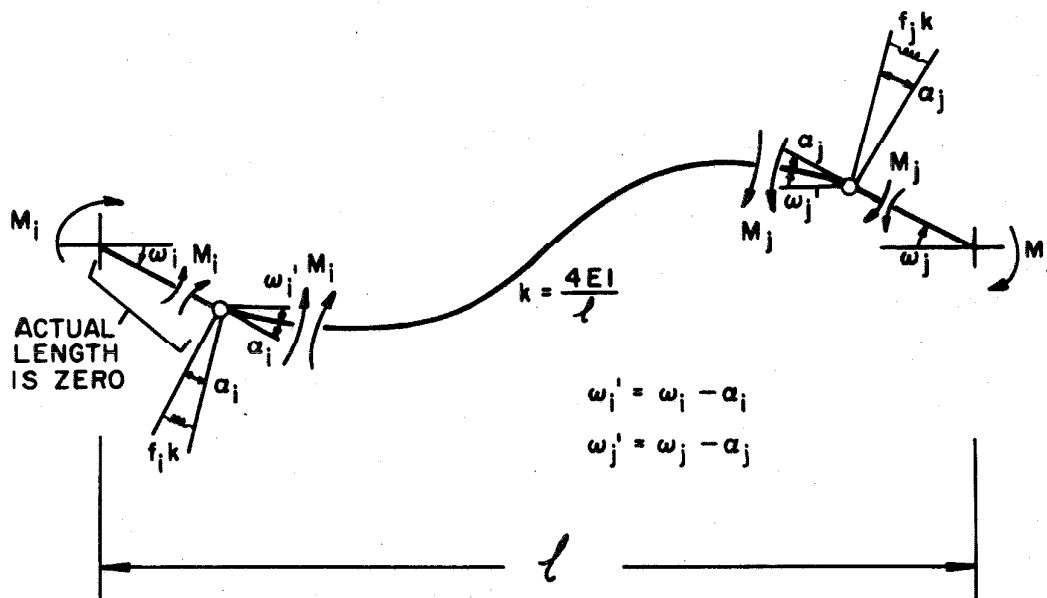


**Fig. 2.10 One-component Model
of a Nonlinear Beam**

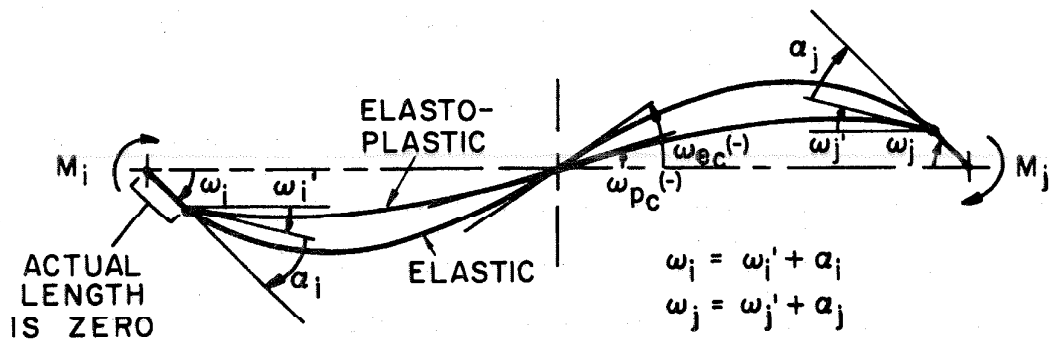


Fig. 2.11a Two-component Model of a Nonlinear Beam

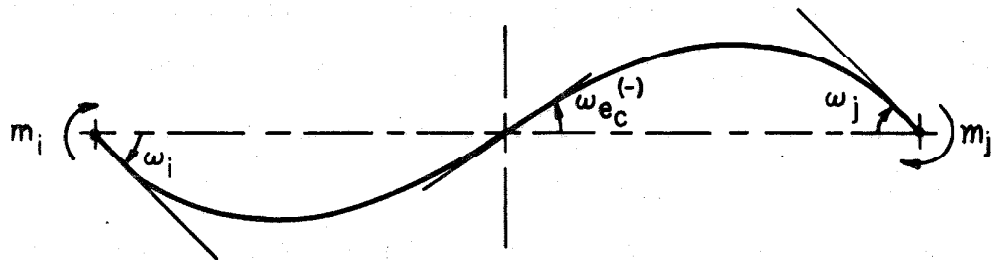


Fig. 2.11b The Linear Component

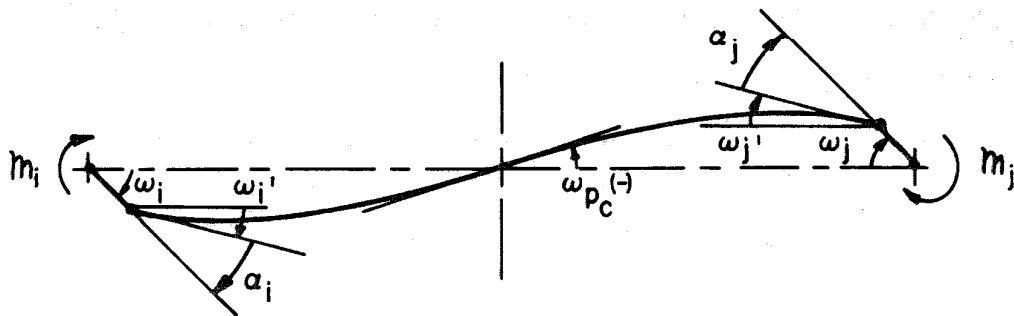


Fig. 2.11c The Ideally Elasto-plastic Component
(Note that the plastic angles α_i and α_j occur only in this component.)

Fig. 2.6 and the "two-component" beam model, Fig. 2.11, is an extension of the springs-in-parallel system, Fig. 2.7.

As seen in Fig. 2.10 and Fig. 2.11, the one-component beam is the more appealing model of a yielding column or girder from the physical point of view. Furthermore, nonlinear (bilinear and curvilinear) hysteresis loops can be used with the one-component beam, the only restriction being that the initial slopes of the hysteresis loops at both ends of the same beam must be equal. On the other hand, the two-component model can have only bilinear hysteresis loops at each end. Although the yield levels can differ, these loops must have identical initial and identical second slopes. For this model, the second slope of the loop is determined by the stiffness, p_k , of the linear component of the beam.

Nevertheless, the two-component beam has been used by other investigators* in the study of nonlinear tall structures with results that are very similar to those obtained using the corresponding one-component beam. Consequently, both of these beam models are studied in the following vis-à-vis presentation.

In the linear state both beam models have stiffness

$$k = \frac{4EI}{l}$$

where

E is Youngs modulus (lbs/in²),

*R. W. Clough and K. L. Benuska, FHA Study, reference 1.

I is the area moment of inertia (in^4), and

l is the length of the beam (in) .

The shear deflection in the beam is neglected.

Although the same symbols are used in the moment-rotation equations for both models, some of the definitions differ slightly, particularly for the plastic angles α . As seen in Figs. 2.10 and 2.11, the symbols have the following meanings:

| | |
|------------------------|--|
| M_i, M_j | bending moments at the ends (i) and (j) (same in both models), |
| m_i, m_j | bending moments at the ends of the linear component of the two-component model, |
| m_i, m_j | bending moments at the ends of the elasto-plastic component of the two-component model, |
| ω_i, ω_j | end rotations (same in both models), |
| ω_i', ω_j' | <div style="display: inline-block; vertical-align: middle; font-size: 3em; line-height: 1;">{</div> <div style="display: inline-block; vertical-align: middle;"> end rotations of central beam in one-component model, or end rotations of central beam of elasto-plastic component in two-component model, </div> |
| α_i, α_j | <div style="display: inline-block; vertical-align: middle; font-size: 3em; line-height: 1;">{</div> <div style="display: inline-block; vertical-align: middle;"> incurred plastic angle at the ends in the one-component model (note correspondence to δ' in Fig. 2.8c); or incurred plastic angle at the ends of the elasto-plastic component in the two-component model (note correspondence to δ in Fig. 2.9c). </div> |

One-component Model (Fig. 2.10)Stiffness distribution:

The central beam has stiffness k . The end beams have zero length and are dropped from further consideration.

Fundamental Bending Moment-End Rotation Equations:

Two-component Model (Fig. 2.11)Stiffness distribution:

The stiffness k of the total beam is apportioned to the two components as follows:

linear component:

$$k_{\text{linear}} = p \cdot k ;$$

elasto-plastic component:

$$k_{\text{elasto-plastic}} = q \cdot k ;$$

where

$$p + q = 1; \text{ (usually } p \approx 0.05).$$

Fundamental Bending Moment-End Rotation Equations:

linear component:

$$m_i = pk(\omega_i + \frac{1}{2}\omega_j)$$

$$m_j = pk(\frac{1}{2}\omega_i + \omega_j)$$

or, in incremental form,

$$\Delta m_i = pk(\Delta\omega_i + \frac{1}{2}\Delta\omega_j)$$

$$\Delta m_j = pk(\frac{1}{2}\Delta\omega_i + \Delta\omega_j)$$

elasto-plastic component:

$$m_i = qk(\omega_i' + \frac{1}{2}\omega_j')$$

$$m_j = qk(\frac{1}{2}\omega_i' + \omega_j')$$

where $q = 1 - p$.

From Fig. 2.11a,

$$\omega_i' = \omega_i - \alpha_i$$

One-component Model, cont.Central beam

$$M_i = k(\omega_i' + \frac{1}{2}\omega_j')$$

$$M_j = k(\frac{1}{2}\omega_i' + \omega_j')$$

From Fig. 2.10,

$$\omega_i' = \omega_i - \alpha_i$$

and

$$\omega_j' = \omega_j - \alpha_j$$

By substitution, the fundamental bending moment-end rotation equations for this beam model are obtained:

$$M_i = k[(\omega_i - \alpha_i) + \frac{1}{2}(\omega_j - \alpha_j)] \quad (2.28.1)$$

$$M_j = k[\frac{1}{2}(\omega_i - \alpha_i) + (\omega_j - \alpha_j)]$$

or, in incremental form:

$$\Delta M_i = k[(\Delta\omega_i - \Delta\alpha_i) + \frac{1}{2}(\Delta\omega_j - \Delta\alpha_j)] \quad (2.29.1)$$

$$\Delta M_j = k[\frac{1}{2}(\Delta\omega_i - \Delta\alpha_i) + (\Delta\omega_j - \Delta\alpha_j)]$$

Two-component Model, cont.

and

$$\omega_j' = \omega_j - \alpha_j$$

By substitution, then,

$$m_i = qk[(\omega_i - \alpha_i) + \frac{1}{2}(\omega_j - \alpha_j)]$$

$$m_j = qk[\frac{1}{2}(\omega_i - \alpha_i) + (\omega_j - \alpha_j)]$$

or, in incremental form:

$$\Delta m_i = qk[(\Delta\omega_i - \Delta\alpha_i) + \frac{1}{2}(\Delta\omega_j - \Delta\alpha_j)]$$

$$\Delta m_j = qk[\frac{1}{2}(\Delta\omega_i - \Delta\alpha_i) + (\Delta\omega_j - \Delta\alpha_j)]$$

For the total beam:

$$M_i = m_i + m_j$$

$$M_j = m_j + m_j$$

similarly in incremental form.

By addition, the fundamental bending moment-end rotation equations for this beam model are obtained:

$$M_i = k[(\omega_i - q\alpha_i) + \frac{1}{2}(\omega_j - q\alpha_j)] \quad (2.28.2)$$

$$M_j = k[\frac{1}{2}(\omega_i - q\alpha_i) + (\omega_j - q\alpha_j)]$$

or, in incremental form:

$$\Delta M_i = k[(\Delta\omega_i - q\Delta\alpha_i) + \frac{1}{2}(\Delta\omega_j - q\Delta\alpha_j)] \quad (2.29.2)$$

$$\Delta M_j = k[\frac{1}{2}(\Delta\omega_i - q\Delta\alpha_i) + (\Delta\omega_j - q\Delta\alpha_j)]$$

The purpose of writing these equations for both beam models in incremental form is that in this form it is possible to solve the equations of motion using finite integration techniques assuming that the state of yield remains constant throughout each time increment. As seen above, the incremental bending moments, ΔM , are related to both the incremental rotations, $\Delta \omega$, and incremental plastic angles, $\Delta \alpha$. Now, if the state of yield is known at the beginning of the time increment, it is possible to establish beforehand an equation of the form

$$\Delta \alpha = \Delta \alpha(\Delta \omega_i, \Delta \omega_j)$$

relating the incremental plastic angles to the end rotations. Using these equations it is possible to eliminate the incremental plastic angles from the incremental moment-rotation equations resulting in equations of the form:

$$\Delta M = \Delta M(\Delta \omega_i, \Delta \omega_j)$$

which are valid for each time increment.

The criteria for establishing the state of yield at the time t (at the beginning of a time increment) are based upon the bending moment at time t and the last incremental bending moment prior to time t . These criteria, which are the same for both beam models, are (see Fig. 2.12) the following:

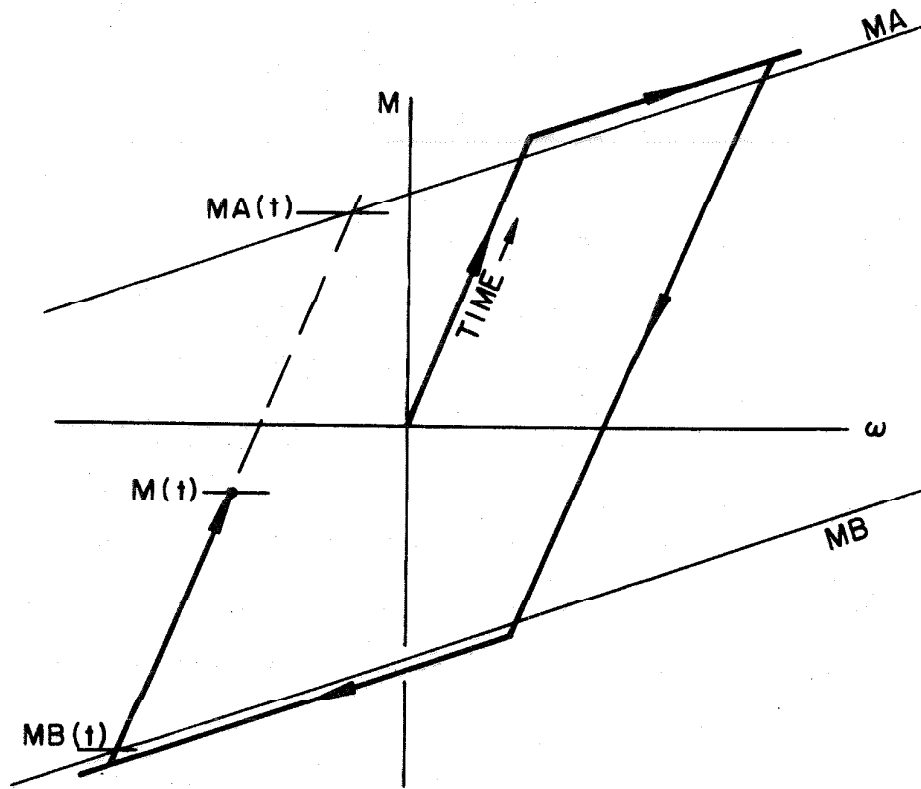


Fig. 2.12 Bilinear Hysteresis Loop Showing "Overshooting"
 Upon Entering the Nonlinear State of Yield and "Backtracking"
 Upon Returning to the Linear State

If $MB(t) < M(t) < MA(t)$, then the state of yield is linear;

if $\left\{ \begin{array}{l} M(t) \geq MA(t) \text{ and } \Delta M(t) > 0, \\ \text{or} \\ M(t) \leq MB(t) \text{ and } \Delta M(t) < 0 \end{array} \right\} \left\{ \begin{array}{l} \text{then the state of} \\ \text{yield is nonlinear;} \end{array} \right.$

where

$M(t)$: total bending moment at time t ,

$MA(t)$: upper yield bending moment at time t ,

$MB(t)$: lower yield bending moment at time t , and

$\Delta M(t)$: the last incremental bending moment prior to time t .

Inherent in this procedure is the phenomena of "overshooting" the yield limit upon entering the nonlinear state and "backtracking" upon returning to the linear state, as shown in Fig. 2.12. This results from the assumption that the state of yield remains constant throughout the time increment.

Although the yield criteria and the general form of the equations relating moments and plastic angles to rotations are the same for both beams, the actual equations for each beam are different as shown below.

One-component Model

When the state of yield is linear at end (i) and/or end (j), the corresponding incremental plastic angle must be zero:

at end (i), $\Delta\alpha_i = 0$;

and/or

Two-component Model

When the state of yield is linear at end (i) and/or end (j), the corresponding incremental plastic angle must be zero:

at end (i), $\Delta\alpha_i = 0$;

and/or

One-component Model, cont.

at end (j), $\Delta\alpha_j = 0$.

When the state of yield is non-linear at end (i) and/or end (j), the corresponding incremental bending moment is proportional to the incremental plastic angle:

$$\text{at end (i), } \Delta M_i = f_i k \Delta\alpha_i ;$$

and/or

$$\text{at end (j), } \Delta M_j = f_j k \Delta\alpha_j ;$$

where f_i and f_j are independent.

These equations are analogous to Eq. 2.27.1 of the springs-in-series system of the previous section.

Two-component Model, cont.

at end (j), $\Delta\alpha_j = 0$.

When the state of yield is non-linear at end (i) and/or end (j), the corresponding incremental total bending moment equals the incremental bending moment of the linear component, and the incremental bending moment in the elasto-plastic component is zero:

$$\text{at end (i), } \Delta M_i = \Delta m_i ,$$

$$\Delta m_i = 0 ;$$

and/or

$$\text{at end (j), } \Delta M_j = \Delta m_j ,$$

$$\Delta m_j = 0 .$$

These equations are analogous to Eq. 2.27.2 of the springs-in-parallel system in the previous section.

Since f_i and f_j are independent, it is possible to use a curvilinear hysteresis loop with the one-component model. The method of determining f_i and f_j is discussed in the next section. On the other hand, for the two-component model, Δm_i and Δm_j are dependent upon the same stiffness parameter (p). Consequently,

this model can have hysteresis loops at the ends with only the two slopes (k) and (pk) although the yield levels may be different.

Since there are two possible states of yield for each yield joint, there are four possible states of yield for a beam. These states, denoted by (a), (b), (c), and (d), are described below.

| <u>One-component Model</u> | <u>Two-component Model</u> |
|--|--|
| <u>State (a) - linear at (i) and (j):</u> | <u>State (a) - linear at (i) and (j):</u> |
| $\Delta\alpha_i = 0 ;$ | $\Delta\alpha_i = 0 ;$ |
| $\Delta\alpha_j = 0 .$ | $\Delta\alpha_j = 0 .$ |
| <u>State (b) - nonlinear at (i); linear at (j):</u> | <u>State (b) - nonlinear at (i); linear at (j):</u> |
| $\Delta M_i = f_i k \Delta\alpha_i ;$ | $\Delta M_i = \Delta m_i ; (\Delta\alpha_i \neq 0) ;$ |
| $\Delta\alpha_j = 0 .$ | $\Delta\alpha_j = 0 .$ |
| <u>State (c) - linear at (i); nonlinear at (j):</u> | <u>State (c) - linear at (i); nonlinear at (j):</u> |
| $\Delta\alpha_i = 0 ;$ | $\Delta\alpha_i = 0 ;$ |
| $\Delta M_j = f_j k \Delta\alpha_j .$ | $\Delta M_j = \Delta m_j ; (\Delta\alpha_j \neq 0) .$ |
| <u>State (d) - nonlinear at (i) and (j):</u> | <u>State (d) - nonlinear at (i) and (j):</u> |
| $\Delta M_i = f_i k \Delta\alpha_i ;$ | $\Delta M_i = \Delta m_i ; (\Delta\alpha_i \neq 0) ;$ |
| $\Delta M_j = f_j k \Delta\alpha_j .$ | $\Delta M_j = \Delta m_j ; (\Delta\alpha_j \neq 0) .$ |
| The functional dependencies of the incremental plastic angles upon rotations are as follows: | The functional dependencies of the incremental plastic angles upon rotations are as follows: |

One-component Model, cont.State (a) - linear at (i) and (j):

$$\Delta\alpha_i = 0 ;$$

$$\Delta\alpha_j = 0 .$$

State (b) - nonlinear at (i);
linear at (j):

from state (b) above and

Eq. 2.29.1,

$$k[(\Delta\omega_i - \Delta\alpha_i) + \frac{1}{2}\Delta\omega_j] = f_i k \Delta\alpha_i .$$

Hence,

$$\Delta\alpha_i = \left(\frac{1}{1 + f_i} \right) (\Delta\omega_i + \frac{1}{2}\Delta\omega_j) ;$$

$$\Delta\alpha_j = 0 .$$

State (c) - linear at (i) ;
nonlinear at (j) :

(similar to state (b); replace (i)

by (j)):

$$\Delta\alpha_i = 0 ;$$

$$\Delta\alpha_j = \left(\frac{1}{1 + f_j} \right) (\frac{1}{2}\Delta\omega_i + \Delta\omega_j)$$

State (d) - nonlinear at (i) and (j):

from state (d) above and

Eq. 2.29.1,

$$k[(\Delta\omega_i - \Delta\alpha_i) + \frac{1}{2}(\Delta\omega_j - \Delta\alpha_j)]$$

$$= f_i k \Delta\alpha_i$$

$$k[\frac{1}{2}(\Delta\omega_i - \Delta\alpha_i) + (\Delta\omega_j - \Delta\alpha_j)]$$

$$= f_j k \Delta\alpha_j$$

Two-component Model, cont.State (a) - linear at (i) and (j):

$$\Delta\alpha_i = 0 ;$$

$$\Delta\alpha_j = 0 .$$

State (b) - nonlinear at (i);
linear at (j):

from state (b) above and

Eq. 2.29.2

$$k[(\Delta\omega_i - q\Delta\alpha_i) + \frac{1}{2}\Delta\omega_j] = pk(\Delta\omega_i + \frac{1}{2}\Delta\omega_j) .$$

Hence,

$$\Delta\alpha_i = (\Delta\omega_i + \frac{1}{2}\Delta\omega_j) ;$$

$$\Delta\alpha_j = 0 .$$

State (c) - linear at (i) ;
nonlinear at (j):

(similar to state (b); replace (i)

by (j)):

$$\Delta\alpha_i = 0 ;$$

$$\Delta\alpha_j = (\frac{1}{2}\Delta\omega_i + \Delta\omega_j) .$$

State (d) - nonlinear at (i) and (j):

from state (d) above and

Eq. 2.29.2,

$$k[(\Delta\omega_i - q\Delta\alpha_i) + \frac{1}{2}(\Delta\omega_j - q\Delta\alpha_j)]$$

$$= pk(\Delta\omega_i + \frac{1}{2}\Delta\omega_j)$$

$$k[\frac{1}{2}(\Delta\omega_i - q\Delta\alpha_i) + (\Delta\omega_j - q\Delta\alpha_j)]$$

$$= pk(\frac{1}{2}\Delta\omega_i + \Delta\omega_j)$$

One-component Model, cont.

rearranging:

$$(1+f_i)\Delta\alpha_i + \frac{1}{2}\Delta\alpha_j = \Delta\omega_i + \frac{1}{2}\Delta\omega_j ;$$

$$\frac{1}{2}\Delta\alpha_i + (1+f_j)\Delta\alpha_j = \frac{1}{2}\Delta\omega_i + \Delta\omega_j .$$

Hence,

$$\Delta\alpha_i = \frac{\left(1 + \frac{4}{3}f_j\right)\Delta\omega_i + \frac{2}{3}f_j\Delta\omega_j}{1 + \frac{4}{3}(f_i + f_j + f_i \cdot f_j)} ;$$

$$\Delta\alpha_j = \frac{\frac{2}{3}f_i\Delta\omega_i + \left(1 + \frac{4}{3}f_i\right)\Delta\omega_j}{1 + \frac{4}{3}(f_i + f_j + f_i \cdot f_j)} .$$

By substitution, the $\Delta\alpha$'s can be eliminated from the incremental moment-rotation equations:

State (a) - linear at (i) and (j):

$$\Delta M_i = k(\Delta\omega_i + \frac{1}{2}\Delta\omega_j) ;$$

$$\Delta M_j = k(\frac{1}{2}\Delta\omega_i + \Delta\omega_j) .$$

State (b) - nonlinear at (i);
linear at (j):

$$\Delta M_i = \left(\frac{1}{1+f_i}\right)k(\Delta\omega_i + \frac{1}{2}\Delta\omega_j) ;$$

$$\Delta M_j = k\left[\frac{1}{2}\left(\frac{1}{1+f_i}\right)\Delta\omega_i + \left(\frac{3+4f_i}{4(1+f_i)}\right)\Delta\omega_j\right] .$$

Two-component Model, cont.

rearranging:

$$(\Delta\omega_i - \Delta\alpha_i) + \frac{1}{2}(\Delta\omega_j - \Delta\alpha_j) = 0 ;$$

$$\frac{1}{2}(\Delta\omega_i - \Delta\alpha_i) + (\Delta\omega_j - \Delta\alpha_j) = 0 .$$

Hence,

$$\Delta\alpha_i = \Delta\omega_i ;$$

$$\Delta\alpha_j = \Delta\omega_j .$$

By substitution, the $\Delta\alpha$'s can be eliminated from the incremental moment-rotation equations:

State (a) - linear at (i) and (j):

$$\Delta M_i = k(\Delta\omega_i + \frac{1}{2}\Delta\omega_j) ;$$

$$\Delta M_j = k(\frac{1}{2}\Delta\omega_i + \Delta\omega_j) .$$

State (b) - nonlinear at (i);
linear at (j):

$$\Delta M_i = pk(\Delta\omega_i + \frac{1}{2}\Delta\omega_j) ;$$

$$\Delta M_j = k\left[\frac{1}{2}p\Delta\omega_i + \left(1 - \frac{q}{4}\right)\Delta\omega_j\right] .$$

One-component Model, cont.

State (c) - linear at (i);
nonlinear at (j):

$$\Delta M_i = k \left[\left(\frac{3+4f_j}{4(1+f_j)} \right) \Delta \omega_i + \frac{1}{2} \left(\frac{f_j}{1+f_j} \right) \Delta \omega_j \right];$$

$$\Delta M_j = \left(\frac{f_j}{1+f_j} \right) k \left(\frac{1}{2} \Delta \omega_i + \Delta \omega_j \right) .$$

State (d) - nonlinear at (i) and (j):

$$\Delta M_i = \frac{f_i k \left[\left(1 + \frac{4}{3} f_j \right) \Delta \omega_i + \frac{2}{3} f_j \Delta \omega_j \right]}{1 + \frac{4}{3} (f_i + f_j + f_i \cdot f_j)} ;$$

$$\Delta M_j = \frac{f_j k \left[\frac{2}{3} f_i \Delta \omega_i + \left(1 + \frac{4}{3} f_i \right) \Delta \omega_j \right]}{1 + \frac{4}{3} (f_i + f_j + f_i \cdot f_j)} .$$

(2.30.1)

Two-component Model, cont.

State (c) - linear at (i);
nonlinear at (j):

$$\Delta M_i = k \left[\left(1 - \frac{q}{4} \right) \Delta \omega_i + \frac{1}{2} p \Delta \omega_j \right] ;$$

$$\Delta M_j = p k \left(\frac{1}{2} \Delta \omega_i + \Delta \omega_j \right) .$$

State (d) - nonlinear at (i) and (j):

$$\Delta M_i = p k (\Delta \omega_i + \frac{1}{2} \Delta \omega_j) ;$$

$$\Delta M_j = p k \left(\frac{1}{2} \Delta \omega_i + \Delta \omega_j \right) .$$

(2.30.2)

Since the incremental bending moment-end rotation equations have a regular pattern for all four states of yield, the following matrix equations using the "effective stiffness" parameters S_A , S_B and S_C can be established:

One-component Model

$$\begin{Bmatrix} \Delta M_i \\ \Delta M_j \end{Bmatrix} = \begin{bmatrix} S_A & S_B \\ S_B & S_C \end{bmatrix} \begin{Bmatrix} \Delta \omega_i \\ \Delta \omega_j \end{Bmatrix}$$

(2.31.1)

Two-component Model

$$\begin{Bmatrix} \Delta M_i \\ \Delta M_j \end{Bmatrix} = \begin{bmatrix} S_A & S_B \\ S_B & S_C \end{bmatrix} \begin{Bmatrix} \Delta \omega_i \\ \Delta \omega_j \end{Bmatrix}$$

(2.31.2)

One-component Model, cont.

where

| | s_A | s_B | s_C |
|-----------------------|------------------------------------|-------------------------------------|------------------------------------|
| state of yield: | | | |
| a | k | $\frac{1}{2}k$ | k |
| b | $\frac{f_i k}{(1+f_i)}$ | $\frac{1}{2} \frac{f_i k}{(1+f_i)}$ | $\frac{(3+4f_i)k}{4(1+f_i)}$ |
| c | $\frac{(3+4f_j)k}{4(1+f_j)}$ | $\frac{1}{2} \frac{f_j k}{(1+f_j)}$ | $\frac{f_j k}{(1+f_j)}$ |
| d | $\frac{f_i(1+\frac{4}{3}f_j)k}{D}$ | $\frac{2}{3} \frac{f_i f_j k}{D}$ | $\frac{f_j(1+\frac{4}{3}f_i)k}{D}$ |

where

$$D = 1 + \frac{4}{3}(f_i + f_j + f_i \cdot f_j)$$

Note that for bilinear hysteresis loops, which are of primary concern here, $f_i = f_j = f$. As a result, some of the effective stiffnesses can be simplified.

Two-component Model, cont.

where

| | s_A | s_B | s_C |
|-----------------------|--------------------|-----------------|--------------------|
| state of yield: | | | |
| a | k | $\frac{1}{2}k$ | k |
| b | pk | $\frac{1}{2}pk$ | $(1-\frac{q}{4})k$ |
| c | $(1-\frac{q}{4})k$ | $\frac{1}{2}pk$ | pk |
| d | pk | $\frac{1}{2}pk$ | pk |

In order to identically match the bilinear hysteretic response of the two beam models, an (f:p) relationship must be found which equates the corresponding incremental moment-rotation equations for each of the four states of yield. Although one (f:p) relationship forms a match between the two beam models for yield states (a), (b),

and (c), and another (f:p) relationship forms a match for yield states (a) and (d), it is not possible to find an (f:p) relationship which forms a match for all four states of yield.

However, in order to compare the response of a nonlinear tall structure using the one-component model to the response of the same nonlinear tall structure using the two-component model, it is necessary to choose the most representative (f:p) relationship. Since it is common in a tall structure for both ends of a girder to rotate symmetrically and to yield at the same time, the (f:p) relationship chosen is the one which matches the incremental moment-rotation equations for yield states (a) and (d). With

$$\Delta M_i = \Delta M_j = \Delta M$$

and

$$\Delta \omega_i = \Delta \omega_j = \Delta \omega ,$$

the following moment-rotation equations are obtained for yield state (d). For the one-component model, Eq. 2.30.1 yields

$$\Delta M = \frac{f}{(1 + \frac{2}{3} f)} k \Delta \omega ; \quad (2.32.1)$$

and for the two-component model, Eq. 2.30.2 yields

$$\Delta M = 1.5 p k \Delta \omega . \quad (2.32.2)$$

By equating the incremental bending moments and end rotations for the two models, the desired (f:p) relationship is found

$$f = \frac{1.5 p}{1 - p} \quad \text{or} \quad p = \frac{f}{1.5 + f} \quad .$$

For example, if $p = 0.050$, then $f = 0.079$.

2.6 Hysteresis Loops and Simple Yielding Systems for Nonlinear Beams

In order to draw an exact two-dimensional hysteresis loop for either end of a beam, it is necessary to have the same functional relationship between the bending moment and the curvature for all states of yield. Such a hysteresis loop, Fig. 2.13d, can be established for end (i) of the one-component model of Fig. 2.13a by defining the "simple yielding beam" shown in Fig. 2.13b having the following properties:

| | |
|---|---|
| M_i | the bending moment at end (i) of the one-component model, |
| α_i | the plastic angle at end (i) of the one-component model, |
| ω_{ii} | the rotation of the simple yielding beam having bending moment M_i and plastic angle α_i , |
| $\omega'_{ii} = \omega_{ii} - \alpha_i$ | an angle representing the curvature at end (i) of the central beam of the one-component model, and |
| $\omega_{ji} = \omega_i - \omega_{ii}$ | the angle representing the cross-effect of end (j) on end (i) where ω_i is the end rotation of the one-component beam. |

A similar "simple yielding beam" can be defined for end (j) of the one-component model having the above properties but with (j) and (i) interchanged. By using the simple yielding beam for end (i),

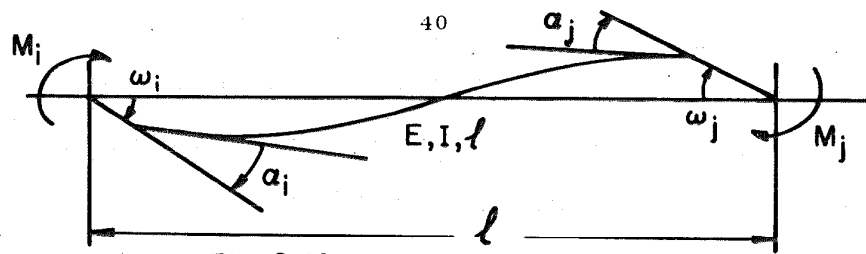


Fig. 2.13a One-component Model of a Nonlinear Beam

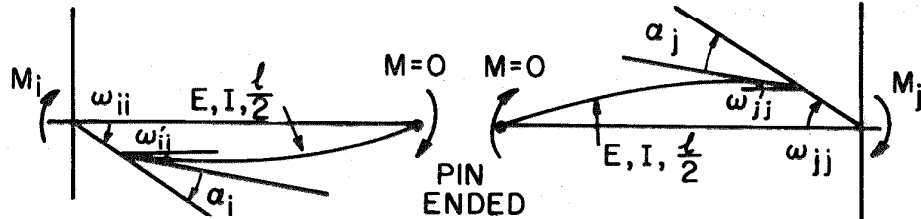


Fig. 2.13b Simple Yielding Beam for End (i)

Fig. 2.13c Simple Yielding Beam for End (j)

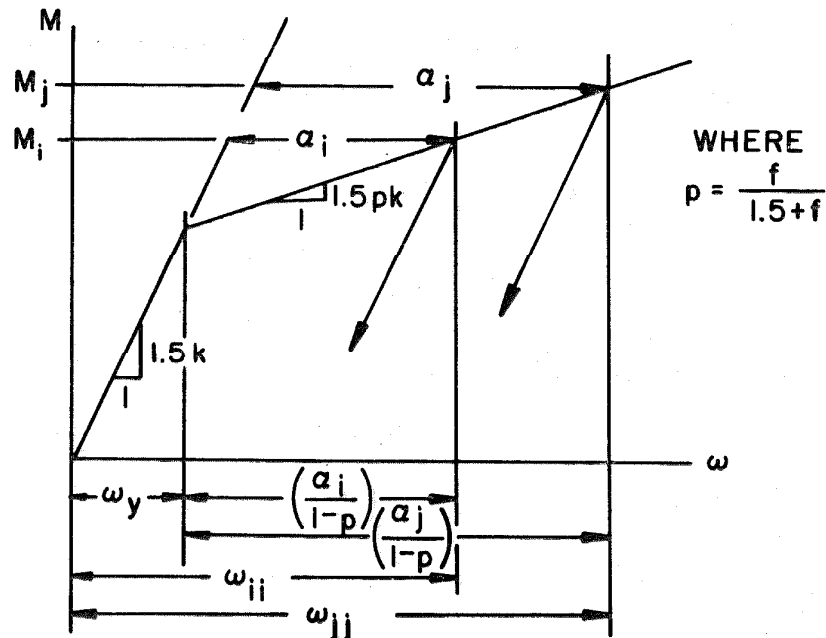


Fig. 2.13d Bilinear Hysteresis Loop for the Simple Yielding Beams for Ends (i) and (j) of the One-component Model of a Nonlinear Beam

the bending moment M_i can be directly related to ω'_{ii} (see Fig. 2.13b) which represents the curvature of the central beam at end (i) as shown below (similarly for end (j)).

The bending moment-end rotation equations for the simple yielding beams are:

$$\begin{aligned} \text{for end (i),} \quad M_i &= 1.5 k(\omega_{ii} - \alpha_i) ; \\ \text{for end (j),} \quad M_j &= 1.5 k(\omega_{jj} - \alpha_j) . \end{aligned} \tag{2.33}$$

Furthermore, in the nonlinear state of yield, the equations relating incremental bending moments to incremental plastic angles for the simple yielding beams are the same ones used at the ends of the one-component model:

$$\begin{aligned} \text{at end (i),} \quad \Delta M_i &= f_i k \Delta \alpha_i ; \\ \text{at end (j),} \quad \Delta M_j &= f_j k \Delta \alpha_j . \end{aligned} \tag{2.34}$$

By equating Eq. 2.33 to Eq. 2.28.1, the general moment rotation equations for M_i and M_j , the following equations for the simple yielding beams are obtained:

$$\begin{aligned} 1.5k(\omega_{ii} - \alpha_i) &= k[(\omega_i - \alpha_i) + \frac{1}{2}(\omega_j - \alpha_j)] ; \\ 1.5k(\omega_{jj} - \alpha_j) &= k[\frac{1}{2}(\omega_i - \alpha_i) + (\omega_j - \alpha_j)] . \end{aligned} \tag{2.35}$$

Hence, equations for ω_{ii} and ω_{jj} are found:

$$\omega_{ii} = \frac{2}{3} \left[\omega_i + \frac{1}{2}\alpha_i + \frac{1}{2}(\omega_j - \alpha_j) \right] ; \quad (2.36)$$

$$\omega_{jj} = \frac{2}{3} \left[\frac{1}{2}(\omega_i - \alpha_i) + \omega_j + \frac{1}{2}\alpha_j \right] .$$

Since

$$\omega_i = \omega_{ii} + \omega_{ji}$$

and

$$\omega_j = \omega_{jj} + \omega_{ij} ,$$

an equation relating the cross-effect angles is obtained:

$$0 = \omega_{ij} + \omega_{ji} ,$$

or

$$\omega_{ij} = - \omega_{ji} . \quad (2.37)$$

This means that the effect of the rotation at end (i) on end (j) is just the negative of the effect of the rotation at end (j) on end (i). Since a definite relationship exists between the bending moment M_i and the angle ω_{ii} and between M_j and ω_{jj} for all states of yield, it is possible to draw a meaningful bilinear hysteresis loop with the abscissa labeled ω_{ii} and ω_{jj} as is done in Fig. 2.13d for both ends of the one-component model of a nonlinear beam. In this case (see Section 2.4),

$$f_i = f_j = f \quad \text{and} \quad p = \frac{f}{1.5 + f} .$$

The above derivation of the equations for ω_{ii} , ω_{jj} , and ω_{ij} (ω_{ji}) are also valid for a curvilinear hysteresis loop such as the one

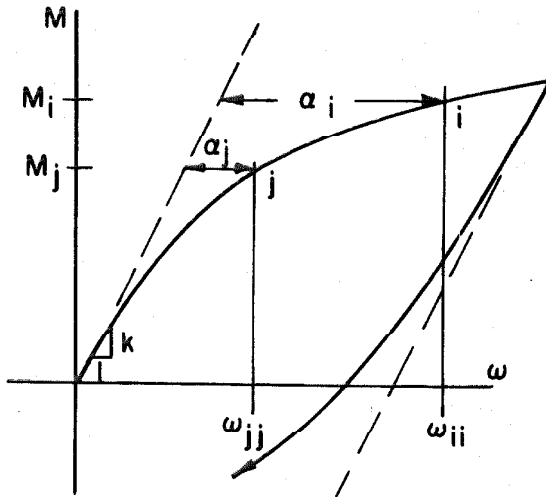


Fig. 2.14a Curvilinear Moment-Rotation Hysteresis Loop of the Simple Yielding Systems for Ends (i) and (j)

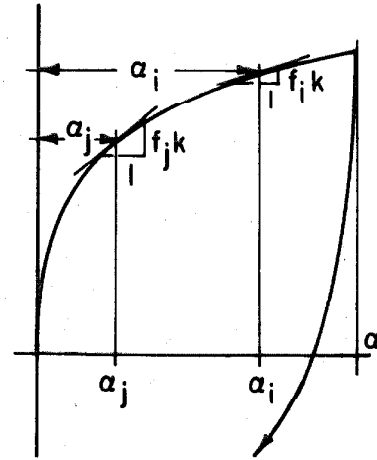


Fig. 2.14b Associated Moment-Plastic Angle Hysteresis Loop of the Simple Yielding Systems for Ends (i) and (j)

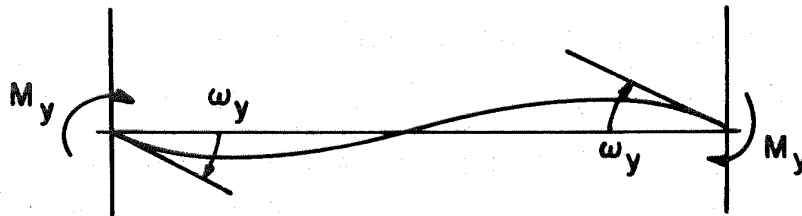


Fig. 2.15 Configuration of Beam at Point of Incipient Yielding

shown in Fig. 2.14a. Such freedom of choice of the hysteresis loop makes the one-component model quite versatile. The points (i) and (j) on the hysteresis loop in Fig. 2.14a represent the moments, rotations, and plastic angles of the ends of a one-component beam at a particular point in time. The values of f_i and f_j to be used in the next time increment are found from the slopes at the corresponding points (i) and (j) on the associated $M - \alpha$ hysteresis loop of Fig. 2.14b.

In the two-component model, the total bending moment at an end is dependent upon the curvatures of both components of the beam at that end. Since these two curvatures have different functional dependencies on the end rotations and plastic angles, when a beam encounters multiple states of yield (at different times), it becomes impossible to draw a two-dimensional hysteresis loop for the two-component model such as was done above for the one-component model.

2.7 Ductility Factors for Nonlinear Beams

In the previous section (Section 2.6) it was shown that by using the concept of simple yielding beams, bilinear and curvilinear hysteresis loops with precise meanings could be found for each end of a one-component model of a nonlinear beam. Consequently, the three ductility factors for simple yielding systems given in Section 2.3 can be directly applied to either end of a one-component beam. Even though an exact hysteresis loop cannot be found for the two-component

beam, two ductility factors can be defined for the two-component model which approximate the corresponding definitions for the one-component model.

It should be recalled that the definition of the plastic angle (α) for the two-component model is different from the definition of (α) for the one-component model. Since no definite hysteresis loop can be drawn for the two-component model which is valid for all states of yield, one can only obtain an approximate relationship between the incurred plastic angles, α , of the two systems. Since the beam usually yields approximately symmetrically, one can approximately relate the α 's of the two systems by

$$\alpha_{\text{one-component}} \doteq (1-p)\alpha_{\text{two-component}} \quad (2.38)$$

The incipient yield angle ω_y appears in the definitions which are used for bilinear hysteretic systems. Knowing the yield moment M_y , ω_y is found from either a simple yielding beam or from the entire beam rotating symmetrically as shown in Fig. 2.15. In either case, the equation relating M_y to ω_y is

$$M_y = \frac{6EI}{l} \omega_y$$

One-component Model

The first definition of ductility factor measures the maximum absolute value of the end rotation of the simple yielding beam with respect to the incipient yield angle (for end (i)):

$$\mu_{1i} = \frac{|\omega_{ii}|_{\max}}{\omega_y}, \quad (2.39.1)$$

but since

$$\omega_{ii} = \omega_y + \left(\frac{\alpha_i}{1-p} \right), \quad (2.40.1)$$

where

$$p = \frac{f}{1.5 + f},$$

Eq. 2.39.1 becomes

$$\mu_{1i} = 1 + \frac{\left| \frac{\alpha_i}{(1-p)} \right|_{\max}}{\omega_y}. \quad (2.41.1)$$

The second definition measures the maximum absolute value of the nonlinear angle, which is the plastic angle (α) for this model, with respect to the incipient yield

Two-component Model

The first definition measures the maximum absolute value of the end rotation of the elasto-plastic component (or of the total beam) with respect to the incipient yield angle of the total beam (for end (i)):

$$\mu_{1i} = \frac{|\omega_i|_{\max}}{\omega_y}, \quad (2.39.2)$$

but since

$$\omega_i = \omega_y + \alpha_i, \quad (2.40.2)$$

Eq. 2.39.2 becomes*

$$\mu_{1i} = 1 + \frac{|\alpha_i|_{\max}}{\omega_y}. \quad (2.41.2)$$

Using Eq. 2.38, it is seen that

Eq. 2.41.1 and Eq. 2.41.2 are approximately equal.

The second definition measures the maximum absolute value of the (approximate) nonlinear angle, which is

$$(1 - p) \cdot \alpha,$$

*This is the definition of ductility factor (or ductility requirement) used in the FHA Study, reference 1.

One-component Model, cont.

angle (for end (i)):

$$\mu_{2i} = 1 + \frac{|\alpha_i|_{\max}}{\omega_y} \quad (2.42.1)$$

The third definition measures the maximum absolute value of the total end rotation of the simple yielding beam with respect to the linear end rotation (for end (i)):

$$\mu_{3i} = \left| \frac{\omega_{ii}}{\omega_{ii} - \alpha_i} \right|_{\max} \quad (2.43.1)$$

The form of Eq. 2.43.1 is useful for curvilinear hysteresis loops; however, for bilinear hysteresis loops, Eq. 2.40.1 can be used to eliminate ω_{ii} . The resulting equation is (for end (i)):

$$\mu_{3i} = 1 + \left| \frac{\alpha_i}{\omega_y + \frac{p\alpha_i}{(1-p)}} \right|_{\max} \quad (2.44.1)$$

Eq. 2.44.1 is the one used in the

Two-component Model, cont.

where (α) is the plastic angle for this model, with respect to the incipient yield angle (for end (i)):

$$\mu_{2i} = 1 + \frac{(1-p)|\alpha_i|_{\max}}{\omega_y} \quad (2.42.2)$$

Using Eq. 2.38, it is seen that Eq. 2.42.1 and Eq. 2.42.2 are approximately equal.

The third definition of ductility factor is not written for the two-component model since it is impossible to use this model for curvilinear hysteresis loops.

One-component Model, cont.

computer studies for finding the ductility factors of one-component beams. The primary reason for using this definition is that it can be used for curvilinear hysteresis loops as well.

Two-component Model, cont.

In this chapter two models of a nonlinear beam were discussed and compared. It was seen that the one-component model was more realistic from the physical point of view. Furthermore, the one-component model was shown to be more versatile since it could treat curvilinear hysteresis loops whereas the two-component model was restricted to bilinear hysteresis loops. Consequently, the one-component model is considered to be the better model of a nonlinear beam and is therefore used in the computer studies of nonlinear tall structures for this report.

In the next chapter the equations of motion of a nonlinear tall structure are derived wherein either of these beam models can be used to represent the girders and columns of the structure.

CHAPTER III

EQUATIONS OF MOTION FOR NONLINEAR TALL STRUCTURES

3.1 Introduction

The purposes of this chapter are to describe the properties of a class of nonlinear tall structures, to present the damping mechanisms appropriate to such structures, to derive the equations of motion, to discuss the integration techniques, and to show how the equations of motion are solved with the aid of a digital computer.

3.2 A Class of Nonlinear Tall Structures

The class of nonlinear structures considered in this report is intended to be representative of modern high-rise buildings with glass and other lightweight walls such as are being built today (1967). This class of structures is characterized by the following assumed properties.

1. The foundation is infinitely rigid.
2. The structure is symmetric in plan view; hence, torsional deformation is neglected.
3. The girders provide all of the stiffness to the floors and they are flexible (not infinitely rigid).
4. The columns provide all of the stiffness to the walls.
5. There are no shear walls; hence, the structures are of the moment-resisting type. This means that the structures resist deformation only by the moments developed at the

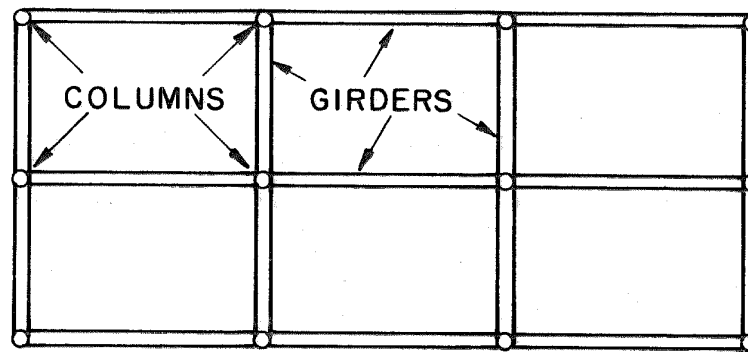


Fig. 3.1a Plan View of a Moment-resisting Frame

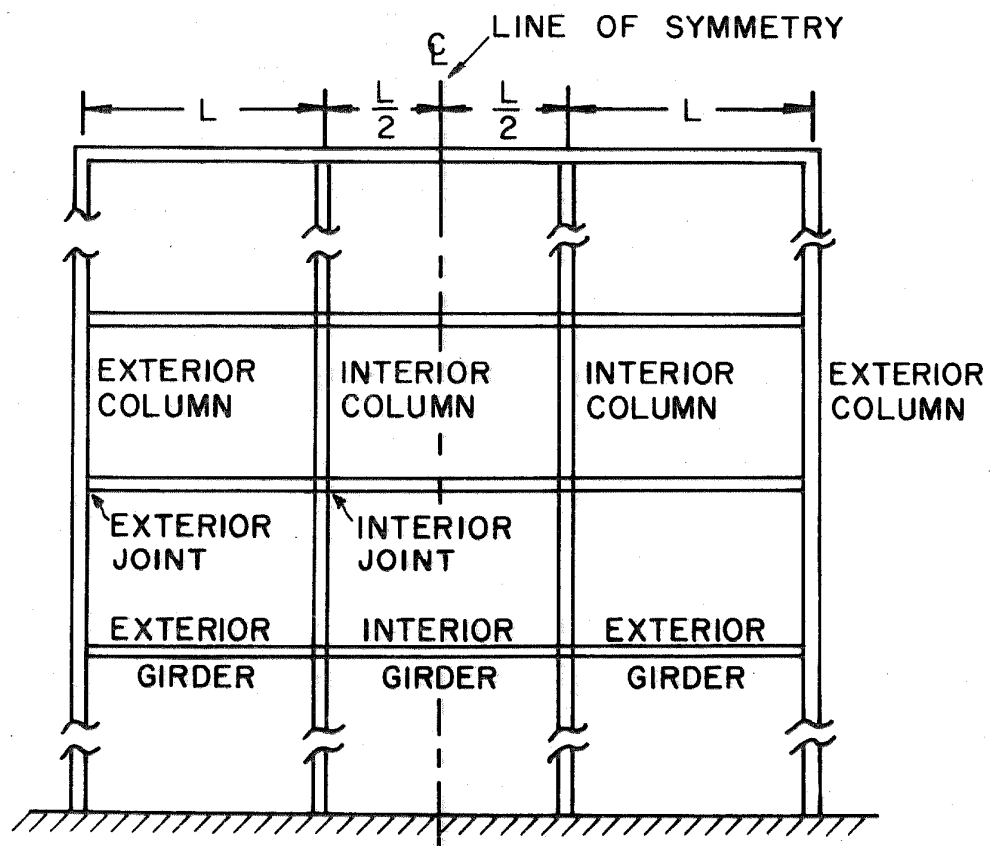


Fig. 3.1b Side View of a Moment-resisting Frame

ends of the girders and columns.

6. Shear deflection in the girders and columns is neglected.
7. As modeled in Chapter II, the girders and columns can yield at each end according to a bilinear bending moment-end rotation hysteresis loop.
8. There is no extension (or contraction) between any joints within the same floor.
9. There is no extension (or contraction) between floors since it is assumed that the structures are infinitely rigid in the vertical direction.
10. All mass is concentrated at the floor levels.
11. The mass of each floor moves only horizontally. Vertical motion is not considered because of property (9). Although the joints rotate, the rotational inertia associated with each joint is neglected.
12. Gravitational effects are negligible for the base overturning moment.

The particular computer program developed in this study can analyze only one (two-dimensional) structural frame at a time. In addition to the properties listed above, the structural frame must also have the following:

- A. It must have three bays (four columns) and be symmetric with respect to the centerline as shown in Fig. 3.1b.
- B. The structural properties of the frame are representative of the three-dimensional structure being considered.

Such a three-dimensional structure is shown in Fig. 3.1a.

- C. The columns are uniformly spaced L inches apart.
- D. There are twenty floors above ground level. With minor alteration, however, the computer program can handle an arbitrary number of floors.

Several properties of the frame are optional:

- E. The mass of each floor;
- F. The distance between any two adjacent floors;
- G. The stiffness properties of the girders and columns in the linear state of yield;
- H. The ratio of the second slope to the first slope of the bilinear hysteresis loops (see Chapter II); and
- I. The yield moments in the hysteresis loops.

Since the frame is subjected to an earthquake accelerogram in the computer program, it is of interest to note the properties of the accelerograms which can be used:

- J. The time history must be digitized.
- K. The time increments can be either uniform or nonuniform.
- L. A multiplicative amplitude scale factor can be used.

One frame having the above structural properties is extensively studied in this report. This is the A/20/2.2/2/6 frame which was designed by R.W. Clough and K. L. Benuska and was used in their studies for the Federal Housing Administration.* An advantage of using this particular frame is that a basis for comparison exists for

* See Section 2.2 of the FHA Study, reference 1.

verifying that the computer program for analyzing nonlinear frames written for this report operates properly (see Section 4.5). Independent studies using this program with various modifications can then be made with confidence in the results.

This frame was designed by means of static analysis using a digital computer. The design moments and design forces in the frame were found in a conventional manner by taking into consideration static gravity loads plus lateral loads as specified by the Uniform Building Code (of 1965). The design of the girders and columns is such that after the static gravity loads (but not the lateral loads) are applied, the positive and the negative yield bending moment for each hysteresis loop have the same absolute value, M_y , as shown in Fig. 2.12.

The identifying numbers of this frame have the following significance:

- A: structural properties are tapered;
- 20: number of floors above ground level;
- 2.2: (approximate) period of the fundamental mode;
- 2: ratio of the yield moments to the corresponding design moments in the girders; and
- 6: ratio of the yield moments to the corresponding design moments in the columns.

For completeness, the structural properties of this frame are given in Fig. 3.2. The stiffness and strength properties of structures are often unrelated and this is reflected in this frame.

A section of a frame having the properties listed above is

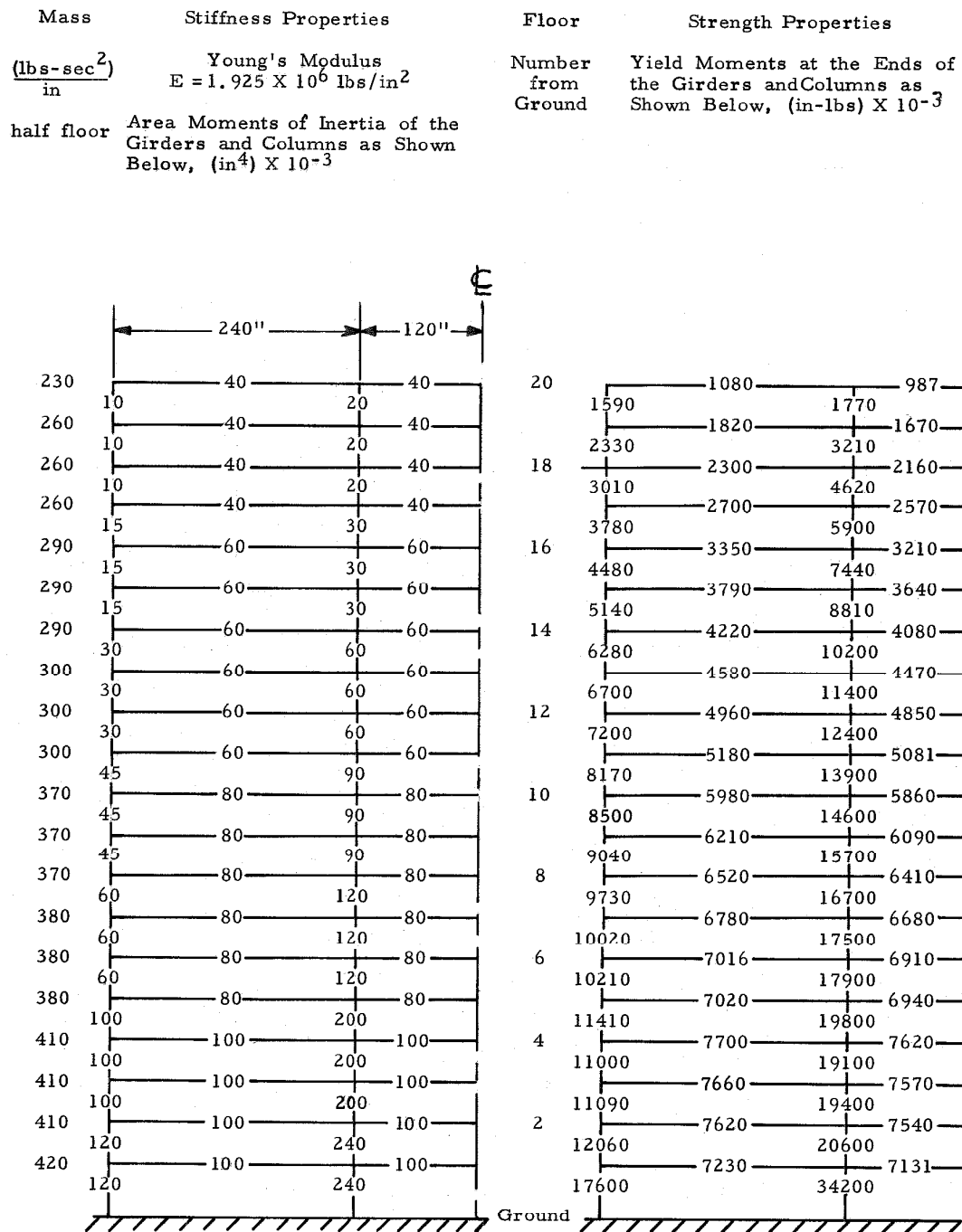


Fig. 3.2. Structural Properties of the A/20/2.2/2/6 Frame. Only Half of the Frame is Shown Since it is Symmetric With Respect to the Centerline (see Fig. 3.1b). The Height Between Floors is 144 Inches Except Between Ground and the First Floor Which is 180 Inches.

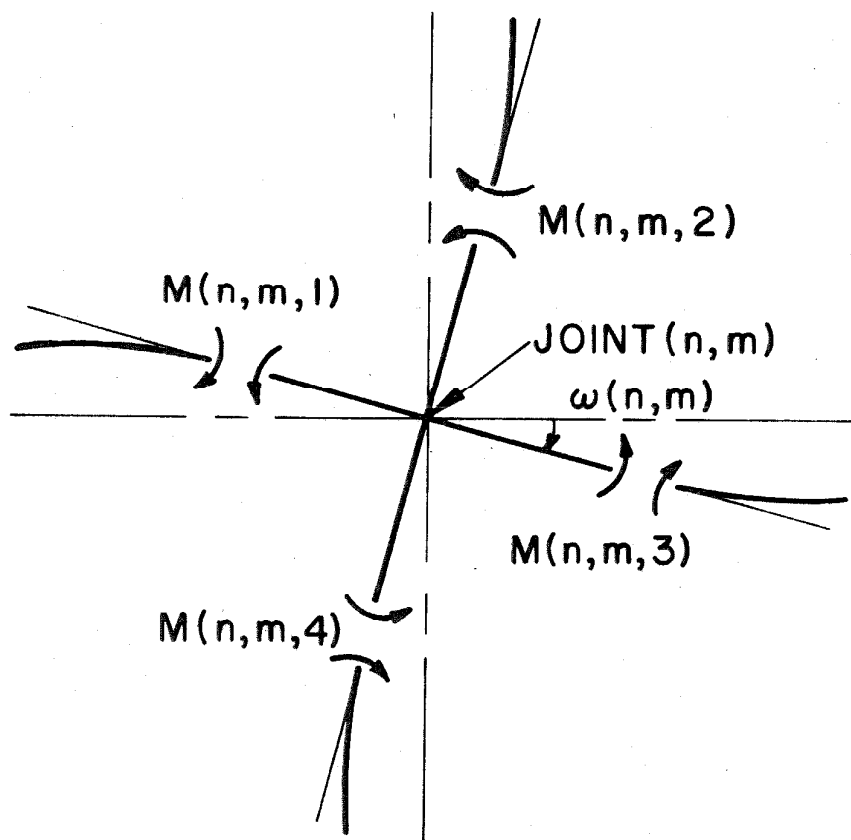


Fig. 3.4 Bending Moments $M(n, m, j)$
at Joint (n, m)

shown in a deformed position in Fig. 3.3 and a typical joint is shown in a rotated position in Fig. 3.4. The coordinates, moments and forces used in this chapter are depicted in Figs. 3.3 and 3.4 in the positive direction unless labeled to the contrary. These coordinates, etc., are defined below.*

| | |
|--|--|
| n | : index, the floor number starting from the roof; |
| m | : index, the column line starting from the left; |
| j ($j = 1, 2, 3, 4$) | : index, the number of the intersecting beam (column or girder); |
| joint (n, m) | : the joint formed by the intersection of girder (n) and column (m); |
| $\omega(n, m)$ | : the angular rotation of joint (n, m); |
| $\alpha(n, m, j)$ | : the plastic angle of the j^{th} beam at joint (n, m) (see Section 2.5); |
| $M(n, m, j)$ | : the (total) bending moment of the j^{th} beam at joint (n, m); |
| $V(n, m)$ | : the shear force in column $C(n, m)$; |
| $HT(n, m)$ | : the height between floor number (n) and ($n+1$) (numbered from roof); |
| $U(n)$ | : the horizontal displacement of floor (n); and |
| $UUH(n) = \frac{U(n) - U(n+1)}{HT(n)}$ | : the interfloor shear angle between floors (n) and ($n+1$). |

Usually floors are numbered from the ground up as shown in Fig. 3.2. However, this method of numbering is not convenient for the computer program since the natural sequence of most operations is from the roof down. Consequently, in the derivation of the

*Some of these coordinates, etc., are labeled in "Fortran notation," e.g., $UUH(n)$: the interfloor shear angle, since this type of notation is used in the resulting computer program (see Appendix E).

equations of motion, the floors are numbered from the roof down, as shown in Fig. 3.3.

3.3 Damping

Because of the difficulty of determining the damping mechanisms in structures, conventional approximations are made. Two approximate damping mechanisms which can be adapted to the equations of motion are described below.

1. As a structure vibrates during an earthquake, energy is dissipated aerodynamically. This dissipation is approximately proportional to the product of the area of the face of the structure perpendicular to the motion and the absolute (or total) velocity of the face. However, for the studies performed here, a pseudo-aerodynamic energy dissipation is assumed which uses the velocity relative to ground. Assuming that the area of the face at a given floor level is proportional to the mass of the associated floor, "mass proportional" viscous damping is obtained. The expression for this type of damping, for an N-floor structure is:

$$\alpha M \dot{\underline{U}} \quad (3.1)$$

where

α : scalar constant,

M : mass matrix ($N \times N$), and

$\dot{\underline{U}}$: vector ($N \times 1$) of the velocities of the floors relative to the ground.

2. When a structure vibrates in an earthquake, the interfloor displacements are large enough to cause the walls and partitions to crack and to rub together, thus dissipating energy. This type of damping in a structure is proportional to the relative interfloor velocity, and a convenient approximation is the expression

$$\beta K \dot{\underline{U}} \quad (3.2)$$

where

β : a scalar constant,

K : a stiffness matrix ($N \times N$), and

$\dot{\underline{U}}$: vector ($N \times 1$) of the velocities of the floors relative to ground.

The form of the stiffness matrix which can be used in Expression 3.2 depends to some degree upon the method of solving the equations of motion. Since the equations of motion are nonlinear, they are solved by means of an incremental integration approach (see Sections 3.4 and 3.5). In this case, if K is a tridiagonal stiffness matrix such as the one for a structure with rigid girders*, Expression 3.2 can be readily adapted to the equations of motion. This type of damping is often referred to as "stiffness proportional" viscous damping.

These two damping mechanisms together comprise "Rayleigh damping" for the structure with rigid girders.

*The ($N \times N$) stiffness matrix for an N -floor structure with flexible girders is, in general, full.

Assume for the moment that the structure with flexible girders remains linear (does not yield) and that the damping matrix, C , is given by

$$C = \alpha M + \beta K' \quad (3.3)$$

where

α, β : scalar constants;

M : diagonal mass matrix ($N \times N$); and

K' : stiffness matrix ($N \times N$) for the structure with flexible girders.

The resulting linear homogeneous matrix equation of motion is

$$M\ddot{\underline{U}} + (\alpha M + \beta K')\dot{\underline{U}} + K'\underline{U} = 0 \quad (3.4)$$

where

\underline{U} is the displacement vector ($N \times 1$).

In this case, classical normal modes can be found.⁽⁴⁴⁾ Hence, for mass proportional damping ($\beta = 0$) only, it can be shown that the fraction of critical damping in the n^{th} mode is

$$\xi_n^m = \frac{\alpha}{2\omega_n} , \quad n = 1, 2, \dots, N ,$$

where ω_n is the natural frequency (circular); therefore,

$$\xi_1^m > \xi_2^m > \xi_3^m > \dots > \xi_N^m . \quad (\text{See footnote, page 61.})$$

Furthermore, for stiffness proportional damping ($\alpha = 0$) only, it can be shown that

$$\xi_n^s = \frac{\beta \omega_n}{2}, \quad n = 1, 2, \dots, N;$$

therefore,

$$\xi_1^s < \xi_2^s < \xi_3^s < \dots < \xi_N^s. \quad *$$

When written in the form of the incremental equations of motion for structures with flexible girders, the Rayleigh damping described above in Expressions 3.1 and 3.2 appears as

$$\Delta \underline{D} = [\alpha M + \beta K] \Delta \underline{\dot{U}} \quad (3.5)$$

where

$\Delta \underline{D}$: incremental damping force vector ($N \times 1$) ;

α, β : scalar constants;

M : diagonal mass matrix ($N \times N$) ;

K : tridiagonal stiffness matrix ($N \times N$) for the structure with rigid girders; and

$\Delta \underline{\dot{U}}$: vector ($N \times 1$) of the velocities of the floors relative to ground.

*For the A/20/2.2/2/6 structure described in the previous section (Section 3.2),

$$\omega_n = 2.84, 6.91, 11.5, 16.0, 20.9, \dots$$

Hence, for mass proportional damping, with 0.10 fraction of critical damping in the fundamental mode,

$$\xi_n^m = 0.10, 0.041, 0.025, 0.018, 0.014, \dots,$$

and for stiffness proportional damping with 0.10 fraction of critical damping in the fundamental mode,

$$\xi_n^s = 0.10, 0.24, 0.40, 0.56, 0.74, \dots$$

In the next section it will be seen how Eq. 3.5 is incorporated into the equations of motion for this class of structures.

3.4 Equations of Motion

In this section the equations of motion are derived for the structural frame described in Section 3.2 having the damping mechanisms of Section 3.3. Two general equations are derived. One of these is for the angular rotation of the joints and the other governs the horizontal motion of the floors. The equation for the rotation of the joints is derived from a balance of bending moments at the ends of the girders and columns at a typical joint and the equation of motion for the floors is derived from a balance of forces on a typical floor. Since the frame is symmetric, as shown in Fig. 3.1b or in Fig. 3.5, these equations of motion are written for only one-half of the frame (the left half) taking symmetry into consideration.

Both of these equations use incremental bending moment-end rotation equations for the girders and columns in the frame. In Chapter II, the moment-rotation equations, Eq. 2.29.1 and Eq. 2.29.2, are developed for beams without making a distinction between columns and girders. However, for the present purpose, a distinction must be made since the interfloor shear angle appears in the moment-rotation equations for the columns but does not appear in the equations for the girders. Using the one-component beam model, the incremental moment-rotation equations for the girders and columns which intersect to form joint (n,m) (see Fig. 3.4) are given in Eq. 3.6. Similar equations can be written for the two-

component beam model.

$$\begin{aligned}
 \Delta M(n, m, 1) &= k_G(n, m-1) \left\{ [\Delta \omega(n, m) - \Delta \alpha(n, m, 1)] \right. \\
 &\quad \left. + \frac{1}{2} [\Delta \omega(n, m-1) - \Delta \alpha(n, m-1, 3)] \right\} ; \\
 \Delta M(n, m, 2) &= k_C(n-1, m) \left\{ [\Delta \omega(n, m) - \Delta UUH(n-1) - \Delta \alpha(n, m, 2)] \right. \\
 &\quad \left. + \frac{1}{2} [\Delta \omega(n-1, m) - \Delta UUH(n-1) - \Delta \alpha(n-1, m, 4)] \right\} ; \\
 \Delta M(n, m, 3) &= k_G(n, m) \left\{ [\Delta \omega(n, m) - \Delta \alpha(n, m, 3)] \right. \\
 &\quad \left. + \frac{1}{2} [\Delta \omega(n, m+1) - \Delta \alpha(n, m+1, 1)] \right\} ; \\
 \Delta M(n, m, 4) &= k_C(n, m) \left\{ [\Delta \omega(n, m) - \Delta UUH(n) - \Delta \alpha(n, m, 4)] \right. \\
 &\quad \left. + \frac{1}{2} [\Delta \omega(n+1, m) - \Delta UUH(n) - \Delta \alpha(n+1, m, 2)] \right\} ;
 \end{aligned} \tag{3.6}$$

where

$k_G(n, m)$: stiffness of girder $G(n, m)^*$ in the linear state of yield^{**} ;

$k_C(n, m)$: stiffness of column $C(n, m)$ in the linear state of yield.

Just as the $\Delta \alpha$'s were eliminated from the incremental bending moment-end rotation equations in Chapter II, the $\Delta \alpha$'s can be eliminated from Eq. 3.6. Consequently, equations analogous to

*See Section 3.2 for nomenclature of $G(n, m)$; $C(n, m)$.

**See Section 2.5 for nomenclature of "linear state of yield."

Eq. 2.31.1 relating the incremental bending moments to end rotations via effective stiffness parameters can be written

for the girders:

$$\begin{Bmatrix} \Delta M(n, m, 3) \\ \Delta M(n, m+1, 1) \end{Bmatrix} = \begin{bmatrix} SGA(n, m) & SGB(n, m) \\ SGB(n, m) & SGC(n, m) \end{bmatrix} \begin{Bmatrix} \Delta \omega(n, m) \\ \Delta \omega(n, m+1) \end{Bmatrix} ; \quad (3.7)$$

for the columns:

$$\begin{Bmatrix} \Delta M(n, m, 4) \\ \Delta M(n+1, m, 2) \end{Bmatrix} = \begin{bmatrix} SCA(n, m) & SCB(n, m) \\ SCB(n, m) & SCC(n, m) \end{bmatrix} \begin{Bmatrix} \Delta \omega(n, m) - \Delta UUH(n) \\ \Delta \omega(n+1, m) - \Delta UUH(n) \end{Bmatrix} . \quad (3.8)$$

In Eq. 3.7, $SGA(n, m)$ is the Fortran name for the effective stiffness parameter which corresponds to S_A in Eq. 2.31.1 (or Eq. 2.31.2) for the girder $G(n, m)$ having stiffness $k_G(n, m)$ in the linear state of yield. A similar correspondence applies for the other effective stiffnesses of the girders and columns.

One of the properties of the class of nonlinear structures considered is that the rotational inertia associated with each joint is neglected (see Section 3.2). Hence, the sum of the bending moments at the ends of the girders and columns at each joint is zero (see Fig. 3.4):

$$\sum_{j=1}^4 \Delta M(n, m, j) = 0 . \quad (3.9)$$

By substituting Eq. 3.7 and Eq. 3.8 with appropriate indices, n , m , and j , into Eq. 3.9, the general equation for the incremental rotation

of joint (n,m) is found:

$$\Delta\omega(n,m) = - \frac{\begin{bmatrix} + SGB(n,m-1) \cdot \Delta\omega(n,m-1) + SGB(n,m) \cdot \Delta\omega(n,m+1) \\ + SCB(n-1,m) \cdot \Delta\omega(n-1,m) + SCB(n,m) \cdot \Delta\omega(n+1,m) \\ - [SCB(n-1,m) + SCC(n-1,m)] \cdot \Delta UUH(n-1) \\ - [SCA(n,m) + SCB(n,m)] \cdot \Delta UUH(n) \end{bmatrix}}{[SGC(n,m-1) + SGA(n,m) + SCC(n-1,m) + SCA(n,m)]} \quad (3.10)$$

For the left half of the symmetrical three bay frame of Fig. 3.5, the joints $(n,2)$ and $(n,3)$ are seen to be typical of the joints of column lines $m = 2$ and $m = 3$, respectively. By considering the characteristics of each of these two joints, different equations for the incremental joint rotations of each column line are derived.

Because the girders $G(n,1)$, $n = 1, \dots, 22$, do not exist in the structure (see Fig. 3.5), an equation for the incremental joint rotation $\Delta\omega(n,2)$ is found by removing the constants $SGB(n,1)$ and $SGC(n,1)$ from Eq. 3.10. Hence, for each joint of column line $m = 2$:

$$\Delta\omega(n,2) = - \frac{\begin{bmatrix} + SGB(n,2) \cdot \Delta\omega(n,3) \\ + SCB(n-1,2) \cdot \Delta\omega(n-1,2) + SCB(n,2) \cdot \Delta\omega(n+1,2) \\ - [SCB(n-1,2) + SCC(n-1,2)] \cdot \Delta UUH(n-1) \\ - [SCA(n,2) + SCB(n,2)] \cdot \Delta UUH(n) \end{bmatrix}}{[SGA(n,2) + SCC(n-1,2) + SCA(n,2)]} \quad (3.11)$$

For column line $m = 3$, the symmetry of the frame is considered in either of two ways. The first and simpler method is to look at the entire frame and to observe that

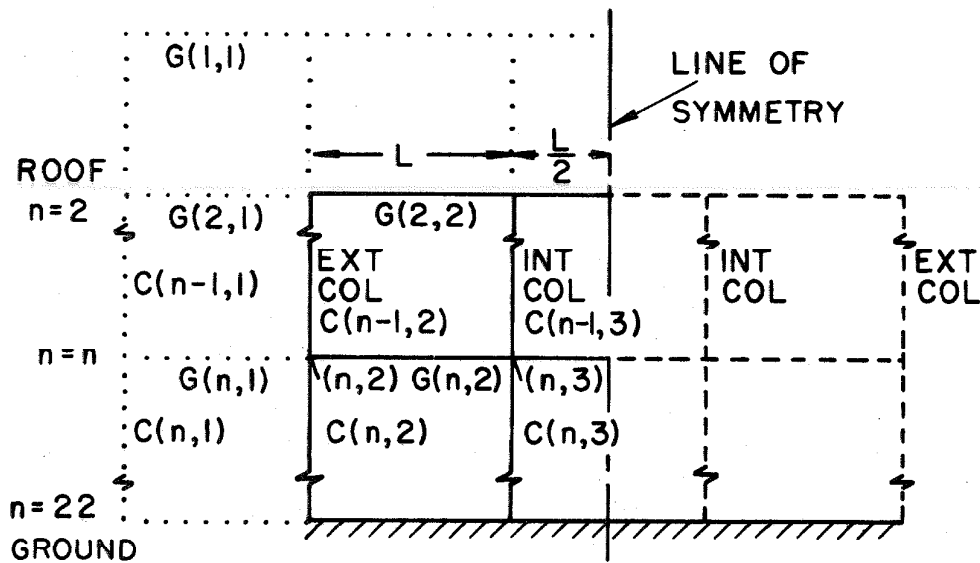


Fig. 3.5 (.....) Dummy Columns and Girders With Stiffnesses Identically Equal to Zero. (Computer Program Artifice)

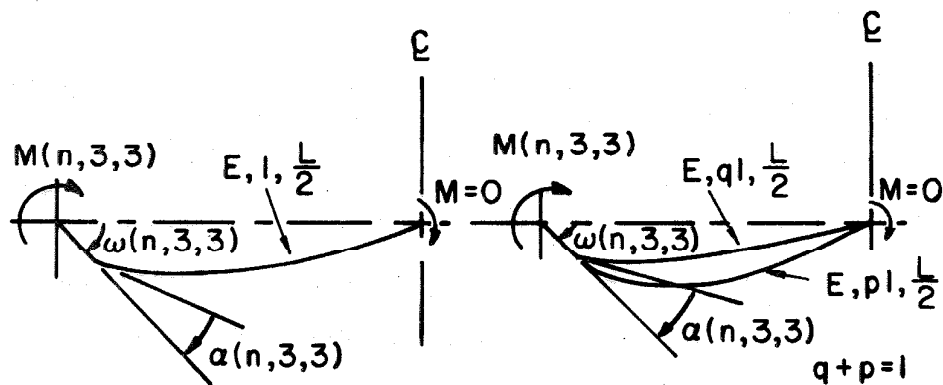


Fig. 3.6a Treatment of Symmetry for One-component Model of Girder G(n, 3). Moment at Centerline Equals Zero.

Fig. 3.6b Treatment of Symmetry for Two-component Model of Girder G(n, 3). Moment at Centerline of Each Component Equals Zero.

$$\Delta\omega(n,4) = \Delta\omega(n,3) . \quad (3.12)$$

Consequently, for the interior girders, $G(n,3)$, $n = 2, \dots, 21$, a simplified bending moment equation is obtained for $\Delta M(n,3,3)$ by substituting Eq. 3.12 into Eq. 3.7):

$$\Delta M(n,3,3) = [SGA(n,3) + SGB(n,3)] \cdot \Delta\omega(n,3) . \quad (3.13)$$

Because the joints at both ends of each interior girder rotate identically the same amount, only the two yield states (a) and (d) need to be considered for either beam model:

State (a) - linear at both ends:

$$\Delta M(n,3,3) = 1.5 \cdot k \cdot \Delta\omega(n,3) ; \quad (3.14)$$

State (d) - nonlinear at both ends:

$$\Delta M(n,3,3) = 1.5 \cdot p \cdot k \cdot \Delta\omega(n,3) ; \quad (3.15)$$

(see Eq. 2.32.1 and Eq. 2.32.2 at the end of Section 2.5). In the second method the girders are cut at the centerline and pinned so that the bending moment at the centerline remains identically zero. For the one-component model this is shown in Fig. 3.6a. For the two-component model, in order to properly treat symmetry, each component must be separately pinned at the centerline as shown in Fig. 3.6b. If, instead, the two components are first connected together and then pinned, certain problems arise, which are discussed in Appendix C. Assuming symmetry is considered correctly, the second method yields the same incremental moment-rotation equations as the first.

Since there are only two states of yield for the interior girders, Eq. 3.14 and Eq. 3.15 are of the form

$$\Delta M(n, 3, 3) = SGA(n, 3) \cdot \Delta \omega(n, 3) \quad (3.16)$$

which uses only one effective stiffness parameter: $SGA(n, 3)$. Hence, for the interior girders, $SGB(n, 3)$ is unnecessary and is merged into $SGA(n, 3)$. The new values of $SGA(n, 3)$ are given (for both beam models) by:

| <u>state of yield</u> | <u>$SGA(n, 3)$</u> |
|-----------------------|-------------------------------|
| linear : | $1.5 \cdot k$ |
| nonlinear : | $1.5 \cdot p \cdot k$ |

Using Eq. 3.16 for $\Delta M(n, 3, 3)$ instead of Eq. 3.13, the following equation is obtained for each joint of column line $m = 3$:

$$\Delta \omega(n, 3) = - \frac{\begin{bmatrix} + SGB(n, 2) \cdot \Delta \omega(n, 2) \\ + SCB(n-1, 3) \cdot \Delta \omega(n-1, 3) + SCB(n, 3) \cdot \Delta \omega(n+1, 3) \\ - [SCB(n-1, 3) + SCC(n-1, 3)] \cdot \Delta UUH(n-1) \\ - [SCA(n, 3) + SCB(n, 3)] \cdot \Delta UUH(n) \end{bmatrix}}{[SGC(n, 2) + SGA(n, 3) + SCC(n-1, 3) + SCA(n, 3)]} \quad (3.17)$$

The differential equation of motion for a typical floor of the structural frame is derived from a balance of forces wherein the sum of the shear forces in the columns, V , damping forces, D , and initial force, I , acting on each floor must be zero. These forces, along with the displacement, U , are depicted in incremental form in Fig. 3.7 and are positive as shown.

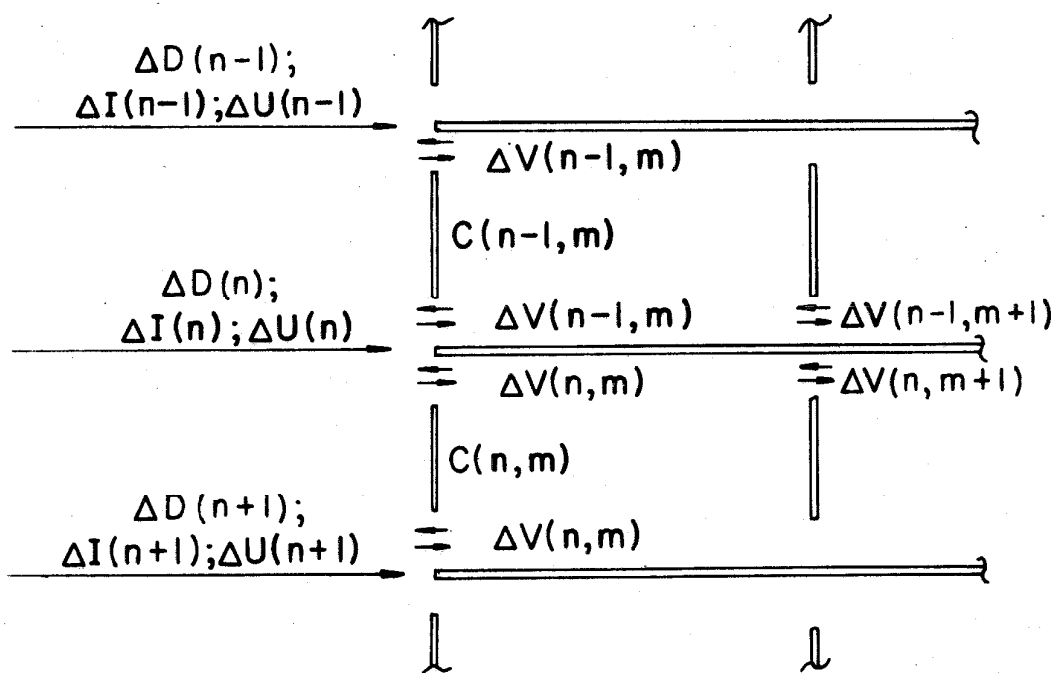


Fig. 3.7

Several constants having Fortran names are used in the equations of motion. Besides those introduced previously, the following ones are used:

$$\begin{aligned}
 \text{SCAB}(n,m) &= \text{SCA}(n,m) + \text{SCB}(n,m) ; \\
 \text{SCBC}(n,m) &= \text{SCB}(n,m) + \text{SCC}(n,m) ; \\
 \text{SCABH}(n,m) &= \frac{\text{SCAB}(n,m)}{\text{HT}(n)} ; \\
 \text{SCBCH}(n,m) &= \frac{\text{SCBC}(n,m)}{\text{HT}(n)} ; \\
 \text{SCD}(n) &= \sum_{m=2}^3 [\text{SCAB}(n,m) + \text{SCBC}(n,m)] ; \text{ and} \\
 \text{SCDHH}(n) &= \frac{\text{SCD}(n)}{[\text{HT}(n)]^2} .
 \end{aligned} \tag{3.18}$$

The incremental shear force in column $C(n,m)$ is

$$\Delta V(n,m) = - \left[\frac{\Delta M(n,m,4) + \Delta M(n+1,m,2)}{\text{HT}(n)} \right] . \tag{3.19}$$

Substituting from Eq. 3.8 and from the list of Fortran constants, Eq. 3.18, Eq. 3.19 becomes

$$\Delta V(n,m) = - \frac{1}{\text{HT}(n)} \left[\begin{aligned} &\text{SCAB}(n,m) \cdot [\Delta \omega(n,m) - \Delta \text{UUH}(n)] \\ &+ \text{SCBC}(n,m) \cdot [\Delta \omega(n+1,m) - \Delta \text{UUH}(n)] \end{aligned} \right] ; \tag{3.20}$$

where

$$\Delta \text{UUH}(n) = \frac{\Delta U(n) - \Delta U(n+1)}{\text{HT}(n)} . \tag{3.21}$$

The resultant incremental shear force acting on (the left half of) the

n^{th} floor of the structural frame in Fig. 3.7 is given by the expression

$$\sum_{m=2}^3 [\Delta V(n-1, m) - \Delta V(n, m)] \quad . \quad (3.22)$$

Using Eq. 3.20 for ΔV and Eq. 3.21 for ΔU_{UH} , and substituting from the list of Fortran constants, Eq. 3.18, an equation for the resultant incremental shear force acting on the n^{th} floor is found:

$$\begin{aligned} & \sum_{m=2}^3 [\Delta V(n-1, m) - \Delta V(n, m)] \\ &= - \sum_{m=2}^3 \text{SCABH}(n-1, m) \cdot \Delta \omega(n-1, m) - \sum_{m=2}^3 \text{SCBCH}(n-1, m) \cdot \Delta \omega(n, m) \\ &+ \sum_{m=2}^3 \text{SCABH}(n, m) \cdot \Delta \omega(n, m) + \sum_{m=2}^3 \text{SCBCH}(n, m) \cdot \Delta \omega(n+1, m) \\ &+ \text{SCDHH}(n) \cdot \Delta U(n+1) + \text{SCDHH}(n-1) \cdot \Delta U(n-1) \\ &- [\text{SCDHH}(n) + \text{SCDHH}(n-1)] \cdot \Delta U(n) \quad . \quad (3.23) \end{aligned}$$

The incremental damping force acting on the n^{th} floor is found from Eq. 3.5:

$$\Delta D(n) = \left\{ \begin{aligned} & - 2\xi_1^m \omega_1 M(n) \cdot \dot{\Delta U}(n) \\ & + \left(\frac{2\xi_1^s}{\omega_1} \right) \cdot \left\{ \begin{aligned} & + \text{SCDHH}(n-1) \cdot \dot{\Delta U}(n-1) \\ & - [\text{SCDHH}(n-1) + \text{SCDHH}(n)] \cdot \dot{\Delta U}(n) \\ & + \text{SCDHH}(n) \cdot \dot{\Delta U}(n+1) \end{aligned} \right\} \end{aligned} \right\}; \quad (3.24)$$

where

- ξ_1^m : the fraction of critical damping for the fundamental mode of the linear structure with only mass proportional damping;
- ξ_1^s : the fraction of critical damping for the fundamental mode of the linear structure with only stiffness proportional damping;
- ω_1 : circular frequency of the fundamental mode,
- $M(n)$: mass of one half of the n^{th} floor, and
- $\Delta \dot{U}(n)$: incremental velocity of the n^{th} floor relative to the foundation.

Although both mass proportional and stiffness proportional damping are included in the equations of motion, only mass proportional damping is used in the computer program for this report (see Subroutine CONV in Appendix E).

The incremental inertial force, ΔI , acting on the n^{th} floor is given by

$$\Delta I(n) = -M(n) \cdot (\Delta \ddot{U}(n) + \ddot{\Delta y}) \quad (3.25)$$

where

- $M(n)$: mass of one half of the n^{th} floor,
- $\Delta \ddot{U}(n)$: incremental acceleration of the n^{th} floor relative to the foundation; and
- $\ddot{\Delta y}$: incremental acceleration of the foundation.

Since the incremental force balance for the n^{th} floor is

$$\Delta I(n) + \Delta D(n) + \sum_{m=2}^3 [\Delta V(n-1, m) - \Delta V(n, m)] = 0 \quad , \quad (3.26)$$

by substituting from Eq. 3.23, Eq. 3.24, and Eq. 3.25, the differential equation of motion in incremental form is obtained:

$$\begin{aligned} & M(n) \cdot \Delta \ddot{U}(n) \\ & + \left[2\xi_1^m \cdot \omega_1 \cdot M(n) + 2\left(\frac{\xi_1^s}{\omega_1}\right) \cdot (SCDHH(n) + SCDHH(n-1)) \right] \cdot \Delta \dot{U}(n) \\ & + [SCDHH(n) + SCDHH(n-1)] \cdot \Delta U(n) \\ & + \sum_{m=2}^3 [SCBCH(n-1, m) - SCABH(n, m)] \cdot \Delta \omega(n, m) \\ & - \left(\frac{2\xi_1^s}{\omega_1}\right) \cdot SCDHH(n-1) \cdot \Delta \dot{U}(n-1) - SCDHH(n-1) \cdot \Delta U(n-1) \\ & + \sum_{m=2}^3 SCABH(n-1, m) \cdot \Delta \omega(n-1, m) \\ & - \left(\frac{2\xi_1^s}{\omega_1}\right) \cdot SCDHH(n) \cdot \Delta \dot{U}(n+1) - SCDHH(n) \cdot \Delta U(n+1) \\ & - \sum_{m=2}^3 SCBCH(n, m) \cdot \Delta \omega(n+1, m) \\ & = - M(n) \cdot \Delta \ddot{y} \quad . \end{aligned} \quad (3.27)$$

In this section, three equations of motion have been derived for the left half of the n^{th} floor of the structural frame taking into consideration the symmetrical properties of the frame. In the next section, the methods used to solve the set of $3N$ equations of motion

for an N-floor nonlinear frame are discussed.

3.5 Solution of the Equations of Motion

As previously mentioned, because of yielding, the stiffness properties of the girders and columns change as a function of time during a strong earthquake. Hence, the equations of motion are nonlinear, which eliminates, for all practical purposes, solutions using modal analysis methods. Nevertheless, the nonlinear equations of motion can be solved by means of an integration technique which uses finite increments of time. In the integration technique used here, it is assumed that the stiffness properties of each girder and column in the structure remain constant throughout each time increment, but that they can change from one time increment to the next. Consequently, within each time increment, the equations of motion are linear.

One criteria for determining the magnitude " ΔT " of the time increment is

$$\Delta T = \frac{1}{10} \tau_{20}$$

where τ_{20} is the period of the 20th mode of the linear structure.

It should be mentioned that in the studies for this report the A/20/2.2/2/6 structure is analyzed with

$$\Delta T = 0.005 \text{ sec} \approx \frac{1}{6} \tau_{20} .$$

The integration technique used to solve the equations of

motion is one presented by E. L. Wilson and R. W. Clough⁽⁴⁰⁾ and is similar to the Newmark β -method^(42,43) with $\beta = 1/6$. For this method, it is assumed that:

1. the acceleration is linear within each time interval; and
2. the acceleration, velocity and displacement at the beginning of the time interval are known.

With these assumptions, for each floor, a set of equations relating the incremental acceleration, velocity, and displacement that occur during the t^{th} time interval can be found. One form of this set of equations is the following:

$$\begin{aligned}\Delta U(n)_t &= \Delta U(n)_t ; \\ \Delta \dot{U}(n)_t &= \frac{3}{\Delta t} \Delta U(n)_t + B(n) ; \\ \Delta \ddot{U}(n)_t &= \frac{6}{(\Delta t)^2} \Delta U(n)_t + A(n) ;\end{aligned}\tag{3.28}$$

where

$$A(n) = - \frac{6}{\Delta t} \ddot{U}(n)_{(t-\Delta t)} - 3 \dot{U}(n)_{(t-\Delta t)} ;$$

$$B(n) = - 3 \dot{U}(n)_{(t-\Delta t)} - \frac{\Delta t}{2} \ddot{U}(n)_{(t-\Delta t)} ;$$

$t-\Delta t$: time at the beginning of the increment; and

t : time at the end of the increment.

$A(n)$ and $B(n)$ appear as constants in Eq. 3.28 since they are determined at the beginning of the time increment. Using Eq. 3.28, the incremental acceleration and incremental velocity are eliminated from the equations of motion leaving only the incremental displacement; hence, it is said to be the " ΔU " form. Furthermore,

Eq. 3.28 can be manipulated into any one of six forms, ΔU , $\Delta \dot{U}$, $\Delta \ddot{U}$, U , \dot{U} , or \ddot{U} , where the name of the form corresponds to the variable that remains in the equations of motion.

Using Eq. 3.28, the equation of motion, Eq. 3.27, becomes

$$\begin{aligned}
 & \left\{ \left(\frac{6}{(\Delta t)^2} + \frac{6\xi_1^m \omega_1}{\Delta t} \right) \cdot M(n) \right. \\
 & \quad \left. + \left(1 + \frac{6\xi_1^s}{\Delta t \cdot \omega_1} \right) \cdot (\text{SCDHH}(n) + \text{SCDHH}(n-1)) \right\} \cdot \Delta U(n) \\
 & + \sum_{m=2}^3 [\text{SCBCH}(n-1, m) - \text{SCABH}(n, m)] \cdot \Delta \omega(n, m) \\
 & - \left(1 + \frac{6\xi_1^s}{\Delta t \cdot \omega_1} \right) \cdot \text{SCDHH}(n-1) \cdot \Delta U(n-1) \\
 & + \sum_{m=2}^3 \text{SCABH}(n-1, m) \cdot \Delta \omega(n-1, m) \\
 & - \left(1 + \frac{6\xi_1^s}{\Delta t \cdot \omega_1} \right) \cdot \text{SCDHH}(n) \cdot \Delta U(n+1) \\
 & - \sum_{m=2}^3 \text{SCBCH}(n+1, m) \cdot \Delta \omega(n+1, m) \\
 & = - [\ddot{\Delta y} + A(n) + 2 \cdot \xi_1^m \cdot \omega_1 \cdot B(n)] \cdot M(n) \\
 & \quad + \left(\frac{2\xi_1^s}{\omega_1} \right) \cdot \left[-[\text{SCDHH}(n) + \text{SCDHH}(n-1)] \cdot B(n) \right. \\
 & \quad \left. + \text{SCDHH}(n-1) \cdot B(n-1) + \text{SCDHH}(n) \cdot B(n+1) \right]
 \end{aligned} \tag{3.29}$$

where the incremental displacements and joint rotations are the only unknowns.

Two methods for solving the equations of motion, Eq. 3.11, Eq. 3.17, and Eq. 3.29, for a nonlinear tall structure are considered here. One is entitled relaxation-iteration and the other, matrix substitution. In the relaxation-iteration method, for each time increment, the three equations of motion are solved for each floor beginning with the top floor (roof) keeping all of the other floors fixed. Then, the equations for the adjacent floor are solved keeping all of the other floors, including the roof, fixed. This procedure is continued sequentially until the equations for all the floors have been "relaxed." By iteration, or repetition of this relaxation process until a convergence criteria is satisfied, the incremental displacements and rotations are found for this time increment. Then the succeeding time interval is considered and the relaxation-iteration process is applied again.

In the matrix substitution method,⁽³⁷⁾ which is described in more detail later in this section, a matrix equation is written involving a large tridiagonal matrix with 3×3 matrices as elements. For each time increment the equations of motion are solved according to a recursion relationship. No iteration is necessary.

In summary, any one of three forms, ΔU , $\Delta \dot{U}$, or $\Delta \ddot{U}$, of the integration technique can conceivably be used with either one of the two methods, iteration or matrix, for solving the incremental equations of motion.

Four of the combinations were studied: $\Delta \ddot{U}$ -iteration, $\Delta \ddot{U}$ -matrix, ΔU -iteration, and ΔU -matrix. Of these, only the

ΔU -matrix does not work well. In this case, some of the 3×3 matrices are ill-conditioned since the relative magnitudes of the elements may be on the order of 10^6 . The other three combinations yield approximately the same answers (resulting displacements are the same to about 4 decimal places) and take about the same amount of computer time, using single precision arithmetic (8 decimal digits). The combination used in all of the computer studies presented in this report is the ΔU -matrix method using double precision arithmetic* (16 decimal digits) for solving the incremental equations of motion and finding the displacements, joint rotations and interfloor displacements. However, the bending moments, shear forces, etc., are calculated using single precision.

Throughout this chapter the roof has been numbered $n = 2$ and the first floor above ground level $n = 21$ for reasons mentioned earlier. However, there is one exception: for the matrix operations described below, $n = 1$ corresponds to the roof and $n = 20$ corresponds to the first floor above the ground level. It should be mentioned that this notation, including the exception for the matrix operations, is consistent with the computer program.

The three equations of motion for the n^{th} floor of the structural frame, Eq. 3.11, Eq. 3.17 and Eq. 3.29, can be written together as a matrix equation, Eq. 3.30, which is of the form of Eq. 3.31. The equations of motion for a tall structure are obtained by writing Eq. 3.31 for each floor. Together, the equations for a

*By using double precision instead of single precision arithmetic, the computing time for the usual run, i.e., without Subroutine MODE, was increased approximately 75 %.

$$\begin{bmatrix}
 -\left(1 + \frac{6\epsilon_1^m}{\Delta t \cdot \omega_1}\right) \cdot \text{SCDHH}(n-1) & +\text{SCABH}(n-1,2) & +\text{SCABH}(n-1,3) & \left(1 + \frac{6\epsilon_1^m}{2\omega_1}\right) \left(\text{SCDHH}(n-1) + \text{SCDHH}(n)\right) + M(n) \left(\frac{6}{\Delta t} + \frac{6\epsilon_1^m}{\Delta t}\right) & +\text{SCBCH}(n-1,2) - \text{SCABH}(n,2) & +\text{SCBCH}(n-1,3) - \text{SCABH}(n,3) & -\left(1 + \frac{6\epsilon_1^m}{\Delta t \cdot \omega_1}\right) \cdot \text{SCDHH}(n) & -\text{SCBCH}(n,2) - \text{SCBCH}(n,3) & \Delta U(n-1) \\
 -\text{SCBCH}(n-1,2) & +\text{SCB}(n-1,2) & 0 & +\text{SCBCH}(n-1,2) + \text{SCA}(n,2) & +\text{SCB}(n,2) & +\text{SCB}(n,2) & +\text{SCABH}(n,2) & 0 & \Delta U(n) \\
 -\text{SCBCH}(n-1,3) & 0 & +\text{SCB}(n-1,3) & +\text{SCBCH}(n-1,3) - \text{SCABH}(n,3) & +\text{SCA}(n,3) & +\text{SCA}(n,3) & +\text{SCABH}(n,3) & +\text{SC3}(n,3) & \Delta U(n-1)
 \end{bmatrix}
 =
 \begin{bmatrix}
 -M(n) \cdot [\Delta \ddot{y} + A(n) + 2\epsilon_1^m \cdot \omega_1 \cdot B(n)] \\
 + \left(\frac{2\epsilon_1^m}{\omega_1}\right) \left[-\text{SCDHH}(n-1) \cdot B(n-1) \right. \\
 \left. - \left[\text{SCDHH}(n) + \text{SCDHH}(n-1) \right] B(n) \right] \\
 0 \\
 0
 \end{bmatrix}
 \quad (3.30)$$

which is of the form

$$\begin{bmatrix} C_{n-1}^T & S & C_n \end{bmatrix} \begin{Bmatrix} \text{DR}(n-1) \\ \text{DR}(n) \\ \text{DR}(n+1) \end{Bmatrix} = \text{DP}(n) \quad (3.31)$$

where

$$\text{DR}(n) = \begin{Bmatrix} \Delta U(n) \\ \Delta u(n,2) \\ \Delta u(n,3) \end{Bmatrix}$$

and

$$\text{DP}(n) = \begin{Bmatrix} -M(n) \cdot [\Delta \ddot{y} + A(n) + 2\epsilon_1^m \cdot \omega_1 \cdot B(n)] + \left(\frac{2\epsilon_1^m}{\omega_1}\right) \left[+\text{SCDHH}(n-1)B(n-1) \right. \\ \left. - \left[\text{SCDHH}(n) + \text{SCDHH}(n-1) \right] B(n) \right] \\ 0 \\ 0 \end{Bmatrix}$$

twenty floor structure form the tridiagonal matrix equation,

Eq. 3.32: *

$$\begin{bmatrix} S_1 & C_1 & & & & \\ C_1^T & S_2 & C_2 & & & \\ & C_2^T & S_3 & C_3 & & \\ & & & \ddots & & \\ & & & & \ddots & \\ & & & & & C_{17}^T \\ & & & & & S_{18} & C_{18} \\ & & & & & C_{18}^T & S_{19} & C_{19} \\ & 0 & & & & C_{19}^T & S_{20} & \\ & & & & & & & \end{bmatrix} \cdot \begin{Bmatrix} DR_1 \\ DR_2 \\ DR_3 \\ \vdots \\ \vdots \\ \vdots \\ DR_{18} \\ DR_{19} \\ DR_{20} \end{Bmatrix} = \begin{Bmatrix} DP_1 \\ DP_2 \\ DP_3 \\ \vdots \\ \vdots \\ \vdots \\ DP_{18} \\ DP_{19} \\ DP_{20} \end{Bmatrix} \quad (3.32)$$

This set of equations is solved by successive substitution followed by successive back-substitution as shown below. The equation for $n = 1$ is

$$S_1 \cdot DR_1 + C_1 \cdot DR_2 = DP_1.$$

Multiplying by S_1^{-1} , an equation for DR_1 is obtained:

$$DR_1 = -S_1^{-1} \cdot C_1 \cdot DR_2 + S_1^{-1} \cdot DP_1. \quad (3.33)$$

DR₁, which is composed of the unknown displacement and joint rotations for floor n = 1, is eliminated from the equation for floor n = 2:

* This closely follows the matrix-substitution method presented by R. W. Clough, I. P. King, and E. L. Wilson in reference 37.

$$C_1(-S_1^{-1} \cdot C_1 \cdot DR_2 + S_1^{-1} \cdot DP_1) + S_2 \cdot DR_2 + C_2 \cdot DR_3 = DP_2$$

or

$$\bar{S}_2 \cdot DR_2 + C_2 \cdot DR_3 = \overline{DP}_2 \quad (3.34)$$

where

$$\bar{S}_2 = S_2 - C_1^T \cdot S_1^{-1} \cdot C_1$$

and

$$\overline{DP}_2 = DP_2 - C_1^T \cdot S_1^{-1} \cdot DP_1 \quad .$$

From Eq. 3.34 a recursive relationship is seen for the n^{th} floor:

$$\bar{S}_n \cdot DR_n + C_n \cdot DR_{n+1} = \overline{DP}_n \quad (3.35)$$

where

$$\bar{S}_n = S_n - C_{n-1}^T \cdot S_{n-1}^{-1} \cdot C_{n-1}$$

and

$$\overline{DP}_n = DP_n - C_{n-1}^T \cdot S_{n-1}^{-1} \cdot DP_{n-1} \quad .$$

Noting that both C_{20} and DR_{21} are nonexistent for a 20 floor structure, the equation for floor $n = 20$ is

$$\bar{S}_{20} \cdot DR_{20} = \overline{DP}_{20} \quad (3.36)$$

where \bar{S}_{20} and \overline{DP}_{20} are found by successive substitution. Since the only unknown in Eq. 3.36 is DR_{20} , it can be found from the equation

$$DR_{20} = \bar{S}_{20}^{-1} \cdot \overline{DP}_{20} \quad (3.37)$$

Having DR_{20} , by means of back-substitution using the recursive relationship

$$DR_n = \bar{S}_n^{-1}(\bar{DP}_n - C_n \cdot DR_{n+1}) \quad (3.38)$$

which is an inverse form of Eq. 3.35, solutions are found for DR_{19} , $DR_{18} \dots DR_1$. In this manner, the incremental equations of motion are solved for each time increment.

In this chapter, the class of nonlinear tall structures treated in this report was described in detail, and the equations of motion for this class of structures were derived using the bending moment-end rotation equations for beams developed in Chapter II. Also, the method used to solve the equations of motion with the aid of a digital computer was outlined.

In order to verify that the resulting computer program operates properly, a number of tests were made. These are discussed in the next chapter.

CHAPTER IV

VERIFICATION OF THE COMPUTER PROGRAM

4.1 Introduction

The computer program developed in connection with this report is based upon the equations of motion derived in the previous chapter. As an overall check on the program, several tests covering various aspects of it were made. The purpose of this chapter is to briefly describe these tests.

4.2 Error Checks in the Program

In the computer solution of the equations of motion, one can anticipate certain round-off error. To evaluate these errors, the "error parameters" $\epsilon_1(n,m)$ and $\epsilon_2(n)$ were introduced into the moment balance and force balance equations, respectively.

For each time increment, the equations of motion were solved for the joint rotations and the displacements of the floors using double precision arithmetic (16 decimal digits). The individual bending moments and forces were found for the girders and columns of the frame using single precision arithmetic (8 decimal digits) since the nature of the round-off error in these computations is not so critical. Having determined the moments and forces, the error $\epsilon_1(n,m)$ in the bending moment balance at each joint in the frame is found according to Eq. 4.1, and the error $\epsilon_2(n)$ in the balance of forces acting on each floor is found according to Eq. 4.2:*

*See Chapter III for the terminology used in these equations.

$$\sum_{j=1}^4 M(n, m, j) = \epsilon_1(n, m) ; \quad (4.1)$$

$$I(n) + D(n) + \sum_{m=2}^3 [V(n-1, m) - V(n, m)] = \epsilon_2(n, m) \quad (4.2)$$

In the printed output at the end of the program, the maximum absolute values of $\epsilon_1(n, m)$ and $\epsilon_2(n)$ are printed along with the times at which they occur. For a typical computer run using an earthquake accelerogram, it is found that

$$|\epsilon_1(n, m)|_{\max} \sim 10^{-6} |M(n, m, j)|_{\max} ; \quad (4.3)$$

and

$$|\epsilon_2(n)|_{\max} \sim 10^{-6} \left| \sum_{m=2}^3 V(n, m) \right|_{\max} . \quad (4.4)$$

It should be noted that for single precision arithmetic, the limit on accuracy is 10^{-8} .

If the values of the error parameters in the printed output of a computer run are consistent with the typical values given in Eq. 4.3 and Eq. 4.4, then there is reason to accept the results of the run. On the other hand, unusual behavior of the error parameters would lead one to suspect some type of program or computer malfunction. Such difficulties were not encountered in the computer runs for the present investigation.

4.3 The Wilson-Clough Integration Technique⁽⁴⁰⁾

To investigate the properties of the Wilson-Clough integration technique, several different programs based on it were examined. At the same time, other programs were developed which used different integration techniques to solve the equations of motion for either the same or an equivalent system. These programs are described below, and the results are compared.

The equations of motion of the damped, three-mass, bilinear hysteretic system of Fig. 4.1, excited by a constant frequency, sinusoidal base acceleration $\ddot{y}(t)$, were solved using three different computer programs. The first program, explicitly written for this system, solved the equations of motion by means of a third order Runge-Kutta integration technique.* The second program, also explicitly developed for this system, used the Wilson-Clough integration technique. The third program was an adaptation of the regular program for analyzing nonlinear frames developed in connection with this report. In this adaptation the number of floors was reduced from twenty to three, and the girders were made rigid. The resulting model is shown in Fig. 4.2. The same approximately steady state initial conditions and the same sinusoidal excitation were used for all three programs. In each case the integration was carried out for fifteen cycles of the input acceleration. The resulting time history plots of the corresponding displacements were within

*This program, written by Dr. W. D. Iwan of California Institute of Technology, uses the standard integration subroutine of the California Institute of Technology Computing Center.

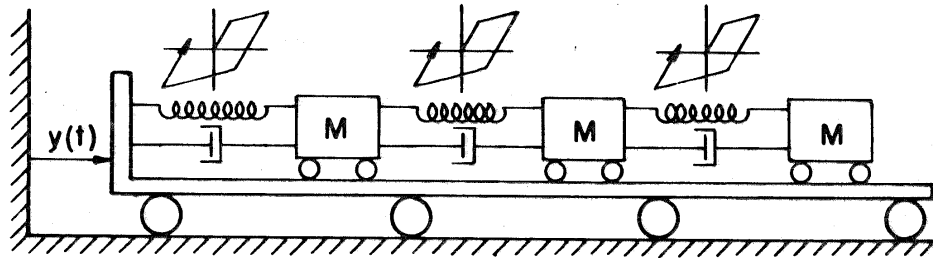


Fig 4.1 Three-mass, Damped, Base Excited System
With Bilinear Hysteretic Springs

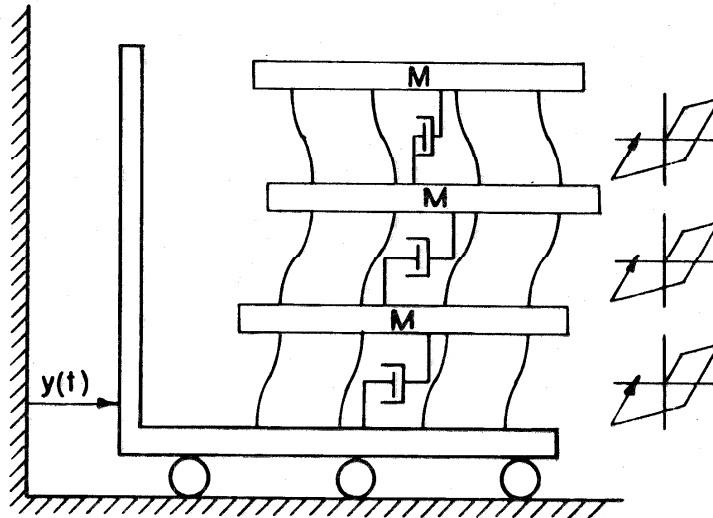


Fig. 4.2 Three-mass, Damped, Base Excited System
With Bilinear Hysteretic Springs

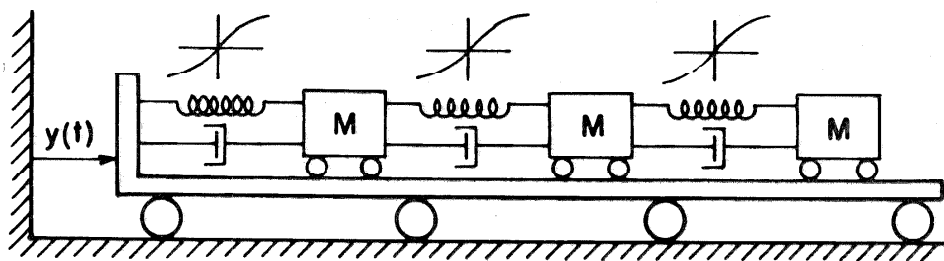


Fig. 4.3 Three-mass, Damped, Base Excited System
With Cubic Nonhysteretic Springs

2% of each other throughout the entire length of the computer runs.

A second system used for comparing the first two programs described above consisted of the damped, three-mass system with cubic-nonhysteretic springs shown in Fig. 4.3. Again, the resulting time history plots of the corresponding displacements were within 2% of each other for the fifteen cycles of the computer run. Even with zero initial conditions, this system achieves steady state motion after nine cycles.

Because of the consistency of the above results, it would appear that the Wilson-Clough integration technique is suitable for the present investigation.

4.4 Excitation of the Linear A/20/2.2/2/6 Frame Near Its Third Natural Frequency

For an additional test of the more complicated system later used in the nonlinear analysis, the computer program was modified so that the base excitation was a constant frequency, sinusoidal accelerogram. Included in this program was a means of checking that the response was approximately steady state.

The A/20/2.2/2/6 frame was used with the yield condition suppressed so that the system remained linear. The specified damping in the fundamental mode was 0.10 fraction of critical. Since mass proportional damping only was used, the effective damping in the higher modes is reduced, being 0.025 fraction of critical in the third mode. The frequencies of the half power points of the steady state resonance curve for a single degree of freedom system

having as a natural frequency the third modal frequency of the frame were analytically calculated (see Table 4-1).

Three computer runs were made in this test: one at each of the three frequencies given in Table 4.1. In each run the initial conditions were zero and the amplitude of the sinusoidal forcing function was the same. After the steady state criteria* were satisfied, the amplitude of the displacement of the 20th floor and the phase angle between that floor and the forcing function were found. The three resulting amplitudes, normalized with respect to the amplitude for the third natural frequency, along with the corresponding phase angles are given in Table 4-1.

For a one degree of freedom system at steady state, the normalized amplitudes at the half-power points are 0.707 instead of 0.69 and 0.77, and the phase angles are 45° and 135° instead of 47° and 140°, respectively. The unnormalized displacement of the 20th floor at the third natural frequency as calculated by the computer was 5% smaller than that found by analytical means using eigenvalue theory wherein it was assumed that the contributions to the excitation by all modes except the third were negligible.

*Within any one complete cycle of the input acceleration, if

$$|U \text{ MAX}(n) + U \text{ MIN}(n)| < 0.05 \cdot U \text{ MAX}(n)$$

for each floor, where

$U \text{ MAX}(n)$: the most positive displacement for the n^{th} floor during that cycle, and

$U \text{ MIN}(n)$: the most negative displacement for the n^{th} floor during that cycle;

then an approximation to steady state is obtained.

TABLE 4-1

| | <u>Lower half- power point</u> | <u>Third natural frequency</u> | <u>Upper half- power point</u> |
|--|------------------------------------|--|------------------------------------|
| Circular frequency | 11.1905 | 11.4748 | 11.7591 |
| Theoretical amplitude, normalized | 0.707 | 1.00 | 0.707 |
| Amplitude of the displace- ment of the 20 th floor, normalized (computer output) | 0.69 | 1.00 | 0.77 |
| Theoretical phase angle | 45° | 90° | 135° |
| Phase angle between displacement of the 20 th floor and the forcing function* (computer output) | 47° | 90° | 140° |

These discrepancies in amplitudes and phase angles can be explained by the following factors:

1. Because the steady state criteria are not exact, the results of the computer program are only approximately steady state.
2. In the analytical calculations it is assumed that only one mode--the third--contributes to the excitation. However, in this test, base excitation is used which does not excite a pure mode in a multi-degree of freedom structure.

*The forcing function used here is

$$f_n(t) = -M(n)\ddot{y}(t)$$

where

$M(n)$: mass of one half of the n^{th} floor, and
 $\ddot{y}(t)$: base acceleration.

Consequently, even though the third mode is the dominant one in this frequency range, the others do contribute.

Since the discrepancies in the results are small and can be explained by these factors, this test provides further assurance that the computer program, including the mass proportional damping mechanism, is working properly.

Another point which reflects upon the accuracy of the computer program concerns the joint rotations of the linear A/20/2.2/2/6 frame. The stiffness properties of this frame (see Fig. 3.2) are designed* so that at each joint within the same floor the ratio of the sum of the column stiffnesses to the sum of the girder stiffnesses is the same. For example, for the first floor above the ground, this ratio for each joint is 2.4. Hence, as long as this frame remains linear, the rotations of the joints within the same floor should be equal. Even though the rotation of each joint is calculated independently, it is seen in the computer output that the rotations of joints within the same floor are the same to eight significant decimal digits, thus giving an additional check on the program. However, such a check cannot be made for the particular nonlinear frame studied in this report. For this frame, the strength properties are not directly proportional to the corresponding stiffness properties, and, therefore, the rotations within the same floor would not be expected to be equal. This difference in joint rotations within the same floor of the nonlinear frame can be seen in the time history plots of Chapter VI.

*See Section 2.2 of the FHA Study, reference 1.

It is especially evident in the plots for the joints of the 20th floor.

4.5 A Comparison With Results Presented in the FHA Study

In another comparison test, the A/20/2.2/2/6 frame was subjected to earthquake excitation and the resulting responses were compared with corresponding ones presented in the FHA Study. Since the yield criteria and the treatment of symmetry used in the regular nonlinear analysis program for this report differ from those used in the program for the FHA Study, the computer program used for this test includes modifications to remove these differences.

It is the author's understanding that the computer program used for the FHA Study is basically the same one presented in a report to the Office of Civil Defense by T. Y. Lin and Associates.⁽²⁾ That program can treat an arbitrary number of girders and columns, but since the two-component beam model is used (see Section 2.5), the symmetrical properties of the three bay (four column) frame cannot be treated exactly by cutting the interior girders at the centerline as is done there. Nevertheless, this is an expedient approximation for that program. The problems that are encountered by using such an approximation are discussed in Appendix C. In order to account for the treatment of symmetry used in the FHA Study, the two-component beam model is used in the program for this test with appropriate modifications to the incremental moment-rotation-plastic angle equations.

As mentioned above, the yield criteria used in the regular

nonlinear analysis program for this report differ from those used in the program for the FHA Study. In order that the criteria be the same in both computations, the criteria used in the FHA Study are adopted for purposes of the comparison test. It is noted that the yield criteria used in the FHA program can, in special cases, lead to incorrect responses. The plastic angles and resulting ductility factors are particularly sensitive to this difficulty. The special situations under which these problems may become troublesome are discussed in Appendix B.

The same input data consisting of the structural properties and the accelerogram of the El Centro (N-S) earthquake of 18 May 1940 were used in both computations. This accelerogram is the same as the one used at the Earthquake Engineering Laboratory of the California Institute of Technology, but rounded off to four decimal places.

The responses obtained from the modified program using this input data are the same as those (within the tolerance of the plots) presented in the FHA Study.

In this Chapter several different tests of the computer program were outlined and the results of each test indicate that the program performs as expected. Consequently, it is believed that the computer program for determining the response of nonlinear tall structures subjected to earthquake excitation operates properly and provides the desired accuracy.

CHAPTER V

MODAL ANALYSIS OF CONTINUOUS CANTILEVER BEAMS
AND OF TALL STRUCTURES5.1 Introduction

In the past a number of authors, M. A. Biot,⁽⁶⁾ G. N. Bycroft,⁽³⁴⁾ R. W. Clough,⁽³⁶⁾ R. L. Jennings,⁽¹⁹⁾ K. Kanai,⁽³²⁾ K. Muto,⁽²⁹⁾ H. M. Westergaard⁽³⁰⁾ and others have mentioned that "higher modes" are important and that "whiplash" is observed in tall structures. This chapter is intended to determine the conditions under which higher modes are important as well as to suggest a definition of whiplash for tall structures.

By studying continuous beams and discretized models of tall structures, it is possible to gain a fuller understanding of why the displacements, strains (interfloor displacements), shear forces, and total accelerations have differing dependencies upon the various modes as well as upon the position in the structure. Two linear elastic continuous cantilever beams which represent limiting cases of tall structures are studied. In one, the stiffness and mass distributions are uniform, while in the other, these distributions taper to a point at the top. Furthermore, a discretized model of a typical structural frame (A/20/2.2/2/6)* is also studied by modal analysis. In Section 5.2 the continuous beams, which are subjected to an ensemble of earthquakes, are analyzed. In particular, the average

*See Section 3.2 for a description of the structural properties.

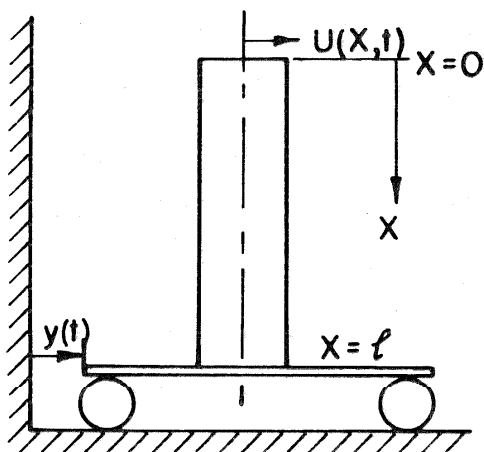


Fig. 5.1 Uniform Cantilever Beam

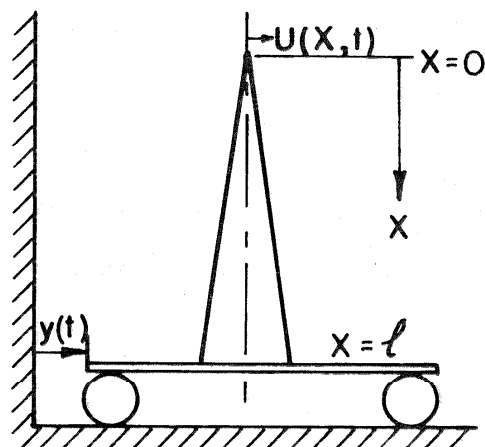


Fig. 5.2 Tapered Cantilever Beam

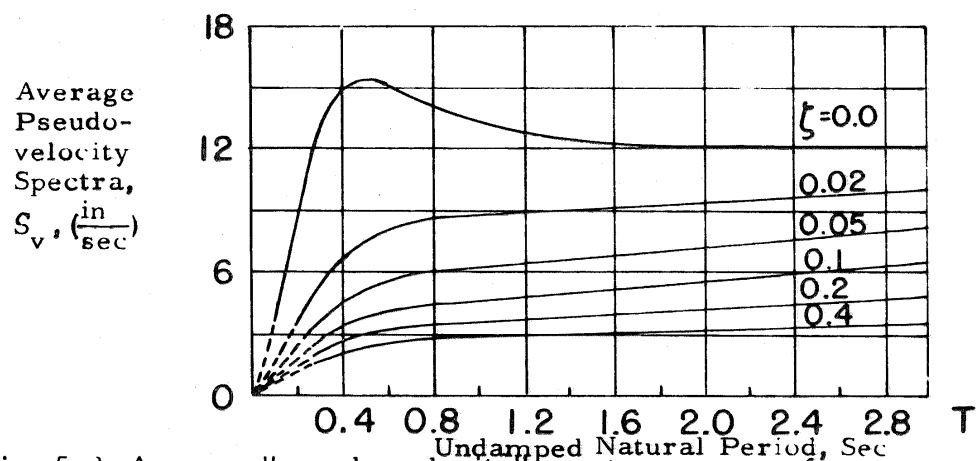


Fig. 5.3 Average "pseudo-velocity" spectrum curves for strongest ground motion. These curves are the average of the four strongest ground motions so far recorded: El Centro, California, May 18, 1940; El Centro, California, Dec. 30, 1934; Olympia, Washington, Apr. 13, 1949; Taft, California, July 21, 1952. Before averaging, each spectrum was normalized so that there was a unit area under the zero-damped curve. To correspond to the respective ground motions, the ordinates must be multiplied by factors as follows: El Centro, 1940 (2.7); El Centro, 1934 (1.9); Olympia, 1949 (1.9); Taft, 1952 (1.6). (Reference 9).

maximum absolute modal contributions to the displacements, strains, shear forces, and total accelerations are related to the average pseudo-velocity spectra S_v . In this chapter, the phrase "average maximum absolute" means average over an ensemble of earthquakes of the maximum absolute value over time of each member of the ensemble. In order to show how these average maximum absolute modal contributions depend upon the taper of the beam and upon the position $(\frac{x}{l})$ in the beam (see Fig. 5.1) some of them are later presented in tabular form.

In Section 5.3, the method used to obtain "equivalent" modal participation factors and the "equivalent" modal contributions to displacements and to interfloor displacements for yielding structures is treated. The results obtained by using this method for a typical yielding structural frame are then discussed.

5.2 Modal Analysis of Continuous Beams

One possible model for approximating a tall structure of uniform properties subjected to horizontal earthquake excitation is the shear-type continuous cantilever beam shown in Fig. 5.1. The general equation for this type of cantilever beam excited by the base acceleration $\frac{d^2 y}{dt^2}(t)$ is

$$\frac{\partial}{\partial x} \left(K(x) \frac{\partial u}{\partial x}(x, t) \right) = \gamma(x) \left(\frac{\partial^2 u}{\partial t^2}(x, t) + \ddot{y} \right) \quad (5.1)$$

with the boundary conditions:

$$\text{at } x = 0 , \quad \frac{\partial u}{\partial x} = 0 ; \quad \text{and}$$

$$\text{at } x = l , \quad u = 0 ;$$

where

$K(x)$ is the shear stiffness in units of lbs ;

$\gamma(x)$ is the mass density in units of $\frac{\text{mass}}{\text{unit length}}$

$u(x,t)$ is the relative displacement; and

$$\ddot{y} = \frac{d^2 y}{dt^2}(t).$$

For the uniform beam, the properties of stiffness and mass density are constants:

$$K(x) = K_o , \quad \text{and}$$

$$\gamma(x) = \gamma_o .$$

The velocity of wave propagation, c , is defined by

$$\frac{1}{c^2} = \frac{\gamma_o}{K_o} .$$

By substituting these values into Eq. 5.1, the general equation for a uniform beam is obtained:

$$\frac{\partial^2 u}{\partial x^2}(x,t) - \frac{1}{c^2} \frac{\partial^2 u}{\partial t^2}(x,t) = \frac{1}{c^2} \ddot{y}(t) . \quad (5.2)$$

The boundary conditions remain the same:

$$x = 0 \quad \frac{\partial u}{\partial x} = 0 , \quad \text{and}$$

$$x = l \quad u = 0 .$$

The solution of this eigenvalue problem with zero initial conditions is

$$u(x, t) = \frac{2c}{l} \sum_{n=1}^{\infty} \frac{(-1)^n}{\omega_n^2} \cos\left(\frac{\omega_n x}{c}\right) \int_0^t \ddot{y}(\tau) \sin(\omega_n(t-\tau)) d\tau \quad (5.3)$$

and the eigenfrequencies are given by

$$\frac{\omega_n l}{c} = \frac{(2n-1)\pi}{2}, \quad n = 1, 2, 3, \dots \quad (5.4)$$

In this section the primary interest in using modal analysis is in making comparisons between the average maximum absolute values of the individual modal contributions of the responses, and not in finding the sums of the modal contributions. Furthermore, there is some question as to the absolute convergence of the total acceleration series. This is discussed briefly later. Consequently, only the n^{th} terms of the various responses are considered.

From Eq. 5.4, the contribution of the n^{th} mode to the displacement is

$$u_n(x, t) = \frac{2c}{l} \frac{(-1)^n}{\omega_n^2} \cos\left(\frac{\omega_n x}{c}\right) \int_0^t \ddot{y}(\tau) \sin(\omega_n(t-\tau)) d\tau. \quad (5.5)$$

Differentiation of Eq. 5.5 with respect to x gives the contribution of the n^{th} mode to the strain:

$$\frac{\partial u_n}{\partial x}(x, t) = \frac{2}{l} \frac{(-1)^{n+1}}{\omega_n} \sin\left(\frac{\omega_n x}{c}\right) \int_0^t \ddot{y}(\tau) \sin(\omega_n(t-\tau)) d\tau. \quad (5.6)$$

It is noted that strain for a continuous model is analogous to the interfloor displacement of a model of a structure.

The contribution of the n^{th} mode to the shear force is obtained by multiplying Eq. 5.6 by K_o :

$$K_o \frac{\partial u_n}{\partial x}(x, t) = \frac{2K_o}{l} \frac{(-1)^{n+1}}{\omega_n} \sin\left(\frac{\omega_n x}{c}\right) \int_0^t \ddot{y}(\tau) \sin(\omega_n(t-\tau)) d\tau. \quad (5.7)$$

From Eq. 5.2 it is seen that the total acceleration is given by

$$\frac{\partial^2 u}{\partial t^2}(x, t) + \ddot{y}(t) = c^2 \frac{\partial^2 u}{\partial x^2}(x, t) \quad (5.8)$$

and the n^{th} modal contribution to the total acceleration is*

$$c^2 \frac{\partial^2 u_n}{\partial x^2}(x, t) = \frac{2c}{l} (-1)^{n+1} \cos\left(\frac{\omega_n x}{c}\right) \int_0^t \ddot{y}(\tau) \sin(\omega_n(t-\tau)) d\tau. \quad (5.9)$$

By taking the maximum value over time of the absolute value of Eqs. 5.5, 5.6, 5.7 and 5.9, one finds the maximum absolute value of the n^{th} modal contribution to each response for a given position $(\frac{x}{l})$ in the beam. Note that a term common to all of these equations is the maximum over time of the absolute value of the integral

$$S_v(\omega_n) = \max_{0 < t} \int_0^t \ddot{y}(\tau) \sin(\omega_n(t-\tau)) d\tau \quad (5.10)$$

which is sometimes called the "spectral velocity." Physically,

*Absolute convergence of this series is discussed below.

$S_v(\omega_n)$ is the absolute value of the maximum pseudo-velocity for an undamped single degree of freedom oscillator with a natural frequency ω_n (or period T_n)* subjected to an earthquake accelerogram $\ddot{y}(t)$. Curves of $S_v(T)$ vs. period T have been made for an ensemble of earthquakes with several damping factors.⁽⁹⁾ By averaging $S_v(T)$ over the ensemble, average spectral pseudo-velocity curves are obtained which are shown in Fig. 4.3. From these curves one can find the average over an ensemble of earthquakes of the maximum absolute value of the pseudo-velocity of a single degree of freedom oscillator with a given period and fraction of critical damping.

Hence, the average maximum absolute values of the n^{th} modal contributions to the various responses are as follows:

for displacement:

$$\left| u_n(x) \right|_{\max_{0 < t}} = \frac{2\ell}{c} \frac{4}{\pi^2 (2n-1)^2} \cos\left(\frac{\omega_n x}{c}\right) S_v(\omega_n) \quad (5.11)$$

for strain:

$$\left| \frac{\partial u_n}{\partial x}(x) \right|_{\max_{0 < t}} = \frac{2}{c} \frac{2}{\pi(2n-1)} \sin\left(\frac{\omega_n x}{c}\right) S_v(\omega_n) \quad (5.12)$$

*For linear systems "pseudo-velocity" equals the displacement times the natural frequency. Studies comparing pseudo-velocity spectra to velocity spectra for a one degree of freedom linear system excited by an ensemble of earthquakes have been performed by C. V. Chelapati, reference 15.

for shear force:

$$\overline{\left| K_o \frac{\partial u_n}{\partial x}(x) \right|}_{\max_{0 < t}} = \frac{2K_o}{c} \frac{2}{\pi(2n-1)} \sin\left(\frac{\omega_n x}{c}\right) S_v(\omega_n) \quad (5.13)$$

and for total acceleration:

$$\overline{\left| c^2 \frac{\partial^2 u_n}{\partial x^2}(x) \right|}_{\max_{0 < t}} = \frac{2c}{l} \cos\left(\frac{\omega_n x}{c}\right) S_v(\omega_n) . \quad (5.14)$$

In Fig. 5.3 it is seen that for periods greater than 0.3 seconds (frequency less than $\frac{2\pi}{0.3}$ radians per second) and for very lightly damped systems the average spectral velocity $S_v(\omega)$ is approximately a constant, to be denoted by \bar{S}_v . Since the periods of only the first five modes of the A/20/2.2/2/6 structure are larger than 0.3 sec, only the first five modes of the continuous beams are considered below.

Looking again at Fig. 5.3, one sees that for periods less than 0.3 sec, as the periods approach zero ($\omega \rightarrow \infty$), the average spectral velocity $S_v(\omega)$ decreases approximately in proportion to T . From Eq. 5.4 then,

$$S_v(\omega_n) \sim \frac{1}{n} .$$

This rate of decrease of $S_v(\omega_n)$ is sufficient to ensure absolute convergence of summations of Eqs. 5.5, 5.6, and 5.7 for displacement, strain, and shear force. However, there may be some

question of the absolute convergence of a summation of Eq. 5.9 in order to obtain the total acceleration, even though the average maximum absolute contribution of the n^{th} mode does decrease as (n) increases beyond some value. By assuming that the base excitation $\ddot{y}(t)$ has a bounded frequency spectrum, absolute convergence can be assured.

In order to show more explicitly the dependence of the average maximum absolute values of these responses upon position in the uniform beam, Eqs. 5.11, 5.12, 5.13, and 5.14 are evaluated at seven different positions in the beam with $S_v(\omega_n)$ replaced by \bar{S}_v . The results are tabulated in Tables 5-2, 5-4, 5-6, and 5-8. From these tables several general trends are seen regarding the dependencies of the various responses upon the modes and upon the position $(\frac{x}{L})$ in the beam.

Table 5-2 shows that the displacements can be expected to be dominated by the first two or three modes, particularly in the upper portion of the beam. In Tables 5-4 and 5-6 it is seen that the strains and shear forces in the lower portion of a uniform beam are highly dependent on the first few modes, while in the upper portion many modes can be expected to contribute significantly.

From Table 5-8 for the total acceleration it is seen that throughout the structure all modes can be expected to contribute. Note, however, that near the base of the beam the expected contribution of the first mode is the smallest of the first five modes.

In order to show the effect of taper on the response of a continuous cantilever beam, subjected to earthquake excitation, the

beam of Fig. 5.2 is examined.

In this case, the stiffness $K(x)$ and the density per unit length $\gamma(x)$ are functions of x :

$$K(x) = K_0 \frac{x}{l}$$

$$\gamma(x) = \gamma_0 \frac{x}{l} .$$

However, the velocity of wave propagation, c , is constant since

$$\frac{1}{c^2} = \frac{\gamma(x)}{K(x)} = \frac{\gamma_0}{K_0} .$$

By substituting these values into the general shear beam equation, Eq. 5.1, the equation for the tapered beam is obtained:

$$\frac{1}{x} \frac{\partial}{\partial x} \left(x \frac{\partial u}{\partial x} (x, t) \right) - \frac{1}{c^2} \frac{\partial^2 u}{\partial t^2} (x, t) = \frac{1}{c^2} \ddot{y} \quad (5.15)$$

with the same boundary conditions:

$$\text{at } x = 0 , \quad \frac{\partial u}{\partial x} = 0 ; \quad \text{and}$$

$$\text{at } x = l , \quad u = 0 .$$

The solution of this eigenvalue problem with zero initial conditions is

$$u(x, t) = -\frac{2c}{l} \sum_{n=1}^{\infty} \frac{1}{\omega_n^2} \frac{J_0\left(\frac{\omega_n x}{c}\right)}{J_1\left(\frac{\omega_n l}{c}\right)} \int_0^t \ddot{y}(\tau) \sin(\omega_n(t-\tau)) d\tau \quad (5.16)$$

and the frequency equation is

$$J_0\left(\frac{\omega_n \ell}{c}\right) = 0 \quad . \quad (5.17)$$

The roots of the Bessel function J_0 are given in Table 5-1.

TABLE 5-1

Natural Frequencies of Uniform and Tapered Beams

| n | Uniform Beam | | Tapered Beam | |
|---|--|------------------|---|------------------|
| | $\cos\left(\frac{\omega_n \ell}{c}\right) = 0$ | Frequency Ratios | $J_0\left(\frac{\omega_n \ell}{c}\right) = 0$ | Frequency Ratios |
| | $\left(\frac{\omega_n \ell}{c}\right)$ | | $\left(\frac{\omega_n \ell}{c}\right)$ | |
| 1 | 1.57 | 1 | 2.4 | 1.00 |
| 2 | 4.71 | 3 | 5.52 | 2.30 |
| 3 | 7.85 | 5 | 8.65 | 3.61 |
| 4 | 10.99 | 7 | 11.8 | 4.92 |
| 5 | 14.13 | 9 | 14.9 | 6.21 |
| 6 | 17.27 | 11 | 18.1 | 7.54 |

Again, because the primary interest is in making comparisons between the average maximum absolute values of the individual modal contributions, the n^{th} terms of the various responses are discussed.

From Eq. 5.16, the n^{th} term of the displacement for the tapered beam is

$$u_n(x,t) = -\frac{2c}{l} \frac{1}{\omega_n} \frac{J_0\left(\frac{\omega_n x}{c}\right)}{J_1\left(\frac{\omega_n l}{c}\right)} \int_0^t \ddot{y}(\tau) \sin(\omega_n(t-\tau)) d\tau. \quad (5.18)$$

By differentiating Eq. 5.18 with respect to x , the n^{th} modal contribution to the strain is obtained:

$$\frac{\partial u_n}{\partial x}(x,t) = \frac{2}{l} \frac{1}{\omega_n} \frac{J_1\left(\frac{\omega_n x}{c}\right)}{J_1\left(\frac{\omega_n l}{c}\right)} \int_0^t \ddot{y}(\tau) \sin(\omega_n(t-\tau)) d\tau. \quad (5.19)$$

The contribution of the n^{th} mode to the shear force in a tapered beam is found by multiplying Eq. 5.19 by $K_o \cdot \frac{x}{l}$:

$$K_o \frac{x}{l} \frac{\partial u_n}{\partial x}(x,t) = \frac{x}{l} \frac{2K_o}{l} \frac{1}{\omega_n} \frac{J_1\left(\frac{\omega_n x}{c}\right)}{J_1\left(\frac{\omega_n l}{c}\right)} \int_0^t \ddot{y}(\tau) \sin(\omega_n(t-\tau)) d\tau. \quad (5.20)$$

From Eq. 5.15 it is seen that the total acceleration for the tapered beam is given by

$$\frac{\partial^2 u}{\partial t^2}(x,t) + \ddot{y}(t) = \frac{c^2}{x} \frac{\partial}{\partial x} \left(x \frac{\partial u(x,t)}{\partial x} \right). \quad (5.21)$$

Hence, the n^{th} modal contribution to the total acceleration is*

$$\frac{c^2}{x} \frac{\partial}{\partial x} \left(x \frac{\partial u_n}{\partial x}(x,t) \right) = \frac{2c}{l} \frac{J_0\left(\frac{\omega_n x}{c}\right)}{J_1\left(\frac{\omega_n l}{c}\right)} \int_0^t \ddot{y}(\tau) \sin(\omega_n(t-\tau)) d\tau. \quad (5.22)$$

*See p.100 for discussion of absolute convergence of this series.

By taking the maximum over time of the absolute value of Eqs. 5.18, 5.19, 5.20 and 5.22; using Eq. 5.10; and letting $z_n = \frac{\omega_n \ell}{c}$; the average maximum absolute values of the contributions of the n^{th} mode to the various responses are obtained:

for displacement:

$$\overline{|u_n(x)|}_{\max_{0 < t}} = \frac{2\ell}{c} \frac{1}{z_n^2} \frac{|J_1(z_n \frac{x}{\ell})|}{|J_1(z_n)|} S_v(\omega_n) , \quad (5.23)$$

for strain:

$$\overline{\left| \frac{\partial u_n(x)}{\partial x} \right|}_{\max_{0 < t}} = \frac{2}{c} \frac{1}{z_n} \frac{|J_1(z_n \frac{x}{\ell})|}{|J_1(z_n)|} S_v(\omega_n) , \quad (5.24)$$

for the shear force:

$$\overline{\left| K_o \frac{x}{\ell} \frac{\partial u_n(x)}{\partial x} \right|}_{\max_{0 < t}} = \frac{x}{\ell} \frac{2K_o}{c} \frac{1}{z_n} \frac{|J_1(z_n \frac{x}{\ell})|}{|J_1(z_n)|} S_v(\omega_n) , \quad (5.25)$$

and for total acceleration:

$$\overline{\left| \frac{c}{x} \frac{\partial}{\partial x} \left(x \frac{\partial u_n(x)}{\partial x} \right) \right|}_{\max_{0 < t}} = \frac{2c}{\ell} \frac{|J_o(z_n \frac{x}{\ell})|}{|J_1(z_n)|} S_v(\omega_n) . \quad (5.26)$$

In order to show the dependencies of displacements, strains, shear forces, and total accelerations upon the first five modes and upon the position $(\frac{x}{l})$ in the tapered beam, Eq. 5.23, 5.24, 5.25 and 5.26 with $S_v(\omega_n)$ replaced by $\overline{S_v}$ have been tabulated in Tables 5-3, 5-5, 5-7 and 5-9. The general trends regarding the dependencies of the responses upon the modes of and upon the position $(\frac{x}{l})$ in the tapered beam are approximately the same as for the uniform beam with two exceptions. These exceptions are the increased emphasis on the higher modes in all of the responses in the tapered beam and the fact that the shear force in the tapered beam is proportional to

$$\frac{x}{l} \left(\frac{\partial u}{\partial x} \right)$$

whereas the shear force in the uniform beam is directly proportional to the strain.

The total acceleration coefficients of the uniform and tapered beams in Tables 5-8 and 5-9 are interesting since they indicate that each of the first five modes of the uniform beam can be expected to contribute about the same amount, except near the base where the contribution of the first mode becomes small. At the top of the tapered beam, however, the higher modes can be expected to dominate the total acceleration.

It appears, then, that a mass particle at the top of a severely tapered structure can be expected to feel very high accelerations. Furthermore, since it is more closely related to strain than to

TABLE 5-2

Displacement Coefficients of $\frac{2l}{c} \bar{S}_v$
for Uniform Beam from Eq. 5.11

| $\frac{x}{l}$ | Mode | | | | |
|---------------|-------|-------|-------|-------|-------|
| | 1 | 2 | 3 | 4 | 5 |
| 0.0 | 0.405 | 0.045 | 0.016 | 0.008 | 0.005 |
| 0.167 | 0.391 | 0.032 | 0.004 | 0.002 | 0.004 |
| 0.333 | 0.351 | 0.000 | 0.014 | 0.007 | 0.000 |
| 0.500 | 0.287 | 0.032 | 0.011 | 0.006 | 0.004 |
| 0.667 | 0.203 | 0.045 | 0.008 | 0.004 | 0.005 |
| 0.833 | 0.105 | 0.032 | 0.016 | 0.008 | 0.004 |
| 1.000 | 0.000 | 0.000 | 0.000 | 0.000 | 0.000 |

Displacement Coefficients of $\frac{2l}{c} \bar{S}_v$
Normalized to Coefficients of Mode 1

| $\frac{x}{l}$ | Mode | | | | |
|---------------|-------|-------|-------|-------|-------|
| | 1 | 2 | 3 | 4 | 5 |
| 0.0 | 1.000 | 0.111 | 0.040 | 0.020 | 0.012 |
| 0.167 | 1.000 | 0.081 | 0.011 | 0.005 | 0.009 |
| 0.333 | 1.000 | 0.000 | 0.040 | 0.020 | 0.000 |
| 0.500 | 1.000 | 0.111 | 0.040 | 0.020 | 0.012 |
| 0.667 | 1.000 | 0.222 | 0.040 | 0.020 | 0.025 |
| 0.833 | 1.000 | 0.304 | 0.149 | 0.076 | 0.034 |
| 1.000 | 0.000 | 0.000 | 0.000 | 0.000 | 0.000 |

TABLE 5-3

Displacement Coefficients of $\frac{2\ell}{c}\bar{S}_v$
for Tapered Beam from Eq. 5.23

| $\frac{x}{l}$ | Mode | | | | |
|---------------|-------|-------|-------|-------|-------|
| | 1 | 2 | 3 | 4 | 5 |
| 0.0 | 0.333 | 0.096 | 0.049 | 0.031 | 0.022 |
| 0.167 | 0.320 | 0.077 | 0.027 | 0.008 | 0.001 |
| 0.333 | 0.282 | 0.031 | 0.011 | 0.012 | 0.004 |
| 0.500 | 0.223 | 0.016 | 0.018 | 0.004 | 0.006 |
| 0.667 | 0.151 | 0.038 | 0.004 | 0.006 | 0.005 |
| 0.833 | 0.074 | 0.029 | 0.014 | 0.007 | 0.003 |
| 1.000 | 0.000 | 0.000 | 0.000 | 0.000 | 0.000 |

Displacement Coefficients of $\frac{2\ell}{c}\bar{S}_v$
Normalized to Coefficients of Mode 1

| $\frac{x}{l}$ | Mode | | | | |
|---------------|-------|-------|-------|-------|-------|
| | 1 | 2 | 3 | 4 | 5 |
| 0.0 | 1.000 | 0.290 | 0.148 | 0.093 | 0.065 |
| 0.167 | 1.000 | 0.241 | 0.084 | 0.024 | 0.003 |
| 0.333 | 1.000 | 0.108 | 0.038 | 0.044 | 0.014 |
| 0.500 | 1.000 | 0.073 | 0.079 | 0.017 | 0.026 |
| 0.667 | 1.000 | 0.254 | 0.027 | 0.042 | 0.035 |
| 0.833 | 1.000 | 0.387 | 0.196 | 0.098 | 0.040 |
| 1.000 | 0.000 | 0.000 | 0.000 | 0.000 | 0.000 |

TABLE 5-4

Strain Coefficients of $\frac{2}{c} \bar{S}_v$
for Uniform Beam from Eq. 5.12

| $\frac{x}{l}$ | Mode | | | | |
|---------------|-------|-------|-------|-------|-------|
| | 1 | 2 | 3 | 4 | 5 |
| 0.0 | 0.000 | 0.000 | 0.000 | 0.000 | 0.000 |
| 0.167 | 0.165 | 0.150 | 0.123 | 0.088 | 0.050 |
| 0.333 | 0.318 | 0.212 | 0.064 | 0.045 | 0.071 |
| 0.500 | 0.450 | 0.150 | 0.090 | 0.064 | 0.050 |
| 0.667 | 0.551 | 0.000 | 0.110 | 0.079 | 0.000 |
| 0.833 | 0.615 | 0.150 | 0.033 | 0.024 | 0.050 |
| 1.000 | 0.637 | 0.212 | 0.127 | 0.091 | 0.071 |

Strain Coefficients of $\frac{2}{c} \bar{S}_v$
Normalized to Coefficients of Mode 1

| $\frac{x}{l}$ | Mode | | | | |
|---------------|-------|-------|-------|-------|-------|
| | 1 | 2 | 3 | 4 | 5 |
| 0.0 | 0.000 | 0.000 | 0.000 | 0.000 | 0.000 |
| 0.167 | 1.000 | 0.911 | 0.746 | 0.533 | 0.304 |
| 0.333 | 1.000 | 0.667 | 0.200 | 0.143 | 0.222 |
| 0.500 | 1.000 | 0.333 | 0.200 | 0.143 | 0.111 |
| 0.667 | 1.000 | 0.000 | 0.200 | 0.143 | 0.000 |
| 0.833 | 1.000 | 0.244 | 0.054 | 0.038 | 0.081 |
| 1.000 | 1.000 | 0.333 | 0.200 | 0.143 | 0.111 |

TABLE 5-5

Strain Coefficients of $\frac{2}{c} \bar{S}_v$
for Tapered Beams from Eq. 5.24

| $\frac{x}{l}$ | Mode | | | | |
|---------------|-------|-------|-------|-------|-------|
| | 1 | 2 | 3 | 4 | 5 |
| 0.000 | 0.000 | 0.000 | 0.000 | 0.000 | 0.000 |
| 0.167 | 0.157 | 0.220 | 0.234 | 0.211 | 0.162 |
| 0.333 | 0.296 | 0.310 | 0.162 | 0.014 | 0.105 |
| 0.500 | 0.400 | 0.225 | 0.077 | 0.108 | 0.041 |
| 0.667 | 0.457 | 0.033 | 0.134 | 0.078 | 0.018 |
| 0.833 | 0.462 | 0.137 | 0.025 | 0.032 | 0.057 |
| 1.000 | 0.416 | 0.181 | 0.116 | 0.085 | 0.067 |

Strain Coefficients of $\frac{2}{c} \bar{S}_v$
Normalized to Coefficients of Mode 1

| $\frac{x}{l}$ | Mode | | | | |
|---------------|-------|-------|-------|-------|-------|
| | 1 | 2 | 3 | 4 | 5 |
| 0.000 | 0.000 | 0.000 | 0.000 | 0.000 | 0.000 |
| 0.167 | 1.000 | 1.398 | 1.486 | 1.342 | 1.030 |
| 0.333 | 1.000 | 1.047 | 0.548 | 0.048 | 0.356 |
| 0.500 | 1.000 | 0.563 | 0.192 | 0.270 | 0.103 |
| 0.667 | 1.000 | 0.072 | 0.294 | 0.170 | 0.039 |
| 0.833 | 1.000 | 0.296 | 0.053 | 0.068 | 0.123 |
| 1.000 | 1.000 | 0.436 | 0.278 | 0.204 | 0.161 |

TABLE 5-6

Shear Force Coefficients of $\frac{2K_o}{c} \bar{S}_v$
for Uniform Beam from Eq. 5.13

| $\frac{x}{l}$ | Mode | | | | |
|---------------|-------|-------|-------|-------|-------|
| | 1 | 2 | 3 | 4 | 5 |
| 0.000 | 0.000 | 0.000 | 0.000 | 0.000 | 0.000 |
| 0.167 | 0.165 | 0.150 | 0.123 | 0.088 | 0.050 |
| 0.333 | 0.318 | 0.212 | 0.064 | 0.045 | 0.071 |
| 0.500 | 0.450 | 0.150 | 0.090 | 0.064 | 0.050 |
| 0.667 | 0.551 | 0.000 | 0.110 | 0.079 | 0.000 |
| 0.833 | 0.615 | 0.150 | 0.033 | 0.024 | 0.050 |
| 1.000 | 0.637 | 0.212 | 0.127 | 0.091 | 0.071 |

Shear Force Coefficients of $\frac{2K_o}{c} \bar{S}_v$
Normalized to Coefficients of Mode 1

| $\frac{x}{l}$ | Mode | | | | |
|---------------|-------|-------|-------|-------|-------|
| | 1 | 2 | 3 | 4 | 5 |
| 0.000 | 0.000 | 0.000 | 0.000 | 0.000 | 0.000 |
| 0.167 | 1.000 | 0.911 | 0.746 | 0.533 | 0.304 |
| 0.333 | 1.000 | 0.667 | 0.200 | 0.143 | 0.222 |
| 0.500 | 1.000 | 0.333 | 0.200 | 0.143 | 0.111 |
| 0.667 | 1.000 | 0.000 | 0.200 | 0.143 | 0.000 |
| 0.833 | 1.000 | 0.244 | 0.054 | 0.038 | 0.081 |
| 1.000 | 1.000 | 0.333 | 0.200 | 0.143 | 0.111 |

TABLE 5-7
 Shear Force Coefficients of $\frac{2K}{c} \bar{S}_v$
 for Tapered Beam from Eq. 5.25

| $\frac{x}{l}$ | Mode | | | | |
|---------------|-------|-------|-------|-------|-------|
| | 1 | 2 | 3 | 4 | 5 |
| 0.000 | 0.000 | 0.000 | 0.000 | 0.000 | 0.000 |
| 0.167 | 0.026 | 0.037 | 0.039 | 0.035 | 0.027 |
| 0.333 | 0.099 | 0.103 | 0.054 | 0.005 | 0.035 |
| 0.500 | 0.200 | 0.113 | 0.038 | 0.054 | 0.021 |
| 0.667 | 0.304 | 0.022 | 0.090 | 0.052 | 0.012 |
| 0.833 | 0.385 | 0.114 | 0.020 | 0.026 | 0.047 |
| 1.000 | 0.416 | 0.181 | 0.116 | 0.085 | 0.067 |

Shear Force Coefficients of $\frac{2K}{c} \bar{S}_v$
 Normalized to Coefficients of Mode 1

| $\frac{x}{l}$ | Mode | | | | |
|---------------|-------|-------|-------|-------|-------|
| | 1 | 2 | 3 | 4 | 5 |
| 0.000 | 0.000 | 0.000 | 0.000 | 0.000 | 0.000 |
| 0.167 | 1.000 | 1.398 | 1.486 | 1.342 | 1.030 |
| 0.333 | 1.000 | 1.047 | 0.548 | 0.048 | 0.356 |
| 0.500 | 1.000 | 0.563 | 0.192 | 0.270 | 0.103 |
| 0.667 | 1.000 | 0.072 | 0.294 | 0.170 | 0.039 |
| 0.833 | 1.000 | 0.296 | 0.053 | 0.068 | 0.123 |
| 1.000 | 1.000 | 0.436 | 0.278 | 0.204 | 0.161 |

TABLE 5-8

Total Acceleration Coefficients of $\frac{2c}{l} \bar{S}_v$
for Uniform Beam from Eq. 5.14

| $\frac{x}{l}$ | Mode | | | | |
|---------------|-------------------------------|-------|-------|-------|-------|
| | 1 | 2 | 3 | 4 | 5 |
| 0.000 | 1.000 | 1.000 | 1.000 | 1.000 | 1.000 |
| 0.167 | 0.966 | 0.707 | 0.259 | 0.259 | 0.707 |
| 0.333 | 0.866 | 0.000 | 0.866 | 0.866 | 0.000 |
| 0.500 | 0.707 | 0.707 | 0.707 | 0.707 | 0.707 |
| 0.667 | 0.500 | 1.000 | 0.500 | 0.500 | 1.000 |
| 0.833 | 0.259 | 0.707 | 0.966 | 0.966 | 0.707 |
| 1.000 | ----- base acceleration ----- | | | | |

Total Acceleration Coefficients of $\frac{2c}{l} \bar{S}_v$
Normalized to Coefficients of Mode 1

| $\frac{x}{l}$ | Mode | | | | |
|---------------|-------------------------------|-------|-------|-------|-------|
| | 1 | 2 | 3 | 4 | 5 |
| 0.000 | 1.000 | 1.000 | 1.000 | 1.000 | 1.000 |
| 0.167 | 1.000 | 0.732 | 0.268 | 0.268 | 0.732 |
| 0.333 | 1.000 | 0.000 | 1.000 | 1.000 | 0.000 |
| 0.500 | 1.000 | 1.000 | 1.000 | 1.000 | 1.000 |
| 0.667 | 1.000 | 2.000 | 1.000 | 1.000 | 2.000 |
| 0.833 | 1.000 | 2.732 | 3.732 | 3.732 | 2.732 |
| 1.000 | ----- base acceleration ----- | | | | |

TABLE 5-9

Total Acceleration Coefficients of $\frac{2c}{l}\bar{S}_v$
for Tapered Beam from Eq. 5.26

| $\frac{x}{l}$ | Mode | | | | |
|---------------|-----------------------------|-------|-------|-------|-------|
| | 1 | 2 | 3 | 4 | 5 |
| 0.000 | 1.926 | 2.939 | 3.684 | 4.302 | 4.842 |
| 0.167 | 1.850 | 2.349 | 2.003 | 1.049 | 0.206 |
| 0.333 | 1.629 | 0.931 | 0.805 | 1.724 | 0.896 |
| 0.500 | 1.290 | 0.495 | 1.312 | 0.520 | 1.311 |
| 0.667 | 0.874 | 1.170 | 0.302 | 0.872 | 1.180 |
| 0.833 | 0.427 | 0.870 | 1.085 | 1.009 | 0.664 |
| 1.000 | -----base acceleration----- | | | | |

Total Acceleration Coefficients of $\frac{2c}{l}\bar{S}_v$
Normalized to Coefficients of Mode 1

| $\frac{x}{l}$ | Mode | | | | |
|---------------|-----------------------------|-------|-------|-------|-------|
| | 1 | 2 | 3 | 4 | 5 |
| 0.000 | 1.000 | 1.526 | 1.912 | 2.233 | 2.513 |
| 0.167 | 1.000 | 1.270 | 1.083 | 0.567 | 0.112 |
| 0.333 | 1.000 | 0.571 | 0.494 | 1.058 | 0.550 |
| 0.500 | 1.000 | 0.384 | 1.017 | 0.403 | 1.016 |
| 0.667 | 1.000 | 1.339 | 0.346 | 0.998 | 1.350 |
| 0.833 | 1.000 | 2.039 | 2.541 | 2.365 | 1.555 |
| 1.000 | -----base acceleration----- | | | | |

displacement, structural damage appears to be more dependent upon the higher modes than upon the lower ones, particularly in the upper portion of a severely tapered structure.

From these tables of response coefficients it can be concluded that in order to minimize the strains and total accelerations in a structure, particularly in the upper portion, it is best to have the stiffness and mass distributions as uniform as possible.

It is also clear from these tables that the extent to which "higher modes" are important depends upon the response of interest, the taper of the structure, and the position within the structure.

Often an analogy is made between either excessive displacements (relative to ground), structural damage, or total accelerations near the top of a building and an energy pulse traveling toward and being reflected from the tip of a whip. These phenomena are said to result from "whiplash" of the structure. Since structural damage and total acceleration are directly related to excessive interfloor displacement and do not necessarily result from large displacements, a suggested definition of "whiplash" in structures is the magnitude of the interfloor displacements.

5.3 Modal Analysis of Discretized Models of Tall Structures

The application of eigenvalue theory to the discretized model of a structure is covered in this section. Using the equations developed here, a computer program subroutine was written which determines the "equivalent" modal participation factors, "equivalent"

modal contributions to the displacements and "equivalent" modal contributions to the interfloor displacements for arbitrarily selected floors in the structure. Using such results a comparison can be made with the results for the continuous beams.

Usually, modal analysis is restricted to structures that remain linear. However, modal analysis can also be useful for structures which yield. Since the eigenvectors of the linear structure form a complete set of base vectors, it is possible to expand any displacement vector in terms of these eigenvectors in order to find what will be called the "equivalent" modal participation factors. These factors can then be used to find "equivalent" modal contributions to the displacements and to the interfloor displacements. In this sense, the concept of the modal participation factor has the same significance for a yielding structure as for a linear one.

It should be noted that, for the excitation used, all of the columns in the A/20/2.2/2/6 structure remain linear except for those between the upper two or three floors. Furthermore, all of the girders yield--but not necessarily all at the same time. Hence, from an overall point of view, the structure is reasonably linear when compared to one in which all of the girders and columns yield at the same time.

The eigenvectors of a linear structure with N floors are found as follows: The homogeneous equation of motion is

$$M\ddot{\underline{u}} + K\underline{u} = 0 \quad (5.27)$$

where

\underline{u} : displacement vector $(N \times 1)$,

M : diagonal mass matrix $(N \times N)$, and

K : symmetric and positive definite stiffness matrix $(N \times N)$.

Letting

$$\underline{u} = M^{-\frac{1}{2}} \underline{\xi} \quad (5.28)$$

and premultiplying by $M^{-\frac{1}{2}}$, Eq. 5.27 becomes

$$I \ddot{\underline{\xi}} + \bar{K} \underline{\xi} = 0 \quad (5.29)$$

where

$$\bar{K} = M^{-\frac{1}{2}} K M^{-\frac{1}{2}} .$$

Since \bar{K} is symmetric and positive definite, a theorem of matrix algebra guarantees the existence of a unitary transformation matrix ϕ such that

$$\phi^T \phi = I \quad \text{and} \quad \phi^T \bar{K} \phi = \begin{bmatrix} \omega_n^2 & \\ & \ddots \end{bmatrix} . \quad (5.30)$$

Therefore, letting

$$\underline{\xi} = \phi \underline{\eta} \quad (5.31)$$

and premultiplying by ϕ^T , Eq. 5.29 becomes

$$\ddot{\underline{\eta}} + \begin{bmatrix} \omega_n^2 & \\ & \ddots \end{bmatrix} \underline{\eta} = 0 \quad (5.32)$$

which is a diagonalized, or separated equation. That is, the solution for the n^{th} modal participation factor η_n is independent of every other mode.

By substituting Eq. 5.31 into Eq. 5.28, an equation relating the displacement vector, \underline{u} , to the modal participation factors, $\underline{\eta}$ is obtained:

$$\underline{u} = M^{-\frac{1}{2}} \phi \underline{\eta} . \quad (5.33)$$

The inverse of Eq. 5.33 is

$$\underline{\eta} = \phi^T M^{+\frac{1}{2}} \underline{u} . \quad (5.34)$$

Equations 5.33 and 5.34 are the ones used in the modal analysis of a tall structure.

As discussed in Section 3.5, a direct integration method is used in the computer program to solve the equations of motion for the yielding structure. Then, knowing the displacement vector \underline{u} , Eq. 5.34 is used to find the vector, $\underline{\eta}$, of "equivalent" modal participation factors. For η_n , Eq. 5.34 becomes

$$\eta_n = \sum_{k=1}^{20} \phi_{kn} M_k^{+\frac{1}{2}} u_k \quad (5.35)$$

for a structure with 20 floors. Similarly, for the displacement, u_j , of the j^{th} floor, Eq. 5.33 becomes

$$u_j = \sum_{n=1}^{20} M_j^{-\frac{1}{2}} \phi_{jn} \eta_n . \quad (5.36)$$

Consequently, after obtaining η_n , the "equivalent" contribution of the n^{th} mode to the displacement of the j^{th} floor, u_{jn} , is found

from

$$u_{jn} = M_j^{-\frac{1}{2}} \phi_{jn} \eta_n . \quad (5.37)$$

Using Eq. 5.37, the "equivalent" contribution of the n^{th} mode to the interfloor displacement, UU_{jn} ,* between floors (j) and (j+1) is found by subtraction:

$$UU_{jn} = u_{jn} - u_{(j+1)n} \quad (5.38)$$

As mentioned earlier, the interfloor displacement of the discretized structure corresponds to the strain in a continuous beam.

Only one modal analysis study of a yielding structure was made on the computer because of the extensive time involved.** In this study the A/20/2.2/2/6 structure with 0.0035 fraction of critical damping*** in the first mode was subjected to the four seconds of the El Centro Earthquake (N-S) of 18 May 1940. Furthermore, the two-component beam model described in Appendix C and the yield criteria with the "test bending moment" described in Appendix B were used. Although the beam model and yield criteria were later

* UU is the Fortran name for interfloor displacement. Also, $j = 2$ at the top floor (roof) and $j = 22$ at the ground level. See Section 3.2 for more details of notation.

** The modal analysis is performed by subroutine MODE, which is optional. A listing of this subroutine is provided in Appendix E--Listing of the Computer Program.

*** This fraction of critical damping is believed to be the same as that used by Clough and Benuska for their studies with essentially no damping in the FHA Study (reference 1).

TABLE 5-10
Modal Contributions to the Largest Displacements for the A/20/2.2/2/6 Structure

| Floor | $\frac{x}{l}$ | Mode | | | | | | | Time of Occurrence |
|-------|---------------|--------|-------|--------|--------|--------|--------|--------|--------------------|
| | | 1 | 2 | 3 | 4 | 5 | 6 | 7 | |
| 19 | .05 | -12.54 | +8.41 | -.640 | -.120 | +0.065 | +0.013 | -.035 | 3.155 sec |
| 14 | .30 | -9.52 | -.121 | +0.316 | +0.076 | +0.143 | -.042 | -.254 | 3.230 sec |
| 9 | .55 | -5.93 | -.597 | -.133 | -.136 | -.154 | +0.014 | +0.044 | 3.155 sec |
| 4 | .80 | -2.058 | -.331 | -.713 | +0.063 | +0.135 | +0.035 | +0.007 | 3.010 sec |

Modal Contributions Normalized to the Contribution of the First Mode

| Floor | $\frac{x}{l}$ | Mode | | | | | | |
|-------|---------------|------|------|------|------|------|------|------|
| | | 1 | 2 | 3 | 4 | 5 | 6 | 7 |
| 19 | .05 | 1.00 | .067 | .051 | .010 | .005 | .001 | .003 |
| 14 | .30 | 1.00 | .013 | .033 | .008 | .015 | .004 | .027 |
| 9 | .55 | 1.00 | .101 | .022 | .023 | .026 | .002 | .007 |
| 4 | .80 | 1.00 | .161 | .346 | .031 | .066 | .017 | .003 |

TABLE 5-11

Modal Contributions to the Largest Inter-floor Displacements for the A/20/2.2/2/6 Structure

| Between Floors | $\frac{x}{l}$ | Mode | | | | | | | Interfloor Displacement (inches) | Time of Occurrence |
|-------------------|---------------|-------|-------|-------|-------|-------|-------|-------|--|-----------------------|
| | | 1 | 2 | 3 | 4 | 5 | 6 | 7 | | |
| 18-19 | .08 | -.038 | -.132 | -.373 | -.360 | -.199 | +.120 | +.020 | -1.11 | 2.525 sec |
| 13-14 | .33 | -.662 | +.122 | +.035 | +.106 | -.041 | -.053 | +.032 | - .519 | 3.210 sec |
| 8- 9 | .58 | -.685 | -.001 | -.018 | -.103 | +.012 | +.019 | +.062 | - .756 | 3.335 sec |
| 3- 4 | .83 | -.617 | -.085 | -.080 | +.011 | -.020 | -.039 | -.026 | - .957 | 3.160 sec |

121

Modal Contributions Normalized to the Contribution of the First Mode

| Between Floors | $\frac{x}{l}$ | Mode | | | | | | |
|-------------------|---------------|------|-------|-------|-------|-------|-------|------|
| | | 1 | 2 | 3 | 4 | 5 | 6 | 7 |
| 18-19 | .08 | 1.00 | 3.478 | 9.847 | 9.488 | 5.256 | 3.161 | .536 |
| 13-14 | .33 | 1.00 | .184 | .053 | .160 | .062 | .080 | .048 |
| 8- 9 | .58 | 1.00 | .001 | .026 | .151 | .017 | .027 | .090 |
| 3- 4 | .83 | 1.00 | .137 | .130 | .018 | .032 | .064 | .042 |

refined (see Chapter II and Appendix C, respectively), it is felt that the general trends of the results presented below are, nevertheless, correct.

The entries in Table 5-10 are the "equivalent" modal contributions to the displacements of the arbitrarily selected floors at the time when the entire displacement (not each modal contribution) reaches its maximum absolute value. Similarly, the entries in Table 5-11 are the "equivalent" modal contributions to the selected interfloor displacements at the time when the entire interfloor displacement (not each modal contribution) reaches its maximum absolute value. Hence, Tables 5-10 and 5-11 are not directly comparable to the corresponding tables for the continuous beams.

At various times during this study, modes as high as the eighth were found to contribute as much as 2% to the displacements. And what is more important, modes as high as the 13th were found to contribute similar amounts to the interfloor displacements. If one either increased the level of the mass proportional damping, or preferably, introduced stiffness proportional damping, the number of modes which contribute significantly would probably decrease.

In Table 5-10 it is seen that, for the instances presented, the fundamental mode dominates the displacements throughout the structure. It is also seen that the higher modes contribute very little to the displacements in the upper portion but somewhat more in the lower portion.

On the other hand, for the cases presented in Table 5-11, the

third and fourth modes contribute the largest amounts to the inter-floor displacement between the 18th-19th floor (which is the largest one occurring anywhere in the structure) with the fundamental mode contributing a relatively small amount. In the lower portion, however, the fundamental is the most important contributor.

Even though the results of this computer study are not directly comparable to the studies of continuous beams, the general trends of the modal contributions are the same. That is, (1) the fundamental mode dominates the displacements, particularly in the upper floors; and (2), for the interfloor displacements, the higher modes usually contribute more than the fundamental in the upper floors, but in the lower floors, the fundamental mode is more important.

In order to learn more about these trends, the time history plots of numerous responses are analyzed in the next chapter.

CHAPTER VI

RESPONSE RESULTS

6.1 Introduction

The purpose of this chapter is to present response results from computer studies of the A/20/2.2/2/6 structural frame (Sec. 3.2) subjected to earthquake excitation. These studies are carried out by the computer program described earlier in the report (Sec. 3.5) using the one-component beam model (Sec. 2.5) for the girders and columns of the frame. The plots given here are time histories of bending moments, interfloor shear forces, joint rotations, total accelerations, displacements and interfloor displacements for a number of stations in the structure.

The first section of this chapter shows the effect of yielding on the response of the structural frame. The excitation used in this investigation is the first four seconds of the accelerogram of the El Centro (N-S) earthquake of 18 May 1940. This is the strongest portion of the earthquake. In a later study in which the nonlinear frame was subjected to the entire length of the earthquake, it was observed that the maximum values of most of the responses occurred during the first four seconds, although several occurred afterwards. It is believed, however, that results based on the first four seconds are indicative of the effect of yielding.

The second section treats the response results for the nonlinear frame subjected to the entire length (30 sec) of the Jennings pseudo-earthquake number 6. In addition to time history plots, the

TABLE 6-1

Nomenclature Used in the Time History
Plots in Chapter VI and in Appendix A

| | |
|-----------------------|--|
| TOTAL ACCEL 17F | : The total horizontal acceleration of the 17 th floor |
| HORIZ DISP 4F | : The horizontal displacement of the 4 th floor relative to ground |
| OVERTURNING MOMT-BASE | : The overturning moment at the base of the three bay structure |
| SHEAR FORCE 18-19F | : One-half of the interfloor shear force between the 18 th and 19 th floors (from only the two columns used in the analysis) |
| INT-FL DISP GD-1F | : The interfloor displacement between the ground and the first floor |
| JNT ROT'N 17F-XC | : The rotation of the joint formed by the intersection of the exterior girder of the 17 th floor and the exterior column line |
| BND MOMT 17F-XG-XC | : The bending moment at station (e) |
| PL ANGLE 4F-XG-XC | : The plastic angle at station (f) |
| PL INDEX 4F-XG-XC | : The plastic index at station (f). This index indicates when yielding occurs and the direction of incremental yielding |
| BND MOMT 20F-IC-BT | : The bending moment at station (d) |
| MOD JNT ROT 20F-IC | : The rotation of the joint formed by the intersection of the 20 th floor and the interior column line modified to include the effect of the interfloor shear angle (see Eq. 3.8) |
| PL ANGLE 2F-XG-IC | : The plastic angle at station (g) |
| BND MOMT 2F-IG-IC | : The bending moment at station (h) |

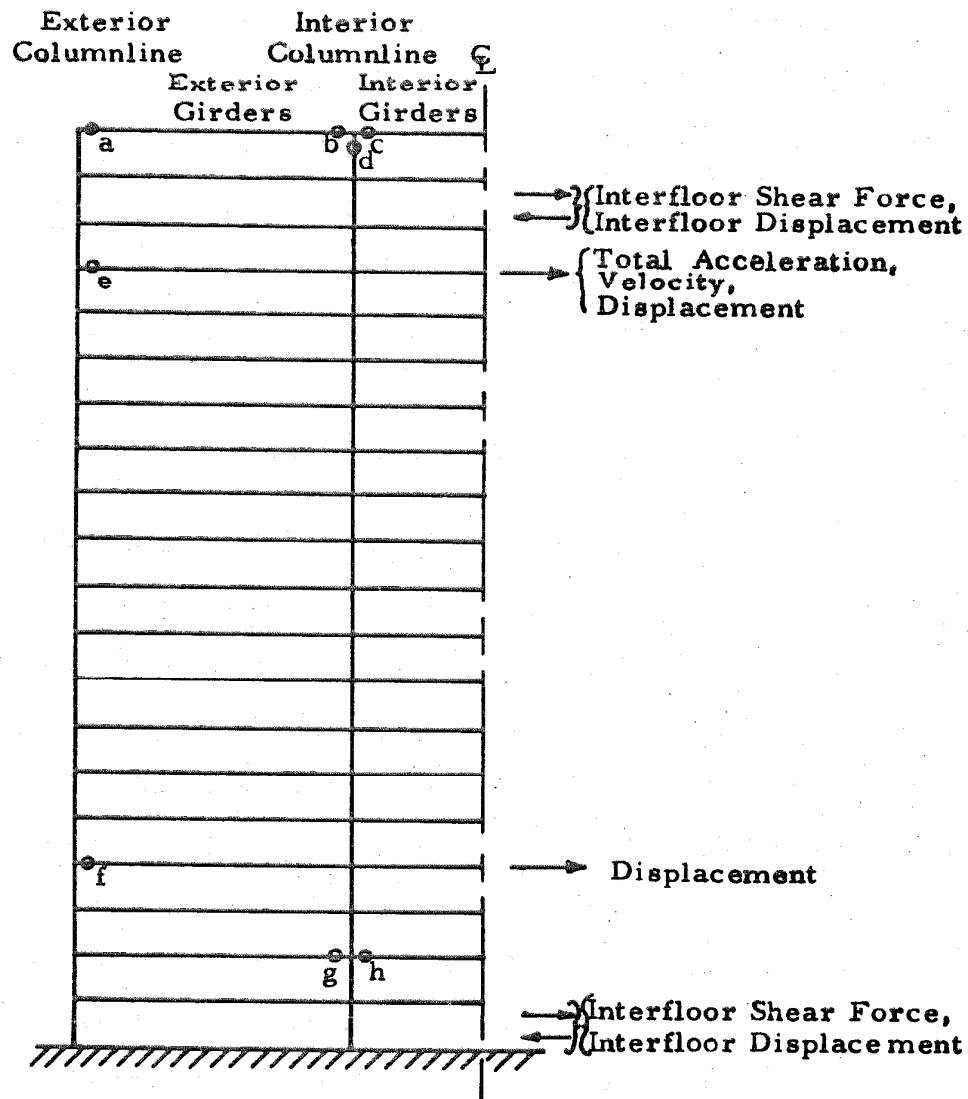


Fig. 6.1 o : Stations for Which the Bending Moment, Joint Rotation (or Modified Joint Rotation), Plastic Angle, and Plastic Index are Plotted .

displacement envelope and the ductility factors are shown. Response plots for similar studies of this frame using the entire length (29.38 sec) of the El Centro (N-S) earthquake of 18 May 1940 and several other pseudo-earthquakes are given in Appendix A.

The nomenclature used in these plots is described in Table 6-1. The unit system used is "in-lbs-sec" with the joint rotations given in radians. The stations for which the time histories of the responses are plotted are shown in Fig. 6.1.

6.2 Comparison of the Linear and Nonlinear Responses of a Structural Frame

In this section a comparison is made between the responses of the linear A/20/2.2/2/6 structural frame and the corresponding nonlinear frame. Each system had 0.10 fraction of critical damping in the fundamental mode and was subjected to approximately the first four seconds of the El Centro (N-S) earthquake of 18 May 1940.

The time histories of the total acceleration of the 17th floor, the horizontal displacements of the 17th floor and the 4th floor as well as the overturning moment at the base of each frame are shown in Fig. 6.2a and Fig. 6.2b. For both the linear and the nonlinear cases, the displacement of the 17th floor and the overturning moment at the base are primarily characterized by the frequency of the fundamental mode. In the time history of the displacement of the 4th floor, higher frequencies are observed in addition to the fundamental for both the linear and nonlinear cases. Many frequencies are noted in the time history of the total acceleration of the 17th floor. These

observations are in agreement with those for the continuous cantilever beam of Chapter V.

Comparing the total acceleration of the 17th floor of the linear structure with that of the nonlinear structure, two features are noted which call for some discussion. The first is that an unusual peak occurs at 2.7 sec in the nonlinear plot in Fig. 6.2b which does not occur in the corresponding linear response, Fig. 6.2a. The second concerns the relatively larger high frequency components of the nonlinear plot.

For the above calculations mass proportional damping was used but no stiffness proportional damping was introduced. As a result, the higher modes are not so effectively damped as the lower. Consequently, there is a limitation on the model for the representation of certain responses which exhibit significant high frequencies.

The first feature to be discussed concerns the unusual peak in the total acceleration record of the 17th floor in the nonlinear frame. This peak has an absolute value of 0.81g and is the maximum absolute value of the total acceleration for any floor during this run for the nonlinear case. However, for the linear frame, the maximum absolute value of the total acceleration at the 17th floor is 0.58g while at the 20th floor it is 1.0g. Since the maximum absolute value of the acceleration of the ground is 0.32g, it appears possible to have amplifications of the total acceleration on the order of 2 or more in this particular nonlinear structure. As a result of yielding, the amplitude and phase of the shear force waves in the nonlinear case

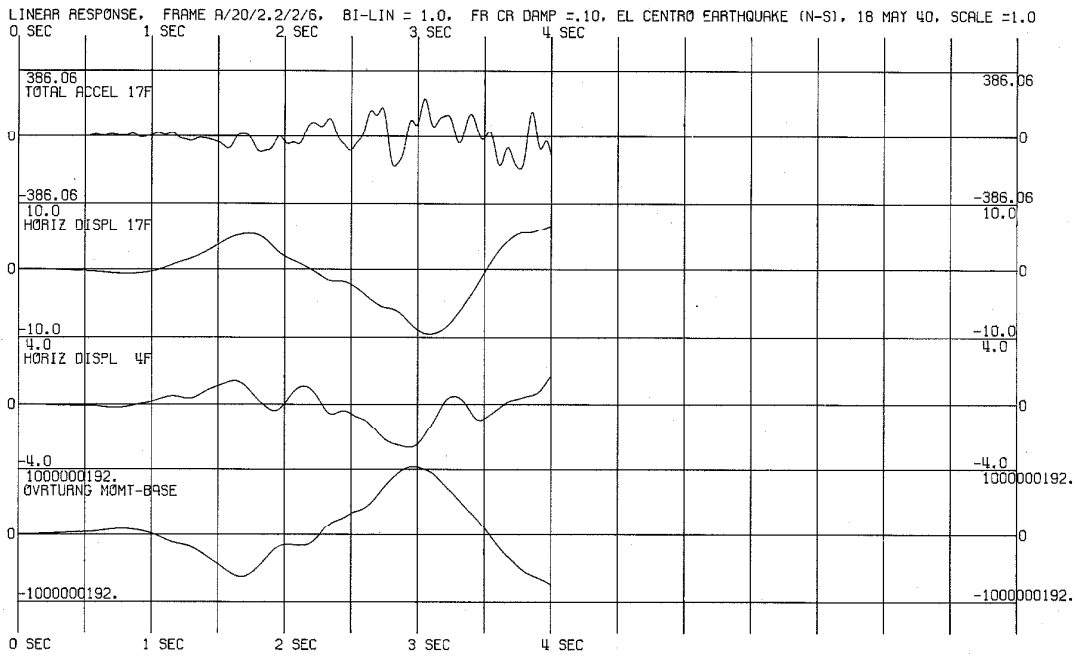


Fig. 6.2a

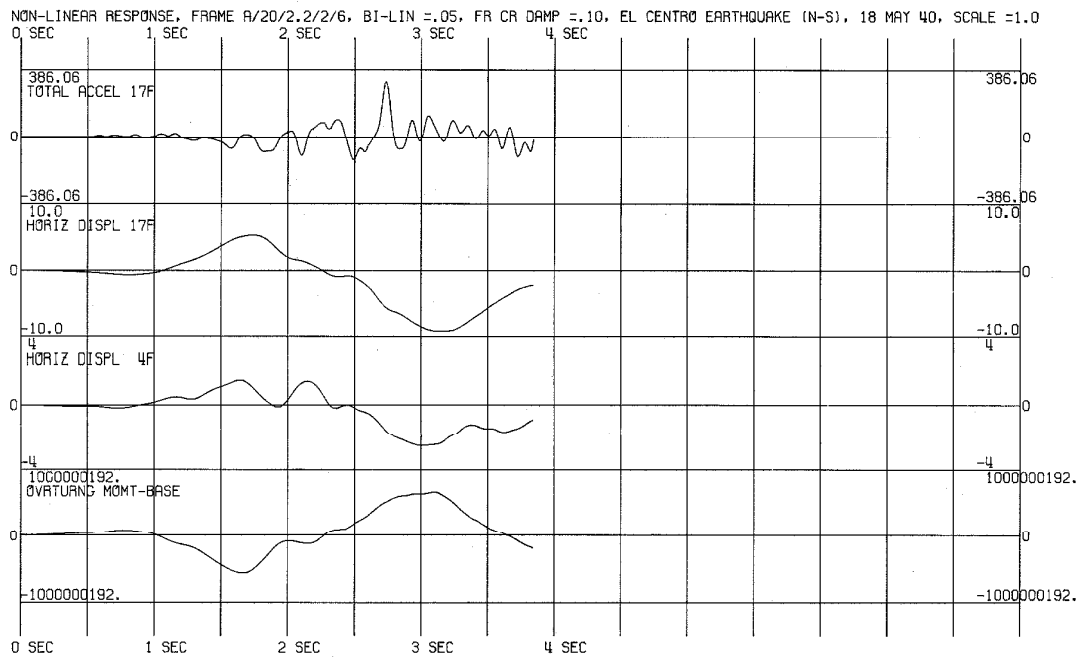


Fig. 6.2b

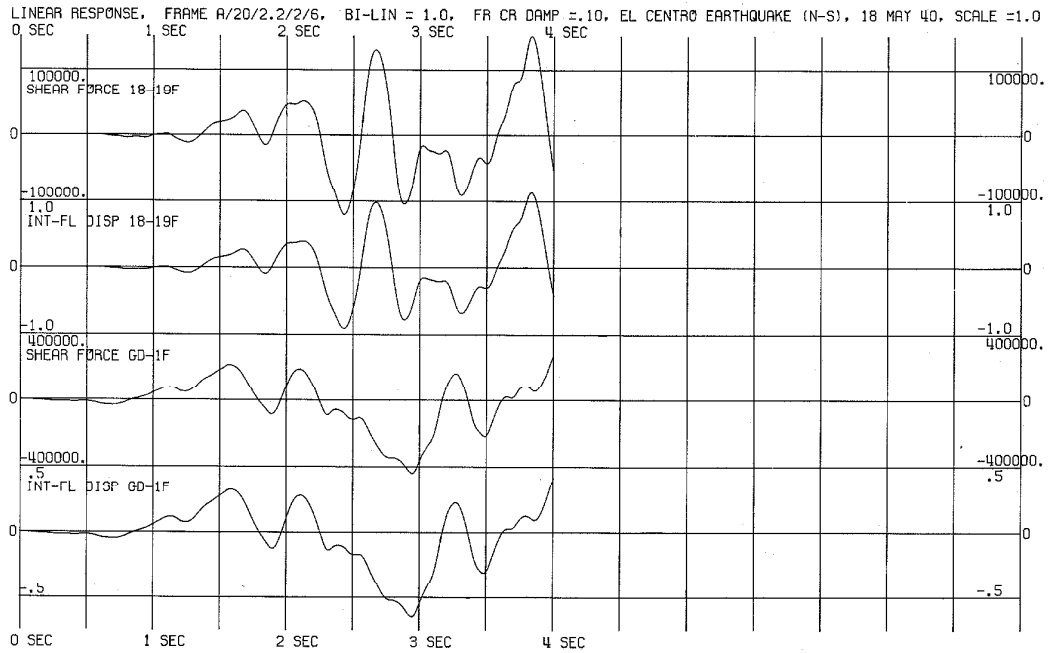


Fig. 6.3a

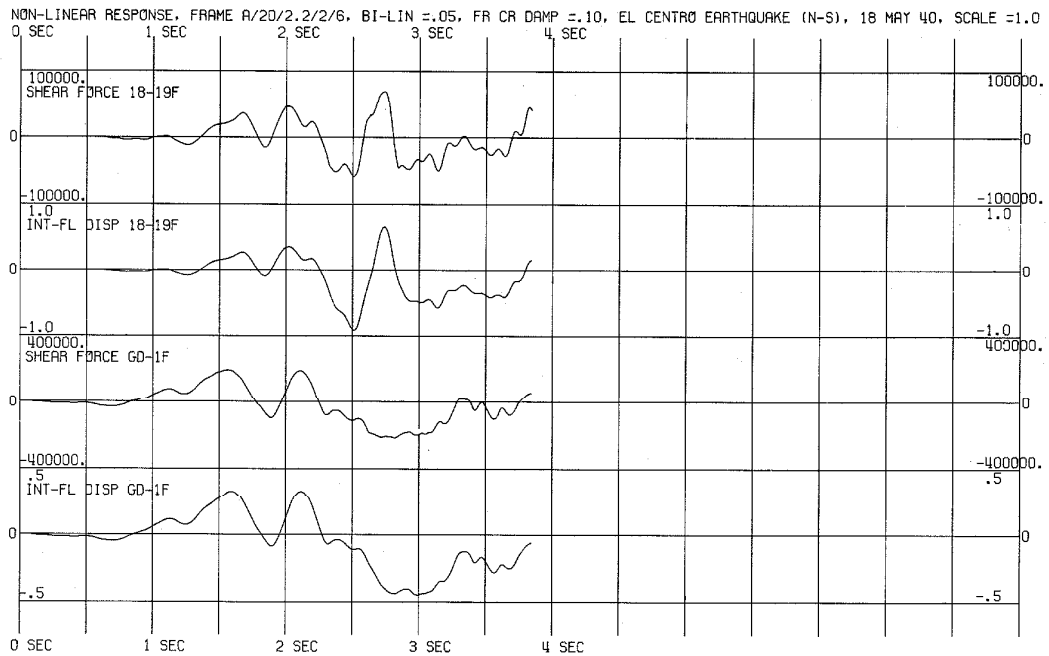


Fig. 6.3b

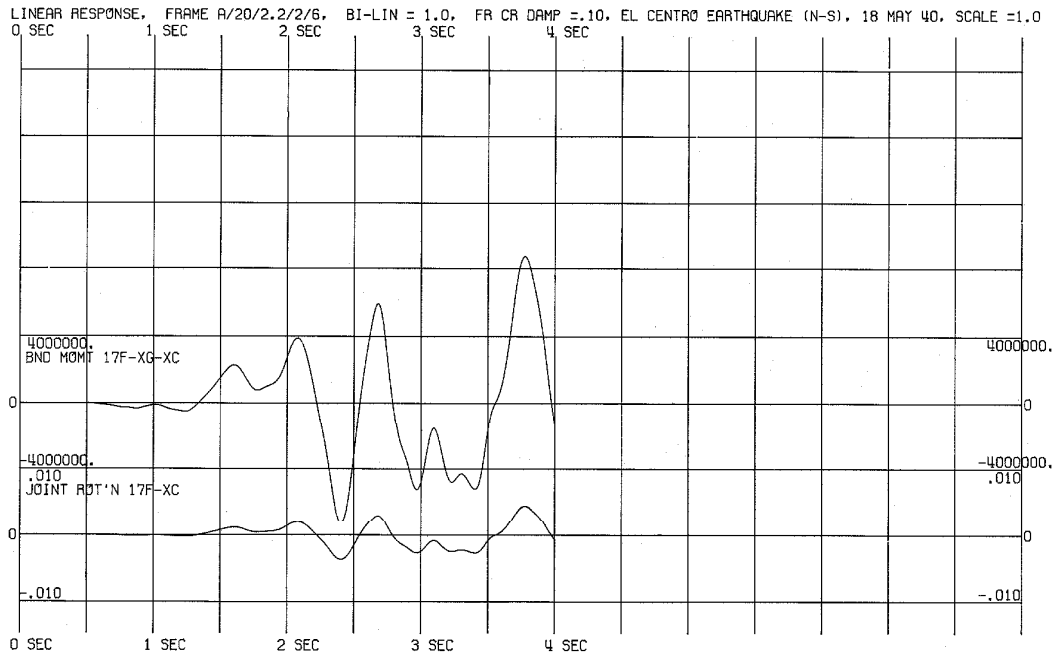


Fig. 6.4a

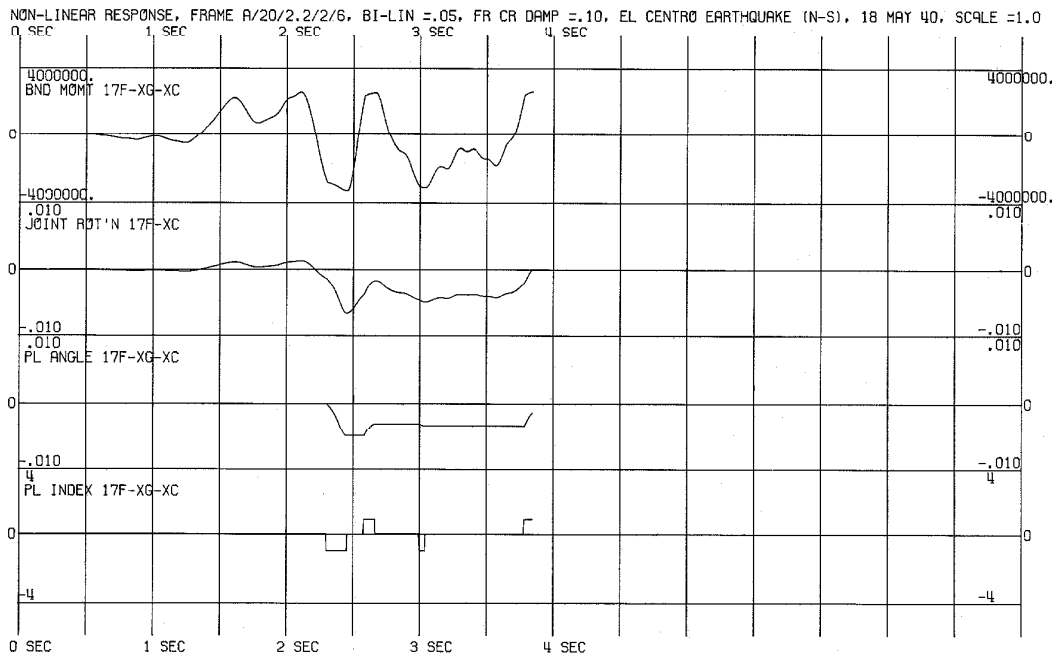


Fig. 6.4b Station (e)

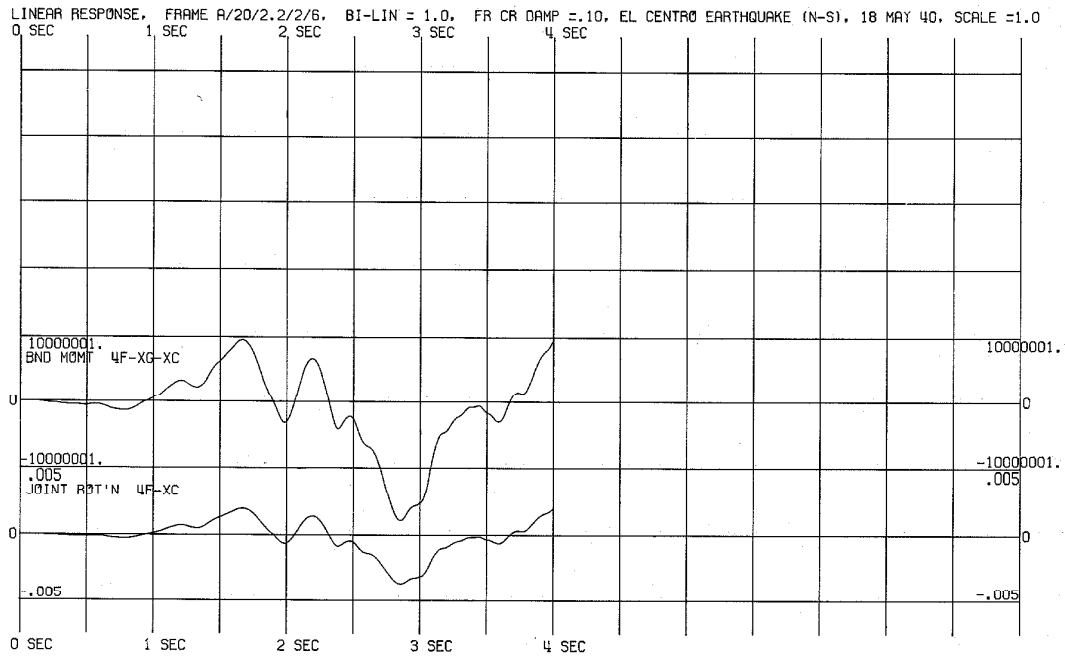


Fig. 6.5a

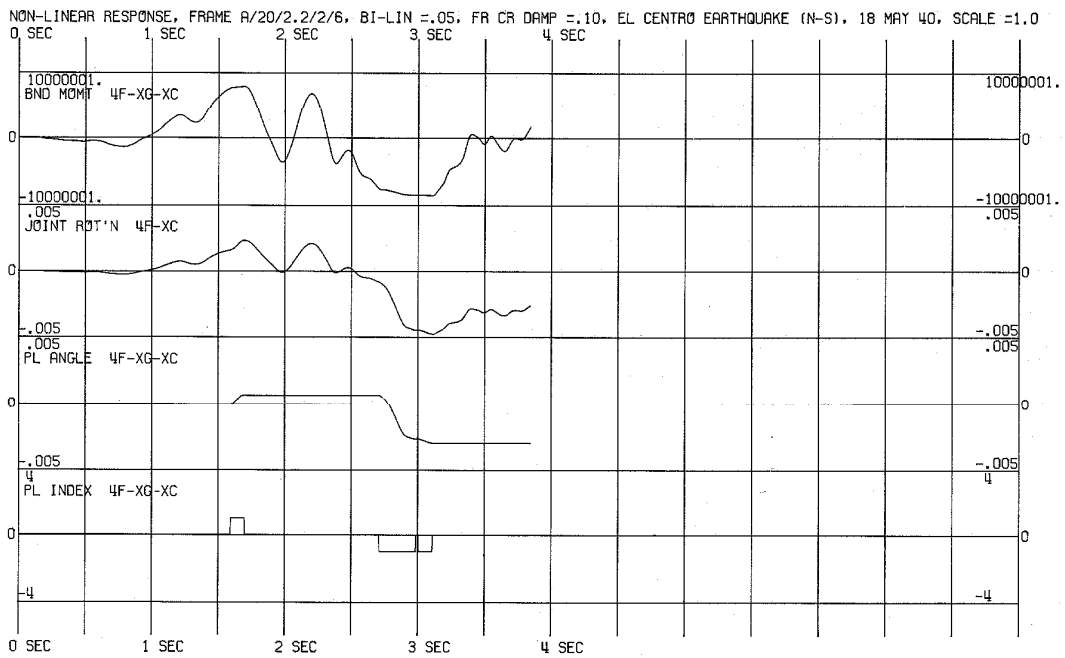


Fig. 6.5b Station (f)

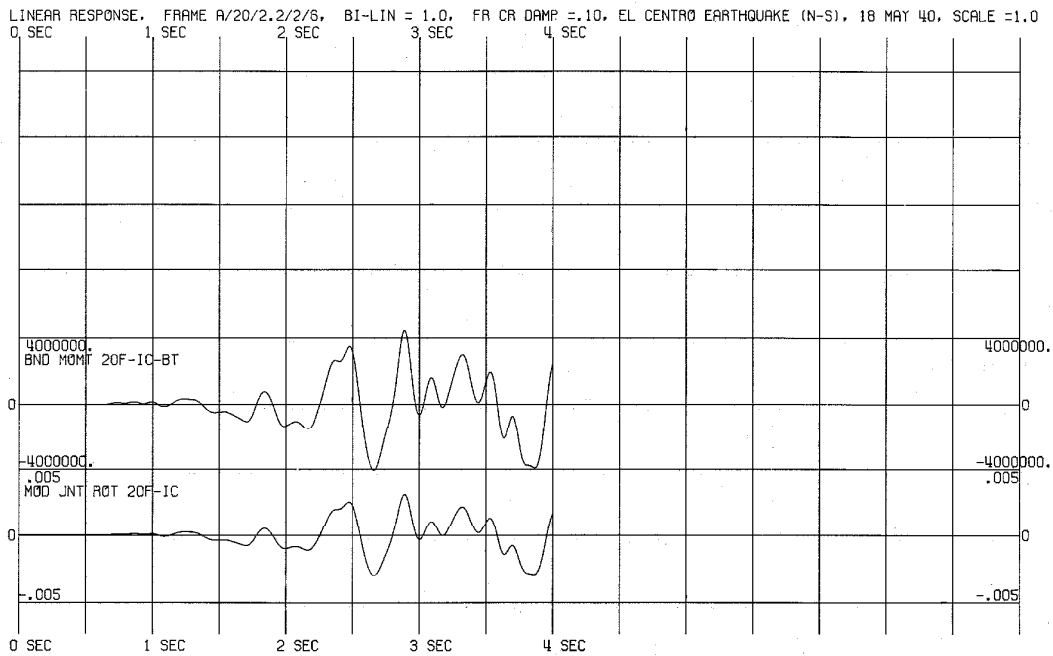


Fig. 6.6a

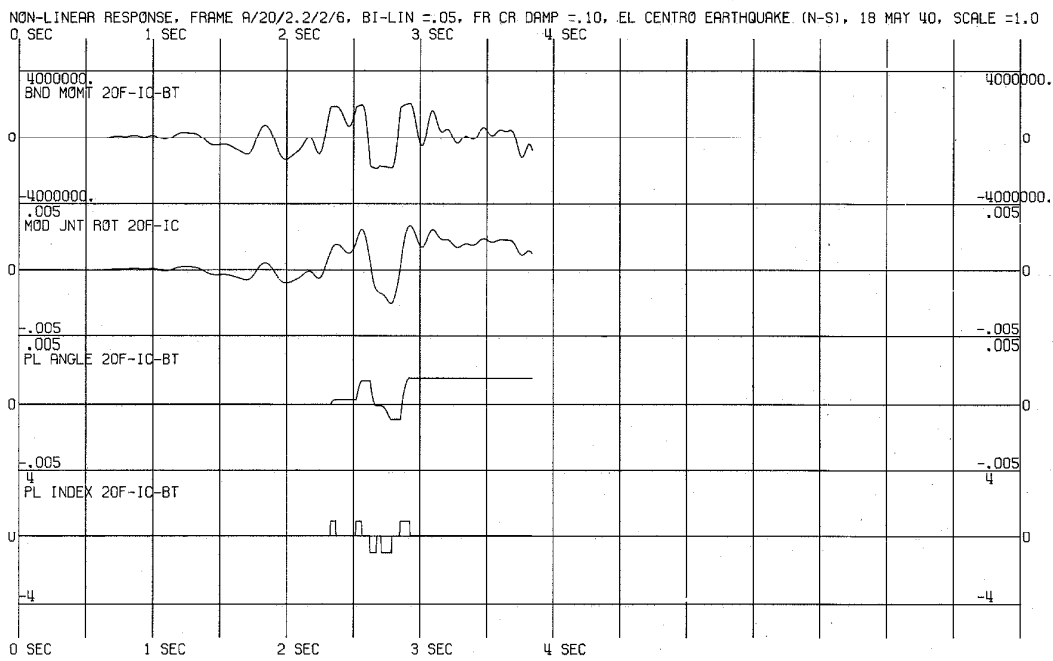


Fig. 6.6b Station (d)

TABLE 6-2

| Floor | Sum of Shear* Forces Above and Below Floor (at Yield Level) lbs $\times 10^{-4}$ | Weight* of Floor lbs $\times 10^{-4}$ | Estimate of Maximum Absolute Value of Total Acceleration fraction g | Maximum Absolute Value of Total Acceleration from a Non- linear Study Using El Centro (N-S), 18 May 1940 fraction g |
|--------|--|---|--|--|
| 20 | 4.31** | 8.88 | 0.49 | 0.54 |
| | 12.00 | 10.04 | 1.20 | 0.58 |
| 18 | 18.29 | 10.04 | 1.82 | 0.45 |
| | 24.04 | 10.04 | 2.39 | 0.81 |
| 16 | 29.99 | 11.20 | 2.67 | 0.65 |
| | 35.93 | 11.20 | 3.21 | 0.61 |
| 14 | 42.27 | 11.20 | 3.77 | 0.66 |
| | 48.03 | 11.58 | 4.14 | 0.45 |
| 12 | 52.36 | 11.58 | 4.52 | 0.53 |
| | 57.87 | 11.58 | 4.99 | 0.50 |
| 10 | 62.73 | 14.28 | 4.39 | 0.48 |
| | 67.44 | 14.28 | 4.72 | 0.43 |
| 8 | 71.06 | 14.28 | 4.97 | 0.39 |
| | 74.92 | 14.67 | 5.10 | 0.45 |
| 6 | 77.26 | 14.67 | 5.26 | 0.39 |
| | 82.39 | 14.67 | 5.61 | 0.45 |
| 4 | 85.15 | 15.83 | 5.37 | 0.50 |
| | 84.15 | 15.83 | 5.31 | 0.37 |
| 2 | 87.71 | 15.83 | 5.54 | 0.41 |
| | 102.92 | 16.21 | 6.34 | 0.37 |
| Ground | - | - | - | 0.32 |

* Calculations based on half of the A/20/2.2/2/6 frame (see Fig. 3.2).

** This one uses the yield moment in the 20th floor girder at the exterior column since it is lower than the one in the exterior column.

are changed from those in the linear case. From a review of the plots for this study, it appears that in the nonlinear case at 2.7 sec, shear force waves fortuitously meet at the 17th floor in a manner sufficient to cause a high total acceleration.

To explore the way in which interfloor shear forces and accelerations may add up at various points in the structure, Table 6-2 has been compiled. The estimate of the maximum absolute value of the total acceleration of a floor is found by dividing the sum of the yield levels of the shear forces in the columns directly above and below that floor by the mass of the floor. These estimates of the maximum total acceleration that the structure could sustain are very high: from 0.49g at the roof to 6.3g near the base. This only means that with respect to total acceleration the columns near the base of the structure are much stronger than would be required for actual earthquake excitation. As shown in Table 6-2 for the El Centro (N-S) earthquake of 18 May 1940, the total acceleration of the 20th floor was calculated to be 0.54g, and near the base it was calculated to be 0.37g. The 0.54g value is in excess of the estimated 0.49g because interfloor shear forces occurred between the 19th and 20th floors in excess of those sufficient to cause yielding in the columns.

The second point to be discussed concerns the larger high frequency components observed in the total acceleration for the nonlinear case in comparison with that for the linear case. This is likely to be a consequence of the sharp corner at the yield level in the bi-linear hysteresis loop. A similar phenomenon was observed in the

previous investigation of the three-mass system with bilinear hysteretic springs shown in Fig. 4.1. In that case it was noted that higher frequency components corresponding to the higher natural modes appeared whenever a spring passed into the yield range. This type of response corresponds to that which would result from a step in the forcing function, i.e., the response would contain all of the natural frequencies of the system. The total acceleration of a real structure may or may not exhibit this high frequency characteristic depending upon the properties of the structure at the yield level. An estimate of the effect of such a sharp corner on the response of a tall structure might be obtained in a future study using curvilinear moment-rotation hysteresis loops such as shown in Fig. 2.14.

In order to observe the effect of yielding on other responses of the structure, Figs. 6.2a and 6.2b are again considered. Comparing the horizontal displacement of the 17th floor for the linear case with that for the nonlinear case, one notes that there is little difference in the maximum displacements or in the time at which they occur. However, it is seen in Fig. A.1.3 of Appendix A that, as a result of yielding, a permanent displacement of about four inches is incurred in the displacement of the 17th floor. Similarly, the maximum absolute displacement of the 4th floor in the linear and the nonlinear cases are approximately equal and occur at about the same time. In the nonlinear case, a permanent displacement of about one inch is incurred.

The maximum absolute value of the overturning moment at the base, Fig. 6.2, is reduced about 30% by yielding. Since the

girders yield, the moments at the ends of the girders and the axial forces in the columns are limited. Consequently, the base overturning moment is also limited. Note that gravitational effects are not considered in the calculation of the base overturning moment of this model.

In the plots of the interfloor shear forces and interfloor displacements, Fig. 6.3, changes in the shape of the shear waves as a result of yielding can be seen. In particular, a shear wave pulse with a period of approximately 0.5 sec, about the period of the third mode, can be traced and changes in its shape observed. This shear force pulse appears between the ground and the 1st floor from 1.6 sec to 2.1 sec in both the linear and nonlinear cases. In the linear case, this pulse appears approximately 0.6 sec later between the 18th and 19th floors. However, in the nonlinear case, the shear force pulse is observed between the 18th and 19th floors with different characteristics than those observed in the linear case. In comparison with the linear case, the amplitude is reduced 50%, the shape is different, and the peaks are delayed by approximately 0.1 sec. This delay is such that the peak in the shear force between the 18th-19th floors at 2.7 sec coincides with the 0.81g peak in the total acceleration plot in Fig. 6.26. The effect of yielding on the wave shape is even more noticeable after 2.8 sec in these time history plots.

Similar effects are observed for the bending moments at different stations in the structure as shown in Figs. 6.4, 6.5 and 6.6. Furthermore, it is seen that the time histories of the bending moments,

joint rotations, and plastic angles differ from one station to another in both the linear and in the nonlinear cases.

To summarize the effects of yielding on the response of the A/20/2.2/2/6 frame subjected to the strongest portion of the El Centro earthquake, it was observed that yielding limits the maximum absolute values of the shear forces to about 60% of the corresponding values in the linear case. However, yielding was not so effective in limiting displacements, interfloor displacements, and joint rotations. For these, the maximum absolute values were reduced to only about 80% of the linear values. Although the maximum absolute values of the total acceleration may be reduced by yielding, it was shown that for the structural properties used, this frame could withstand total horizontal accelerations in excess of 6g near the base and in excess of 1g near the top without the columns yielding (the girders do yield). It was also seen that during the time of severe yielding, the phase of the response was significantly altered.

In the next section, the response of this nonlinear structure to a pseudo-earthquake is presented. By a visual analysis of the time history plots of various responses, it is possible to obtain an understanding of the frequency components expected in each response.

6.3 Response of the Nonlinear A/20/2.2/2/6 Frame Subjected to Earthquake Excitation

Several response studies of the bilinear hysteretic A/20/2.2/2/6 frame subjected to different earthquakes are performed using the computer program developed in connection with this report.

In addition to the El Centro (N-S) earthquake of 18 May 1940, six of the pseudo-earthquakes generated from a random process by P. C. Jennings are used. Since the corresponding responses of the structure are similar in amplitude and frequency content for the pseudo-earthquakes used, the plots for one earthquake only are analyzed in this section. The plots for the other earthquakes are given in Appendix A.

The pseudo-earthquake accelerograms have spectral properties similar to those for the recorded strong motion accelerograms of real earthquakes. However, the pseudo-earthquake accelerograms are more nearly uniform in amplitude over time than are the real ones. In an attempt to obtain approximately the same amount of yielding in the structure for the pseudo-earthquakes as occurred in the structure for the El Centro earthquake, they were scaled so that the rms value of each accelerogram is approximately 1.2 times that of El Centro. The actual rms values used are given in Table 6-3. In all cases the bilinearity (the ratio of the second slope to the first in the hysteresis loop) was 0.05. The fraction of critical damping in the fundamental mode was 0.10 in all runs except one which used 0.05 fraction of critical damping in order to observe the effect of damping on the response. A summary of the combinations of parameters used in the studies is shown in Table 6-3.

The response plots for the nonlinear A/20/2.2/2/6 frame using pseudo-earthquake number 6 with 0.10 fraction of critical damping in the fundamental mode are presented in this section. In addition, the displacement responses (in inches) of seven one-degree of freedom

TABLE 6-3

| Earthquake | Fraction Critical Damping in Frame | rms Scale Factor (with respect to El Centro) | Max. Abs. Acceleration of Earthquake (frac.grav.) | Spectrum Intensity $S_{0.0}$ | Max. Abs. Displacement (inches) | Max. Abs. Interfloor Displacement (inches) | Maximum Ductility Factors | | |
|-----------------------------|------------------------------------|--|---|------------------------------|---------------------------------|--|---------------------------|-----------------|---------------------|
| | | | | | | | All Girders | Interior Column | Exterior Column |
| El Centro (N-S) 18 May 1940 | 0.10 | 1.0 | 0.316 | 8.94 | 11.52 | 1.29 | 4.44 | 2.99 | 0.83 |
| Pseudo-Earthquake No. 1 | 0.10 | 1.15 | 0.246 | 11.45 | 8.98 | 0.98 | 3.58 | 1.74 | 0.71 |
| Pseudo-Earthquake No. 2 | 0.10 | 1.18 | 0.267 | 13.23 | 14.43 | 1.31 | 5.00 | 3.11 | 0.81 |
| Pseudo-Earthquake No. 4 | 0.10 | 1.26 | 0.267 | 12.21 | 10.96 | 0.93 | 3.96 | 2.02 | 0.80 |
| Pseudo-Earthquake No. 5 | 0.10 | 1.19 | 0.271 | 12.25 | 9.69 | 0.91 | 3.63 | 2.23 | 0.76 ¹⁴⁰ |
| Pseudo-Earthquake No. 6 | 0.10 | 1.22 | 0.313 | 10.96 | 8.91 | 0.99 | 4.01 | 2.58 | 0.78 |
| Pseudo-Earthquake No. 6 | 0.05 | 1.22 | 0.313 | 10.96 | 10.28 | 1.08 | 4.32 | 2.91 | 0.80 |
| Pseudo-Earthquake No. 7 | 0.10 | 1.20 | 0.328 | 12.06 | 8.52 | 0.97 | 3.75 | 2.53 | 0.79 |

Notes:

These pseudo-earthquakes were chosen by flipping coins.

In all cases the bilinearity is 0.05.

Max. Abs. = Maximum Absolute.

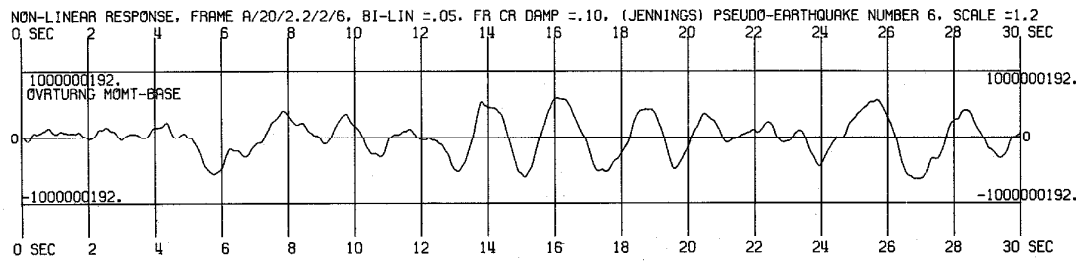


Fig. 6.7

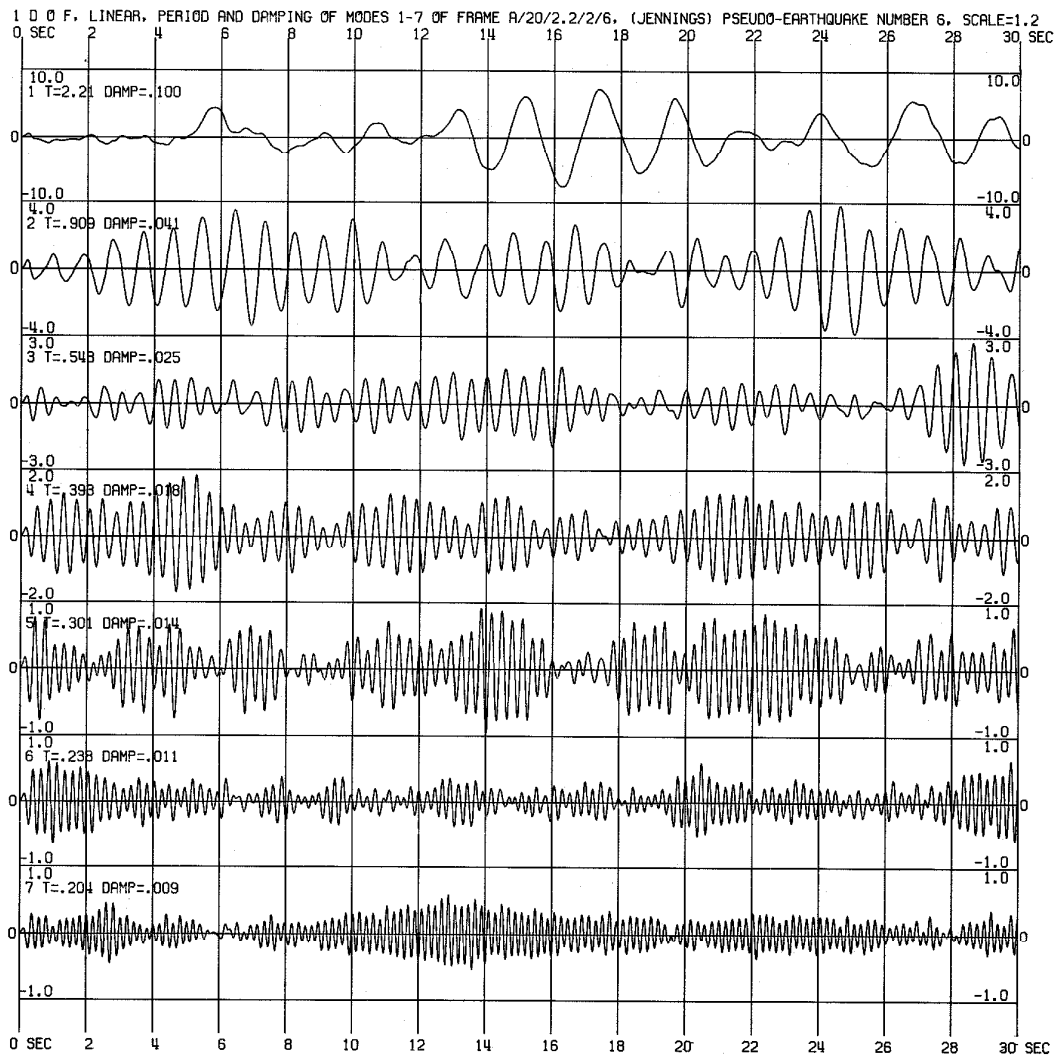


Fig. 6.8

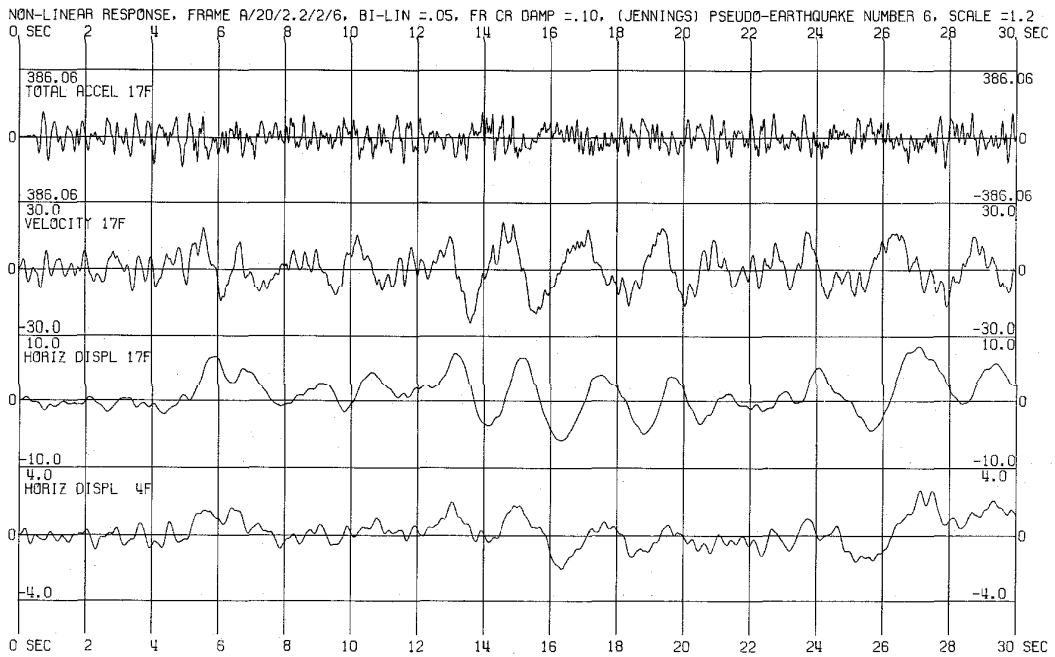


Fig. 6.9

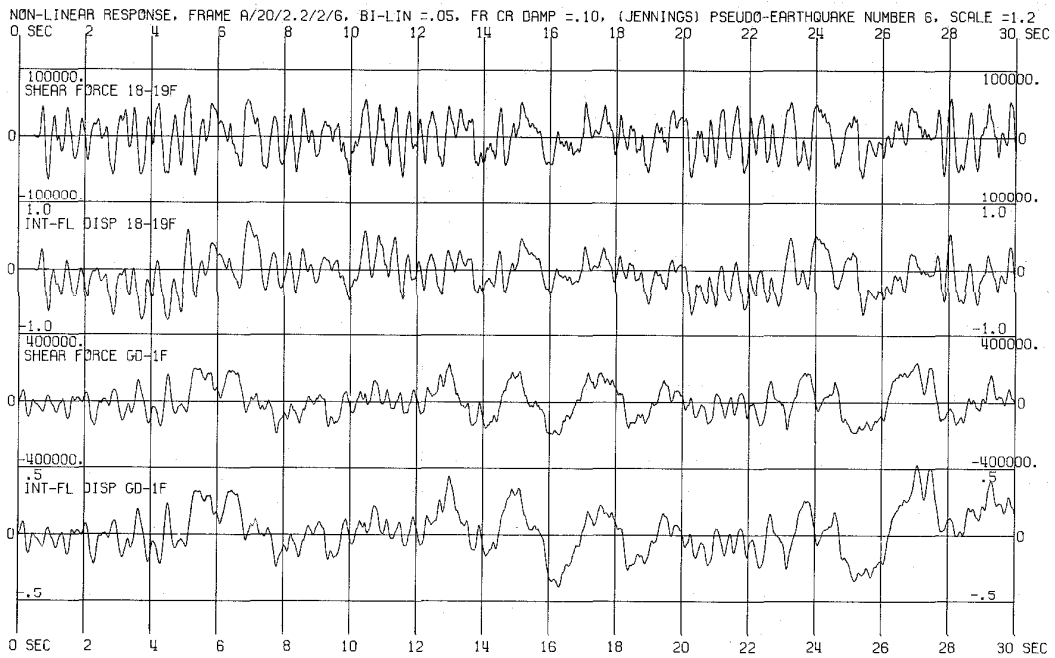


Fig. 6.10

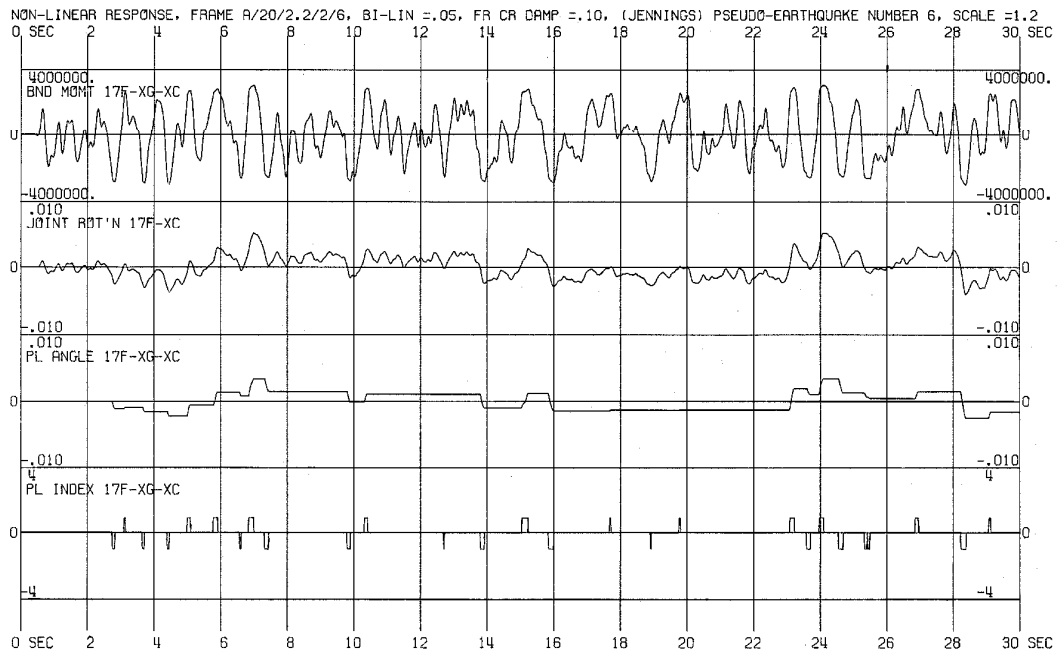


Fig. 6.11 Station (e)

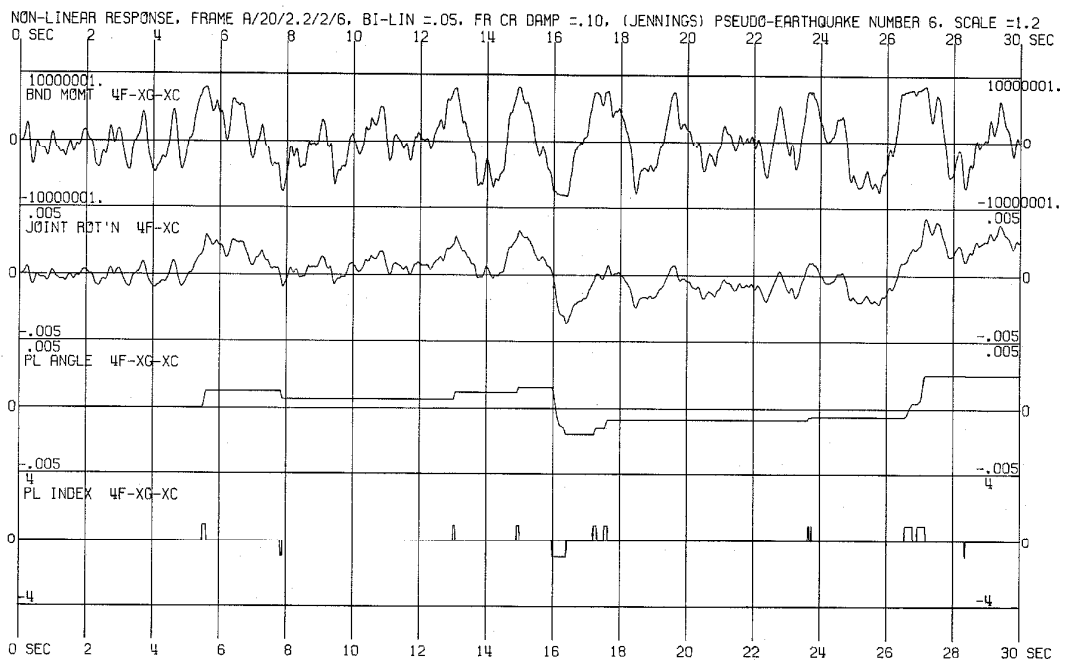


Fig. 6.12 Station (f)

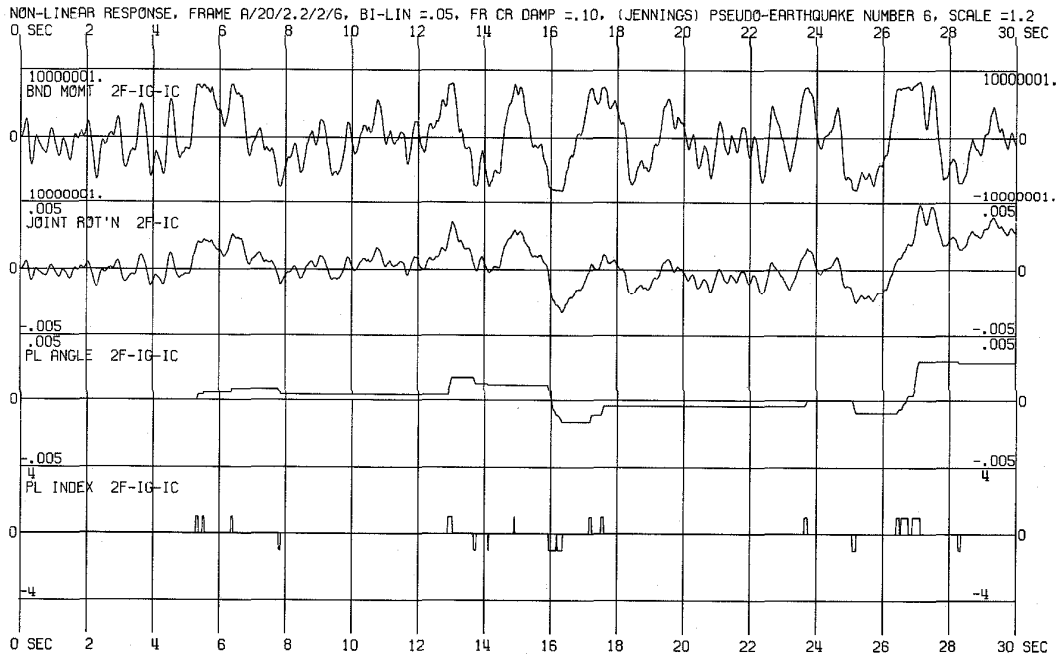


Fig. 6.13 Station (h)

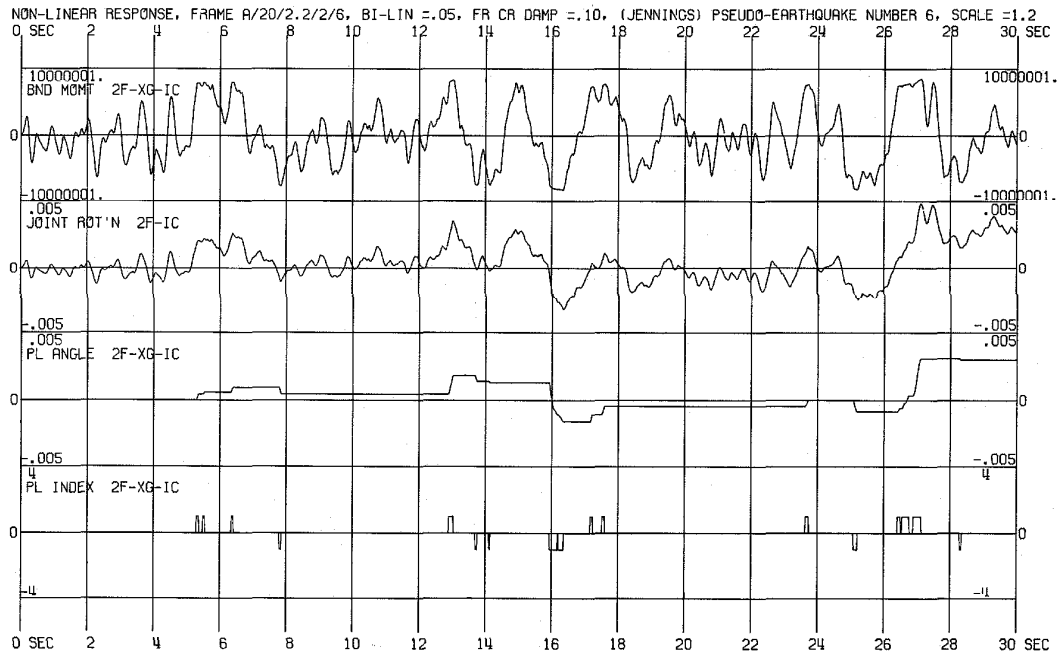


Fig. 6.14 Station (g)

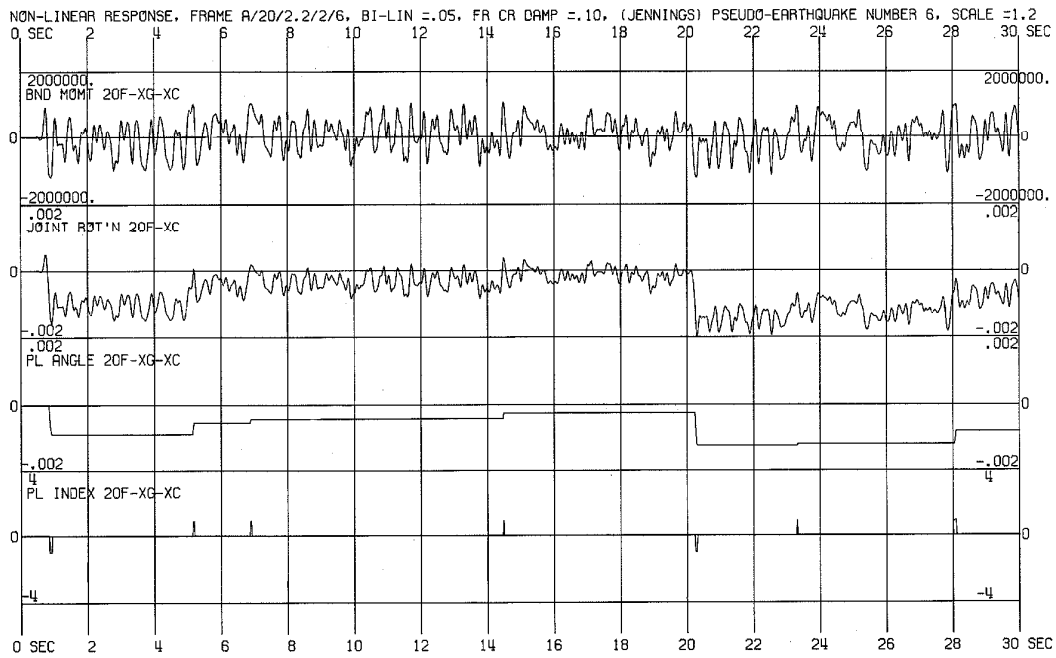


Fig. 6.15 Station (a)

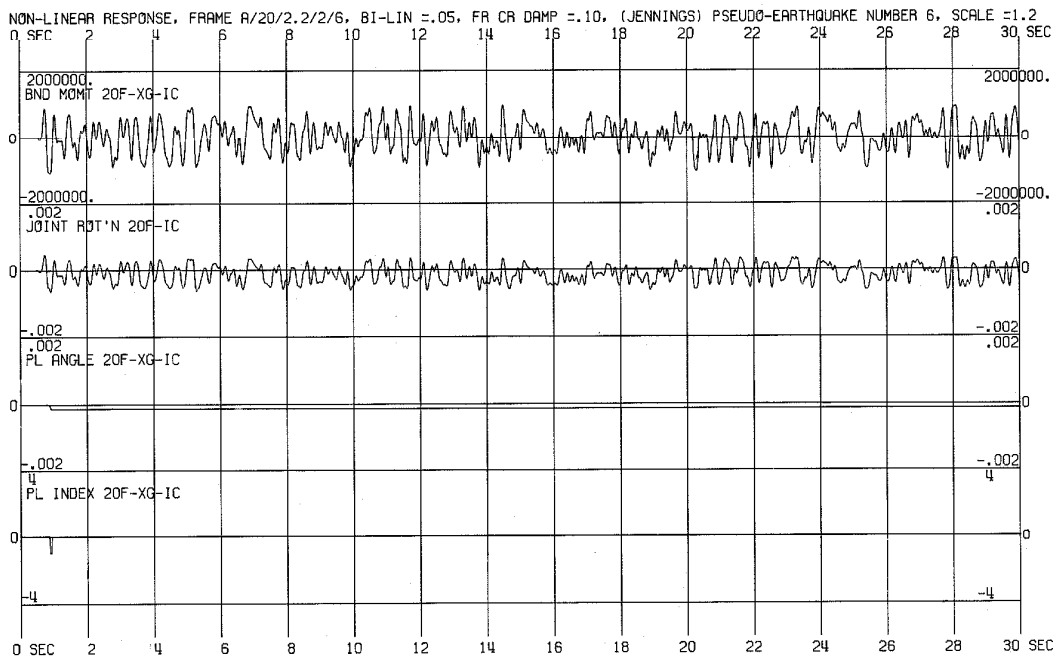


Fig. 6.16 Station (b)

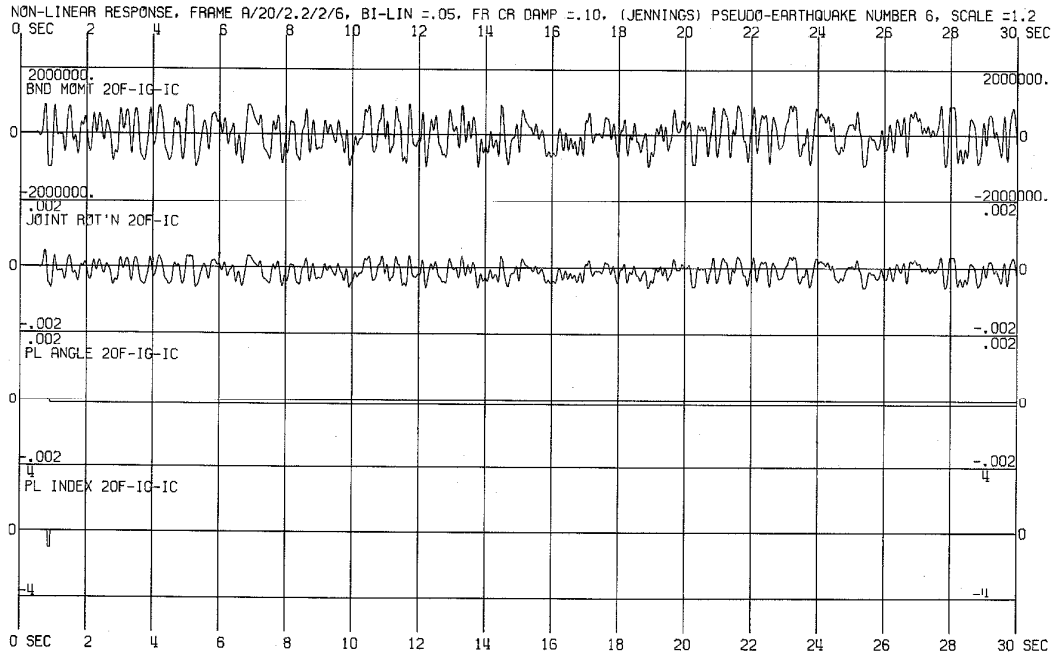


Fig. 6.17 Station (c)

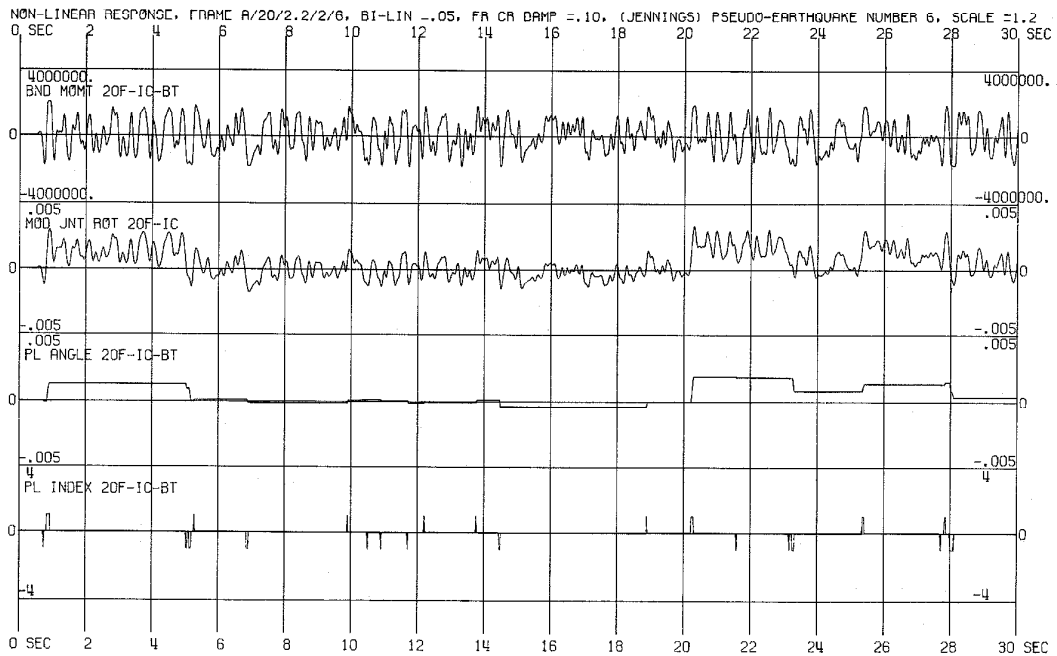


Fig. 6.18 Station (d)

NONLINEAR RESPONSE OF FRAME A/20/2.2/2/6
 BILINEARITY = 0.05, FRACTION OF CRITICAL DAMPING = 0.10
 (JENNINGS) PSEUDO-EARTHQUAKE NUMBER 6, SCALE = 1.2

MOST NEGATIVE AND MOST POSITIVE DISPLACEMENTS IN INCHES

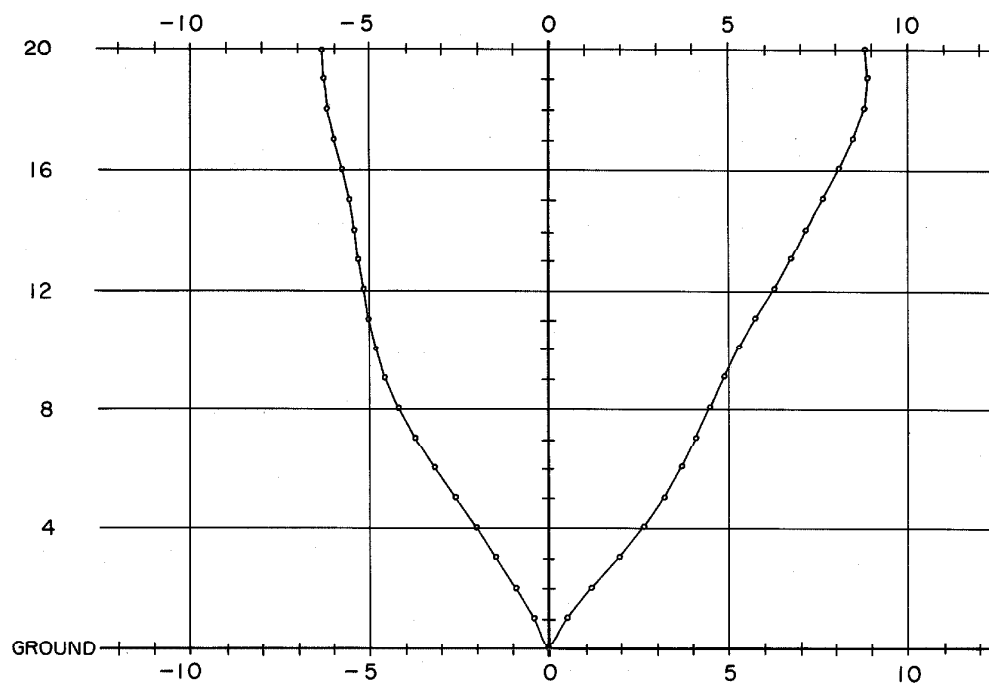


Fig. 6.19

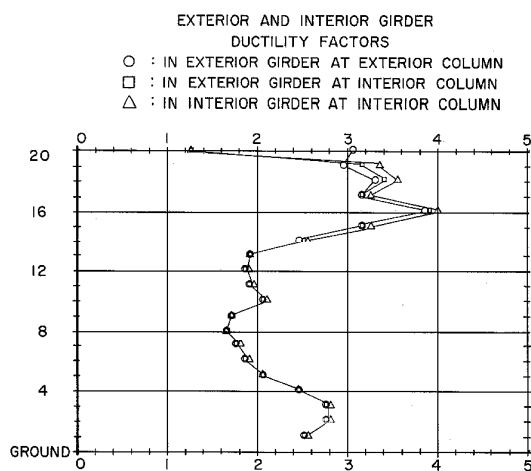


Fig. 6.20a

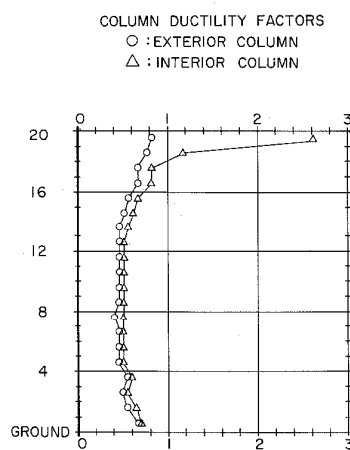


Fig. 6.20b

linear oscillators subjected to the same excitation are presented in Fig. 6.8. There is a one-to-one correspondence between these oscillators and the first seven modes of the linear A/20/2.2/2/6 frame with respect to period and damping. For example, the first oscillator has the period and the fraction of critical damping of mode 1. In Fig. 6.8 the response of this oscillator is labeled

$$1 \quad T = 2.21 \quad \text{DAMP} = .100 \quad .$$

The time history of the displacement of the 17th floor is shown in Fig. 6.9. By comparison with the response of the linear oscillator corresponding to the first mode of the linear frame, henceforth called the first modal oscillator, it is seen that the two are closely correlated. This is in accordance with the analytical results for continuous cantilever beams in Chapter V which indicate that the horizontal displacements in the upper portion of the structure are expected to be dominated by the first few modes, primarily the fundamental.

By design, the distribution of yield bending moments in the A/20/2.2/2/6 frame is such that throughout most of the structure the girders yield at a much lower level than the neighboring columns. The purpose for such a design is "to maintain vertical load integrity of the structure."* For all of the earthquake excitations used, the interior columns of the nonlinear structure yield in only the upper 2 or 3 floors and the girders spend at most 10% of the time in yield. Consequently, the time histories of the gross responses of this particular structure,

*Clough and Benuska, FHA Study, p.1-7.

such as the displacements, should be highly correlated with those of the linear structure. If the yield moment distribution were changed so that more of the columns yielded, a lower correlation with the response of the linear system would probably occur.

The overturning moment at the base, Fig. 6.7, is observed to be closely correlated with the displacement at the 17th floor and with the response of the first modal oscillator (with opposite sign). This correlation should exist for the following reason: When a floor is displaced, shear forces develop in the girders which appear as forces in the axial direction in the columns. Only when many of the floors are displaced in the same direction, such as in the fundamental mode, do the axial column forces add together to cause a significant resultant moment at the base.

A comparison of the 4th floor displacement with the 17th floor displacement, Fig. 6.9, indicates that higher frequency response (corresponding to the higher modes in a linear structure) of the structure influences the displacement (not interfloor displacement) of the 4th floor more than it influences the displacement of the 17th floor. This is in agreement with the studies of continuous beams.

In addition to a fundamental modal response component, higher frequency response is observed in the plot of the velocity (relative to ground) of the 17th floor. This is expected since the velocity is a first derivative of the displacement and differentiations characteristically tend to amplify higher frequencies.

As seen in Fig. 6.9, the total acceleration, which is the sum

of the acceleration relative to ground and the acceleration of the ground, has many frequency components. Again, this is in agreement with the results of the continuous beam studies.

In Fig. 6.10, the time histories of the shear force and of the interfloor displacements between the 18th and 19th floors as well as between the ground and 1st floors are shown. By comparison, it is seen that the time history of the shear force between the 18th and 19th floors and the time history of the corresponding interfloor displacement are very similar in appearance. The small differences between them occur because the shear force is a function of the joint rotations in addition to the interfloor displacement and because permanent displacement occurs as a result of yielding.

In the propagation of the first shear force pulse from the base to the 19th floor in the linear A/20/2.2/2/6 frame a time lag of about 0.6 seconds is observed. This time lag is seen throughout most of the earthquake, but it is usually not so clear. For the shear-type continuous cantilever beams described in Chapter V, the time necessary for a shear force pulse to travel from the base to the top is:

for the uniform beam:

$$\frac{T_1}{4} = 0.55 \text{ sec and}$$

for the tapered (to a point) beam:

$$\frac{T_1}{2.6} = 0.85 \text{ sec}$$

where T_1 is the period of the fundamental mode in each case. Since

this frame has mass and stiffness properties which are partially tapered (Fig. 3.2), the observed time lag of 0.6 sec is in good agreement with those predicted for the continuous beams. In these plots it is seen that the shear force and interfloor displacement between the ground and first floor have a strong dependence upon the fundamental mode. However, many modes contribute to the shear force and interfloor displacement near the top of the frame.

Time history plots of the bending moment, joint rotation, plastic angle, and plastic index are shown for several stations in the frame.* Each of the figures 6.11 through 6.18 corresponds to one of these stations. If the station is in a girder, the joint rotation is given; if the station is in a column, the modified joint rotation (Eq. 3.8) taking into account the interfloor displacement is plotted. During yielding the plastic index is (+1) or (-1) depending upon the direction in which the associated plastic angle moves. For example, at station (e) in the exterior girder in the 17th floor, Fig. 6.11, the initial yielding occurs with negative bending moment; hence, the incurred plastic angle is negative and the plastic index is (-1). By making visual comparisons of the time history plot of the bending moment at station (e), Fig. 6.11, with the response of each of the linear modal oscillators, Fig. 6.8, correlations can be observed which indicate the importance of the modes to the response at that station. Between 3 sec and 10 sec a

* All of these time history plots were made on the California Computer Products "Model 763 Plotter" programmed with the IBM 7094-7040 Computer at the California Institute of Technology Computing Center. For the 30 seconds of the earthquake there were 6000 time increments. After every 4th time increment, a point was plotted; hence, 50 points per earthquake second were plotted.

strong correlation with the 2nd modal response is observed; hence, it is concluded that the 2nd mode is responsible for most of the yielding during this time at this station. Between 13 sec and 19 sec, correlation with the first modal response occurs. Similarly, it is concluded that during this interval the first mode is responsible for most of the yielding at this station. At times combinations of modes are responsible for the yielding since the contribution of each mode by itself does not appear to be sufficient to cause yielding.

For an accurate determination of the relative importance of each mode at a particular instant, it is usually necessary to make a modal decomposition of the motion of the structure at that instant. Only at the times when one or two modes dominate a response does it appear possible to visually determine the importance of these modes. Such a modal analysis is made for this nonlinear structure in each time increment throughout the first four seconds of the El Centro earthquake according to a technique described in Section 5.3. The modal contributions to the largest displacements and inter-floor displacements that occurred in that analysis are given in Table 5-10 and Table 5-11. The results presented in those tables indicate that often more modes than can be observed by the eye are important for the interfloor displacements. However, because extensive computer time is used in making modal decompositions, an analysis of this type was not performed for the present study. Consequently, in this chapter the discussion of modal contributions (or frequency components) is based upon visual analysis.

At station (f) in the 4th floor, the fundamental mode appears to be the largest contributor to the bending moment and, hence, is the most important for yielding at this station. At times, however, the second and higher modes are observed to add to the fundamental mode, thereby contributing to the yielding.

As the frame is deformed, the ends of the girders within the same floor may or may not yield simultaneously depending upon the distribution of strength properties, i.e., yield moments, in that portion of the frame. In the lower portion, the yield moments in the interior and exterior girders within the same floor are approximately equal and the yield moments in the girders are lower than those in the neighboring columns. As a result, the columns remain linear and the girders yield. In the time history plots, Fig. 6.13 and Fig. 6.14, for stations (h) and (g), it is observed that the girders in the second floor yield almost simultaneously.

Near the top of the frame the yield moments within the same floor differ by as much as 10%. In the top two floors the yield moments in the girders approximate the yield moments in the neighboring columns. Consequently, in this portion of the frame, the girders within the same floor usually do not yield at the same time or by the same amount. This can be seen by comparing the time history plots, Fig. 6.15 and Fig. 6.16, of the plastic angles incurred at the opposite ends of the exterior girder in the 20th floor. (Note that different scale factors are used in the various plots for the 20th floor.)

For stations (h) and (g) in the second floor, there are some

TABLE 6-4

Times at which the most positive and most negative displacements and interfloor displacements occur for each floor of the A/20/2.2/2/6 frame with 0.10 fraction of critical damping (mass proportional) in the fundamental mode. Pseudo-earthquake number 1 is used. See Fig. A.2.3 in Appendix A for plots of corresponding displacements at the 4th and 17th floors and Fig. A.2.4 for the interfloor displacements between ground and the 1st floor and between the 18th and 19th floors.

| <u>Time (sec) of Occurrence of the Most Negative:</u> | | | <u>Time (sec) of Occurrence of the Most Positive:</u> | |
|---|------------------------------------|--------------|---|------------------------------------|
| <u>Displacement</u> | <u>Interfloor Displacement</u> | <u>Floor</u> | <u>Displacement</u> | <u>Interfloor Displacement</u> |
| 14.6 sec | | 20 | 18.0 sec | |
| | 29.5 sec | 19 | | 24.5 sec |
| 14.6 | 10.1 | 18 | 18.0 | 24.5 |
| 14.6 | 29.6 | 17 | 18.0 | 24.5 |
| 4.0 | 29.0 | 16 | 18.0 | 3.2 |
| 4.0 | 4.1 | 15 | 25.3 | 3.2 |
| 3.9 | 4.1 | 14 | 25.3 | 18.0 |
| 3.8 | 12.0 | 13 | 25.3 | 18.0 |
| 3.8 | 12.0 | 12 | 25.3 | 25.3 |
| 3.8 | 12.0 | 11 | 15.6 | 25.4 |
| 3.8 | 16.5 | 10 | 13.1 | 25.4 |
| 3.8 | 16.5 | 9 | 13.1 | 25.4 |
| 3.8 | 3.8 | 8 | 13.1 | 15.3 |
| 21.5 | 3.8 | 7 | 13.1 | 15.6 |
| 21.5 | 9.7 | 6 | 13.1 | 13.2 |
| 21.5 | 9.7 | 5 | 13.1 | 13.1 |
| 21.5 | 16.3 | 4 | 13.1 | 13.1 |
| 21.5 | 21.5 | 3 | 13.0 | 13.1 |
| 21.4 | 21.5 | 2 | 13.0 | 13.0 |
| 21.4 | 21.4 | 1 | 13.0 | 13.0 |
| 21.4 | 21.4 | Ground | 13.0 | 13.0 |

high frequency components in the bending moments, but it appears that most of the yielding occurs in connection with the response of the fundamental mode. On the other hand, in the time history plots of the bending moments in the 20th floor, many frequencies are observed. It is not obvious that any one frequency dominates the bending moments or the yielding in the 20th floor. Furthermore, the times at which yielding occurs in the 20th floor are different from those at which yielding occurs in either the 2nd, 4th, or the 17th floor.

In Fig. 6.19a the displacement envelope is given. Although the points are connected together, this does not necessarily imply that either all of the most positive displacements or all of the most negative displacements occur at the same time. Typically three or four times are represented for either side of the envelope as shown in Table 6-4 for the study using pseudo-earthquake number 1. However, in the study being analyzed in this section, which uses pseudo-earthquake number 6, all floors do reach their most positive displacements at the same time and the most negative displacements at the same time.

The 20th floor (roof) usually, but not always, is the floor which incurs the maximum absolute displacement of any floor in the frame during an earthquake. As indicated in Table 6-3, for the various studies using 0.10 fraction of critical damping in the frame, the maximum absolute displacements range between 8.5 and 14.4 inches. The ductility factors for the individual girders and columns are shown in

Fig. 6.20a and Fig. 6.20b, respectively. The ductility factors greater than 1.0 indicate that yielding occurred and are calculated according to Eq. 2.44.1. However, when yielding does not occur, the ductility factors are less than 1.0 and are given by the maximum absolute values of the ratios of the incurred bending moments to the corresponding yield bending moments. For the girders, the ductility factor for each end is shown, but for the columns, only the maximum value that occurs at either end is plotted. The maximum values of the ductility factors for each study are presented in Table 6-3. For the pseudo-earthquakes, with 0.10 fraction of critical damping in the frame, the maximum values of the ductility factors for the girders range from 3.6 to 5.0. For the exterior columns, which do not yield, the maximum values range from 0.71 to 0.81. For the interior columns, which yield in the upper two or three floors only, the maximum values are between 1.74 and 3.11.

This range in the maximum values of the structural responses appears to result from statistical variation. Such a range might be expected because the exact time histories of the earthquake accelerograms differ and because there is some variation in the statistics of the properties of the accelerograms.

In order to observe the effect of viscous damping on the response of this frame, a computer run using pseudo-earthquake number 6 with 0.05 fraction of critical damping was made. The plots for this run are shown in Fig. A.6.1 through Fig. A.6.8 in Appendix A. The effect of viscous damping is seen by comparing the various responses in those plots with the corresponding ones

presented in this section. The summary of these response results tabulated in Table 6-3 indicates that by decreasing the fraction of critical damping from 0.10 to 0.05, the maximum absolute values of the various responses increase: the displacement by 15%; the interfloor displacement by 9%; the ductility factors in the girders by 8%, in the interior columns by 12%, and in the exterior columns (moment ratio) by 3%.

6.4 Relationships Between Structural Responses and the Strength of an Earthquake

Three common measurements of the strength of an earthquake are the following:

1. The maximum absolute value of the ground acceleration during the earthquake;
2. The rms value of the acceleration of the earthquake:

$$\left[\frac{1}{30} \int_0^{30} [\ddot{y}(t)]^2 dt \right]^{\frac{1}{2}} ;$$

3. The spectrum intensity of the earthquake: The spectrum intensity SI_{ξ} is defined as the area under the velocity spectrum curve* from period $T = 0.1$ to $T = 2.5$ for a

*If \dot{z} is the relative velocity of a linear, base excited oscillator having period T and fraction of critical damping ξ , then the velocity spectrum value for this system is

$$S_{vel}(\xi, \frac{2\pi}{T}, t') = |\dot{z}|_{max}$$

where t' is the length of the earthquake excitation. Other points of the same velocity spectra curve are obtained by using different natural periods of the system. The average spectra curves in Fig. 5.3 are based upon the "pseudo-velocity" spectrum values

$$S_{ps-vel}(\xi, \omega, t') = \omega |z|_{max} .$$

given damping factor, ξ , and earthquake excitation^(9,14):

$$SI_{\xi} = \int_{T=0.1}^{T=2.5} S_{vel}(\xi, \frac{2\pi}{T}, 30) dT$$

The numerical values of these three strength measurements of the earthquakes used to excite the nonlinear structure are listed in Table 6-3. Note that the spectrum intensities are given for $\xi = 0.0$.

In an attempt to find a means for predicting the magnitude of structural response, it is of interest to compare the earthquake strengths as defined above with the magnitudes of the corresponding structural responses. Unfortunately, it is seen that none of these three measurements correctly predicts the trend of the maximum absolute values of either the displacements or ductility factors of the structure.

The first two measurements, maximum absolute value and rms value of an earthquake, do not take any properties of the structure into consideration and, therefore, they should not be expected to accurately estimate the maximum absolute value of the various responses of a tall structure. However, if the same earthquake is used with two different amplitude scale factors, the response corresponding to the larger scale factor can be expected to be larger.

The period range chosen for the spectrum intensity includes many of the natural periods of a typical tall structure. However, because the modes of a particular structure are not specifically considered, the spectrum intensity should not be expected to accurately predict the amplitude of the response of that structure. Nevertheless,

the spectrum intensity may be indicative of the amplitude of the average response of numerous structures taken together.

Another method for estimating the maximum values of the horizontal displacement, $y_{j_{\max}}$, in the structure is⁽⁹⁾

$$y_{j_{\max}} = \left\{ \sum_{i=1}^{20} \left[\frac{\sum_{k=1}^{20} \phi_{ki} M_k}{\sum_{k=1}^{20} \phi_{ki}^2 M_k} \frac{\phi_i}{\omega_i} S_{ps-vel_i} \right]^2 \right\}^{\frac{1}{2}}$$

where

- j : floor number,
- i : mode number,
- S_{ps-vel_i} : the pseudo-velocity spectrum value at T_i ,
- ϕ_{ki} : the k^{th} component of the i^{th} mode shape, and
- ω_i : the i^{th} modal frequency.

Since this method takes the modes of the structure into account, it might be more successful in predicting the trends of the maximum absolute displacements of the structure as a function of the earthquakes. It is noted that this method does not consider the time dependence of the modes. From the results of Section 6.3, it appears necessary to take the time dependence into consideration in order to accurately predict the maximum values of the various responses. One such method of approximating the magnitude of a given response in a structure might use the maximum absolute value of a time dependent sum of the linear modal responses, such as shown in Fig. 6.8, with

each mode weighted according to its expected contribution to the response of interest. The abilities of these methods to predict the trends could be evaluated in a future study by applying them to the structure and earthquakes discussed in this chapter.

CHAPTER VII

CONCLUSIONS

The following is a summary of the conclusions reached for the investigation described in this report:

- 1) Since the one-component nonlinear beam model can have a different curvilinear or bilinear hysteresis loop at each end, it is more versatile than the two-component model which is restricted to bilinear hysteresis loops at the ends.
- 2) Of the three definitions of ductility factor presented, only one is adaptable to both bilinear and curvilinear hysteresis loops. In the computer studies, this one was used with the one-component model having bilinear hysteretic behavior.
- 3) As an overall check on the computer program for analyzing the response of a nonlinear multi-story structure subjected to earthquake excitation, several tests covering various aspects of the computations were made. The results of each test indicate that the program operates properly and provides the desired accuracy.
- 4) For a nonlinear structure, it is possible to find "equivalent" modal participation factors which describe the contributions of the various modes to the structural response. These can be obtained by expanding the displacement vector for the nonlinear structure in terms of the eigenvectors of the linear system.

Such an analysis indicates that more modes may contribute to the interfloor displacements than can be visually observed in the time history response plots, particularly in the upper portion of the structure.

- 5) The effects of yielding on the response of the A/20/2.2/2/6 frame subjected to the first four seconds of the El Centro (N-S) earthquake of 18 May 1940 are, generally,
 - (a) to reduce the forces and moments to approximately 60% of the values for the linear system, and
 - (b) to reduce the displacements, interfloor displacements, and total accelerations to about 80% of the corresponding values for the linear system.

During severe yielding, the shapes of the response time history plots are significantly changed from the shapes of the corresponding responses for the linear structure.

- 6) In different computer runs, the nonlinear A/20/2.2/2/6 frame with 0.10 fraction of critical damping in the fundamental mode was subjected to the entire El Centro (N-S) earthquake of 18 May 1940 and to six pseudo-earthquakes. The time history plots for a given response at a given position in the structure were compared for the earthquakes used. Characteristic patterns of response behavior were noted which were in qualitative agreement with similar responses of linear elastic, shear-type, continuous cantilever beams. A brief summary of

these characteristic response patterns follows:

- (a) For the overturning moment at the base, the fundamental mode dominates.
- (b) For the horizontal displacements in the upper portion, the fundamental mode dominates; in the lower portion, the fundamental mode is important, but the 2nd and 3rd modes are also significant.
- (c) For the interfloor displacements in the upper portion, as many as eight modes may be important. The fundamental mode decreases in importance approaching the roof. In the lower portion, the fundamental mode increases in importance approaching the base, but the 2nd, 3rd and 4th modes also contribute significantly.
- (d) For the total accelerations, frequencies of almost all modes are observed. This is partly a consequence of the relatively low damping in the higher modes.
- (e) Results of the studies of the continuous systems indicate that, with increasing taper of the structure, the higher modes become more important for all of the responses throughout the structure.

The distribution of ductility factors in the girders are similar for the different earthquakes used. Column ductility factor distributions were also similar for the different earthquakes.

Because these results are consistent for all of the earthquakes used, it is believed that the characteristic patterns of

modal contributions to the responses and the shapes of the ductility factor distributions are a function more of the structure than of the earthquake.

The maximum absolute value of a particular structural response differs between earthquakes because this value is highly dependent upon:

- (a) the extent to which individual modes are excited at a particular time, and
- (b) the phase relationships between the contributing modes at that time.

These modal responses differ from one earthquake to another because the exact time histories of the earthquakes are different.

- 7) Comparing maximum responses of the yielding structure for the series of pseudo-earthquakes having similar statistics, the following percentage deviations were found:

| | |
|---|-----|
| (a) maximum absolute displacements | 50% |
| (b) maximum absolute interfloor displacements | 40% |
| (c) girder ductility factors | 35% |
| (d) interior column ductility factors | 55% |
| (e) exterior column ductility factors | 15% |

- 8) The effect of decreasing the fraction of critical damping from 0.10 to 0.05 in the fundamental mode of this particular structure excited by pseudo-earthquake number 6 is to increase the maximum values of the displacement response by 15% and of the ductility factor by 8%.

APPENDIX A
RESPONSE PLOTS FOR A NONLINEAR MULTI-STORY
STRUCTURE SUBJECTED TO SEVERAL
EARTHQUAKE EXCITATIONS

In this appendix response plots for the A/20/2.2/2/6 structure subjected to several earthquakes are presented. Sets of response plots consisting of the displacement envelope, distributions of ductility factors in the girders and in the columns, and time history response plots for various stations in the structure are given for seven structure-earthquake combinations. The positions in the structure of the stations indicated in the plots are shown in Fig. 6.1. The structural and earthquake parameters used are listed in the heading at the top of each plot. They are also tabulated in Table 6-3.

NONLINEAR RESPONSE OF FRAME A/20/2.2/2/6
 BILINEARITY = 0.05, FRACTION OF CRITICAL DAMPING = 0.10
 EL CENTRO EARTHQUAKE (N·S), 18 MAY 1940, SCALE = 1.0

MOST NEGATIVE AND MOST POSITIVE DISPLACEMENTS IN INCHES

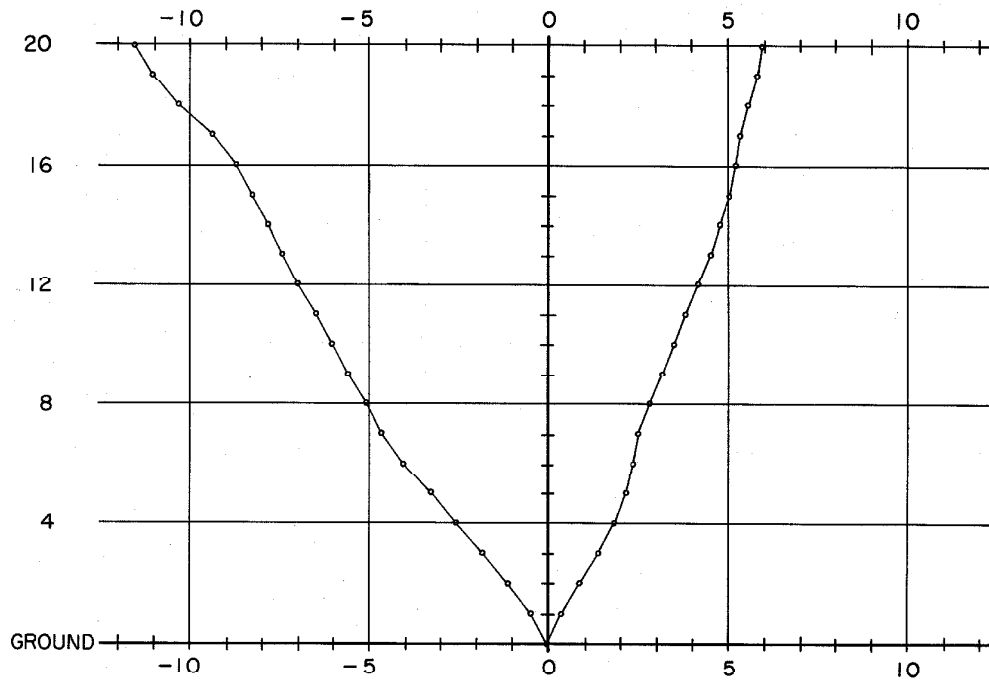


Fig. A.1.1

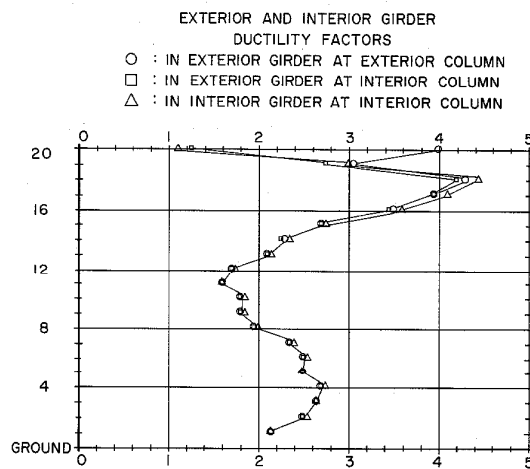


Fig. A.1.2.a

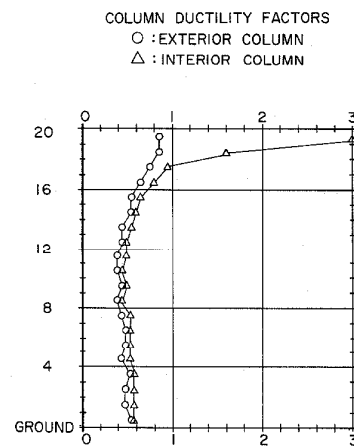


Fig. A.1.2.b

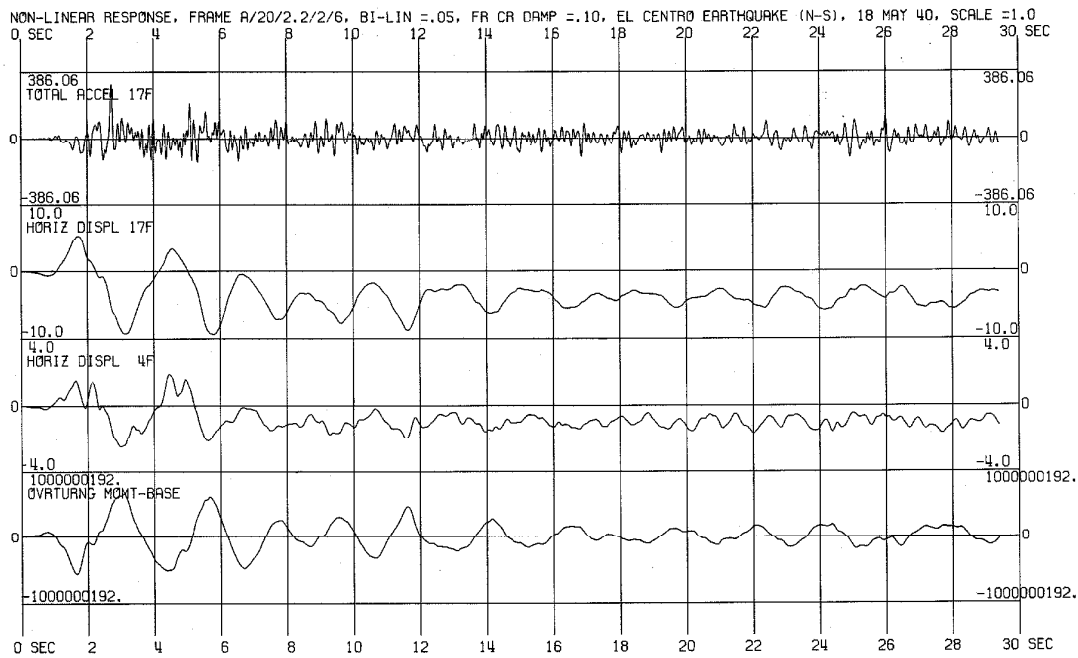


Fig. A.1.3

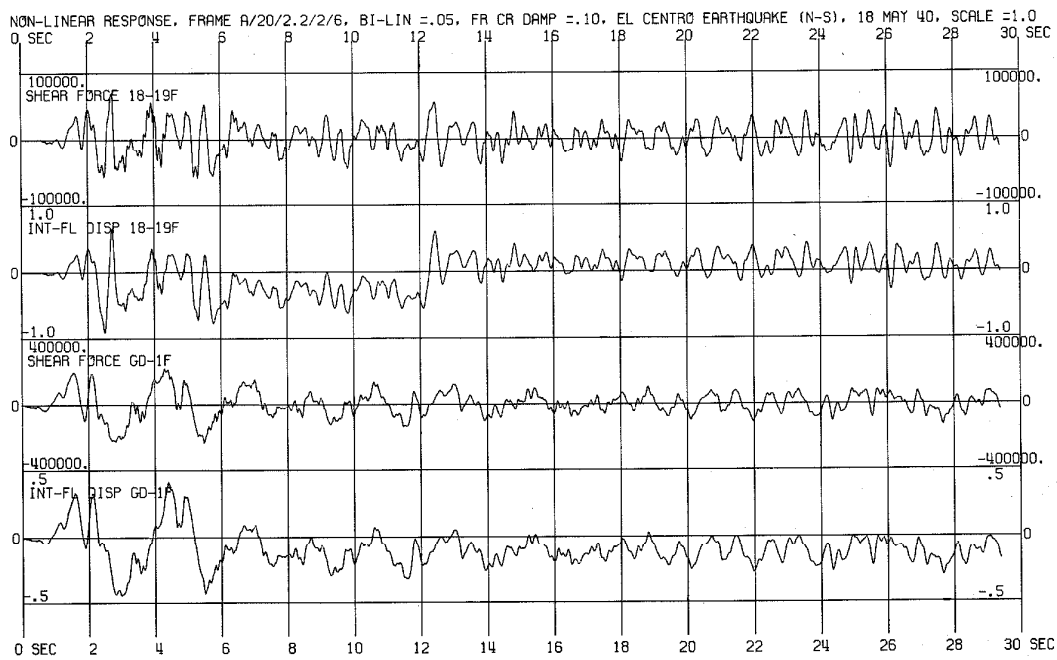


Fig. A.1.4

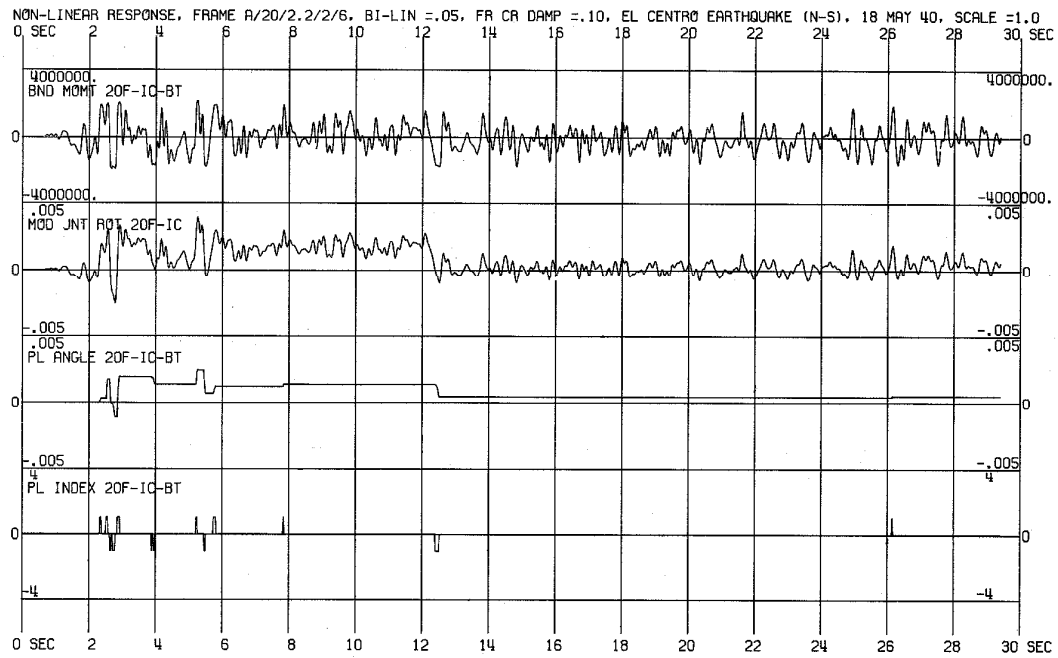


Fig. A.1.5 Station (d)

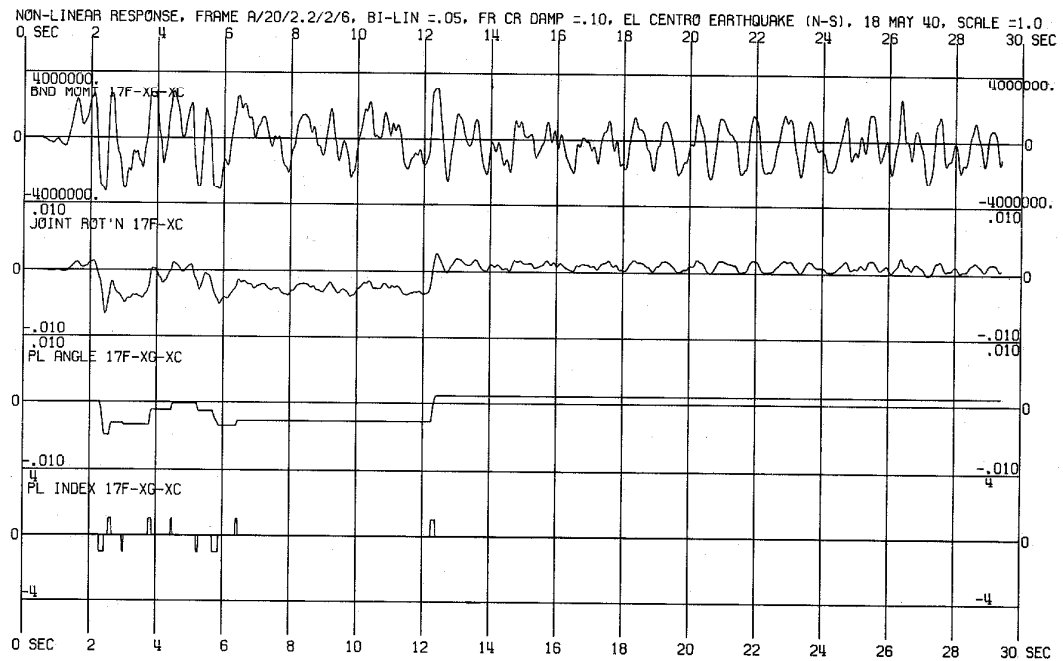


Fig. A.1.6 Station (e)

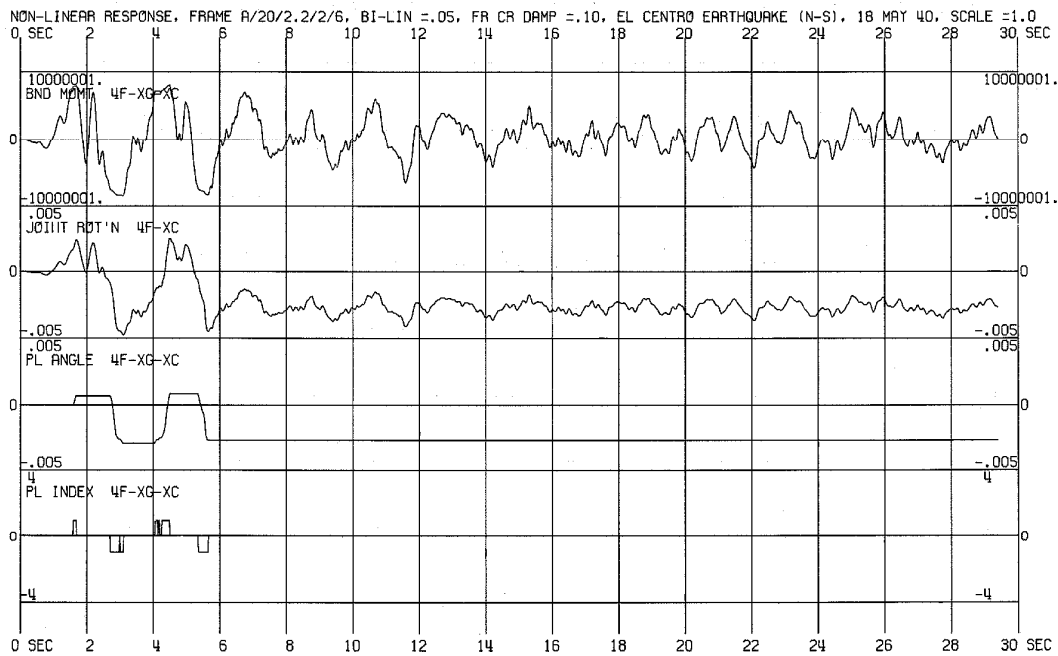


Fig. A.1.7 Station (f)

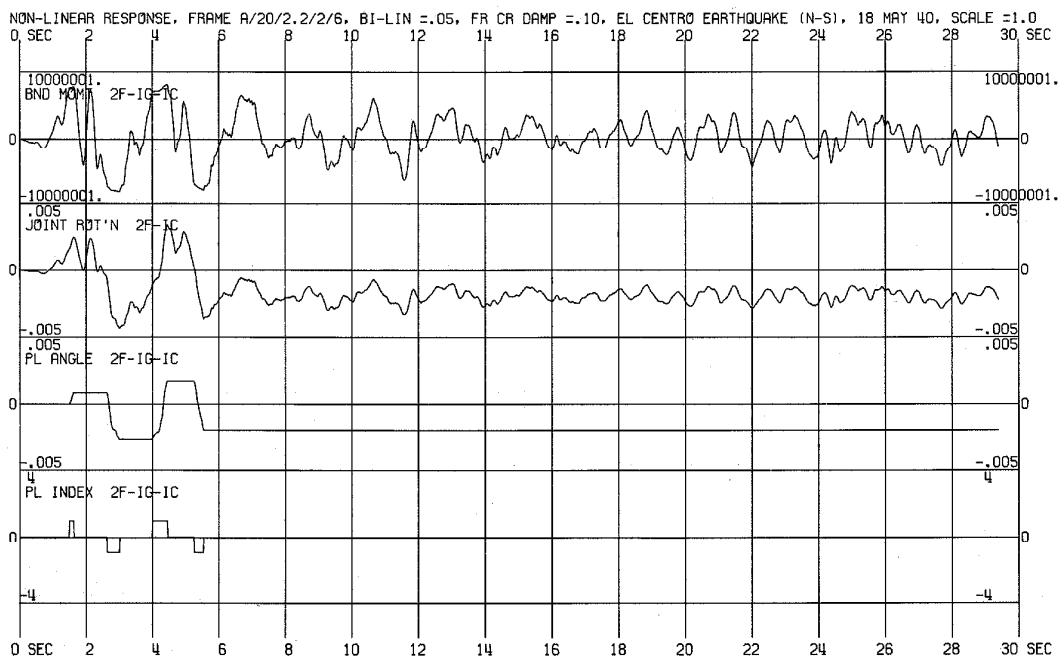


Fig. A.1.8 Station (h)

NONLINEAR RESPONSE OF FRAME A/20/2.2/2/6
 BILINEARITY=0.05, FRACTION OF CRITICAL DAMPING=0.10
 (JENNINGS) PSEUDO-EARTHQUAKE NUMBER 1, SCALE=1.2

MOST NEGATIVE AND MOST POSITIVE DISPLACEMENTS IN INCHES

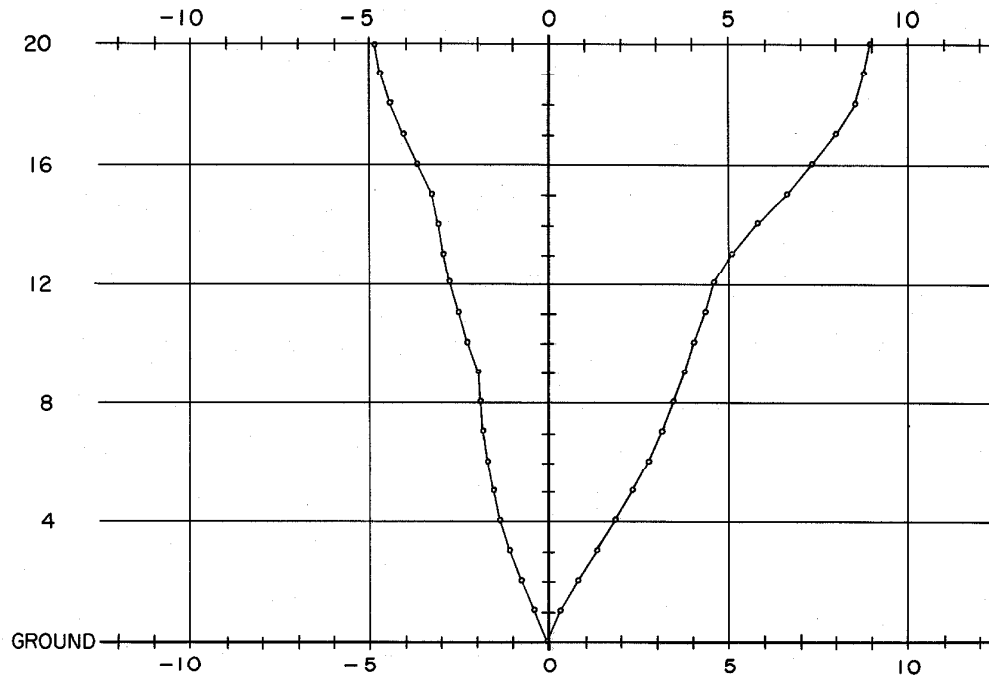


Fig. A.2.1

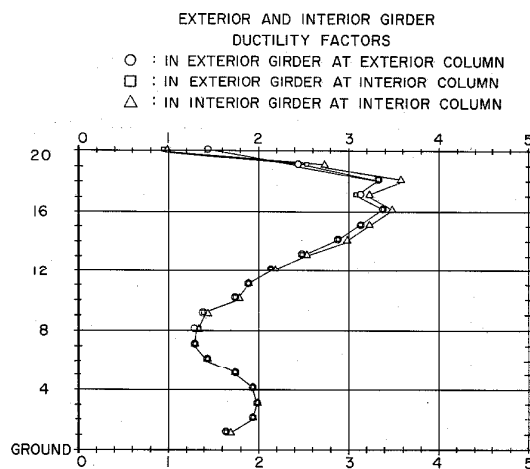


Fig. A.2.2.a

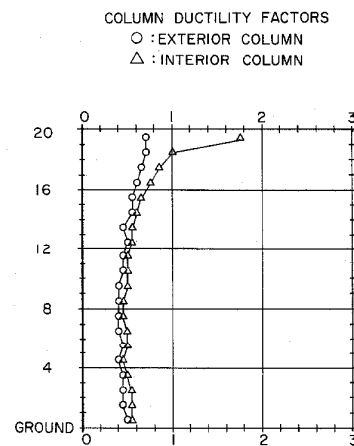


Fig. A.2.2.b

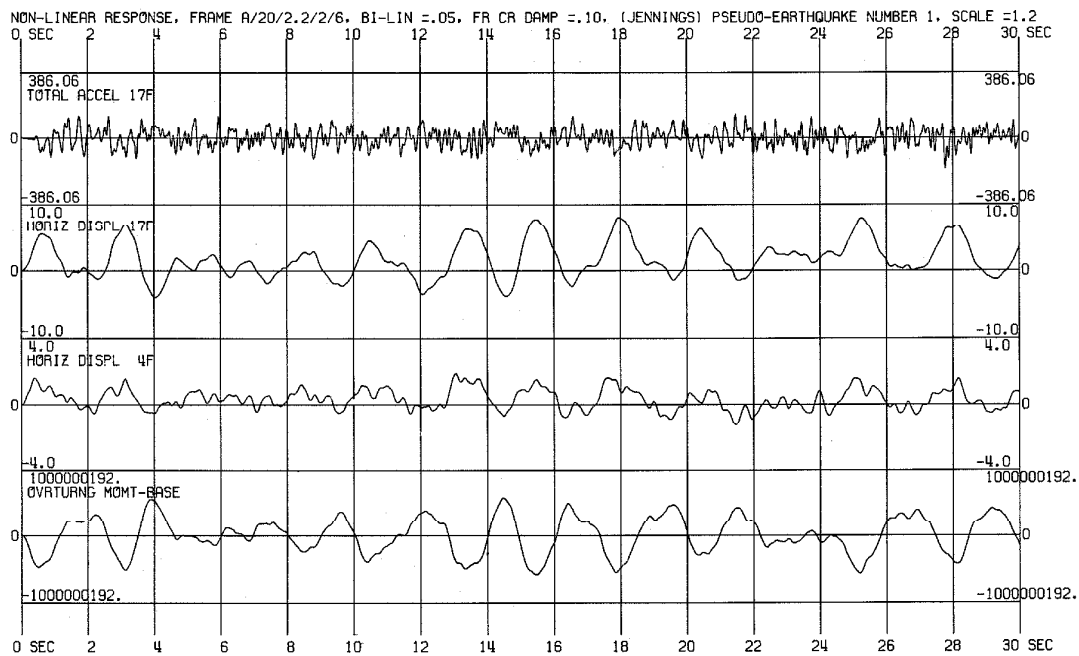


Fig. A.2.3

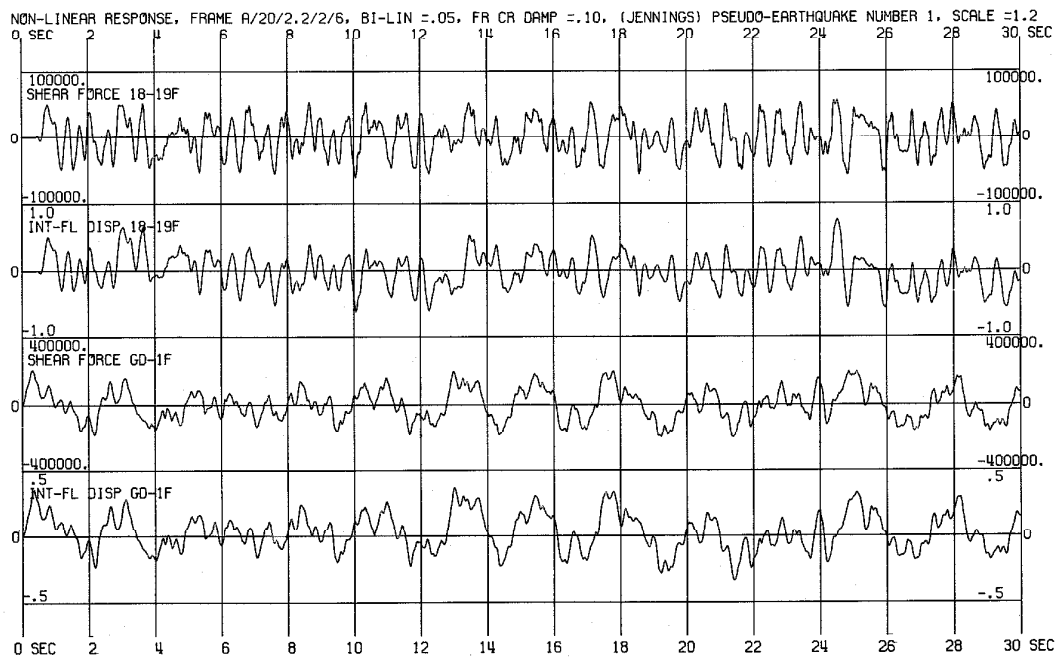


Fig. A.2.4

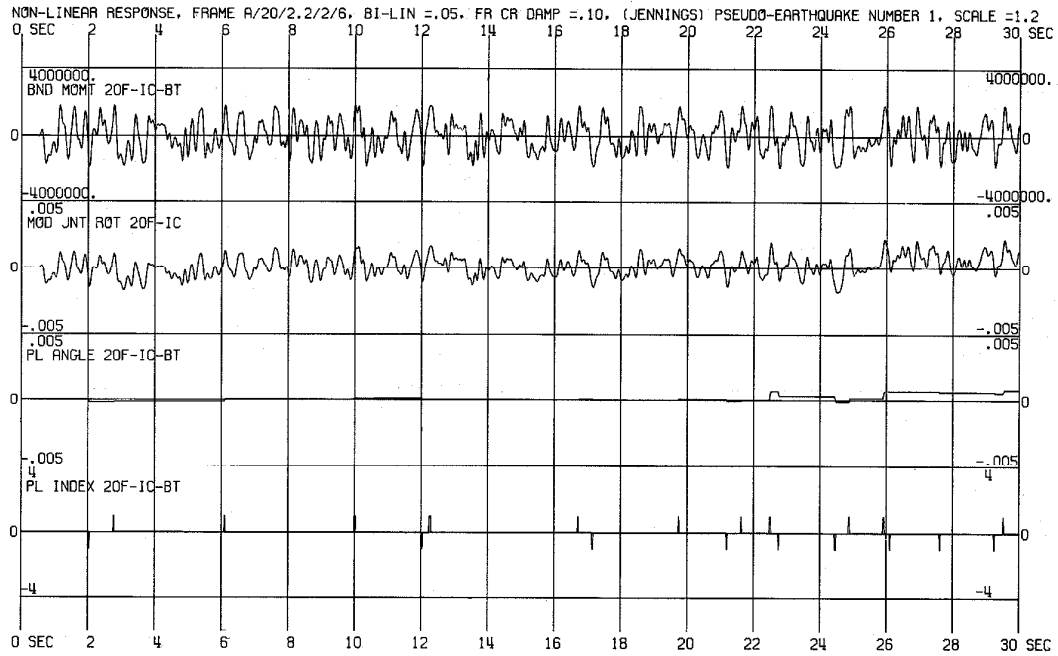


Fig. A.2.5 Station (d)

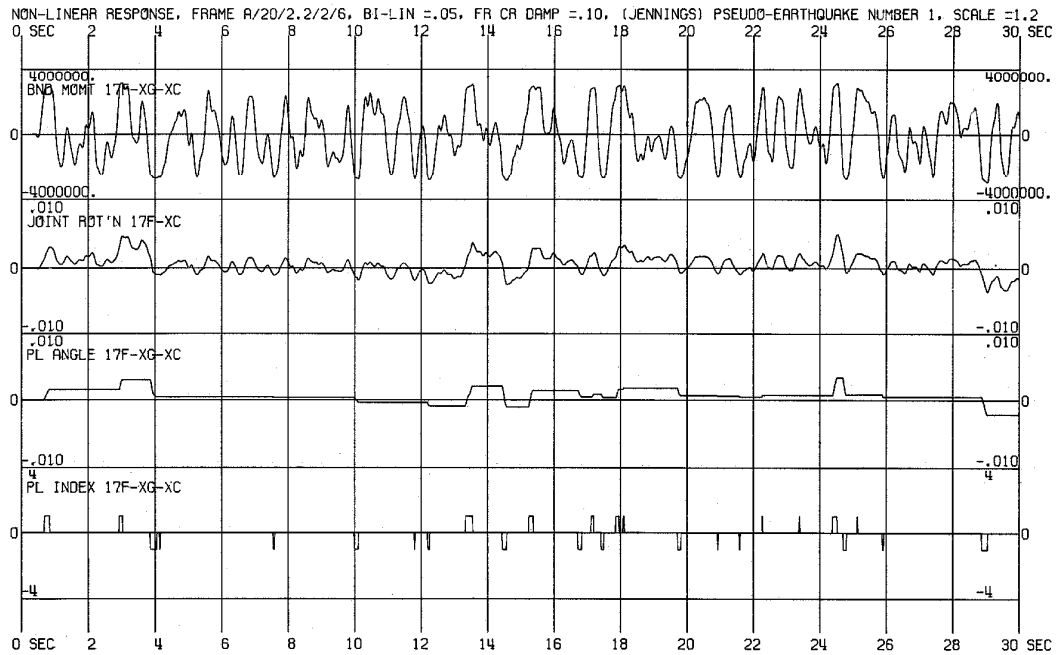


Fig. A.2.6 Station (e)

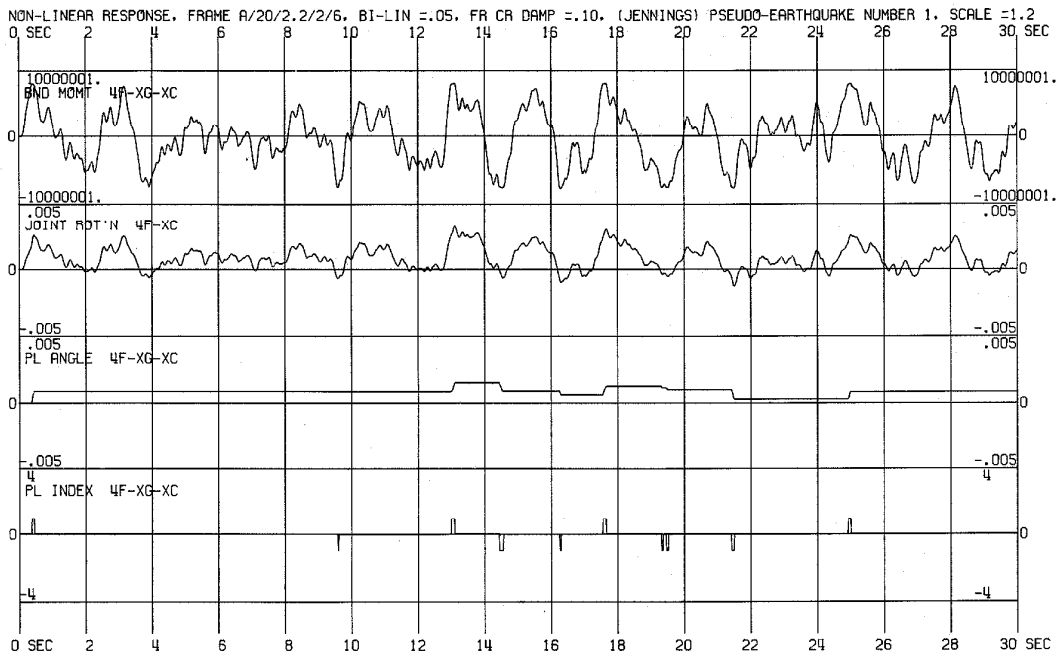


Fig. A.2.7 Station (f)

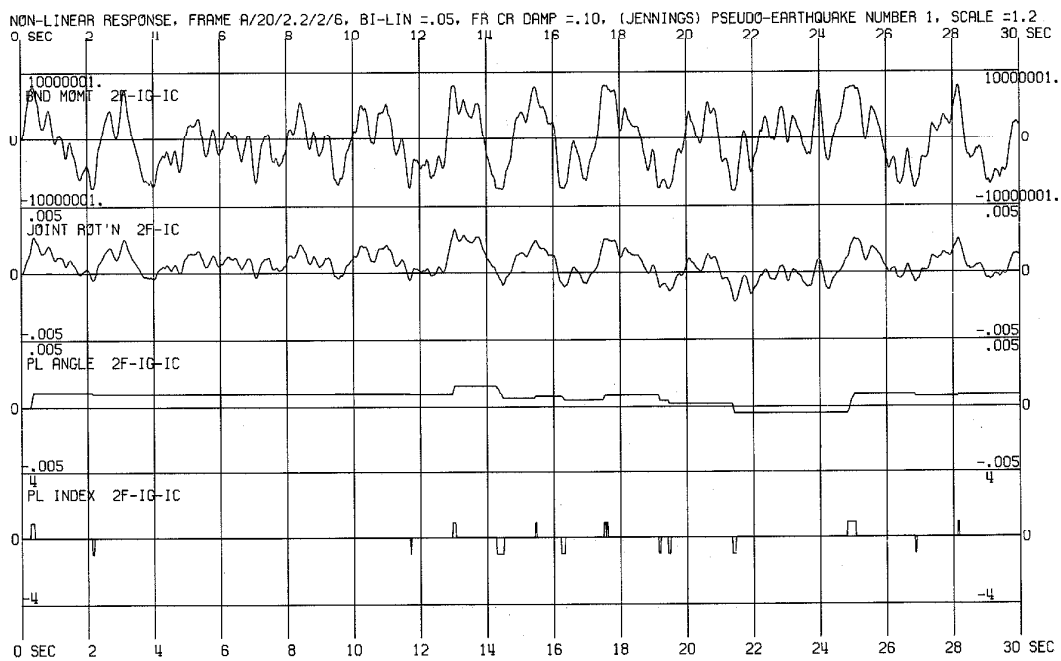


Fig. A.2.8 Station (h)

NONLINEAR RESPONSE OF FRAME A/20/2.2/2/6
 BILINEARITY = 0.05, FRACTION OF CRITICAL DAMPING = 0.10
 (JENNINGS) PSEUDO-EARTHQUAKE NUMBER 2, SCALE = 1.2

MOST NEGATIVE AND MOST POSITIVE DISPLACEMENTS IN INCHES

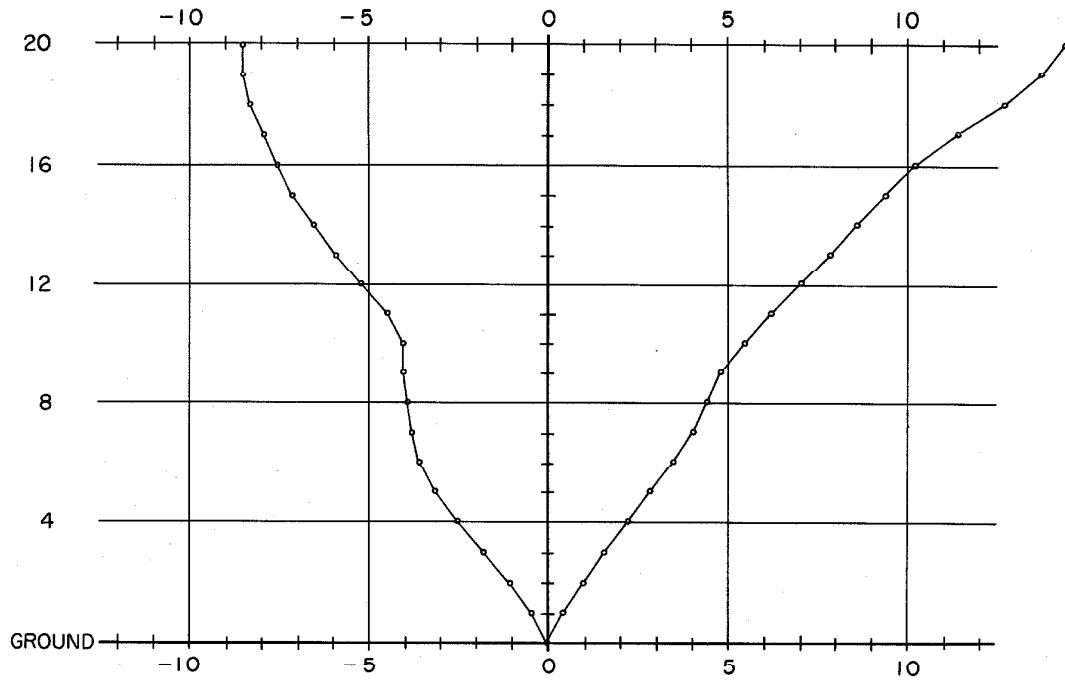


Fig. A.3.1

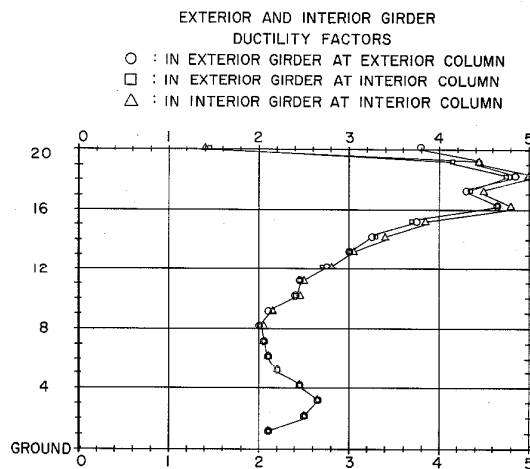


Fig. A.3.2.a

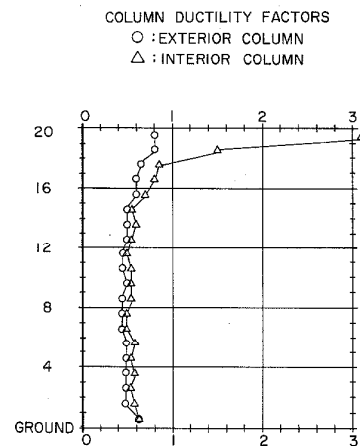


Fig. A.3.2.b

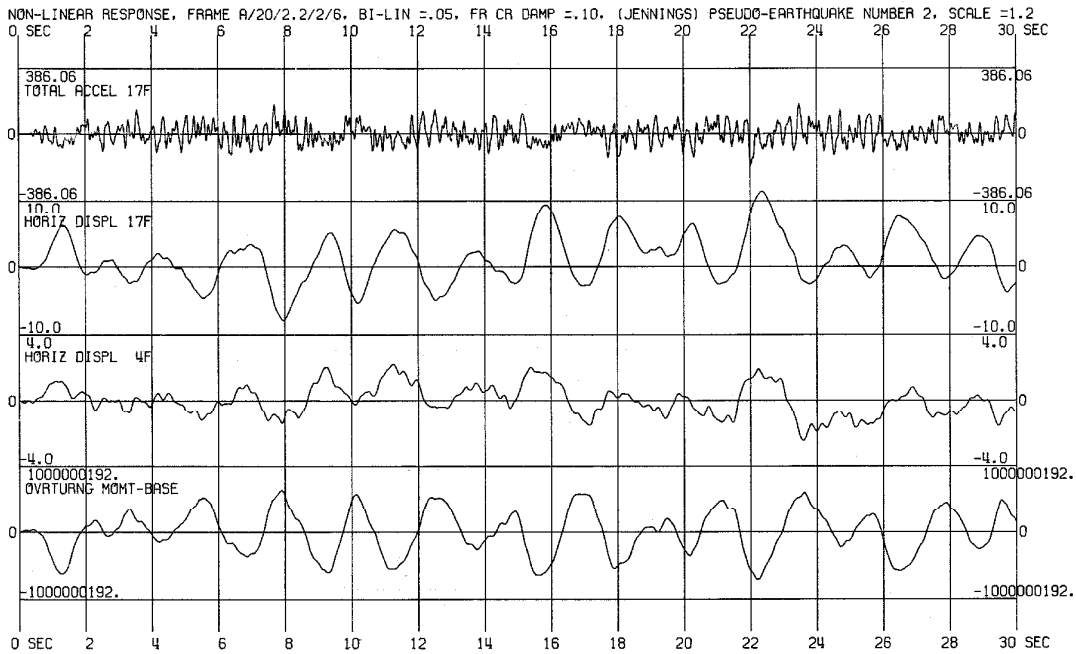


Fig. A.3.3

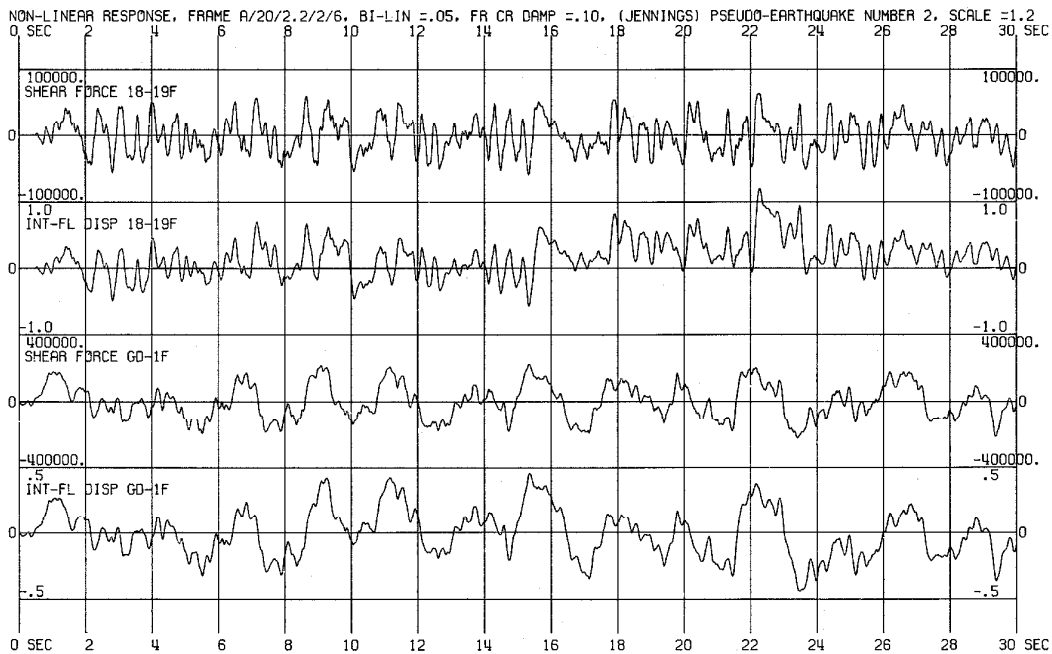


Fig. A.3.4

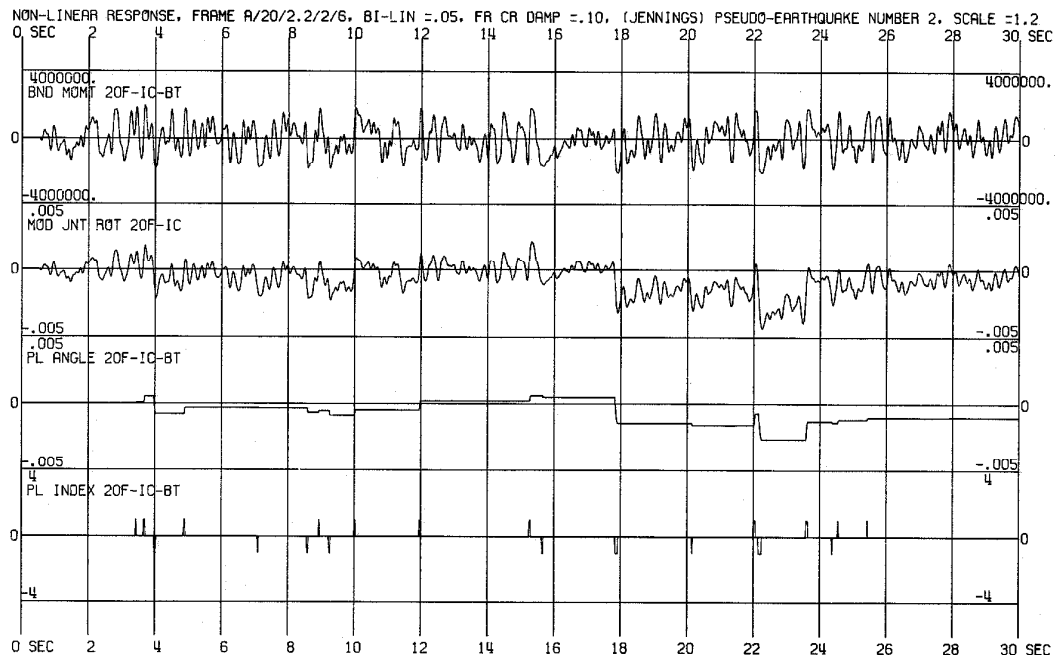


Fig. A.3.5 Station (d)

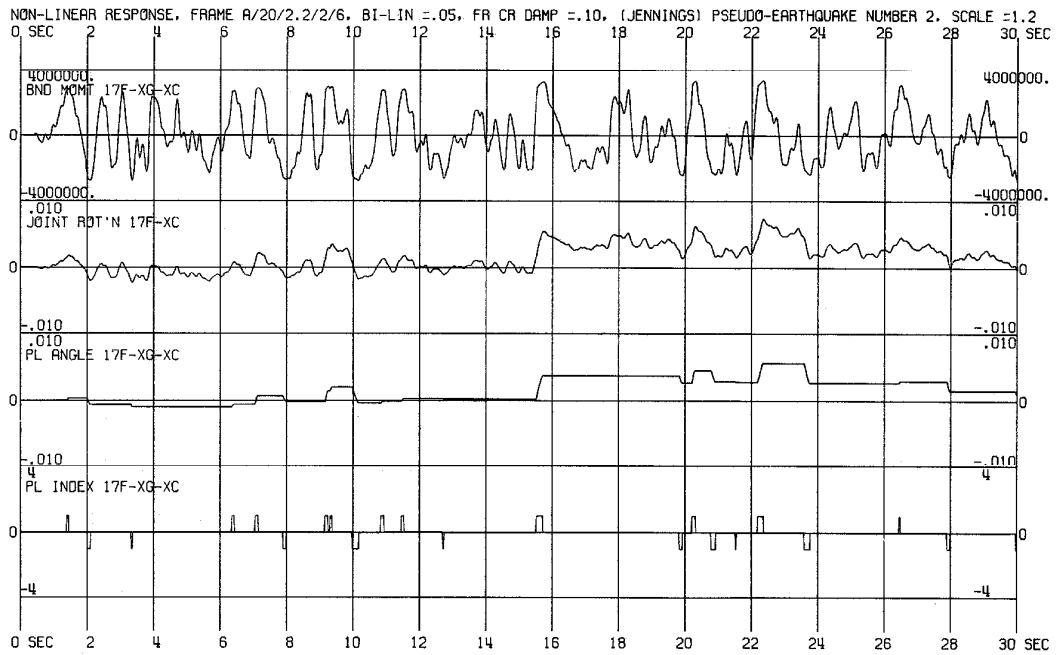


Fig. A.3.6 Station (e)

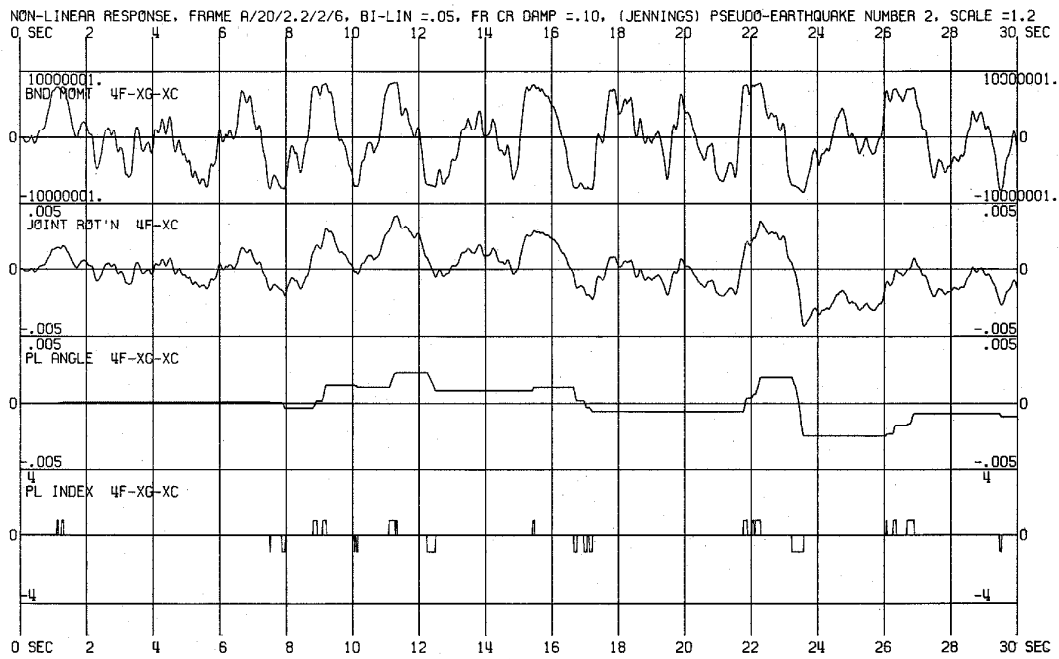


Fig. A.3.7 Station (f)

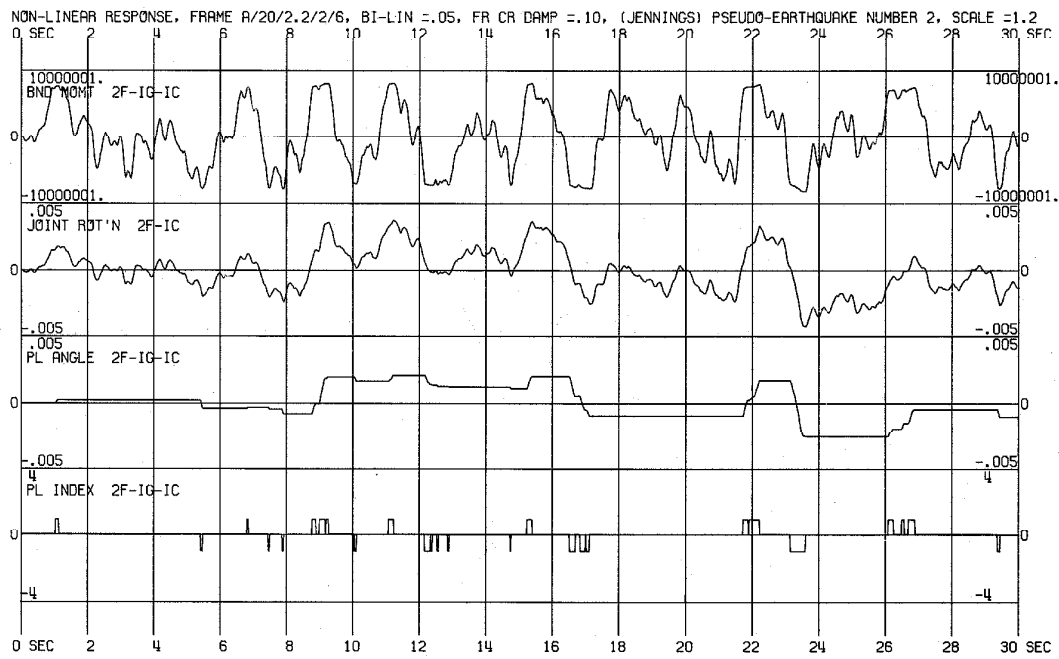


Fig. A.3.8 Station (h)

NONLINEAR RESPONSE OF FRAME A/20/2.2/2/6
 BILINEARITY = 0.05, FRACTION OF CRITICAL DAMPING = 0.10
 (JENNINGS) PSEUDO-EARTHQUAKE NUMBER 4, SCALE = 1.2

MOST NEGATIVE AND MOST POSITIVE DISPLACEMENTS IN INCHES

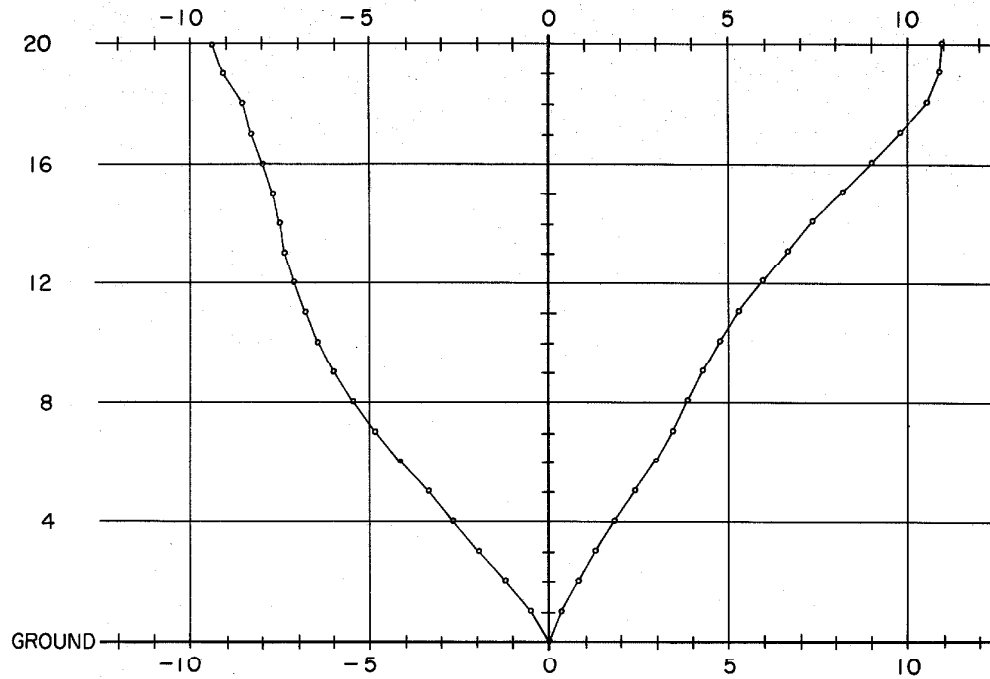


Fig. A.4.1

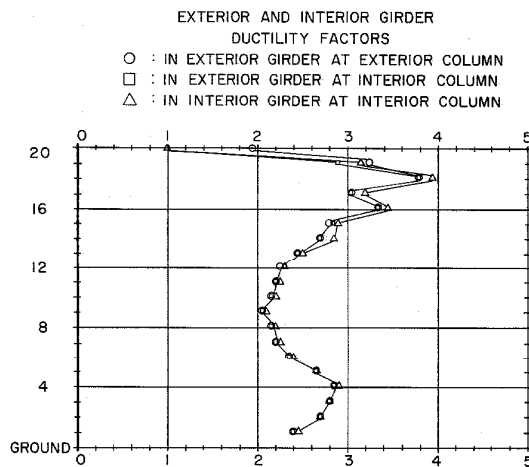


Fig. A.4.2.a

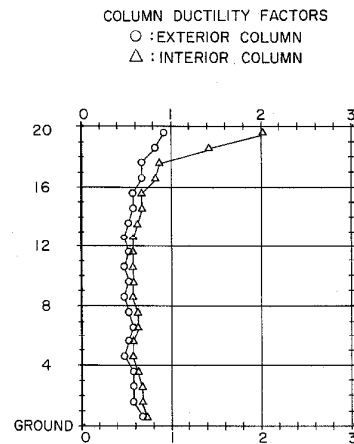


Fig. A.4.2.b

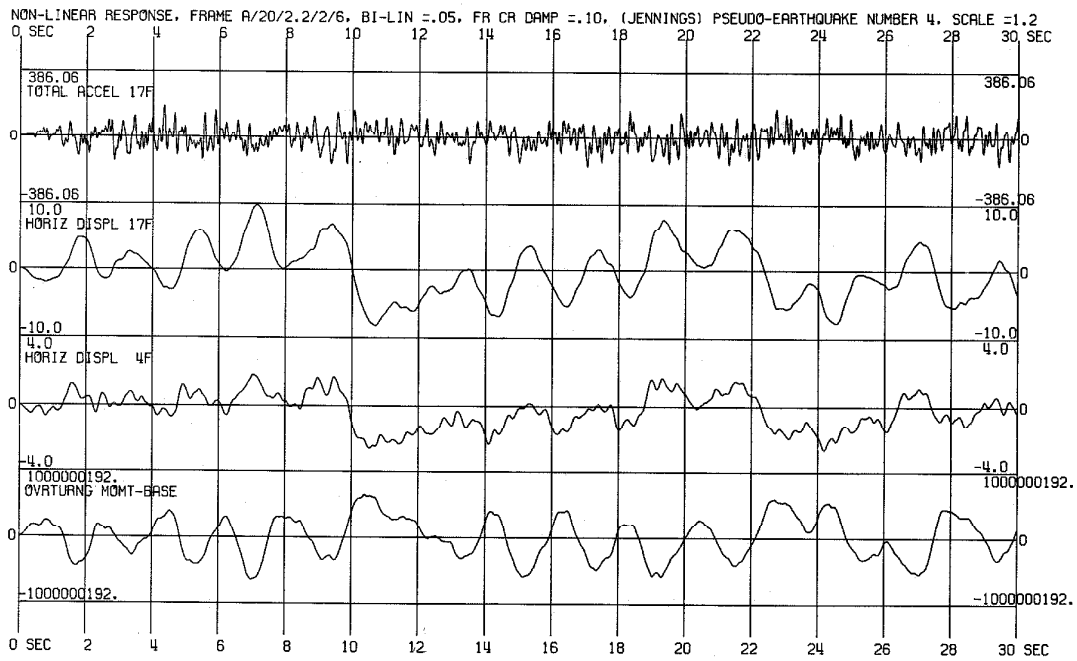


Fig. A.4.3

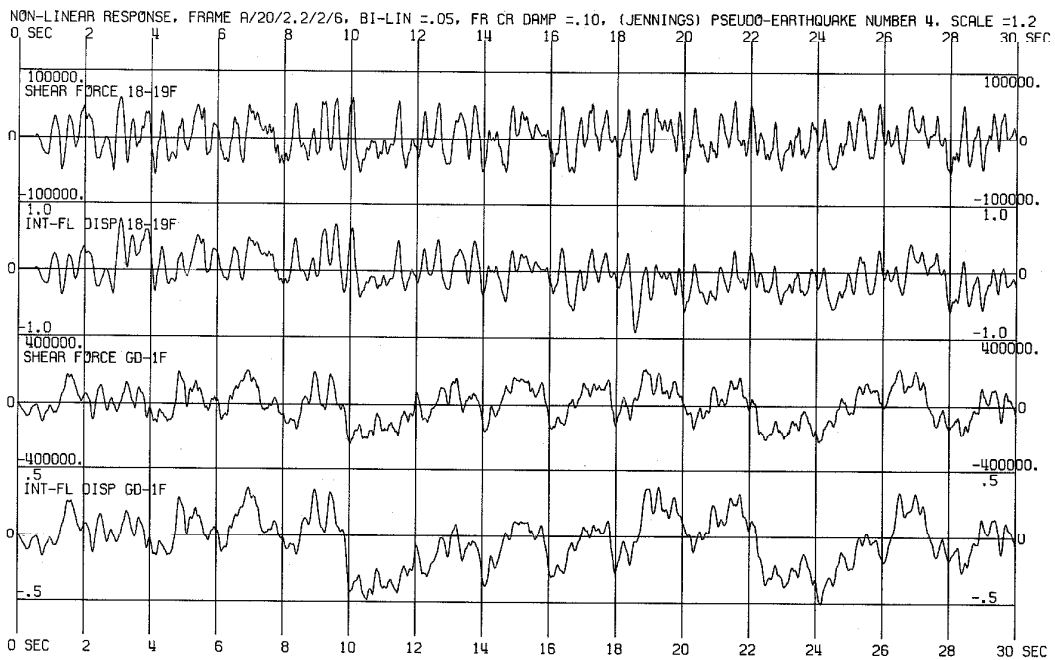


Fig. A.4.4

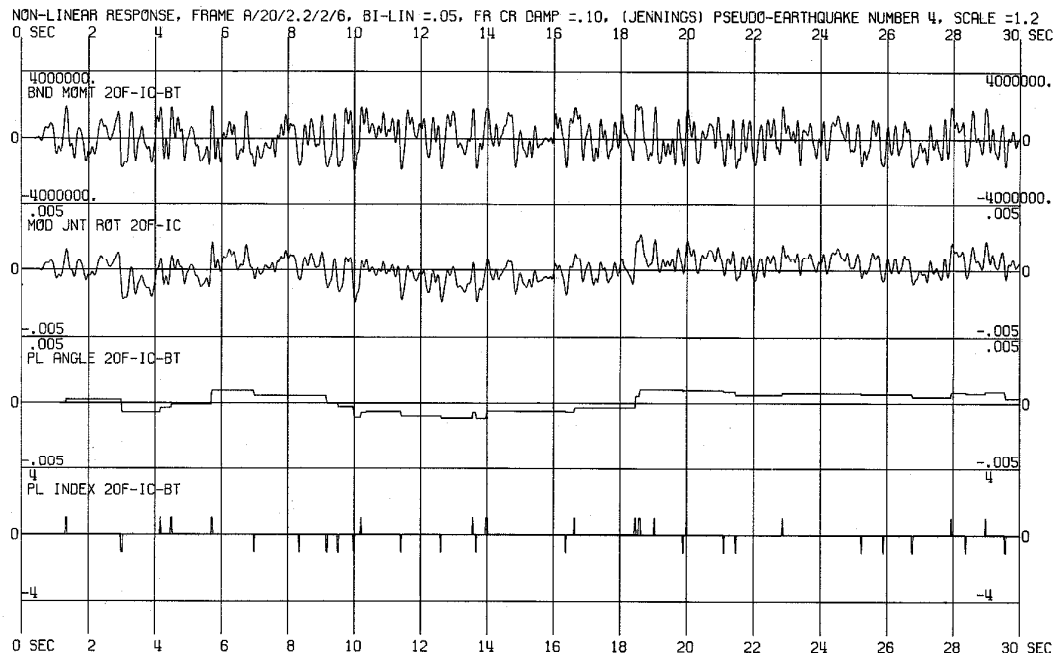


Fig. A.4.5 Station (d)

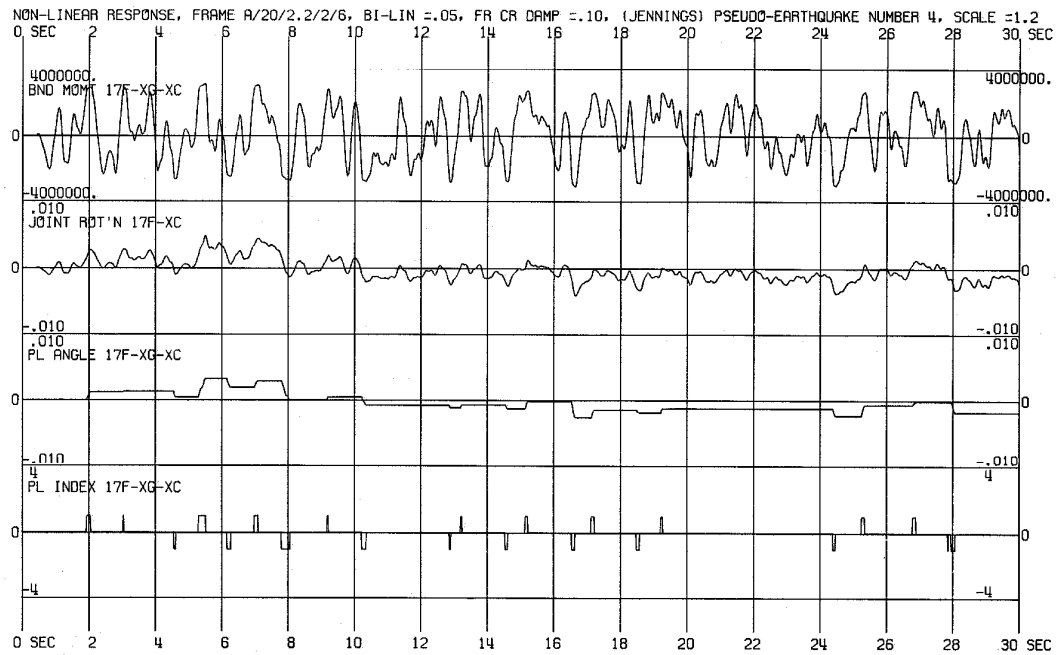


Fig. A.4.6 Station (e)

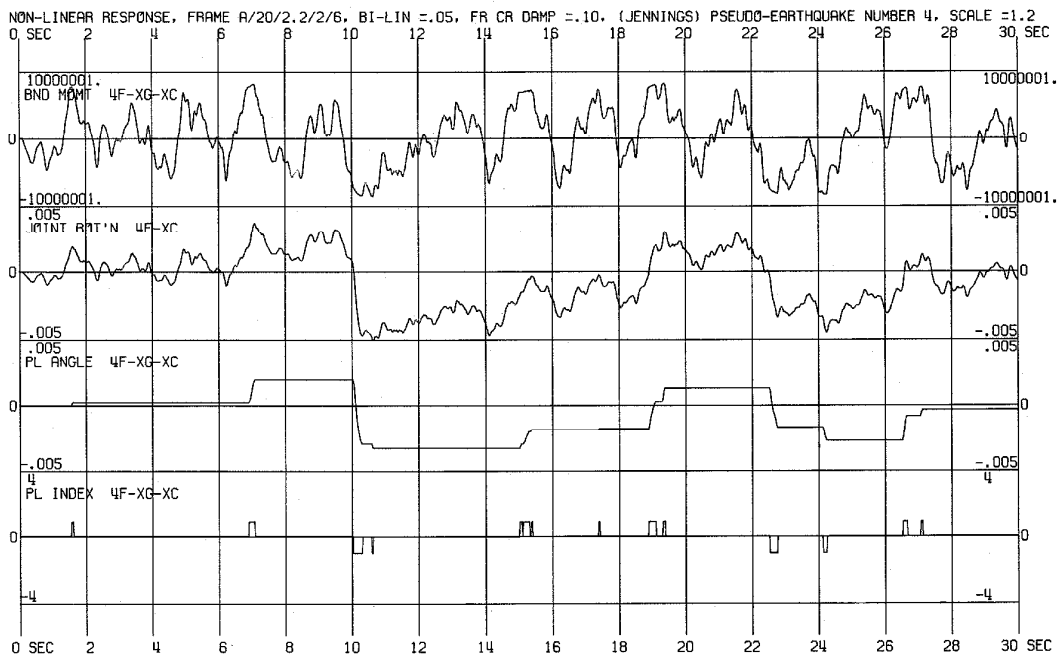


Fig. A.4.7 Station (f)

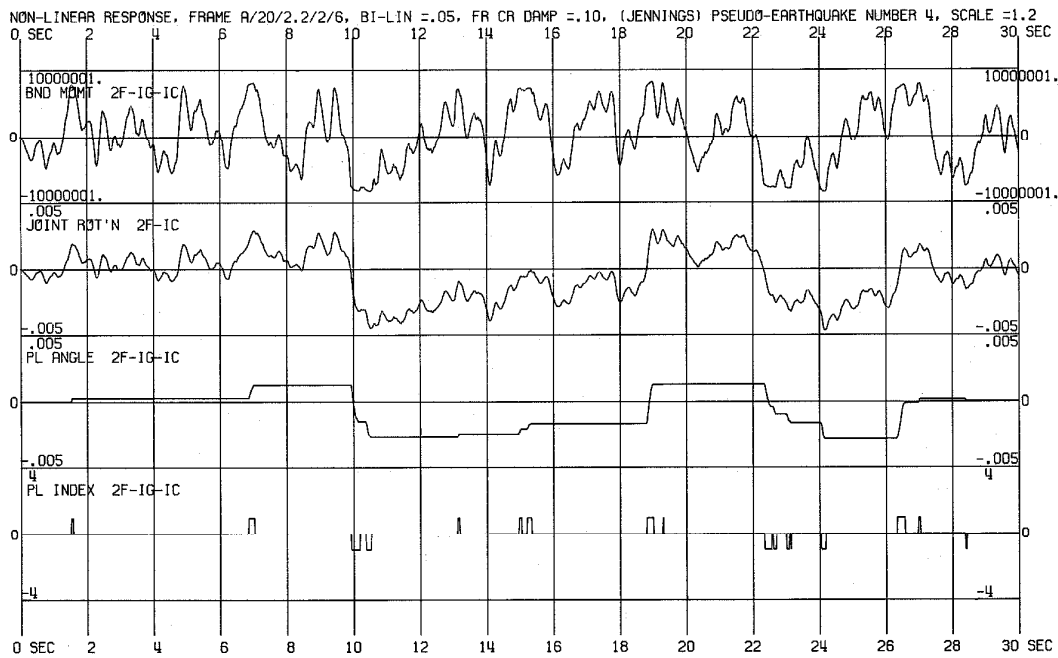


Fig. A.4.8 Station (h)

NONLINEAR RESPONSE OF FRAME A/20/2.2/2/6
 BILINEARITY = 0.05, FRACTION OF CRITICAL DAMPING = 0.10
 (JENNINGS) PSEUDO-EARTHQUAKE NUMBER 5, SCALE = 1.2

MOST NEGATIVE AND MOST POSITIVE DISPLACEMENTS IN INCHES

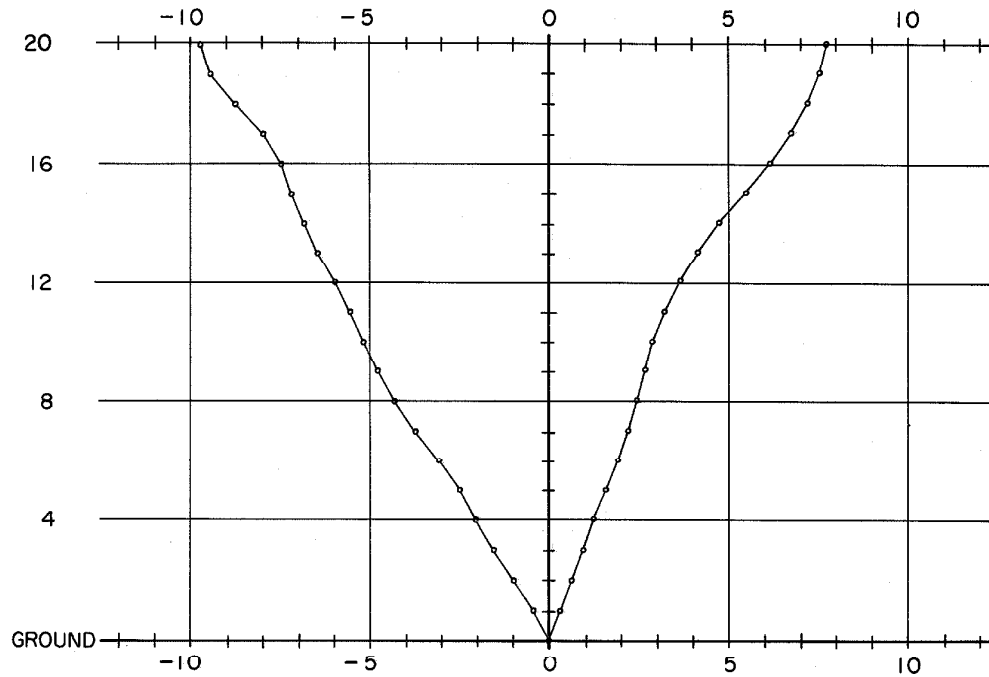


Fig. A.5.1

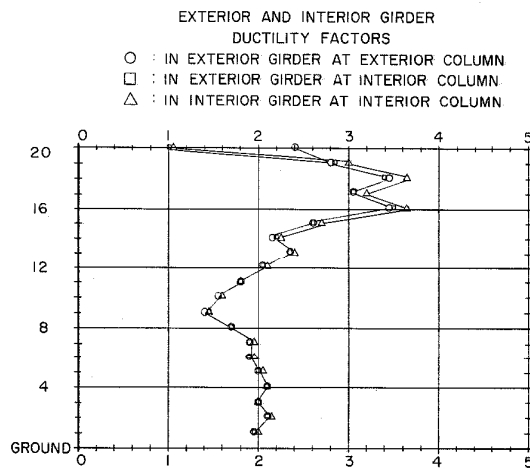


Fig. A.5.2.a

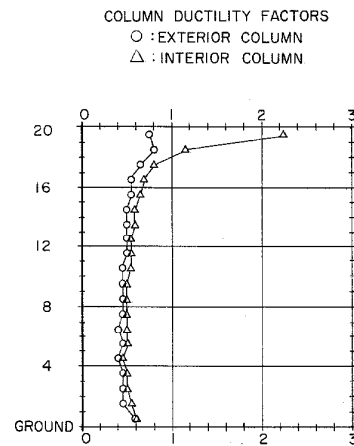


Fig. A.5.2.b

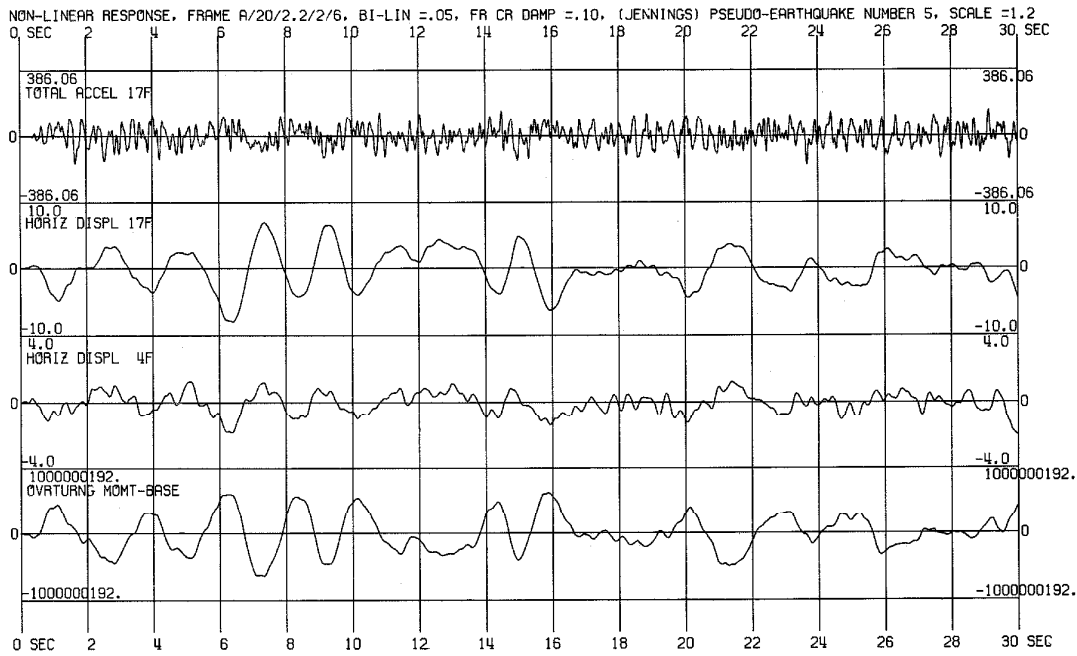


Fig. A.5.3

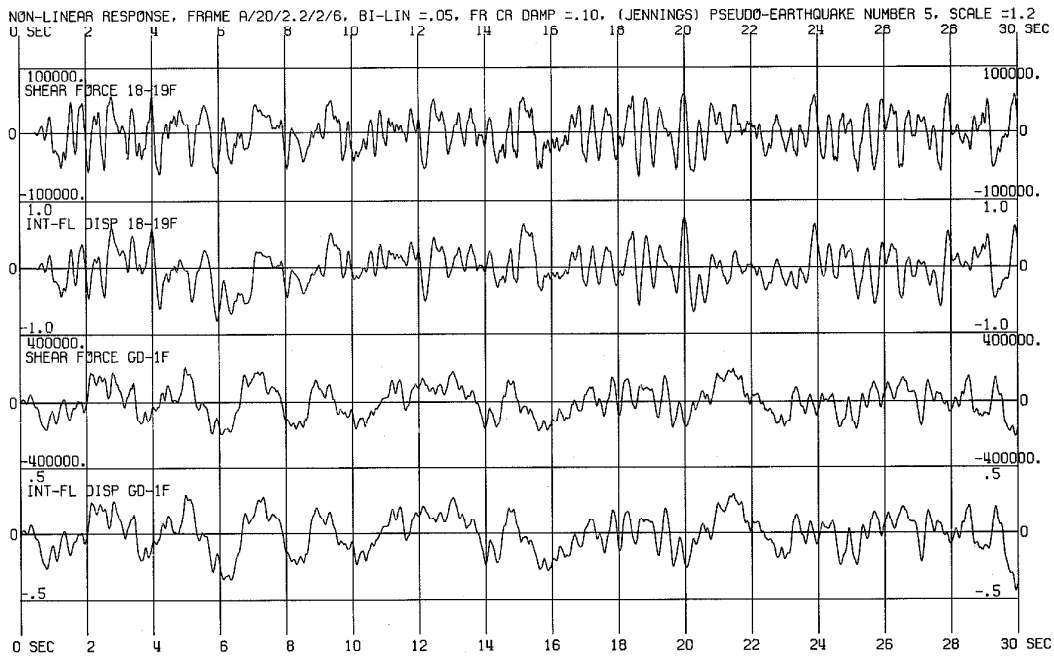


Fig. A.5.4

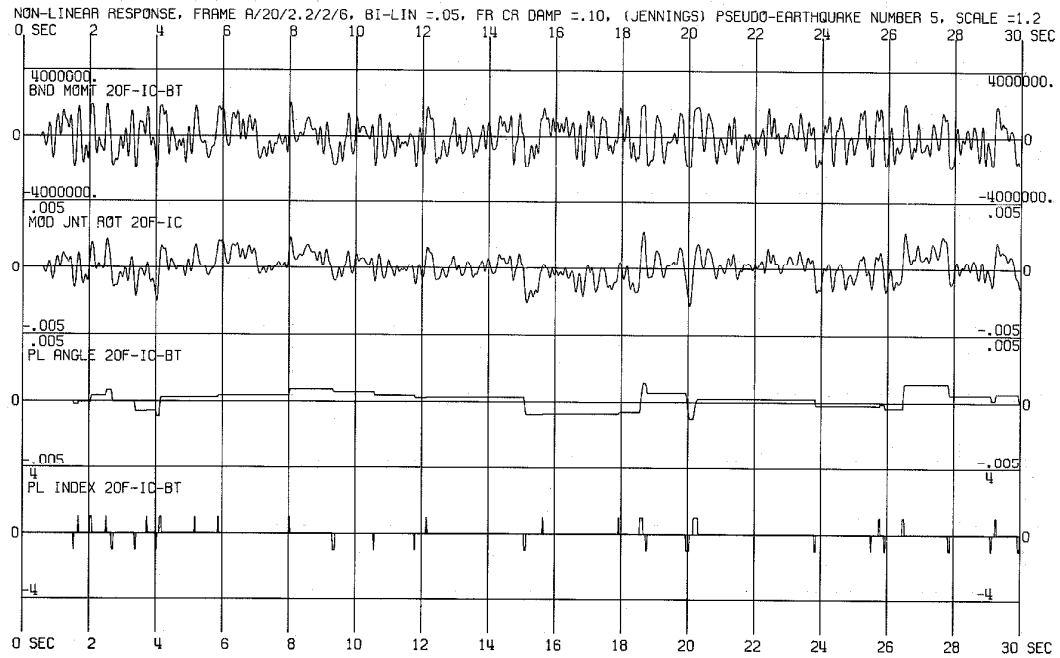


Fig. A.5.5 Station (d)

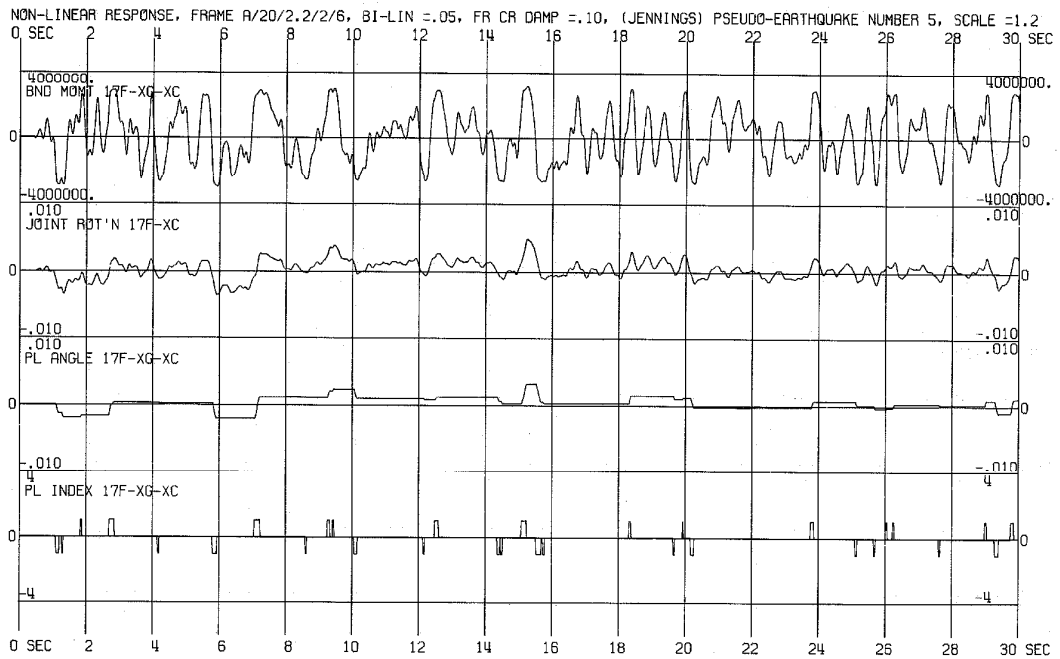


Fig. A.5.6 Station (e)

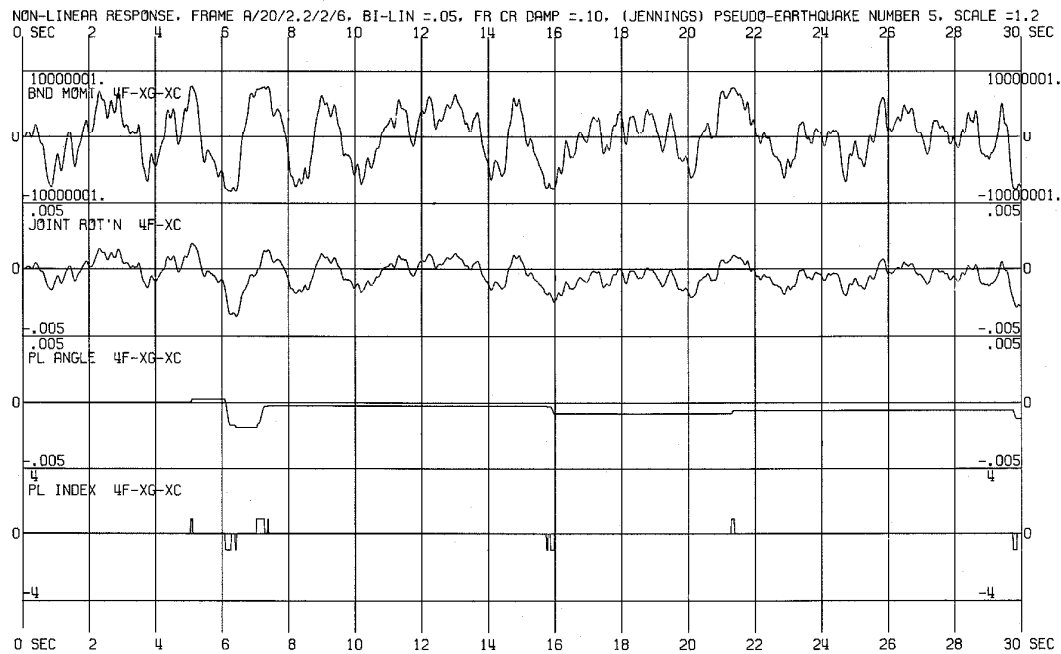


Fig. A.5.7 Station (f)

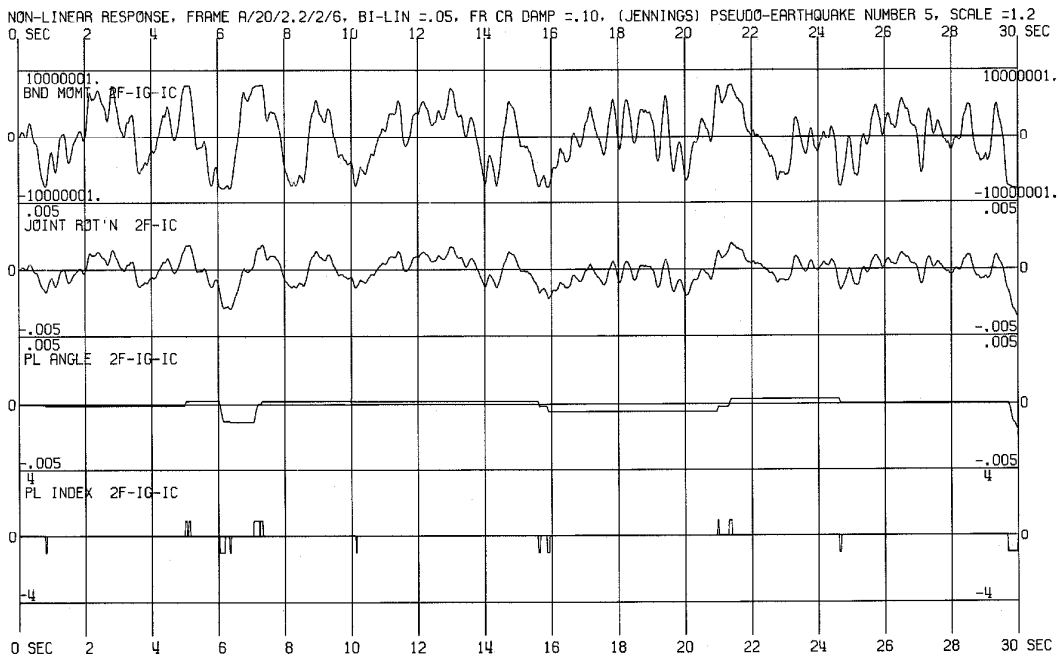


Fig. A.5.8 Station (h)

NONLINEAR RESPONSE OF FRAME A/20/2.2/2/6
 BILINEARITY = 0.05, FRACTION OF CRITICAL DAMPING = 0.05
 (JENNINGS) PSEUDO-EARTHQUAKE NUMBER 6, SCALE = 1.2

MOST NEGATIVE AND MOST POSITIVE DISPLACEMENTS IN INCHES

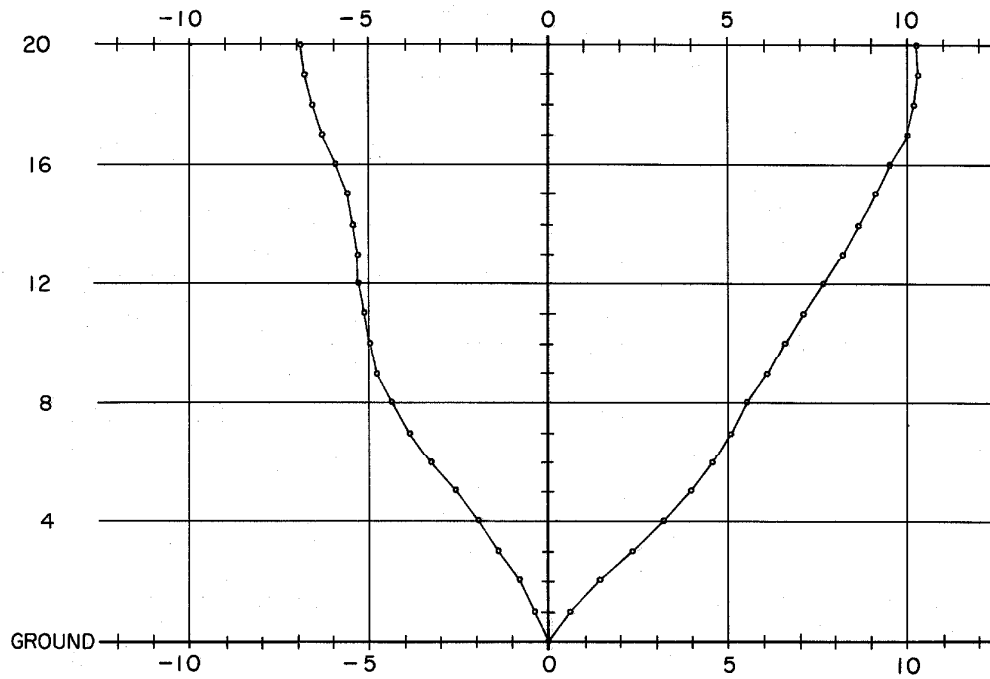


Fig. A.6.1

EXTERIOR AND INTERIOR GIRDER
 DUCTILITY FACTORS

- : IN EXTERIOR GIRDER AT EXTERIOR COLUMN
- : IN EXTERIOR GIRDER AT INTERIOR COLUMN
- △ : IN INTERIOR GIRDER AT INTERIOR COLUMN

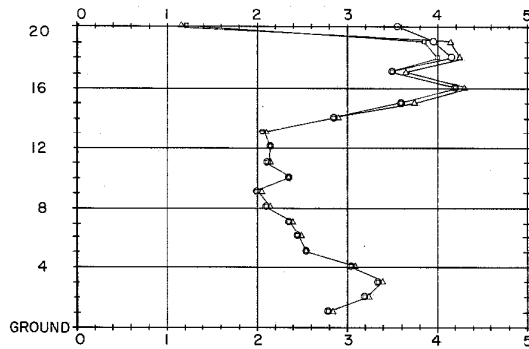


Fig. A.6.2.a

COLUMN DUCTILITY FACTORS

- : EXTERIOR COLUMN
- △ : INTERIOR COLUMN

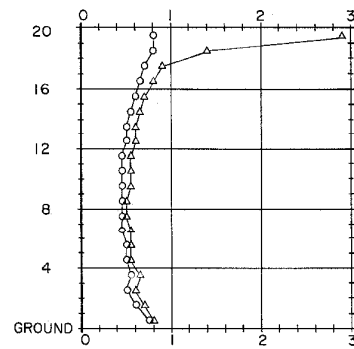


Fig. A.6.2.b

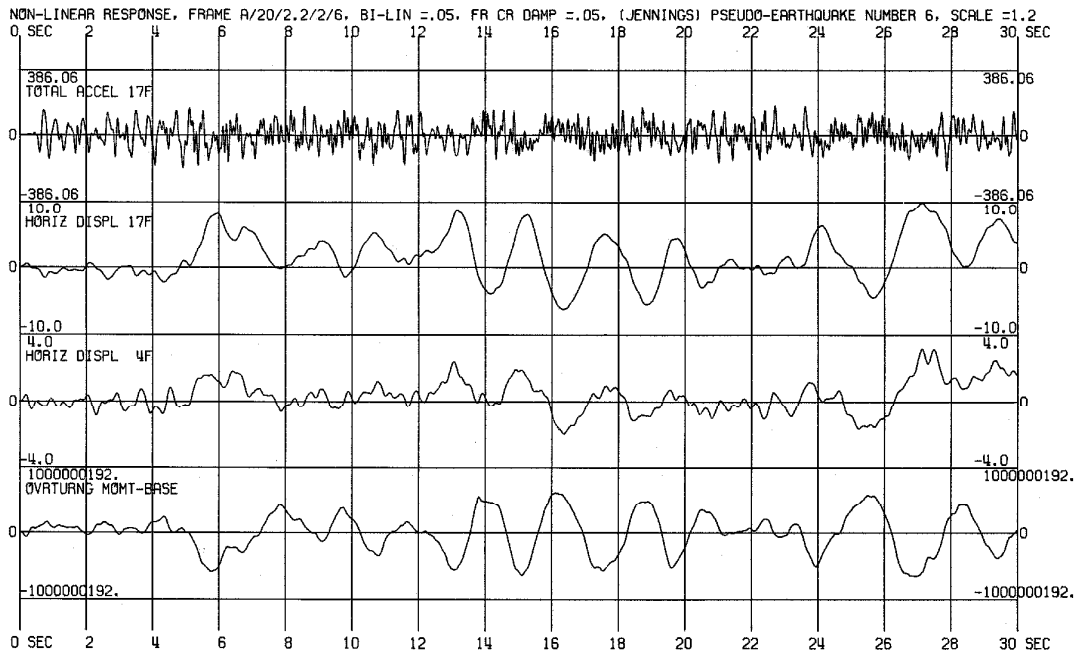


Fig. A.6.3

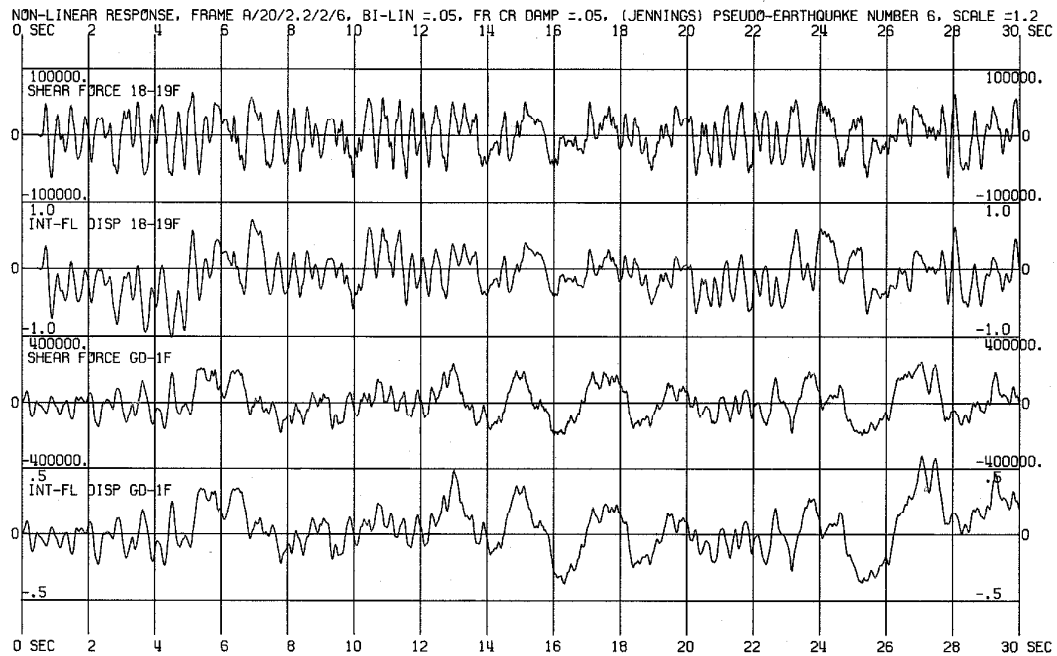


Fig. A.6.4

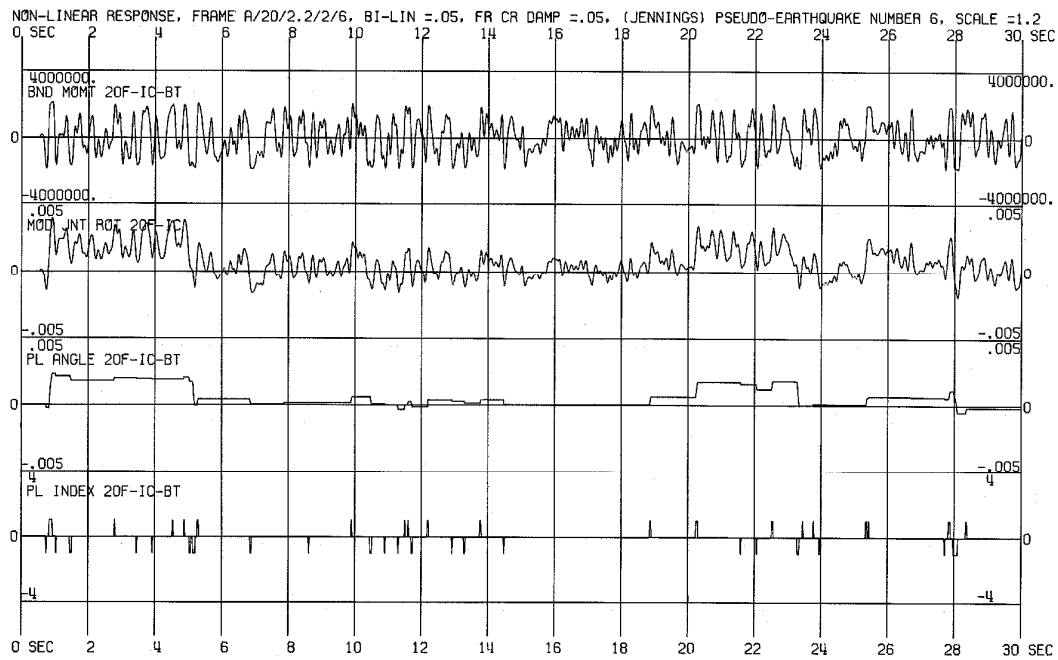


Fig. A.6.5 Station (d)

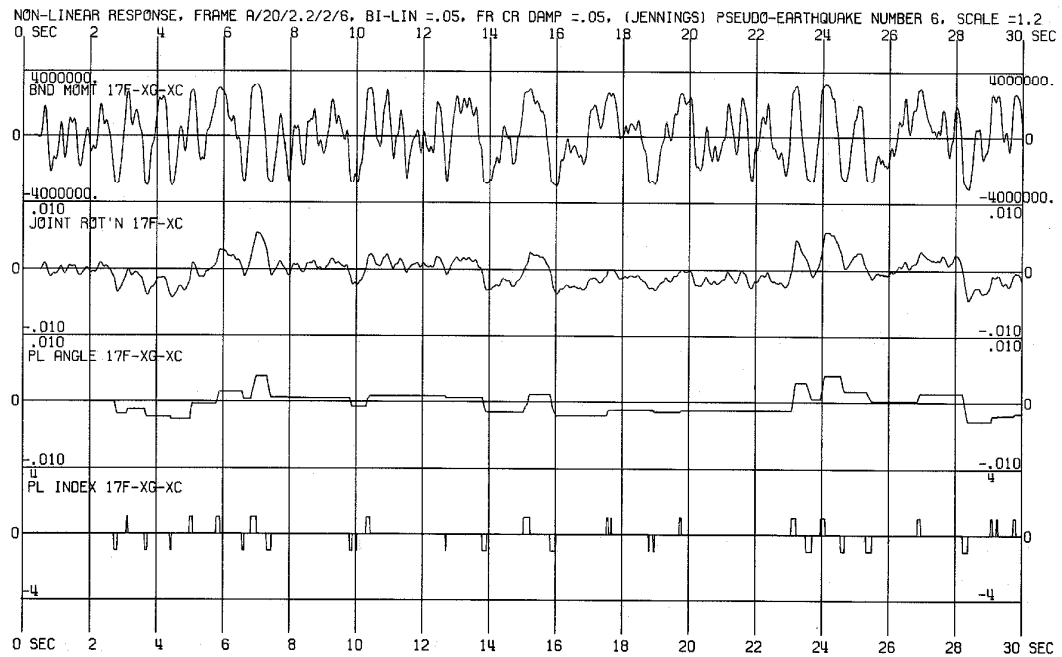


Fig. A.6.6 Station (e)

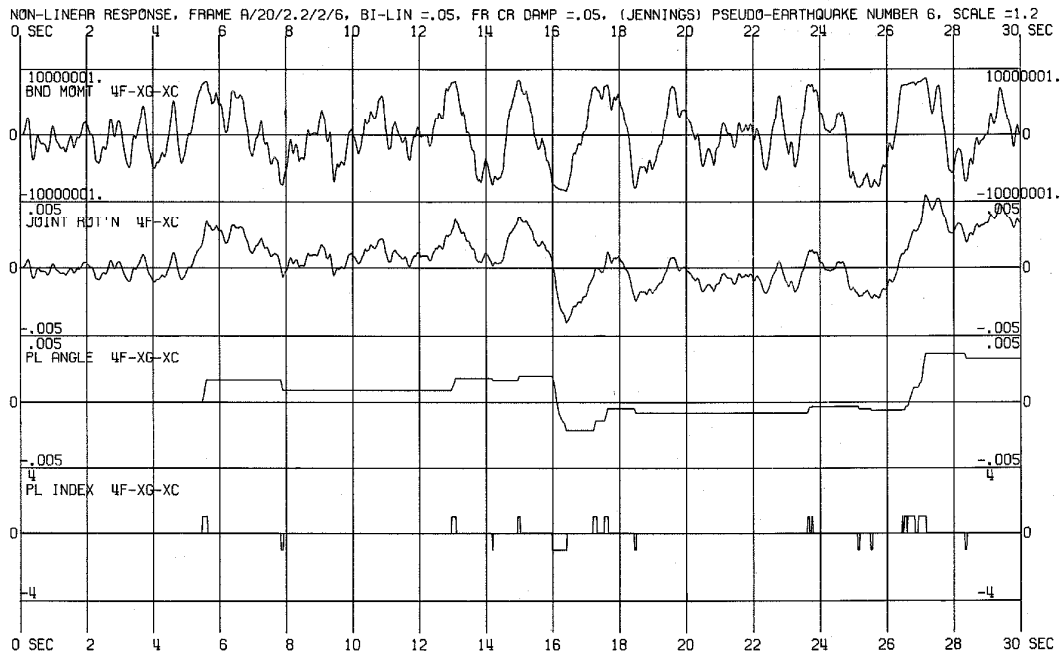


Fig. A.6.7 Station (f)

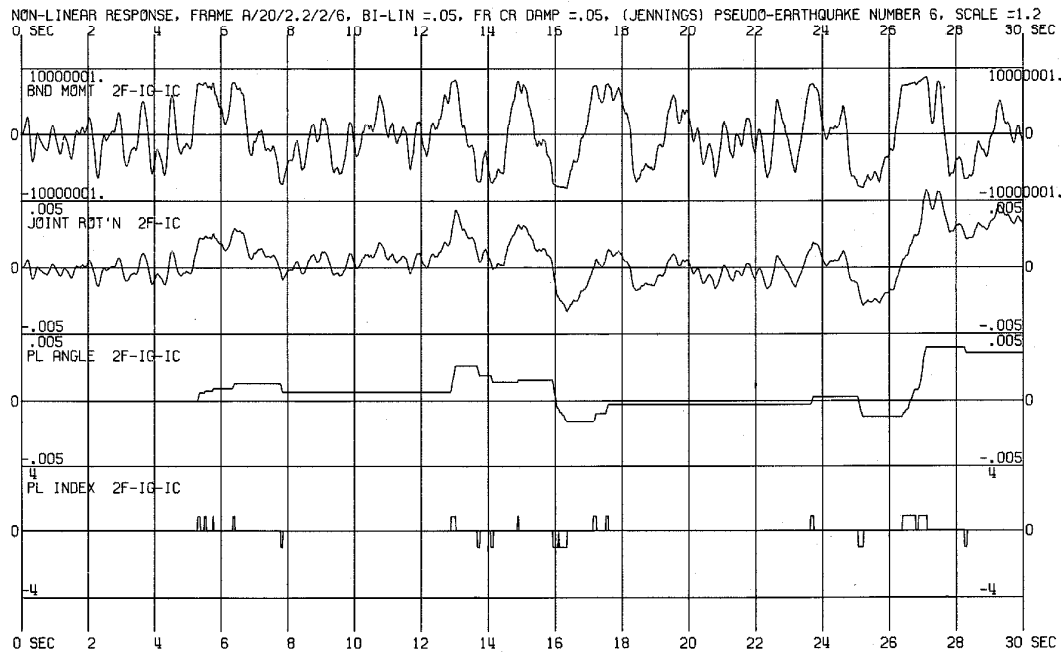


Fig. A.6.8 Station (h)

NONLINEAR RESPONSE OF FRAME A/20/2.2/2/6
 BILINEARITY=0.05, FRACTION OF CRITICAL DAMPING=0.10
 (JENNINGS) PSEUDO-EARTHQUAKE NUMBER 7, SCALE=1.2

MOST NEGATIVE AND MOST POSITIVE DISPLACEMENTS IN INCHES

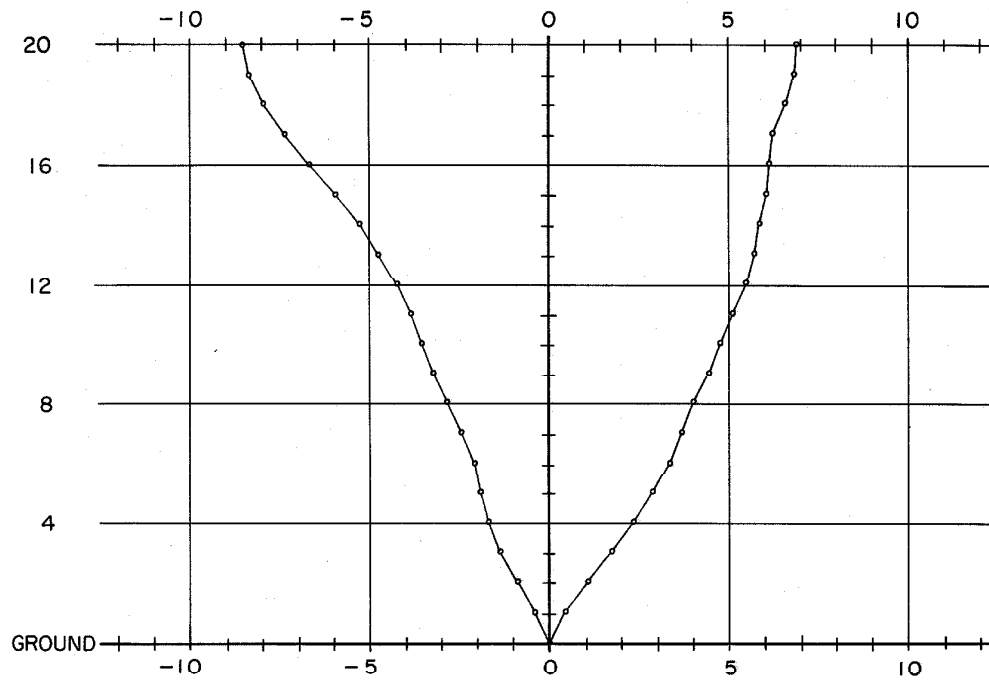


Fig. A.7.1

EXTERIOR AND INTERIOR GIRDER
 DUCTILITY FACTORS

- : IN EXTERIOR GIRDER AT EXTERIOR COLUMN
- : IN EXTERIOR GIRDER AT INTERIOR COLUMN
- △ : IN INTERIOR GIRDER AT INTERIOR COLUMN

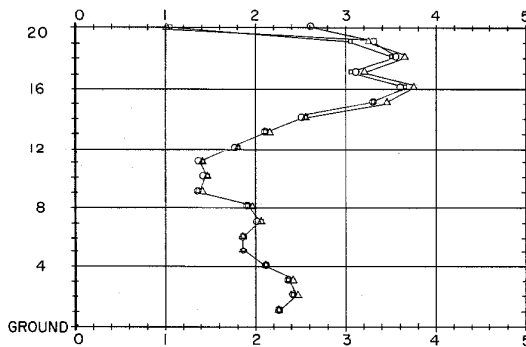


Fig. A.7.2.a

COLUMN DUCTILITY FACTORS

- : EXTERIOR COLUMN
- △ : INTERIOR COLUMN

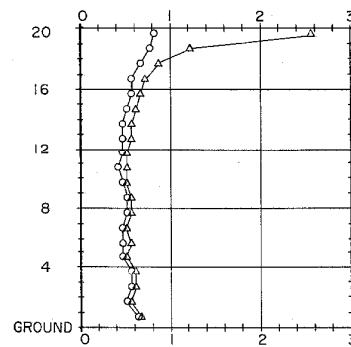


Fig. A.7.2.b

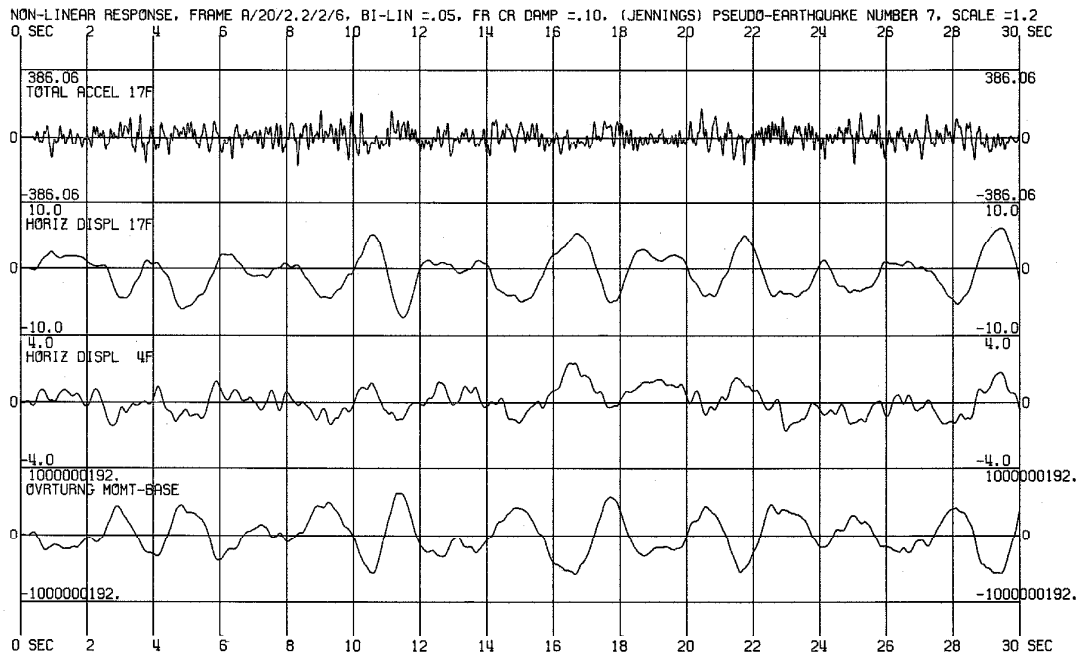


Fig. A.7.3

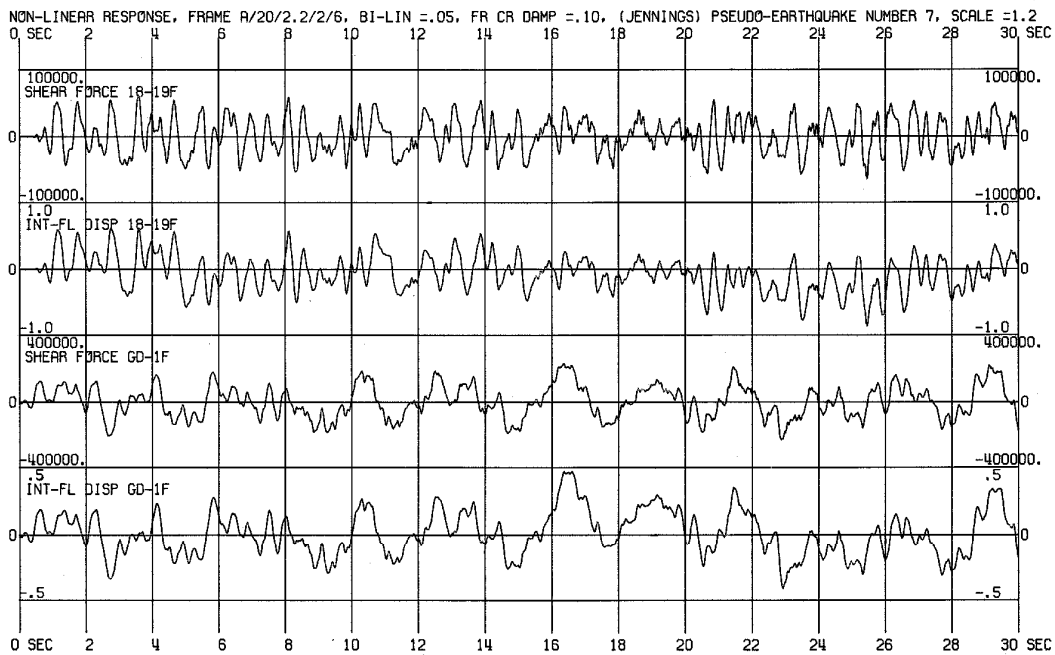


Fig. A.7.4

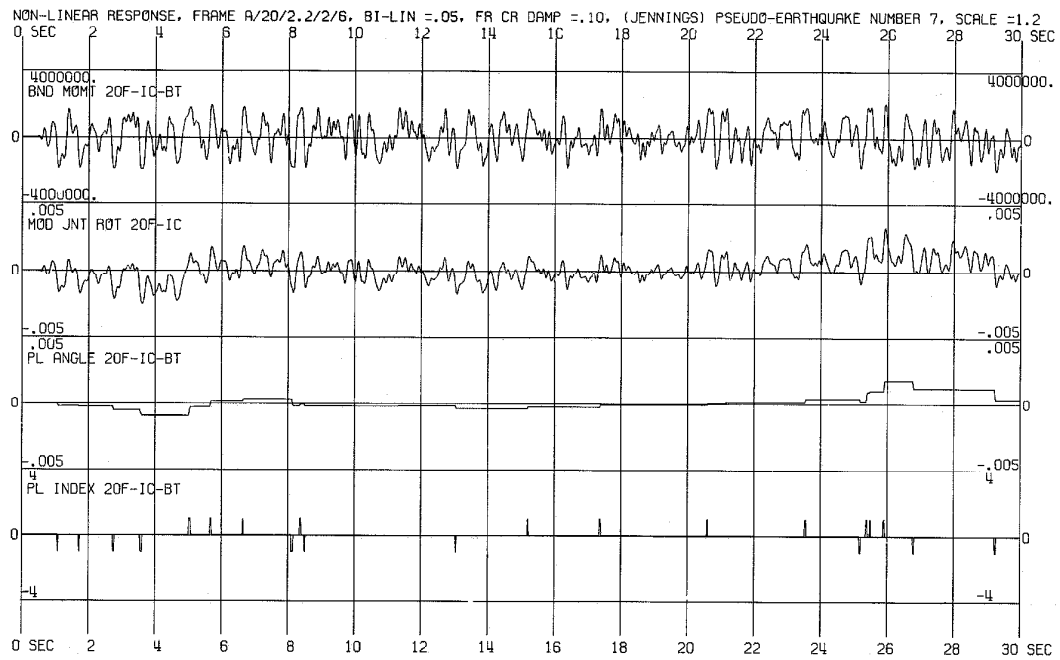


Fig. A.7.5 Station (d)

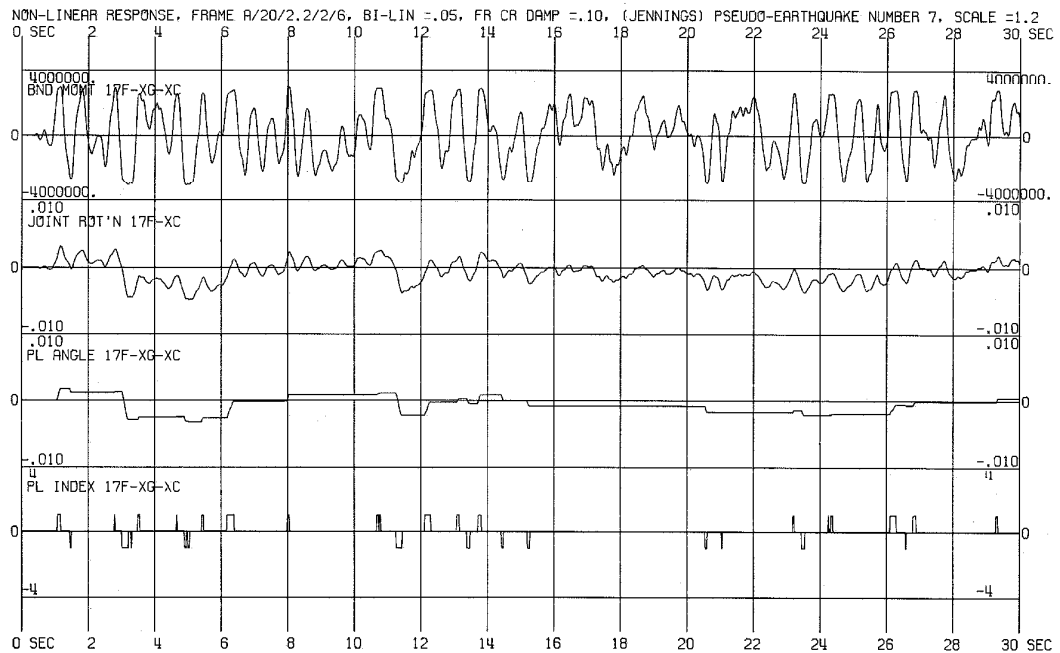


Fig. A.7.6 Station (e)

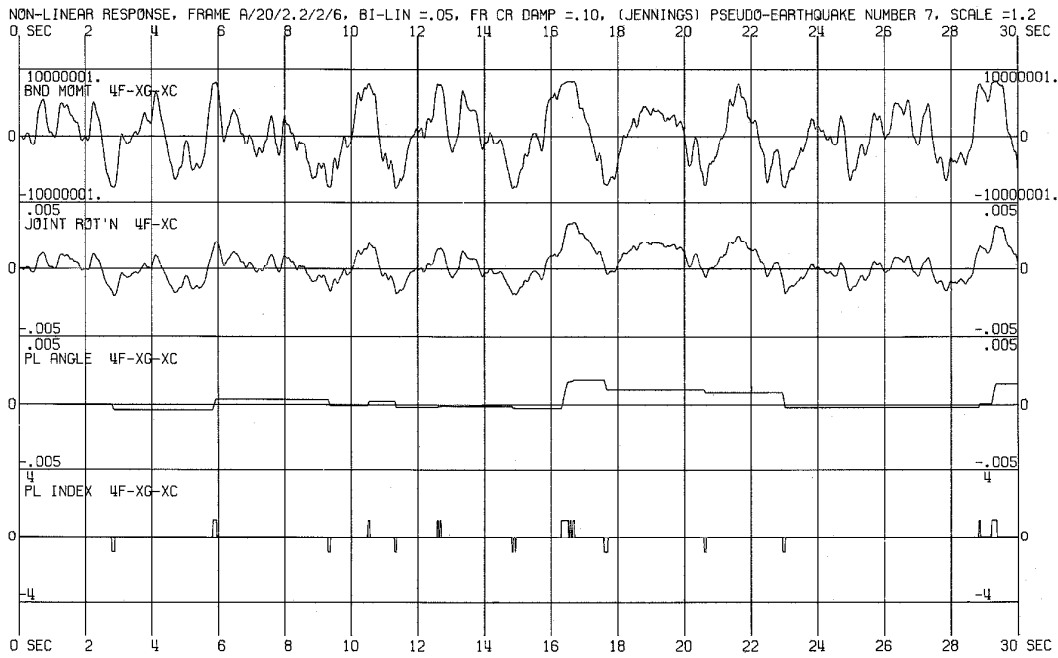


Fig. A.7.7 Station (f)

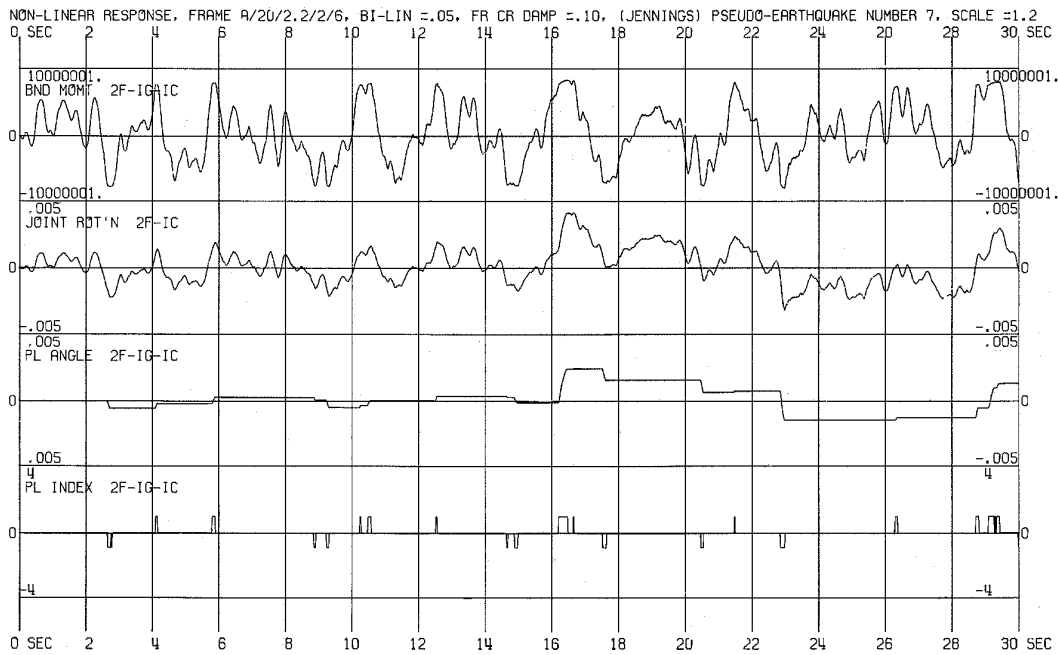


Fig. A.7.8 Station (h)

APPENDIX B

DISCUSSION OF THE YIELD CRITERIA USED IN THE FHA STUDY

The purpose of this appendix is to describe the special situation which causes the yield criteria used in the computer program for the FHA Study to lead to computational difficulties. Instead of the actual bending moment, this criteria compares a corresponding "test bending moment" with the yield bending moment in order to determine whether the end of a beam is in the linear range or in the yield range. By following the actual and corresponding test bending moments for a number of time increments along the paths shown in Fig. B.1a and Fig. B.1b, respectively, the special situation can be seen.

Usually, the bending moments are written as a function of the rotations and plastic angles of both ends of the beam; however, a simpler form in which the moment is a function of the rotation and plastic angle at one end only is sufficient for the present purpose. The equations written below are those for a simplified two-component beam. The usual moment-rotation equations for a two-component beam are described in Section 2.5.

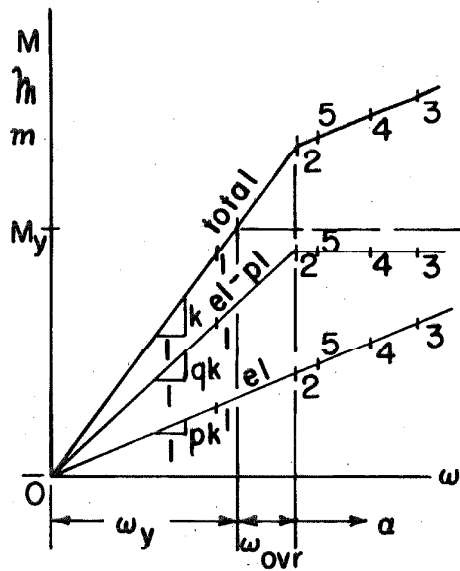


Fig. B.1a Actual
Bending Moment

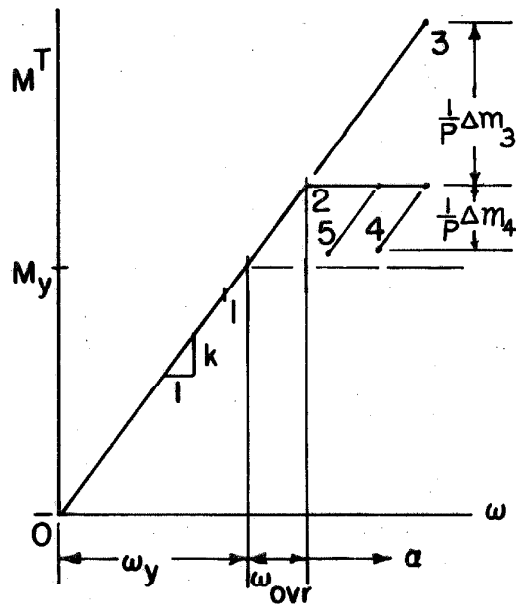


Fig. B.1b Test
Bending Moment

Actual Bending Moment

(See Fig. B.1a)

General equations:elasto-plastic component:

$$m_t = qk(\omega_t - \alpha_t) ;$$

elastic component:

$$m_t = pk(\omega_t) ;$$

total actual bending moment:

$$M_t = k(\omega_t - q\alpha_t) ;$$

end rotation:

$$\omega_t = \omega_{t-\Delta t} + \Delta\omega_t ;$$

plastic angle:

$$\alpha_t = \alpha_{t-\Delta t} + \Delta\alpha_t ;$$

$t = 1, 2, 3, \dots$ the integration
step number, i.e., the time
at the end of the increment; and
 $p + q = 1$ (usually $p \approx 0.05$).

Test Bending Moment

(See Fig. B.1b)

General equations:test bending moment:

$$M_t^T = k(\omega_t - \alpha_{t-\Delta t}) ;$$

however, with

$$\omega_t = \omega_{t-\Delta t} + \Delta\omega_t ,$$

$$M_t^T = k(\omega_{t-\Delta t} - \alpha_{t-\Delta t}) + k\Delta\omega_t ,$$

or

$$M_t^T = \frac{1}{q} m_{t-\Delta t} + \frac{1}{p} \Delta m_t$$

where

$$m_t, m_{t-\Delta t}, p, q, \text{ and } t$$

are the same as those for the
"actual bending moment."

Follow the process for
a number of time increments.

$t = 0$, initial point.

$$\omega_0 = 0,$$

$$\alpha_0 = 0,$$

$$m_0 = 0,$$

$t = 0$

Initially in the linear range;

hence,

PLASTIC INDEX (1) = 0.

Actual Moment, cont.

$$m_o = 0, \text{ and}$$

$$M_o = 0.$$

Test Moment, cont.

Integration step number 2,

calculate $\Delta\omega_1$.

$$t = 1$$

Since PLASTIC INDEX (1) = 0,

$$\Delta\alpha_1 = 0.$$

$$\therefore \alpha_1 = 0,$$

$$m_1 = qk(\omega_1 - 0),$$

$$m_1 = pk\omega_1, \text{ and}$$

$$M_1 = k\omega_1.$$

$$(M_1 = M_1^T)$$

$$t = 1$$

$$M_1^T = \frac{1}{q} m_o + \frac{1}{p} \Delta m_1,$$

with

$$m_o = 0,$$

$$\Delta m_1 = pk\Delta\omega_1,$$

and

$$\Delta\omega_1 = \omega_1,$$

$$M_1^T = k\omega_1.$$

Compare M_1^T with M_y . From point (t = 1) in Fig. B.1b, find that $M_1^T < M_y$.

\therefore PLASTIC INDEX (2) = 0, i.e.,

in the linear range for integration step number 2.

Integration step number 2,

calculate $\Delta\omega_2$.

Actual Moment, cont.

$t = 2$

Since PLASTIC INDEX (2) = 0,

$$\Delta \alpha_2 = 0.$$

$$\therefore \alpha_2 = 0,$$

$$m_2 = qk(\omega_2 - 0),$$

$$m_2 = pk\omega_2, \text{ and}$$

$$M_2 = k\omega_2.$$

$$(M_2 = M_2^T)$$

Test Moment, cont.

$t = 2$

$$M_2^T = \frac{1}{q} m_1 + \frac{1}{p} \Delta m_2$$

With

$$m_1 = qk\omega_1,$$

$$\Delta m_2 = pk\Delta\omega_2,$$

and

$$\Delta\omega_2 = \omega_2 - \omega_1,$$

it follows that

$$M_2^T = k\omega_2.$$

Compare M_2^T with M_y . From point ($t = 2$) in Fig. B.1b, find that

$$M_2^T > M_y.$$

\therefore PLASTIC INDEX (3) = 1, i.e.,

in the yield range for integration step number 3. From Fig. B.1b, note that

$$M_2^T = M_y + k\omega_{\text{ovr}}$$

where the overshoot ω_{ovr} is

$$\omega_{\text{ovr}} = \omega_2 - \omega_y.$$

Integration step number 3,

calculate $\Delta\omega_3$.

Actual Moment, cont.

$t = 3$

Since PLASTIC INDEX (3) = 1,

$$\Delta\alpha_3 = \Delta\omega_3 = \omega_3 - \omega_2.$$

Since $\alpha_3 = \alpha_2 + \Delta\alpha_3$,

and $\alpha_2 = 0$,

it follows that

$$\alpha_3 = \omega_3 - \omega_2.$$

Furthermore,

$$m_3 = qk\omega_2,$$

or

$$m_3 = m_2;$$

$$m_3 = pk\omega_3;$$

and

$$M_3 = k(\omega_3 - q\alpha_3).$$

Also,

$$M_3 = M_2 + \Delta M_3$$

or

$$M_3 = M_2 + \Delta m_3$$

where

$$\Delta m_3 = pk\Delta\omega_3.$$

Test Moment, cont.

$t = 3$

$$M_3^T = \frac{1}{q} m_2 + \frac{1}{p} \Delta m_3$$

With

$$m_2 = qk\omega_2,$$

$$\Delta m_3 = pk\Delta\omega_3,$$

it follows that

$$M_3^T = k\omega_3.$$

Compare M_3^T with M_y . From Fig. B.1b, find that $M_3^T > M_y$.

\therefore PLASTIC INDEX (4) = 1, i.e.,

in the yield range for integration

step number 4.

Note that

$$M_3^T = M_2^T + k\Delta\omega_3.$$

Since

$$M_2^T = M_y + k\omega_{\text{ovr}},$$

$$M_3^T = M_y + k(\omega_{\text{ovr}} + \Delta\omega_3).$$

If

$$(\omega_{\text{ovr}} + \omega_3) > 0,$$

then

$$M_3^T > M_y.$$

As seen in Fig. B.1b,

$$\Delta\omega_3 = \omega_3 - \omega_2 > 0.$$

In this instance, the criteria indi-

cate that the system is in the

Actual Moment, cont.Test Moment, cont.

yield range during the next time interval, as it should be. Hence, PLASTIC INDEX (4) = 1.

Integration step number 4,
calculate $\Delta\omega_4$.

t = 4

Since PLASTIC INDEX (4) = 1,

$$\Delta\alpha_4 = \Delta\omega_4 = \omega_4 - \omega_3,$$

$$m_4 = m_2.$$

Also,

$$M_4 = M_3 + \Delta m_4$$

where

$$\Delta m_4 = pk\Delta\omega_4.$$

In this time increment "back-tracking" occurred, i.e.,

$$\Delta\omega_4 < 0,$$

as shown in Fig. B.1b.

Hence,

$$\alpha_4 < \alpha_3$$

$$\text{and } M_4 < M_3.$$

The first increment of back-tracking is unavoidable but additional ones are undesirable.

t = 4

$$M_4^T = \frac{1}{q} m_3 + \frac{1}{p} \Delta m_4.$$

With

$$m_3 = m_2 = qk\omega_2$$

and

$$\Delta m_4 = pk\Delta\omega_4,$$

it follows that

$$M_4^T = k\omega_2 + k\Delta\omega_4.$$

Since

$$k\omega_2 = M_y + k\omega_{\text{ovr}},$$

$$M_4^T = M_y + k(\omega_{\text{ovr}} + \Delta\omega_4).$$

As shown in Fig. B.1b,

$$\Delta\omega_4 < 0,$$

but

$$\omega_{\text{ovr}} + \Delta\omega_4 > 0.$$

Consequently, the criteria for yielding:

$$M_4^T > M_y$$

Actual Moment, cont.Test Moment, cont.

is still satisfied indicating that
the system continues in the yield
range:

PLASTIC INDEX (5) = 1.

As long as

$$\omega_{\text{ovr}} + \Delta\omega_t > 0$$

for

$$t = 4, 5, 6, \dots,$$

the criteria for being in the yield range will be satisfied even though

$$\Delta\omega_t < 0 \quad \text{for } t = 4, 5, 6, \dots$$

In this special situation, the bending moment as well as the yield angle will continue to "backtrack," that is, decrease according to the equations for the yield range when they should have returned to the linear range. The system will not return to the linear range until some $\Delta\omega_t$ is sufficiently negative so that

$$\omega_{\text{ovr}} + \Delta\omega_t < 0.$$

Fortunately, $\Delta\omega_t$ is usually sufficiently negative, or what is the same, ω_{ovr} is usually sufficiently small so that this problem with the yield criteria does not often cause serious difficulties.

APPENDIX C

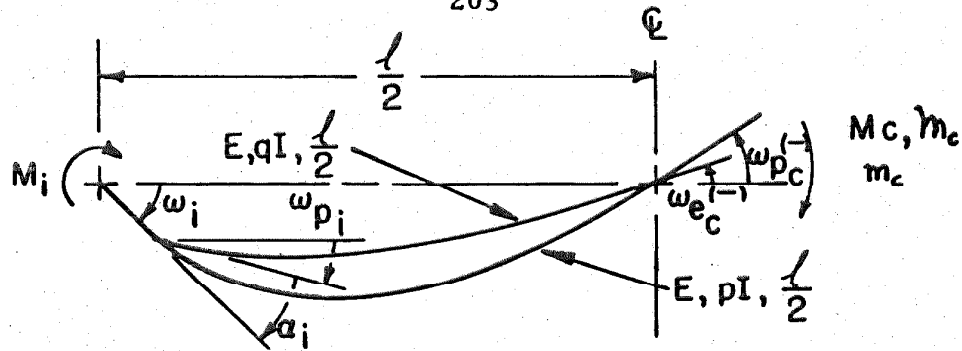
DISCUSSION OF THE TREATMENT OF SYMMETRY
FOR THE TWO-COMPONENT BEAM MODEL

The purpose of this appendix is to discuss an approximate treatment of symmetry for the two-component model of the interior girder of a three-bay (four-column) structural frame. This approximation is convenient for the computer program used for the FHA Study⁽¹⁾. In this treatment, the interior girder is cut at the centerline and the resulting "centerline" end, end (c), is treated the same as the end of any other beam. That is, the ends of both components of the girder are connected together and then pinned so that they rotate identically, as shown in Fig. C.1b. In this case, the sum of the bending moments of both components of the girder at end (c) is zero.

The correct treatment of symmetry is achieved by cutting the girder at the centerline and separately pinning the resulting end of each component so that they can rotate independently. In this case, the bending moment at end (c) of each component is zero, as shown in Fig. C.1a.

The nomenclature used in this appendix closely follows that for the two-component beam in Chapter II, with the usage for each system being indicated in Fig. C.1a and Fig. C.1b. The appropriate boundary conditions are also given in these figures.

The bending moment-end rotation-plastic angle equations for both the correct and approximate treatments of symmetry are given



left end:

$$\Delta M_i = \Delta m_i + \Delta m_i;$$

$$\Delta \omega_i = \Delta \omega_{pi} + \Delta \alpha_i;$$

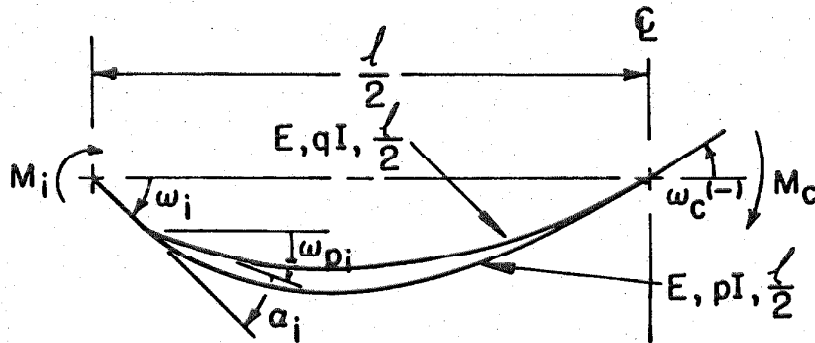
$$\Delta \alpha_i \neq 0.$$

"centerline" end:

$$\Delta m_c = 0; \Delta m_c = 0;$$

$$\omega_{ec} \neq \omega_{pc}; \Delta \alpha_c = 0.$$

Fig. C.1a Treatment of Symmetry
of an Interior Girder



left end:

$$\Delta M_i = \Delta m_i + \Delta m_i;$$

$$\Delta \omega_i = \Delta \omega_{pi} + \Delta \alpha_i;$$

$$\Delta \alpha_i \neq 0.$$

"centerline" end:

$$\Delta M_c = \Delta m_c + \Delta m_c = 0;$$

$$\Delta m_c = -\Delta m_c; \Delta \alpha_c = 0;$$

$$\Delta \omega_c = \Delta \omega_{pc} = \Delta \omega_{ec}.$$

Fig. C.1b Approximate Treatment of Symmetry
of an Interior Girder

below. In both systems, the stiffness
of the elastic component is:

$$pk' = p \left(\frac{EI}{l/2} \right) ;$$

and of the elasto-plastic component is:

$$qk' = q \left(\frac{EI}{l/2} \right) ;$$

where $p + q = 1$. In this case $k' = 2k$ where

$$k = \frac{EI}{l}$$

and l is the length of the entire interior girder. Since no yielding occurs at end (c) for either system, only two yield cases are considered: end (i) is either linear or yielding.

Correct Treatment

(See Fig. C.1a)

Boundary Conditions:

end (i):

$$\Delta M_i = \Delta m_i + \Delta m_i ,$$

$$\Delta \omega_{p_i} = \Delta \omega_i - \Delta \alpha_i ;$$

end (c):

$$\Delta m_c = 0 ,$$

$$\Delta m_c = 0 ,$$

$$\Delta \omega_{p_c} \neq \Delta \omega_{e_c} .$$

With these boundary conditions,
the general moment-rotation

Approximate Treatment

(See Fig. C.1b)

Boundary Conditions:

end (i):

$$\Delta M_i = \Delta m_i + \Delta m_i ,$$

$$\Delta \omega_{p_i} = \Delta \omega_i - \Delta \alpha_i ;$$

end (c):

$$\Delta M_c = \Delta m_c + \Delta m_c = 0$$

or

$$\Delta m_c = - \Delta m_c ,$$

and

$$\Delta \omega_{p_c} = \Delta \omega_{e_c} = \Delta \omega_c .$$

Correct Treatment, cont.

equations in incremental form are:

for the elasto-plastic component:

$$\Delta m_i = qk' [\Delta \omega_i - \Delta \alpha_i + \frac{1}{2} \Delta \omega_{p_c}]$$

$$\Delta m_c = qk' [\frac{1}{2} (\Delta \omega_i - \Delta \alpha_i) + \Delta \omega_{p_c}] ;$$

for the elastic component:

$$\Delta m_i = pk' [\Delta \omega_i + \frac{1}{2} \Delta \omega_{e_c}]$$

$$\Delta m_c = pk' [\frac{1}{2} \Delta \omega_i + \Delta \omega_{e_c}] .$$

Apply boundary conditions at end (c):

$$\Delta m_c = 0$$

and

$$\Delta m_c = 0 .$$

Hence,

$$\Delta \omega_{p_c} = - \frac{1}{2} (\Delta \omega_i - \Delta \alpha_i) ,$$

$$\Delta \omega_{e_c} = - \frac{1}{2} \Delta \omega_i .$$

For the total beam at end (i):

$$\Delta M_i = \Delta m_i + m_i .$$

Eliminating $\Delta \omega_{p_c}$ and $\Delta \omega_{e_c}$, this becomes

$$\Delta M_i = \frac{3}{4} k' (\Delta \omega_i - q \Delta \alpha_i) .$$

Approximate Treatment, cont.

With these boundary conditions, the general moment-rotation equations in incremental form are:

for the elasto-plastic component:

$$\Delta m_i = qk' [(\Delta \omega_i - \Delta \alpha_i) + \frac{1}{2} \Delta \omega_c]$$

$$\Delta m_c = qk' [\frac{1}{2} (\Delta \omega_i - \Delta \alpha_i) + \Delta \omega_c] ;$$

for the elastic component:

$$\Delta m_i = pk' [\Delta \omega_i + \frac{1}{2} \Delta \omega_c]$$

$$\Delta m_c = pk' [\frac{1}{2} \Delta \omega_i + \Delta \omega_c] .$$

Apply boundary conditions at end (c):

$$\Delta M_c = \Delta m_c + \Delta m_c = 0 .$$

Hence

$$\Delta \omega_c = - \frac{1}{2} (\Delta \omega_i - q \Delta \alpha_i) .$$

For the total beam at end (i):

$$\Delta M_i = \Delta m_i + \Delta m_i .$$

Eliminating $\Delta \omega_c$, this becomes

$$\Delta M_i = \frac{3}{4} k' (\Delta \omega_i - q \Delta \alpha_i) .$$

Correct Treatment, cont.

Since

$$k' = 2k ,$$

where $k = \frac{EI}{l}$ is the stiffness of the entire interior girder,

$$\Delta M_i = 1.5(\Delta \omega_i - q\Delta \alpha_i) .$$

The moment-rotation equation

for the total beam at end (i) for the linear case

with

$$\Delta \alpha_i = 0 ,$$

is

$$\Delta M_i = 1.5 k \Delta \omega_i .$$

Approximate Treatment, cont.

Since

$$k' = 2k ,$$

where $k = \frac{EI}{l}$ is the stiffness of the entire interior girder,

$$\Delta M = 1.5(\Delta \omega_i - q\Delta \alpha_i) .$$

The moment-rotation equation

for the total beam at end (i) for the linear case

with

$$\Delta \alpha_i = 0 ,$$

is

$$\Delta M_i = 1.5 k \Delta \omega_i .$$

These equations for both systems are
the same in the linear case.

Incremental plastic angle at

end (i). During yielding, for the two-component beam (see Sec. 2.5),

$$\Delta M_i = \Delta m_i$$

or

$$1.5k[\Delta \omega_i - q\Delta \alpha_i] = 1.5pk\Delta \omega_i .$$

Incremental plastic angle at

end (i). During yielding, for the the two-component beam (see Sec. 2.5),

$$\Delta M_i = \Delta m_i$$

or

$$1.5k[\Delta \omega_i - q\Delta \alpha_i] = 1.5pk[\Delta \omega_i + \frac{q}{3} \Delta \alpha_i] .$$

Correct Treatment, cont.

Hence

$$\Delta\alpha_i = \Delta\omega_i .$$

Moment-rotation equation for the total beam at end (i) during yielding. By eliminating $\Delta\alpha_i$, this equation becomes:

$$\Delta M_i = 1.5 pk \Delta\omega_i .$$

Approximate Treatment, cont.

Hence

$$\Delta\alpha_i = \left(\frac{3}{3+p} \right) \Delta\omega_i .$$

Moment rotation equation for the total beam at end (i) during yielding. By eliminating $\Delta\alpha_i$, this equation becomes:

$$\Delta M_i = \left(\frac{6}{3+p} \right) pk \Delta\omega_i .$$

For $p = 0.05$, as used in this report,

$$\Delta M_i = 1.97 pk \Delta\omega_i .$$

Comparing these two moment-rotation equations, it is observed that for the value of (p) used, the effective stiffness of the approximate technique during yielding is about $4/3$ times that for the correct method. Because each joint of the frame is in the linear case about 90% of the time, and because the equations are the same for both systems in the linear case, only small differences in the structural responses occur. By comparing the computer results for the two methods with each other, these differences are seen to be on order of 1%, being small enough to justify the use of the approximate technique for treating symmetry.

APPENDIX D

FUTURE STUDIES

As a result of the investigation described in this report, several analyses are suggested which would provide additional understanding of how multi-story structures respond to earthquake excitation. These are briefly mentioned below.

1) Stiffness proportional damping in the form of Eq. 3.24 could be added to the computer program, thereby making it possible to observe the effect of this type of damping on the response. Combinations of the two types of damping would make it possible to match more closely the modal damping distribution in actual buildings.

2) An energy balance subroutine could be developed and added to the program. Such a balance might consist of the energy in (and out) at the base, dissipation by yielding, dissipation by damping mechanisms, kinetic energy and (recoverable) potential energy. Such an analysis would provide insight into the distribution of energy dissipation in a multi-story structure.

3) Instead of bilinear hysteresis loops which inherently have a sharp corner at the yield level, curvilinear hysteresis loops could be used with the one-component beam model. This would permit the effect of the sharp corner upon the response of the structure to be observed.

4) Analyses of nonlinear elastic, shear type, base excited, continuous cantilever beams might be considered. The excitation could be either pulse, sinusoidal, or earthquake.

5) Static moments could be applied to the ends of the girders to account for static loads in the structure. This would require the use of the entire frame because the yielding characteristics would no longer be symmetric with respect to the centerline.

APPENDIX E

LISTING OF THE COMPUTER PROGRAM

The computer program used for determining the response of nonlinear multi-story structures subjected to earthquake excitation is listed in this appendix. A flow chart is also provided. Numerous comment cards are used so that the program will be understandable to the reader with some background in Fortran II or Fortran IV.

This program was written in Fortran IV for use on the IBM 7090/7094 Computer at the Computer Center of the California Institute of Technology. The computer has a 32,000-cell memory core which is filled by this program and the necessary library sub-routines. Alterations may be necessary to adapt this program to the computers at other installations.

A typical run in which the nonlinear A/20/2.2/2/6 frame was subjected to 30 seconds of pseudo-earthquake took 40 minutes of computer time. Since the time increment is 0.005 sec (earthquake time), there were 6000 integration steps. After every fourth time interval, most of the responses of the structure were written onto binary tape. After every second of earthquake time, the most positive and most negative (cumulative) values of all of the responses, along with the times at which they occurred, were written out on paper.

The resulting 2400 ft, 560 bit-per-inch binary tape was scanned to obtain the time histories of the responses to be plotted. The time history for each response was punched into a deck of cards.

The plots were made from these decks. The time necessary to scan a tape for 30 responses was about 10 minutes. Each page of four response plots took the computer 30 sec to set up; however, it took 7 minutes to actually plot.

When a modal analysis was made, the "equivalent" modal participation factors, the "equivalent" modal contributions to four displacements and to four interfloor displacements were found. This information was calculated and written out for every time increment. Such an analysis doubles the computer time required. One run of this nature was made for the first four seconds of the El Centro (N-S) earthquake of 18 May 1940.

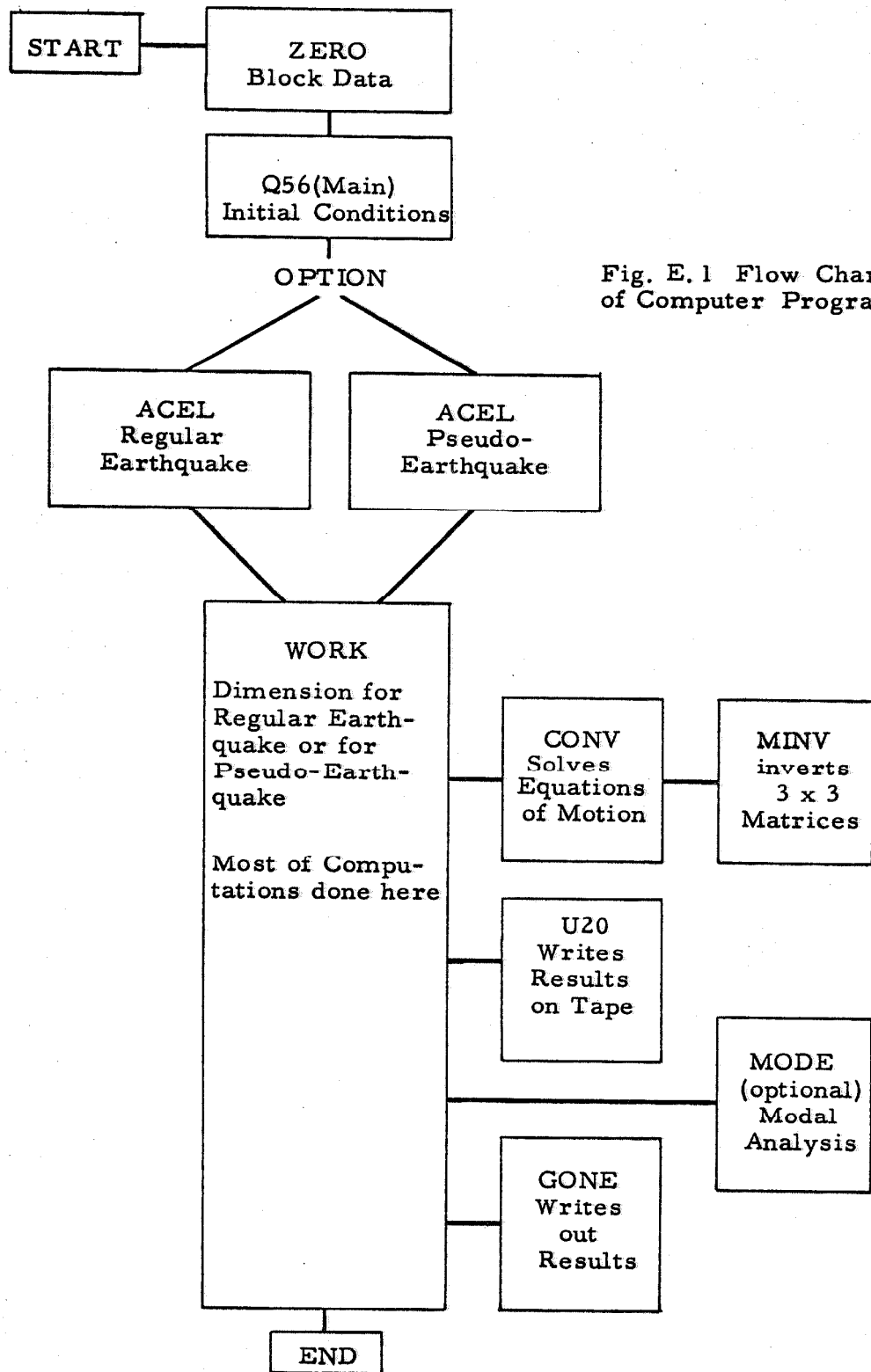


Fig. E.1 Flow Chart of Computer Program


```

50  YIELD(N,3,1)=YIELD(N,2,3)
C  CONTINUE
DO 80 M=1,3
DO 80 J=1,6
DO 80 N=1,22
  BM(N,M,J) = -BM(N,M,J)
C  CONTINUE
60  C..... EVALUATE BILINEAR STIFFNESS PARAMETERS *F, A, S* .....
C  F = 1.5*F/(1.0-P)
C
C  A(1) = 1.0/(1.0 + F)
C  A(2) = 0.5*A(1)
C  D = 1.0 + 2.6666667*F + 1.3333333*F*F
C  A(3) = (1.0 + 1.3333333*F)/D
C  A(4) = 0.6666667*F/D
C  A(5) = (1.0 + 2.0*F)/D
C
C  S(3) = F*A(1)
C  S(4) = F*A(2)
C  S(5) = (C.75 + F)/(1.0 + F)
C  S(6) = F*A(3)
C  S(7) = F*A(4)
C  S(8) = F*A(5)
C
C  C..... WRITE OUT INPUT DATA AND INITIAL CONDITIONS .....
C  WRITE(6,1069) A,S,F,P,D
1069  FORMAT(10X,1P,E17.7)
C
1003  WRITE(6,1003) NAMES1,P,ZETA,FUNDFQ,TINEND,NAMEOK
1003  FORMAT(1X,10A6,15H BILINEARITY = ,7F2.3,16H,FRAC CR DAMP = ,
3 5X,15H,ELONG THE FIRST *F(10.5), 15H SECONDS OF THE , 13A6,2X,/)
C  WRITE(6,1060)
1060  FORMAT(132H STORY  CE  BMA  YIELD  CI  BMA  YIELD
3  HT  ZM  )
NN=21
DO 70 N=2,22
NN = NN-1
WRITE(6,1070) NN,CE(N),BMA(N,2,4),YIELD(N,2,4),CI(N),BMA(N,3,4),
2  YIELD(N,3,4),GE(N),BMA(N,2,3),YIELD(N,2,3),GI(N),BMA(N,3,3),
3  YIELD(N,3,3),HT(N),ZMIN)
1070  FORMAT(1X,13,4(10PE8.0,0PF11.0,1PE10.3), 0P2F6.0)
70  CONTINUE
C
1002  WRITE(6,1002)
1002  FORMAT(1X,10A6,15H BILINEARITY = ,7F2.3,16H,FRAC CR DAMP = ,
3 5X,15H,ELONG THE FIRST *F(10.5), 15H SECONDS OF THE , 13A6,2X,/)
C  WRITE(6,1080)
1080  FORMAT(12X,7HCAIN,2), 10X,7HCAIN,3), 10X,7HCAIN,2), 10X,7HCAIN,3))
NN=21
DO 80 N=2,22
NN = NN-1
WRITE(6,1090)NN,CA(N,21),CAIN,3),GA(N,21),CAIN,3)
1090  FORMAT(12X,13,1P,E17.7)
80  CONTINUE
C  CALL ACCEL
C  CALL WORK
C  STOP
C  END

```

```

MAIN 141
MAIN 142
MAIN 143
MAIN 144
MAIN 145
MAIN 146
MAIN 147
MAIN 148
MAIN 149
MAIN 150
MAIN 151
MAIN 152
MAIN 153
MAIN 154
MAIN 155
MAIN 156
MAIN 157
MAIN 158
MAIN 159
MAIN 160
MAIN 161
MAIN 162
MAIN 163
MAIN 164
MAIN 165
MAIN 166
MAIN 167
MAIN 168
MAIN 169
MAIN 170
MAIN 171
MAIN 172
MAIN 173
MAIN 174
MAIN 175
MAIN 176
MAIN 177
MAIN 178
MAIN 179
MAIN 180
MAIN 181
MAIN 182
MAIN 183
MAIN 184
MAIN 185
MAIN 186
MAIN 187
MAIN 188
MAIN 189
MAIN 190
MAIN 191
MAIN 192
MAIN 193
MAIN 194
MAIN 195
MAIN 196
MAIN 197
MAIN 198
MAIN 199
MAIN 200
MAIN 201
MAIN 202
MAIN 203
MAIN 204

```



```

$10FTC ACCL DEC*ACCELEROGAM FROM REGULAR EARTHQUAKE*      056 ACRG 1
SUBROUTINE ACCL                                           ACRG 2
C*****ACRG 3
C THE PURPOSE OF THIS PROGRAM IS TO CALCULATE VARIOUS RESPONSES ACRG 4
C OF NONLINEAR TALL STRUCTURES SUBJECTED TO EARTHQUAKE EXCITATION. ACRG 5
C ACRG 6
C ACRG 7
C ACRG 8
C EACH OF THE TWO 'ACCL' SUBROUTINES SETS-UP AN ACCELEROGAM ACRG 9
C WITH UNITS OF 'FRACTIONS OF G' AT EQUAL TIME INTERVALS 'DBDT' ACRG 10
C FOR USE BY SUBROUTINE 'WORK'. THE DIFFERENCE BETWEEN THEM IS ACRG 11
C THE FORMAT OF THE INPUT ACCELEROGAM. ACRG 12
C THE 'JENINGS' PSEUDO-EARTHQUAKE* IS GIVEN WITH VALUES OF ACRG 13
C ACCELERATION IN UNITS OF 'FT/SEC**2' AT EQUAL TIME INTER- ACRG 14
C VALS OF 0.025 SEC. THE CORRESPONDING TIMES MUST BE GENERATED. ACRG 15
C THE REGULAR EARTHQUAKE ACCELEROGAMS ARE GIVEN IN ACRG 16
C 'TIME-ACCELERATION' PAIRS AT UNEQUAL TIME INTERVALS AND THE ACRG 17
C UNITS OF ACCELERATION ARE 'FRACTIONS OF G'. ACRG 18
C ACRG 19
C THIS 'ACCL' SUBROUTINE HANDLES THE 'REGULAR EARTHQUAKES'. ACRG 20
C ACRG 21
C THIS PROGRAM INCLUDING ALL SUBROUTINES WAS WRITTEN BY MELBOURNE ACRG 22
C F. GIBERSON, DEPARTMENT OF APPLIED MECHANICS, CALIFORNIA INSTI- ACRG 23
C TUTE OF TECHNOLOGY, PASADENA, CALIFORNIA. ACRG 24
C LAST REVISION - 4 DECEMBER 1966 ACRG 25
C*****ACRG 26
C*****ACRG 27
C DOUBLE PRECISION DBTIME,DBDT,ED,DBTIM3,DBZK ACRG 28
C COMMON/ACENOK/ DBTIME,DBDT,ED,DBTIM3,IOPION, ACRG 29
C 2 TIM3(601),DDY3(601),DDY1(601), KEND ACRG 30
C ACRG 31
C ACRG 32
C ACRG 33
C READ(5,1110) NCARD,DBDT,ENDREC,IOPION,SCALE ACRG 34
C FORMAT(110,010,010,010,010,010,010,010) ACRG 35
C READ(5,1120) (TIM3(I),DDY3(I),I=1,NCARD) ACRG 36
C DD = DBLE(DDY3(1)/DBDT) ACRG 37
C KEND = SNGL(KEND) ACRG 38
C KEND = SNGL(ED) + 1.5 ACRG 39
C INC = KEND - 1 ACRG 40
C ACRG 41
C ACRG 42
C ACRG 43
C ACRG 44
C ACRG 45
C ACRG 46
C ACRG 47
C ACRG 48
C ACRG 49
C ACRG 50
C ACRG 51
C ACRG 52
C ACRG 53
C ACRG 54
C ACRG 55
C ACRG 56
C ACRG 57
C ACRG 58
C ACRG 59
C ACRG 60
C ACRG 61
C ACRG 62
C ACRG 63
C ACRG 64
C ACRG 65
C ACRG 66
C ACRG 67
C ACRG 68
C ACRG 69
C ACRG 70
C ACRG 71

```

```
C*****SUBROUTINE ACCEL DECK *ACCELEROGRAM FROM PSEUDO-EARTHQUAKE* Q66 ACPS
C*****SUBROUTINE ACCEL *****ACPS 3
C*****ACPS 4
C*****ACPS 5
C*****ACPS 6
C*****ACPS 7
C*****ACPS 8
C*****ACPS 9
C*****ACPS 10
C*****ACPS 11
C*****ACPS 12
C*****ACPS 13
C*****ACPS 14
C*****ACPS 15
C*****ACPS 16
C*****ACPS 17
C*****ACPS 18
C*****ACPS 19
C*****ACPS 20
C*****ACPS 21
C*****ACPS 22
C*****ACPS 23
C*****ACPS 24
C*****ACPS 25
C*****ACPS 26
C*****ACPS 27
C*****ACPS 28
C*****ACPS 29
C*****ACPS 30
C*****ACPS 31
C*****ACPS 32
C*****ACPS 33
C*****ACPS 34
C*****ACPS 35
C*****ACPS 36
C*****ACPS 37
C*****ACPS 38
C*****ACPS 39
C*****ACPS 40
C*****ACPS 41
C*****ACPS 42
C*****ACPS 43
C*****ACPS 44
C*****ACPS 45
C*****ACPS 46
C*****ACPS 47
C*****ACPS 48
C*****ACPS 49
C*****ACPS 50
C*****ACPS 51
C*****ACPS 52
C*****ACPS 53
C*****ACPS 54
C*****ACPS 55
C*****ACPS 56
C*****ACPS 57
C*****ACPS 58
C*****ACPS 59
C*****ACPS 60
C*****ACPS 61
C*****ACPS 62
C*****ACPS 63
C*****ACPS 64
C*****ACPS 65
C*****ACPS 66
C*****ACPS 67
C*****ACPS 68
C*****ACPS 69
C*****ACPS 70
```

THE PURPOSE OF THIS PROGRAM IS TO CALCULATE VARIOUS RESPONSES
OF NONLINEAR TALL STRUCTURES SUBJECTED TO EARTHQUAKE EXCITATION.

EACH OF THE TWO 'ACEL' SUBROUTINES SETS-UP AN ACCELEROGRAM
WITH UNIT OF 'G'. EACH OF THESE SUBROUTINES TAKES AS INPUT
FOR USE IN THE 'ACCEL' SUBROUTINE, THE DIFFERENCE BETWEEN THEIR IS
THE FORMAT OF THE INPUT ACCELEROGRAM. THE DIFFERENCE BETWEEN THEM IS
THE 'JENNINGS' PSEUDO-EARTHQUAKE. IS GIVEN WITH VALUES OF
ACCELERATION IN UNITS OF 'FT/SEC**2)' AT EQUAL TIME INTER-
VALS OF 0.025 SEC. THE CORRESPONDING TIMES MUST BE GENERATED.
THE REGULAR EARTHQUAKE ACCELEROGRAMS ARE GIVEN IN
'TIME-ACCELERATION' PAIRS AT UNEQUAL TIME INTERVALS AND THE
UNITS OF ACCELERATION ARE 'FACTORS OF G'.

THIS 'ACEL' SUBROUTINE HANDLES THE 'JENNINGS' PSEUDO-EARTHQUAKES'.
THIS PROGRAM INCLUDING ALL SUBROUTINES WAS WRITTEN BY MELBOURNE
F. GIBERSON, DEPARTMENT OF APPLIED MECHANICS, CALIFORNIA INSTI-
TUTE OF TECHNOLOGY, PASADENA, CALIFORNIA.

LAST REVISION - 4 DECEMBER 1966

*****EQUIVALENCE (DDY1(=ELL), DDY3(1))

DOUBLE PRECISION DBTIME,DBDT,ED,OBDTM3,DBZK
DOUBLE PRECISION DBDT5,DBZT1

DIMENSION NAME(13),TIM3(1201),DDY3(1201)

COMMON/ACEWOR/ DBTIME,DBDT,ED,OBDM3,IOPDM,
2 DDY1(=ELL), KEND

READ(15,110) NCARD,OBOT,ENDREC,IOPDM,SCALE
FORMAT(10,D10.0,F10.0,F10.0,F10.0)
READ(15,1120) (TIM3(I),DDY3(I)),I=1,NCARD)
CILL20 FORMATTICXA2F10.0)

C ***** THE FOLLOWING STATEMENTS READ IN THE PSUEDO-EARTHQUAKES *****

C *****

READ(15,1123) NAME
FORMAT(12A6)
READ(15,1125) DDY3
FORMAT(6F11.7,1X)
DBDT3 = 0.025D+00
SSCALE = 3.16*SSCALE
DO 100 I = 1,NCARD
Z11 = I - 1
DBZ1 = DDY3(Z11)
DBZ11 = SNGL(DBZ1+DBDT3)
CONTINUE
WRITE(6,1123) NAME
WRITE(6,1127) (I,TIM3(I),DDY3(I)),I=1,NCARD)
FORMAT(10X,I5,F12.6,F12.7)
DO 105 I=1,NCARD
DDY3(I) = DDY3(I)*SSCALE/32.171667
CONTINUE
DOT = SNGL(DBDT3)
ED = DLE(ENDREC)/DBDT
KEND = SNGL(DOT) + 1.5
INC = KEND - 1
WRITE(6,1130) NCARD,DOT,ENDREC,INC
FORMAT(1H, 25H NO. TIME-ACCEL. PAIRS = ,I4,,/,

100
1105
1123
1125
1127
1130

```

1256 WORK DECK ** MOST OF THE WORK IS DONE HERE**
1257 SUBROUTINE WORK
1258 C*****
1259 C THE PURPOSE OF THIS PROGRAM IS TO CALCULATE VARIOUS RESPONSES
1260 C OF NONLINEAR TALL STRUCTURES SUBJECTED TO EARTHQUAKE EXCITATION.
1261 C
1262 C THE PURPOSE OF SUBROUTINE 'WORK' IS TO EVALUATE THE PARAMETERS
1263 C NEEDED BY SUBROUTINE 'CONV' IN ORDER TO SOLVE THE EQUATIONS OF
1264 C MOTION FOR EACH TIME INTERVAL. THEN THE VARIOUS RESPONSES ARE
1265 C MONITORED CUMULATIVELY FROM TIME ZERO FOR THE MOST POSITIVE AND
1266 C MOST NEGATIVE VALUES AND THE TIMES THEY OCCUR. AFTER EVERY
1267 C SECOND OF REAL TIME AND AT THE END OF THE RUN THESE MAXIMA AND
1268 C TIMES ARE WRITTEN OUT BY SUBROUTINE 'GONE'.
1269 C
1270 C THIS PROGRAM INCLUDING ALL SUBROUTINES WAS WRITTEN BY MELBOURNE
1271 C F. GIBSON, DEPARTMENT OF APPLIED MECHANICS, CALIFORNIA INSTI-
1272 C TUTE OF TECHNOLOGY, PASADENA, CALIFORNIA.
1273 C LAST REVISION - 11 JANUARY 1967
1274 C*****
1275 C
1276 C DOUBLE PRECISION DBU,DBUU
1277 C DOUBLE PRECISION DBTIME,DBOT,ED,DBTIM3,DBZJJ
1278 C
1279 C DIMENSION TAC(122),AXCLD(22,3),GSR(22,3),SHEAR(122),
1280 C 2 L(22,3,4),ALP(122,3,4),BML(22,3,4),BMLAST(22,3,4),BMT(22,3),
1281 C 3 OTMOM(122),SRT(122)
1282 C
1283 C COMMON/WRKCON/UMAX(122),UMIN(122),TMXU(122),TMNU(122),
1284 C 2 VMAX(122),VMIN(122),TMXV(122),TMNV(122),
1285 C 3 UMAX(122),UMIN(122),TMXU(122),TMNU(122),
1286 C 4 SMAX(122),SMIN(122),TMXS(122),TMNS(122),
1287 C 5 ALPMA(122,3,4),ALPMIN(122,3,4),TMXALP(122,3,4),TMNALP(122,3,4),
1288 C 6 BMAX(122,3,4),BMIN(122,3,4),TMXB(122,3,4),TMNB(122,3,4),
1289 C 7 TACMX(122),TACMIN(122),TMXTAC(122),TMNTAC(122),
1290 C 8 GSRMX(122,3),GSRMIN(122,3),TMXGSR(122,3),TMNGSR(122,3),
1291 C 9 CLDMAX(122,3),CLDMIN(122,3),TMXCLD(122,3),TMNCLD(122,3),
1292 C 10 OTMOM(122),OTMOM(122),TMXOT(122),TMNOTM(122),
1293 C 3 ABSBMT(122,3),TABSSRT(122),TABSSR(122)
1294 C
1295 C COMMON/MNMGON/NAMEST(10),NAMEBK(13),BMA(122,3,4),BME(122,3,4),
1296 C 2 GA(122,3),CA(122,3),HT(122),H(122),ZM(122),A(15),S(16),P,F,ZETA,FUNDOF,
1297 C 3 ZL,AL,TIMEND,ALAMDA,BLAMDA,IELPL,TIML,LRTST
1298 C
1299 C ***** THERE ARE TWO OPTIONS FOR THE SECOND CARD OF 'COMMON/ACEWOR/'
1300 C ***** ONE FOR 'JENKINGS' PSEUDO-EARTHQUAKES, THE OTHER FOR REG-
1301 C ***** ULAR EARTHQUAKES. SEE EITHER SUBROUTINE 'ACEL' FOR FURTHER
1302 C ***** EXPLANATION.*****
1303 C
1304 C COMMON/ACEWOR/ DBTIME,DBOT,ED,DBTIM3,IUPTON,
1305 C 2 DDY1(6011),JJEND
1306 C
1307 C 2 TIM3(6011),DDY3(6011),JJEND (USED FOR REG EQKS)
1308 C
1309 C COMMON/HKCONV/S:A(22,3),SCB(122,3),SCC(122,3),SCABH(122,3),
1310 C 2 SCBCH(122,3),SCDHH(122),SGAI(22,3),SGB(122,3),SGC(122,3),
1311 C 3 DU(122),UI(122),DUUH(122),DUUH(122),DU(122),VI(122),
1312 C 4 DACC(122),ACC(122),DM(122,3),W(122,3),DDDY,DT,KG,N22
1313 C
1314 C COMMON/COMMONOD/ DBU(122),DBUU(122)
1315 C
1316 C COMMON/MKGNIN/LLX,LLI,LLB,ALLS,LLD,LLP, LGO(2),LINE(129)
1317 C
1318 C ZG=386.06
1319 C
1320 C JJ = 1
1321 C ITIME = 1
1322 C ZTIME = ITIME
1323
1324 DT = SNGL(DBOT)
1325 DBTIME = DBTIM3
1326 TTIL = SNGL(DBTIME)
1327
1328 C DDY1ZG = DDY1(1)*ZG
1329 DO 5 N=2,21
1330 ACC(N) = -DDY1ZG
1331
1332 C WRITE(20) NAMEST,NAMEBK
1333
1334 C WRITE(20) JJ,LLI,LLSHEAR,BM,OTMOM,AXCLD,ACC,TACC,V,
1335 C 2 DBU,DBUU,W,UMH,ALP,TIML,DT,DDY1(JJ)
1336
1337 C WRITE(6,1001)
1338 C 1001 FORMAT(1H1)
1339
1340 C WRITE(6,1075) DT
1341 C 1075 FORMAT(15H DT = ,1PE15.7)
1342
1343 C WRITE(6,1076)
1344 C 1076 FORMAT(48H JJ TIM1 DDY1 U(2) L1 )
1345
1346 C MR:TE(6,1077) JJ,TIM1,DDY1(JJ),U(2),L1
1347 C 1077 FORMAT(1X,14,1F10.6,1P2E15.7,13)
1348
1349 C ***** BEGIN NEW TIME INTERVAL *****
1350
1351 C 10 CONTINUE
1352 C JJ = JJ+1
1353 C DBZJJ = DBZJJ+DBOT
1354 C TTIL = SNGL(DBTIME)
1355 C JJML = JJ
1356 C DDY1 = DDY1(JJ) - DDY1(JJML)*ZG
1357 C IF(ABS(DT),GT,0.000001) GO TO 80
1358 C DO 70 N=2,21
1359 ACC(N) = ACC(N) - DDY1
1360 C 70 CONTINUE
1361 C WRITE(6,1111) LLX,TIM1,DT,DDY1
1362 C 1111 FORMAT(2X,AL,2X,2F12.5,13X,1PE18.7)
1363 C GO TO 10
1364 C 80 CONTINUE
1365
1366 C ***** EVALUATE 'EFFECTIVE STIFFNESSES SCA, SCB, SCC' FOR COLUMNS *****
1367 C
1368 DO 150 N=2,3
1369 DD 145 N=2,3
1370 CANH = CA(N,M)
1371 IF(ILL(N,M),NE,0) GO TO 120
1372 IF(ILL(N+1,M,2),NE,0) GO TO 110
1373 C----- NO HINGES IN COLUMN -----
1374 SCAIN(M) = CANH
1375 SC3IN(M) = 0.5*CANH
1376 SC2IN(M) = CANH
1377 GO TO 140
1378
1379 C----- HINGE IN COLUMN AT (N+1,M,2) -----
1380 SCAIN(M) = S(1)*CANH
1381 SC3IN(M) = S(1)*CANH
1382 SC2IN(M) = S(1)*CANH
1383 GO TO 140
1384
1385 C----- HINGE IN COLUMN AT (N,M,4) -----
1386 SCAIN(M) = S(3)*CANH
1387 SC3IN(M) = S(4)*CANH
1388 SC2IN(M) = S(5)*CANH
1389 GO TO 140
1390
1391 C----- HINGES IN COLUMN AT BOTH ENDS -----
1392 SCAIN(M) = S(6)*CANH
1393 SC3IN(M) = S(7)*CANH
1394
1395
1396
1397
1398
1399
1400
1401
1402
1403
1404
1405
1406
1407
1408
1409
1410
1411
1412
1413
1414
1415
1416
1417
1418
1419
1420
1421
1422
1423
1424
1425
1426
1427
1428
1429
1430
1431
1432
1433
1434
1435
1436
1437
1438
1439
1440

```



```

      BM(NIN,M,J)=BM(N,M,J)
      TMSGR(N,M,J)=TIM1
      CONTINUE
495 CONTINUE
500 CONTINUE
      C
      C..... EVALUATE *GIRDER SHEAR FORCES, COLUMN AXIAL FORCES, AND
      C..... OVERTURNING MOMENTS* .....
      C
      DO 510 N=2,22
        GSR(N,2) = -(18*MIN(2,3) + BM(N,3,1)) *AL
        GSR(N,3) = -(2.0*BM(N,3,1)*AL)
        AXCLD(N,2) = AXCLD(N,1,2) + (GSR(N,2) - GSR(N,2))
        AXCLD(N,3) = AXCLD(N,1,3) + (GSR(N,2) - GSR(N,2))
        OTMOM(N) = 2.1*(AXCLD(N,1,3) + 5.0*AXCLD(N,1,2))
        OTMOM(N) = 2.0*(BM(N,2,2) + BM(N,3,2))
      C
      C..... MONITOR FOR MAXIMUM AND MINIMUM *OVERTURNING MOMENTS - OTMOM*
      C
      IF(OTMOM(N).GE.OTMOM(N)) GO TO 505
      OTMAX(N) = OTMOM(N)
      TMAXOT(N) = TIM1
      GO TO 510
505 CONTINUE
      IF(OTMOM(N).LE.OTMOM(N)) GO TO 510
      OTMIN(N) = OTMOM(N)
      TMINOT(N) = TIM1
      CONTINUE
510 CONTINUE
      C
      C..... EVALUATE *CHECK-SUM* OF BENDING MOMENTS AT EACH JOINT ...
      C
      DO 550 N=2,3
        DO 545 J=1,22
          BMT(N,M) = 0.0
          DO 520 J=1,4
            BMT(N,M) = BMT(N,M) + BM(N,M,J)
          CONTINUE
          IF(ABS(BMT(N,M).GE.ABS(BMT(N,M))) GO TO 525
          ABSBMT(N,M) = ABS(BMT(N,M))
          TABSBMT(N,M) = TIM1
          CONTINUE
525 CONTINUE
      C
      C..... MONITOR FOR MAXIMUM AND MINIMUM *GIRDER SHEAR - GSR* .....
      C
      IF(GSR(N,M).GE.GSR(N,M)) GO TO 530
      GSRMAX(N,M)=GSR(N,M)
      TMSGSR(N,M)=TIM1
      GO TO 535
530 CONTINUE
      IF(GSR(N,M).LE.GSR(N,M)) GO TO 535
      GSRMIN(M)=GSR(N,M)
      TMSGSR(N,M)=TIM1
      CONTINUE
535 CONTINUE
      C
      C..... MONITOR FOR MAXIMUM AND MINIMUM *AXIAL COLUMN LOAD - AXCLD*
      C
      IF(AXCLD(N,M).GE.AXCLD(N,M)) GO TO 540
      AXCLD(N,M)=AXCLD(N,M)
      TMAXCLD(N,M)=TIM1
      GO TO 545
540 CONTINUE
      IF(AXCLD(N,M).LE.AXCLD(N,M)) GO TO 545
      AXCLD(N,M)=AXCLD(N,M)
      TMINCLD(N,M)=TIM1
      CONTINUE
545 CONTINUE
550 CONTINUE
      C
      CALL MODE
      LWRITE = LWRITE + 1

```

```

      IF(LWRITE.LT.LRTEST) GO TO 560
      LWRITE = 0
      WRITE(6,1077) JJ,TIM1,DDY1(JJ),UI(2),LL1
      C
      WRITE(20) JJ,LL1,AL,SHEAR,BM,OTMOM,AXCLD,ACC,TACC,V,
      2 DBU,DBDU,M,UUH,ALP,TIM1,DT,DDY1(JJ)
560 CONTINUE
      C
      C..... END OF TIME INCREMENT .....
      C
      IF(ABS(TIM1-ZTIME).GT.2.5000002E-03.AND.TIM1.LT.TIMEND) GO TO 10
      ITIME = ITIME + 1
      ZTIME = ITIME
      CALL GONE
      WRITE(6,1001)
      C
      C IF(TIM1.LT.TIMEND) GO TO 10
      C
      CALL GONE
      WRITE(6,1090) JJ
      1090 FORMAT(10H JEND = ,I4)
      C
      C..... TERMINATION OF RUN .....
      C
      RETURN
      END

```

```

      WORK 491
      WORK 492
      WORK 493
      WORK 494
      WORK 495
      WORK 496
      WORK 497
      WORK 498
      WORK 499
      WORK 500
      WORK 501
      WORK 502
      WORK 503
      WORK 504
      WORK 505
      WORK 506
      WORK 507
      WORK 508
      WORK 509
      WORK 510
      WORK 511
      WORK 512
      WORK 513
      WORK 514
      WORK 515
      WORK 516

```



```

1 $IBFC MINV DECK *INVERTS *3X3 SYMMETRIC* MATRIX, DOUBLE PREC*
2 C
3 C*****
4 C
5 C
6 C
7 C
8 C
9 C
10 C
11 C
12 C
13 C
14 C
15 C
16 C
17 C
18 C
19 C
20 C
21 C
22 C
23 C
24 C
25 C
26 C
27 C
28 C
29 C
30 C
31 C
32 C
33 C
34 C
35 C
36 C
37 C
38 C
39 C
40 C
41 C
42 C
43 C
44 C
45 C
46 C
47 C
48 C
49 C
50 C
51 C
52 C
53 C
54 C
55 C
56 C
57 C
58 C
59 C
60 C
61 C
62 C
63 C
64 C
65 C
66 C
67 C
68 C
69 C
70 C
71 C
72 C
73 C
74 C
75 C
76 C
77 C
78 C
79 C
80 C
81 C
82 C
83 C
84 C
85 C
86 C
87 C
88 C
89 C
90 C
91 C
92 C
93 C
94 C
95 C
96 C
97 C
98 C
99 C
100 C
101 C
102 C
103 C
104 C
105 C
106 C
107 C
108 C
109 C
110 C
111 C
112 C
113 C
114 C
115 C
116 C
117 C
118 C
119 C
120 C
121 C
122 C
123 C
124 C
125 C
126 C
127 C
128 C
129 C
130 C
131 C
132 C
133 C
134 C
135 C
136 C
137 C
138 C
139 C
140 C
141 C
142 C
143 C
144 C
145 C
146 C
147 C
148 C
149 C
150 C
151 C
152 C
153 C
154 C
155 C
156 C
157 C
158 C
159 C
160 C
161 C
162 C
163 C
164 C
165 C
166 C
167 C
168 C
169 C
170 C
171 C
172 C
173 C
174 C
175 C
176 C
177 C
178 C
179 C
180 C
181 C
182 C
183 C
184 C
185 C
186 C
187 C
188 C
189 C
190 C
191 C
192 C
193 C
194 C
195 C
196 C
197 C
198 C
199 C
200 C
201 C
202 C
203 C
204 C
205 C
206 C
207 C
208 C
209 C
210 C
211 C
212 C
213 C
214 C
215 C
216 C
217 C
218 C
219 C
220 C
221 C
222 C
223 C
224 C
225 C
226 C
227 C
228 C
229 C
230 C
231 C
232 C
233 C
234 C
235 C
236 C
237 C
238 C
239 C
240 C
241 C
242 C
243 C
244 C
245 C
246 C
247 C
248 C
249 C
250 C
251 C
252 C
253 C
254 C
255 C
256 C
257 C
258 C
259 C
260 C
261 C
262 C
263 C
264 C
265 C
266 C
267 C
268 C
269 C
270 C
271 C
272 C
273 C
274 C
275 C
276 C
277 C
278 C
279 C
280 C
281 C
282 C
283 C
284 C
285 C
286 C
287 C
288 C
289 C
290 C
291 C
292 C
293 C
294 C
295 C
296 C
297 C
298 C
299 C
300 C
301 C
302 C
303 C
304 C
305 C
306 C
307 C
308 C
309 C
310 C
311 C
312 C
313 C
314 C
315 C
316 C
317 C
318 C
319 C
320 C
321 C
322 C
323 C
324 C
325 C
326 C
327 C
328 C
329 C
330 C
331 C
332 C
333 C
334 C
335 C
336 C
337 C
338 C
339 C
340 C
341 C
342 C
343 C
344 C
345 C
346 C
347 C
348 C
349 C
350 C
351 C
352 C
353 C
354 C
355 C
356 C
357 C
358 C
359 C
360 C
361 C
362 C
363 C
364 C
365 C
366 C
367 C
368 C
369 C
370 C
371 C
372 C
373 C
374 C
375 C
376 C
377 C
378 C
379 C
380 C
381 C
382 C
383 C
384 C
385 C
386 C
387 C
388 C
389 C
390 C
391 C
392 C
393 C
394 C
395 C
396 C
397 C
398 C
399 C
400 C
401 C
402 C
403 C
404 C
405 C
406 C
407 C
408 C
409 C
410 C
411 C
412 C
413 C
414 C
415 C
416 C
417 C
418 C
419 C
420 C
421 C
422 C
423 C
424 C
425 C
426 C
427 C
428 C
429 C
430 C
431 C
432 C
433 C
434 C
435 C
436 C
437 C
438 C
439 C
440 C
441 C
442 C
443 C
444 C
445 C
446 C
447 C
448 C
449 C
450 C
451 C
452 C
453 C
454 C
455 C
456 C
457 C
458 C
459 C
460 C
461 C
462 C
463 C
464 C
465 C
466 C
467 C
468 C
469 C
470 C
471 C
472 C
473 C
474 C
475 C
476 C
477 C
478 C
479 C
480 C
481 C
482 C
483 C
484 C
485 C
486 C
487 C
488 C
489 C
490 C
491 C
492 C
493 C
494 C
495 C
496 C
497 C
498 C
499 C
500 C
501 C
502 C
503 C
504 C
505 C
506 C
507 C
508 C
509 C
510 C
511 C
512 C
513 C
514 C
515 C
516 C
517 C
518 C
519 C
520 C
521 C
522 C
523 C
524 C
525 C
526 C
527 C
528 C
529 C
530 C
531 C
532 C
533 C
534 C
535 C
536 C
537 C
538 C
539 C
540 C
541 C
542 C
543 C
544 C
545 C
546 C
547 C
548 C
549 C
550 C
551 C
552 C
553 C
554 C
555 C
556 C
557 C
558 C
559 C
560 C
561 C
562 C
563 C
564 C
565 C
566 C
567 C
568 C
569 C
570 C
571 C
572 C
573 C
574 C
575 C
576 C
577 C
578 C
579 C
580 C
581 C
582 C
583 C
584 C
585 C
586 C
587 C
588 C
589 C
590 C
591 C
592 C
593 C
594 C
595 C
596 C
597 C
598 C
599 C
600 C
601 C
602 C
603 C
604 C
605 C
606 C
607 C
608 C
609 C
610 C
611 C
612 C
613 C
614 C
615 C
616 C
617 C
618 C
619 C
620 C
621 C
622 C
623 C
624 C
625 C
626 C
627 C
628 C
629 C
630 C
631 C
632 C
633 C
634 C
635 C
636 C
637 C
638 C
639 C
640 C
641 C
642 C
643 C
644 C
645 C
646 C
647 C
648 C
649 C
650 C
651 C
652 C
653 C
654 C
655 C
656 C
657 C
658 C
659 C
660 C
661 C
662 C
663 C
664 C
665 C
666 C
667 C
668 C
669 C
670 C
671 C
672 C
673 C
674 C
675 C
676 C
677 C
678 C
679 C
680 C
681 C
682 C
683 C
684 C
685 C
686 C
687 C
688 C
689 C
690 C
691 C
692 C
693 C
694 C
695 C
696 C
697 C
698 C
699 C
700 C
701 C
702 C
703 C
704 C
705 C
706 C
707 C
708 C
709 C
710 C
711 C
712 C
713 C
714 C
715 C
716 C
717 C
718 C
719 C
720 C
721 C
722 C
723 C
724 C
725 C
726 C
727 C
728 C
729 C
730 C
731 C
732 C
733 C
734 C
735 C
736 C
737 C
738 C
739 C
740 C
741 C
742 C
743 C
744 C
745 C
746 C
747 C
748 C
749 C
750 C
751 C
752 C
753 C
754 C
755 C
756 C
757 C
758 C
759 C
760 C
761 C
762 C
763 C
764 C
765 C
766 C
767 C
768 C
769 C
770 C
771 C
772 C
773 C
774 C
775 C
776 C
777 C
778 C
779 C
780 C
781 C
782 C
783 C
784 C
785 C
786 C
787 C
788 C
789 C
790 C
791 C
792 C
793 C
794 C
795 C
796 C
797 C
798 C
799 C
800 C
801 C
802 C
803 C
804 C
805 C
806 C
807 C
808 C
809 C
810 C
811 C
812 C
813 C
814 C
815 C
816 C
817 C
818 C
819 C
820 C
821 C
822 C
823 C
824 C
825 C
826 C
827 C
828 C
829 C
830 C
831 C
832 C
833 C
834 C
835 C

```


[illegible]

```

WRITE(6,1445)
1445 FORMAT(204,80H SUM-CHECK OF ALL OF THE FORCES ACTING ON EACH FLOOR,
2 AND THE TIME OF OCCURRENCE )
NN=21
DO 845 N=2,22
NN=NN-1
WRITE(6,1445) NN,ABSRT(N),TABSSR(N)
845 CONTINUE
C
WRITE(6,1402)
WRITE(6,1403)
WRITE(6,1404)
1450 FORMAT(114,90H SUM-CHECK OF THE BENDING MOMENTS AT EACH
2M1, AND THE TIME OF OCCURRENCE )
NN=21
DO 850 N=2,22
NN=NN-1
WRITE(6,1445) NN,TABSBMT(N,M),TABSBM(N,M),P=2,3)
850 CONTINUE
C
WRITE(6,1401) NAMEST,P,ZETA,FUNDFQ,TIM1,NAMEQK
WRITE(6,1460)
1460 FORMAT(104,100H OVERTURNING MOMENTS IN INCH LBS, AND THE TIME OF
2 OCCURRENCE ** OTMMX,IMXOTM, OTMMN,IMNOTM )
NN=21
DO 855 N=2,22
NN=NN-1
WRITE(6,1445) NN,OTMMX(N),TXOTM(N),OTMMN(N),IMNOTM(N)
855 CONTINUE
C
WRITE(6,1402)
WRITE(6,1465)
1465 FORMAT(142H ((DUCTIL(N,M,J),J=1,4),M=2,3) GIBERSON )
NN=21
DO 860 N=2,22
NN=NN-1
WRITE(6,1413) NN,((DUCTIL(N,M,J),J=1,4),M=2,3)
860 CONTINUE
C
WRITE(6,1401) NAMEST,P,ZETA,FUNDFQ,TIM1,NAMEQK
WRITE(6,1470)
1470 FORMAT(140,65H MOST NEGATIVE AND MOST POSITIVE DISPLACEMENTS IN
2 INCHES )
NN=21
DO 865 N=2,22
NN=NN-1
WRITE(6,1480)
1480 FORMAT(112H -16 -15 -14 -13 -12 -11 -10 -9 -8 -7 -6 -5 -4 -3 -2 -1 0 1 2 3 4 5 6 7 8 9 10 11 12 13
3 14 15 16 )
1485 FORMAT(131,14H+1)
NN=21
DO 610 N=2,21
NN=NN-1
LINE(65)=LLP
IF(LUMIN(N,LE,-16,0) GO TO 605
I=IFIX(4,0*UMIN(N) -0.5) + 65
LINE(11)=LLD
605 IF(UMAX(N,-GT,16,0) GO TO 608
J=IFIX(4,0*UMAX(N) + 0.5) + 65
LINE(11)=LLD
608 WRITE(6,1490) NN,LINE
1490 FORMAT(112,129A1)
LINE(11)=LLB
610 CONTINUE
C
LINE(65)=LLP
WRITE(6,1495) LCD,LINE
1495 FORMAT(112,2A1,129A1)
LINE(65)=LLB
WRITE(6,1485)
C
WRITE(6,1402)

```

```

CONE 141
CONE 142
CONE 143
CONE 144
CONE 145
CONE 146
CONE 147
CONE 148
CONE 149
CONE 150
CONE 151
CONE 152
CONE 153
CONE 154
CONE 155
CONE 156
CONE 157
CONE 158
CONE 159
CONE 160
CONE 161
CONE 162
CONE 163
CONE 164
CONE 165
CONE 166
CONE 167
CONE 168
CONE 169
CONE 170
CONE 171
CONE 172
CONE 173
CONE 174
CONE 175
CONE 176
CONE 177
CONE 178
CONE 179
CONE 180
CONE 181
CONE 182
CONE 183
CONE 184
CONE 185
CONE 186
CONE 187
CONE 188
CONE 189
CONE 190
CONE 191
CONE 192
CONE 193
CONE 194
CONE 195
CONE 196
CONE 197
CONE 198
CONE 199
CONE 200
CONE 201
CONE 202
CONE 203
CONE 204
CONE 205
CONE 206
CONE 207
CONE 208
CONE 209
CONE 210

NN = NN - 1
WRITE(6,1312) NN,((ALPMIN(N,M,J),J=1,4),M=2,3)
CONTINUE
C
WRITE(6,1002)
WRITE(6,1380)
FORMAT(36H ((BMMIN(N,M,J),J=1,4),M=2,3)
NN = 21
DO 830 N=2,22
NN=NN-1
WRITE(6,1313) NN,((BMMIN(N,M,J),J=1,4),M=2,3)
CONTINUE
C
WRITE(6,1001) NAMEST,P,ZETA,FUNDFQ,TIM1,NAMEQK
WRITE(6,1390)
FORMAT(50H ((GSRMX, TXGSR, GSRMN, TMNGSR), M=2,3)
NN = 21
DO 790 N=2,22
NN=NN-1
WRITE(6,1311) NN,(GSRM(N,M),TXGSR(N,M),GSRMN(N,M),TMNGSR(N,M),
2 M=2,3)
CONTINUE
C
WRITE(6,1002)
WRITE(6,1400)
FORMAT(50H ((CLDMAX, IMXCLD, CLDMIN, IMNCLD), M=2,3)
NN = 21
DO 800 N=2,22
NN=NN-1
WRITE(6,1311) NN,(CLDMAX(N,M),IMXCLD(N,M),CLDMIN(N,M),IMNCLD(N,M),
2 M=2,3)
CONTINUE
C
WRITE(6,1001) NAMEST,P,ZETA,FUNDFQ,TIM1,NAMEQK
FORMAT(36H ((BMX(N,M,J),J=1,4),M=2,3)
NN = 21
DO 810 N=2,22
NN=NN-1
WRITE(6,1312) NN,((BMX(N,M,J),J=1,4),M=2,3)
CONTINUE
C
WRITE(6,1002)
WRITE(6,1420)
FORMAT(36H ((TMXBM(N,M,J),J=1,4),M=2,3)
NN = 21
DO 820 N=2,22
NN=NN-1
WRITE(6,1313) NN,((TMXBM(N,M,J),J=1,4),M=2,3)
CONTINUE
C
WRITE(6,1001) NAMEST,P,ZETA,FUNDFQ,TIM1,NAMEQK
FORMAT(36H ((BMMIN(N,M,J),J=1,4),M=2,3)
NN = 21
DO 830 N=2,22
NN=NN-1
WRITE(6,1312) NN,((BMMIN(N,M,J),J=1,4),M=2,3)
CONTINUE
C
WRITE(6,1002)
WRITE(6,1440)
FORMAT(36H ((TMNBM(N,M,J),J=1,4),M=2,3)
NN = 21
DO 840 N=2,22
NN=NN-1
WRITE(6,1313) NN,((TMNBM(N,M,J),J=1,4),M=2,3)
CONTINUE
C
WRITE(6,1001) NAMEST,P,ZETA,FUNDFQ,TIM1,NAMEQK

```



```

C
DO 645 J=1,17,8
  ABSAMV= 0.0D+00
  MODE 71
  MODE 72
  MODE 73
  MODE 74
  IF (ABSAMV.GE.DABSNAMEV(K,J)) GO TO 642
  ABSAMV =DABSNAMEV(K,J)
  MODE 75
  MODE 76
  MODE 77
  MODE 78
  MODE 79
  MODE 80
  MODE 81
  MODE 82
  MODE 83
  MODE 84
  MODE 85
  MODE 86
  C..... EVALUATE (TRANPOSED EIGENVECTOR)*(MASS*(1/2)) .....
  C
  DO 660 J=1,20
    ZMH = ZMHAF(J)
    MODE 87
    MODE 88
    MODE 89
    MODE 90
    MODE 91
    MODE 92
    MODE 93
    MODE 94
    MODE 95
    MODE 96
    MODE 97
    MODE 98
    MODE 99
    MODE 100
    MODE 101
    MODE 102
    MODE 103
    MODE 104
    MODE 105
    MODE 106
    MODE 107
    C..... EVALUATE THE MODAL CONTRIBUTIONS TO THE DISPLACEMENTS AND .....
    C..... INTER-FLOOR DISPLACEMENTS OF SELECTED (ARBITRARY) FLOORS ...
    JN = 0
    DO 690 I = 2,17,5
      JN=JN+1
      TUUM(JN) = 0.0D+00
      TUUM(JN) = 0.0D+00
      DO 682 J=1,20
        UUM(JN,J) = AMEV(I,J)*AIDA(J)
        UUM(JN,J) = (AMEV(I,J) - AMEV(I+1,J))*AIDA(J)
        TUUM(JN) = TUUM(JN) + UUM(JN,J)
      CONTINUE
    WRITE(6,1230) (N,(UUM(JN,N), UUM(JN,N),JN=1,4),N=1,20)
    FORMAT(1X,I2,4(2X,1P2E15.7) )
    N = 21
    WRITE(6,1230) N,(TUUM(JN), TUUM(JN),JN=1,4)
    WRITE(6,1230) N,(DBL(J),DBUU(J),J=3,18,5)
    WRITE(6,11001)
    FORMAT(1H1)
    RETURN
  END
  MODE 108
  MODE 109
  MODE 110
  MODE 111
  MODE 112
  MODE 113
  MODE 114
  MODE 115
  MODE 116
  MODE 117
  MODE 118
  MODE 119
  MODE 120
  MODE 121
  MODE 122
  MODE 123
  MODE 124
  MODE 125
  MODE 126
  MODE 127
  MODE 128
  MODE 129
  MODE 130

```

```

1
2
3
4
5
6
7
8
9
10
11
12
13
14
15
16
17
18
19
20
21
22
23
24
25
26
27
28
29
30
31
32
33
34
35
36
37
38
39
40
41
42
43
44
45
46
47
48
49
50
51
52
53
54
55
56
57
58
59
60
61
62
63
64
65
66
67
68
69
70
71
72
73
74
75
76
77
78
79
80
81
82
83
84
85
86
87
88
89
90
91
92
93
94
95
96
97
98
99
100
101
102
103
104
105
106
107
108
109
110
111
112
113
114
115
116
117
118
119
120
121
122
123
124
125
126
127
128
129
130
131
132
133
134
135
136
137
138
139
140
141
142
143
144
145
146
147
148
149
150
151
152
153
154
155
156
157
158
159
160
161
162
163
164
165
166
167
168
169
170
171
172
173
174
175
176
177
178
179
180
181
182
183
184
185
186
187
188
189
190
191
192
193
194
195
196
197
198
199
200
201
202
203
204
205
206
207
208
209
210
211
212
213
214
215
216
217
218
219
220
221
222
223
224
225
226
227
228
229
230
231
232
233
234
235
236
237
238
239
240
241
242
243
244
245
246
247
248
249
250
251
252
253
254
255
256
257
258
259
260
261
262
263
264
265
266
267
268
269
270
271
272
273
274
275
276
277
278
279
280
281
282
283
284
285
286
287
288
289
290
291
292
293
294
295
296
297
298
299
300
301
302
303
304
305
306
307
308
309
310
311
312
313
314
315
316
317
318
319
320
321
322
323
324
325
326
327
328
329
330
331
332
333
334
335
336
337
338
339
340
341
342
343
344
345
346
347
348
349
350
351
352
353
354
355
356
357
358
359
360
361
362
363
364
365
366
367
368
369
370
371
372
373
374
375
376
377
378
379
380
381
382
383
384
385
386
387
388
389
390
391
392
393
394
395
396
397
398
399
400
401
402
403
404
405
406
407
408
409
410
411
412
413
414
415
416
417
418
419
420
421
422
423
424
425
426
427
428
429
430
431
432
433
434
435
436
437
438
439
440
441
442
443
444
445
446
447
448
449
450
451
452
453
454
455
456
457
458
459
460
461
462
463
464
465
466
467
468
469
470
471
472
473
474
475
476
477
478
479
480
481
482
483
484
485
486
487
488
489
490
491
492
493
494
495
496
497
498
499
500
501
502
503
504
505
506
507
508
509
510
511
512
513
514
515
516
517
518
519
520
521
522
523
524
525
526
527
528
529
530
531
532
533
534
535
536
537
538
539
540
541
542
543
544
545
546
547
548
549
550
551
552
553
554
555
556
557
558
559
560
561
562
563
564
565
566
567
568
569
570
571
572
573
574
575
576
577
578
579
580
581
582
583
584
585
586
587
588
589
590
591
592
593
594
595
596
597
598
599
600
601
602
603
604
605
606
607
608
609
610
611
612
613
614
615
616
617
618
619
620
621
622
623
624
625
626
627
628
629
630
631
632
633
634
635
636
637
638
639
640
641
642
643
644
645
646
647
648
649
650
651
652
653
654
655
656
657
658
659
660
661
662
663
664
665
666
667
668
669
670
671
672
673
674
675
676
677
678
679
680
681
682
683
684
685
686
687
688
689
690
691
692
693
694
695
696
697
698
699
700
701
702
703
704
705
706
707
708
709
710
711
712
713
714
715
716
717
718
719
720
721
722
723
724
725
726
727
728
729
730
731
732
733
734
735
736
737
738
739
740
741
742
743
744
745
746
747
748
749
750
751
752
753
754
755
756
757
758
759
760
761
762
763
764
765
766
767
768
769
770
771
772
773
774
775
776
777
778
779
780
781
782
783
784
785
786
787
788
789
790
791
792
793
794
795
796
797
798
799
800
801
802
803
804
805
806
807
808
809
810
811
812
813
814
815
816
817
818
819
820
821
822
823
824
825
826
827
828
829
830
831
832
833
834
835
836
837
838
839
840
841
842
843
844
845
846
847
848
849
850
851
852
853
854
855
856
857
858
859
860
861
862
863
864
865
866
867
868
869
870
871
872
873
874
875
876
877
878
879
880
881
882
883
884
885
886
887
888
889
890
891
892
893
894
895
896
897
898
899
900
901
902
903
904
905
906
907
908
909
910
911
912
913
914
915
916
917
918
919
920
921
922
923
924
925
926
927
928
929
930
931
932
933
934
935
936
937
938
939
940
941
942
943
944
945
946
947
948
949
950
951
952
953
954
955
956
957
958
959
960
961
962
963
964
965
966
967
968
969
970
971
972
973
974
975
976
977
978
979
980
981
982
983
984
985
986
987
988
989
990
991
992
993
994
995
996
997
998
999
1000

```

[illegible]

THE FOLLOWING IBM® TAPE CONTROL PROGRAM IS USED BY PROGRAM 'Q56'.

| | | | |
|--------|--------|--|---|
| SIBNA? | U20 | DECK | 1 |
| ENTRY | .UN20. | X | 2 |
| UN20, | PZE | RESULT TAPE=6(1),HOLD,BLK=256,BIN,POUNT,OUTPUT | 3 |
| X | K | FILE | 4 |
| END | | END | 5 |

```

1      $IBFC ZERO   DECK *INITIALIZING BY *BLOCK DATA**
2      C*****
3      C*****
4      C*****
5      C THE PURPOSE OF THIS PROGRAM IS TO CALCULATE VARIOUS RESPONSES
6      C OF NONLINEAR TALL STRUCTURES SUBJECTED TO EARTHQUAKE EXCITATION.
7      C*****
8      C THE PURPOSE OF "BLOCK DATA" IS TO PLACE PRESCRIBED NON-ZERO
9      C VALUES IN CERTAIN MEMORY CELLS AT THE TIME OF LOADING.
10     C*****
11     C THIS PROGRAM INCLUDING A.L. SUBROUTINES WAS WRITTEN BY MELBOURNE
12     C F. GIBERSON, DEPARTMENT OF APPLIED MECHANICS, CALIFORNIA INSTI-
13     C TUTE OF TECHNOLOGY, PASADENA, CALIFORNIA.
14     C LAST REVISION - 4 DECEMBER 1966
15     C*****
16     C*****
17     C BLOCK DATA
18     C*****
19     C COMMON/MKGNIN/LX,LLI,LL3,LLS,LLD,LLP, LGO(12),LINE(129)
20     C*****
21     C COMMON/MNCCCN/NAMEST(11),NAMEQ(113),BMA(12),3,4),BMH(12),3,5),
22     C GA(12),3,3),CA(12),3,3),H(12),H(12),ZM(12),5),S(18),P,F,ZETA,FUNDFQ,
23     C ZL,AL,TIMEND,ALAMDA,BLAMDA,TPL,TTL,LRTST
24     C*****
25     C DATA LLX,LLI,LL3,LLS,LLD,LLP/LHX,IHI,1,H ,IH8,IH9,1HH+1,
26     C LG(11),LG(12)/LHG,IHO*, / LINE(11),1,1,129/ 129=IH /
27     C 3 ((1BMA(N,M,J),N=1,2,,J=1,4),M=1,3)/264*1./0/
28     C *****
29     C *****

```

REFERENCES

1. Clough, R. W., K. L. Benuska and T. Y. Lin & Associates. FHA Study of Seismic Design Criteria for High-Rise Buildings, (HUD TS-3), Federal Housing Administration, Washington, D.C., (August 1966).
2. T. Y. Lin & Associates. A Computer Program to Analyze the Dynamic Response of High Rise Buildings to Nuclear Blast Loading, Vol. I: Elastic Analysis, Vol. II: Dynamic Nonlinear Response Analysis. (OCD-OS-63-44), Office of the Secretary of the Army, Department of the Army, Washington, D.C., (October 1963).
3. Sano, R., and K. Muto. Earthquake and Typhoon Resistant Construction, (Japanese), Tokyo, Japan, 1935.
4. Suyehiro, K. "Engineering Seismology," ASCE, Proceedings, v.58, no.5, pt.2, (May 1932), 110p.
5. Biot, M. A. "Theory of Elastic Systems Vibrating Under Transient Impulse With an Application to Earthquake Proof Buildings," National Academy of Science, Proceedings, v.19 (1933) 262-268.
6. Biot, M. A. "Analytical and Experimental Methods in Engineering Seismology," ASCE, Transactions, v.108 (1943) 262-268.
7. Freeman, J. R. Earthquake Damage and Earthquake Insurance, N.Y., McGraw-Hill, 1932.
8. Hudson, D. E. "Response Spectrum Techniques in Engineering Seismology." In World Conference on Earthquake Engineering, Berkeley, California, 1956, Proceedings. San Francisco, Earthquake Engineering Research Institute, 1956, Paper No. 4.
9. Housner, G. W. "Vibration of Structures Induced by Seismic Waves, Part I: Earthquakes," (Chapter 50). In Shock and Vibration Handbook, v.3. Edited by Cyril M. Harris and Charles E. Crede. N.Y., McGraw-Hill, 1961.
10. Caughey, T. K. "Random Excitation of a System with Bilinear Hysteresis," Journal of Applied Mechanics, v.27, no.4 (December 1960) 649-652.
11. Berg, G. V. and S. S. Thomaidis. "Energy Consumption by Structures in Strong Motion Earthquakes." In World Conference on Earthquake Engineering, 2d, Tokyo and Kyoto, Japan 1960, Proceedings. Tokyo, Science Council of Japan, 1960.

12. Penzien, J. "Dynamic Response of Elasto-Plastic Frames," ASCE, Structural Division, Journal, v.86, no.ST7 (July 1960) 81-94.
13. Iwan, W. D. The Dynamic Response of Bilinear Hysteretic Systems, Earthquake Engineering Research Laboratory (Ph.D. Thesis), California Institute of Technology, 1961.
14. Jennings, Paul C. Response of Simple Yielding Structures to Earthquake Excitation, Earthquake Engineering Research Laboratory (Ph. D. Thesis), California Institute of Technology, 1963.
15. Chelapati, C. V. Response of Simple Inelastic Systems to Ground Motion, Ph.D. Thesis, University of Illinois, Urbana, Illinois, 1962.
16. Lutes, L. D. Stationary Random Response of Bilinear Hysteretic Systems, Earthquake Engineering Research Laboratory (Ph.D. Thesis), California Institute of Technology, 1967.
17. Jacobsen, L. S. and R. S. Ayre. "Experimentally Determined Dynamic Shears in a Fifteen Story Model," Seismological Society of America, Bulletin, v.28, no.4 (October 1938) 269-311.
18. Tung, T. P. and N. M. Newmark. "Numerical Analysis of Earthquake Response of a Tall Structure," Seismological Society of America, Bulletin, v.45, no.4 (October 1955) 269-278.
19. Jennings, Richard L. The Response of Multistoried Structures to Strong Ground Motion, M.S. Thesis, University of Illinois, Urbana, Illinois, 1958.
20. Jennings, Richard L. and N. M. Newmark. "Elastic Response of Multi-story Shear Beam Type Structures Subjected to Strong Ground Motion." In World Conference on Earthquake Engineering, 2d, Tokyo and Kyoto, Japan, 1960, Proceedings, Tokyo, Science Council of Japan, 1960, v.2, 699-718.
21. Clough, R. W. "On the Importance of Higher Modes of Vibration in the Earthquake Response of a Tall Building," Seismological Society of America, Bulletin, v.45, no.4 (October 1955) 289-301.
22. Blume, J. A. "Structural Dynamics in Earthquake-Resistant Design," ASCE, Structural Division, Journal, v.84, no.ST4 (July 1958) Proc. Paper 1695.

23. Blume, J. A., L. Corning and N. M. Newmark. Design of Multi-Story Reinforced Concrete Buildings for Earthquake Motions. Chicago, Illinois, Portland Cement Association, 1961.
24. Goldberg, J. E., J. L. Bogdanoff and Z. L. Moh. "Forced Vibration and Natural Periods of Tall Building Frames," Seismological Society of America, Bulletin, v. 49, no. 1 (1959) 33-48.
25. Penzien, J. "Elasto-Plastic Response of Idealized Multi-Story Structures." In World Conference on Earthquake Engineering, 2d, Tokyo and Kyoto, Japan, 1960, Proceedings, Tokyo, Science Council of Japan, 1960, v. 2, Session II, 739-760.
26. Bustamante, J. I. "Seismic Shears and Overturning Moments in Buildings." In World Conference on Earthquake Engineering, 3d, Auckland and Wellington, New Zealand, 1965, Proceedings, Wellington, New Zealand National Committee on Earthquake Engineering, 1965, v. 3, Session IV, 144-160.
27. Umemura, H., Y. Osawa and A. Shibato. "Study on Shearing Forces in Structures Caused by Medium Earthquakes Recorded in Japan." In World Conference on Earthquake Engineering, 3d, 1965, Auckland and Wellington, 1965, Proceedings, Wellington, New Zealand National Committee on Earthquake Engineering, 1965, v. 3, Session IV, 539-571.
28. Berg, G. V. "Response of Multi-Story Structures to Earthquakes," ASCE, Engineering Mechanics Division, Journal, v. 87, no. EM2 (April 1961) 1-16.
29. Muto, K. "Recent Trends in High Rise Building Design in Japan." (Special Address) In World Conference on Earthquake Engineering, 3d, Auckland and Wellington, New Zealand, 1965, Proceedings, Wellington, New Zealand National Committee on Earthquake Engineering, 1965, v. 1, 119-146.
30. Westergaard, H. M. "Earthquake Shock Transmission in Tall Buildings," Engineering News-Record, v. 111 (November 30, 1933) 654-656.
31. Jacobsen, L. S. "Vibrational Transfer from Shear Buildings to Ground," ASCE, Engineering Mechanics Division, Journal, v. 90, no. EM3 (June 1964) 21-38.

32. Kanai, K. "Some New Problems of Seismic Vibrations of a Structure." In World Conference on Earthquake Engineering, 3d, Auckland and Wellington, New Zealand, 1965, Proceedings, Wellington, New Zealand National Committee on Earthquake Engineering, 1965, v.2, Session II, 260-275.
33. Bycroft, G. N. "Yield Displacements in Multi-Story Aseismic Design," Seismological Society of America, Bulletin, v.50, no.3 (July 1960) 441-453.
34. Bycroft, G. N. "Effect of Stiffness Taper in Aseismic Design," Seismological Society of America, Bulletin, v.50, no.4 (October 1960) 537-552.
35. Murphy, M. J., G. N. Bycroft and L. W. Harrison, "Electrical Analog for Earthquake Shear Stresses in a Multi-Story Building." In World Conference on Earthquake Engineering, Berkeley, California, USA, 1956, Proceedings, San Francisco, Earthquake Engineering Research Institute, 1956, Paper No.9.
36. Clough, R. W. "Earthquake Analysis by Response Spectrum Superposition," Seismological Society of America, Bulletin, v.52, no.3 (July 1962) 647-660.
37. Clough, R. W., I. P. King and E. L. Wilson. "Large Capacity Multistory Frame Analysis Programs," ASCE, Structural Division, Journal, v.89, no.ST4 (August 1963) 179-204.
38. Clough, R. W., I. P. King and E. L. Wilson. "Structural Analysis of Multistory Buildings," ASCE, Structural Division, Journal, v.90, no.ST3 (June 1964) 19-34.
39. Clough, R. W., K. L. Benuska and E. L. Wilson. "Inelastic Earthquake Response of Tall Buildings." In World Conference on Earthquake Engineering, 3d, Auckland and Wellington, New Zealand, 1965, Proceedings, Wellington, New Zealand National Committee on Earthquake Engineering, 1965, v.2, Session II, 68-89.
40. Clough, R. W. and E. L. Wilson. "Dynamic Response by Step-by-Step Matrix Analysis," Symposium on the Use of Computers in Civil Engineering, Lisbon, Portugal, 1962.
41. Richard, R. M. and J. E. Goldberg. "Analysis of Nonlinear Structures, Force Method," ASCE, Structural Division, Journal, v.91, no.ST6 (December 1965) 33-48.
42. Melin, J. "Numerical Integration by the Beta Method." American Society of Civil Engineers, Conference on Electronic Computation, 1st, 1958, Kansas City, Missouri, 227-236.

43. Newmark, N. M. "A Method of Computation for Structural Dynamics," ASCE, Engineering Mechanics Division, Journal, v.85, no.EM3 (July 1959) 67-94.
44. O'Kelley, M. E. J. Vibration of Viscously Damped Linear Dynamic Systems, Dynamics Laboratory (Ph.D. Thesis), California Institute of Technology, 1964.

Several textbooks on the design of indeterminate structures such as those modeled in this report are available. Among them are the following:

45. Ferguson, P. M. Reinforced Concrete Fundamentals, (1st ed., 1958), (2d ed., rev. 1965), N.Y., J. Wiley.
46. Hurty, W. C. and M. F. Rubenstein. Dynamics of Structures, Englewood Cliffs, N.J., Prentice-Hall, 1964.
47. Timoshenko, S. and D. H. Young. Theory of Structures, (2nd ed.), N.Y., McGraw-Hill, 1965.

Two bibliographies of research work covering the entire earthquake engineering field are noted:

48. Hollis, E. P. Bibliography of Engineering Seismology (2nd ed.), San Francisco, Earthquake Engineering Research Institute, 1966.
49. Rosenblueth, E. "Earthquake Resistant Design," Applied Mechanics Review, v.14, no.12 (December 1961) 923-926.